Evaluating the Effect of Glyco-engineered Monoclonal Antibodies on Natural Killer Cell and Dendritic Cell Activation and the Potential to Promote CD8+ T-cell Mediated Cancer Immunity

Etuk, Aniekan

Awarding institution:
King's College London

Evaluating the Effect of Glyco-engineered Monoclonal Antibodies on Natural Killer Cell and Dendritic Cell Activation and the Potential to Promote $CD8^+$ T-cell Mediated Cancer Immunity

Aniekan Etuk MSc

A thesis submitted for the degree of
Doctor of Philosophy (PhD)

January 2019

Supervisors: Dr Linda Barber | Professor Farzin Farzaneh

King's College London

Faculty of Life Sciences and Medicine

School of Cancer and Pharmaceutical Sciences

The Rayne Institute

123 Coldharbour Lane

London

SE5 9NU

KING'S College LONDON

Abstract

Therapeutic monoclonal antibodies (mAbs) can inhibit the function of tumour antigens (TA) and additionally those of IgG_1 subclass can recruit natural killer (NK) cells to kill tumours via antibody-dependent cellular cytotoxicity (ADCC). One such example is cetuximab, which is specific for the epidermal growth factor receptor (EGFR) that is overexpressed in more than 70% of colorectal cancer cases. Importantly the efficacy of cetuximab is limited in patients who have the low affinity FCγRIIIa (CD16) polymorphism, thus a glyco-engineered (GE) anti-EGFR mAb was developed called GA201GE (imgatuzumab), that reportedly mediates high affinity CD16 binding and enhanced ADCC, irrespective of CD16 genotype. In a similar vein, the anti-CD20 GE-mAb obinutuzumab (GA101GE) was developed to improve upon the unmodified anti-CD20 rituximab currently used in the treatment of B-cell malignancies. It is important to evaluate whether ADCC facilitated by therapeutic mAbs has the potential to stimulate $CD8^+$ T-cell mediated immunity, which is essential for long-term tumour immune-surveillance. The complex cross talk between NK cells and dendritic cells (DC) is a precursor to the generation of TA-specific T cells. DC can ingest and process exogenous antigen released from target cells lysed by NK cells, and subsequently cross present TA epitopes to TA-specific $CD8^+$ T cells. Cetuximab-activated NK cells are known to induce DC maturation but whether GE mAb-activated NK cells can induce DC maturation is currently unknown. This study therefore aimed to assess the ability of GE-mAbs to induce DC maturation and other functions necessary for the stimulation of adaptive immunity. An *in vitro* co-culture model was established to assess interactions between tumour cells, NK cells, DC and TA-specific $CD8^+$ T cells. In keeping with a precedent set by previous studies of GE-mAbs, comparisons were made with wild type counterpart mAbs or clinically utilised unmodified mAbs. Principally, GE-mAbs were shown to induce NK-cell activation in terms of both activation marker up-regulation and cytokine production. Imgatuzumab-mediated NK-cell activation was achieved across various tumour-cell EGFR expression levels, indicating an ability to provoke responses to heterogeneous tumours and GE-mAb-activated NK cells were shown to induce DC maturation. Antigen uptake by DC and cross presentation of TA to TA-specific T cells were also examined in the presence of GE-mAbs. In a secondary manner, when compared at equivalent concentrations, GE-mAbs induced multiple measures of NK-cell function and DC maturation to a significantly greater extent than unmodified mAbs. These findings suggest that GE-mAbs may have greater potential to promote presentation of TA to $CD8^+$ T cells than unmodified mAbs.

Declaration of originality

The work presented in this thesis was performed by Aniekan Etuk; all else has been appropriately referenced. The copyright of this thesis rests with the author and no quotation or information derived from it may be published without proper acknowledgement.

Acknowledgements

At the end of every journey, it is always heartening to remember the people who guided you and made that journey possible. I would first like to express my deepest gratitude to Professor Farzin Farzaneh, who turned a ‘one year in the first instance’ employment contract into 3 years, and then gave me the opportunity of a lifetime with a further 3 years of funding for this PhD. Thank you for finding a way to keep me. I will never forget what you have done for me. The same goes to Dr Linda Barber, who has been a supervisor in every sense of the word. Thank you for putting up with me, thank you for your time, your patience and your guidance through my hardest years.

The road to this thesis was paved with a number of lessons, but not all of these were learned in the lab. Specifically, as part of a lasting friendship Giulia Giunti and Cinzia Benfatto regularly provided support and suggestions but also taught me that a risotto with chicken in it is categorically not Italian. Countless other extremely talented scientists - David Oppenheim, Monera Al Rukhayes (Bnt Saoud), surrogate lab mother Ruby Quartey-Papafio, Maeve McEnery, Kiki Ioannou, Sabine Domning and Laura McLaughlin provided enthusiasm and ideas, but most importantly taught me that tissue culture room 2.03 is the epicentre of lab gossip and the place to go to raise spirits when experiments have failed. This was closely followed by room 2.10, the home of my faithful friend the BD FACS Canto II and the legendary Thomas Seidl, who I bugged, relentlessly, and who never gave me a short answer. To every member of the Rayne Institute family, I have been honoured to call you my colleagues and to wear the King’s College London badge every single day. You have been the making of me.

To my dad watching from heaven and to my brothers - years ago you taught me to ride my little blue bike and were always there to catch me if I fell; so it follows to this day that you have never let me fall. To my husband Sausage, the kindest, most wonderful man on the planet - I am so very lucky that I can call you mine; I would have crumbled without your love. And to my mother - my best friend, my nurse, my counsellor, my cheerleader, my bank, my reality check, my rock and my inspiration - I dedicate this thesis to you.

Your Annie. x

“One only understands the things that one tames,” said the fox.

“What must I do, to tame you?" asked the little prince.

"You must be very patient," replied the fox.

The Little Prince - Antoine de Saint-Exupéry

Presentations at internal, national and international conferences

Etuk A, Farzaneh F, Barber LD - "Evaluation of the Ability of Glyco-engineered Therapeutic Antibodies to Promote Adaptive Immunity".

Poster Presentation: King's College London - Annual Division of Cancer Studies PhD Symposium

London, UK - June 2014

Awarded prize for "Best Poster"

Etuk A, Farzaneh F, Barber LD - "Glyco-engineering of Monoclonal Antibodies Enhances Potential to Promote Adaptive Immunity".

Oral Presentation: King's College London - Annual Division of Cancer Studies PhD Symposium

London, UK - June 2015

Shortlisted for prize of "Best Oral Presentation"

Etuk A, Klein C, Gerdes C, Passioukov A, Farzaneh F, Barber LD - "Glyco-engineering of Monoclonal Antibodies Enhances Potential to Promote Adaptive Immunity".

Oral Presentation: 4th European Congress of Immunology (ECI)

Vienna, Austria - September 2015

Etuk A, Georgiadis C, Preece R, Qasim W - "Universal antibody-mediated cell therapy (uACT)"

Oral Presentation: British Society for Gene and Cell Therapy - Autumn Conference

London, UK - November 2018

List of publications

Oppenheim DE, Spreafico R, **Etuk A**, Malone D, Amofah E, Pena-Murillo C*,* Murray T, McLaughlin L, Choi BS, Allan S, Belousov A, Passioukov A, Gerdes C, Umaña P, Farzaneh F and Ross P "Glyco-engineered anti-EGFR mAb elicits ADCC by NK cells from colorectal cancer patients irrespective of chemotherapy". *British Journal of Cancer* 2014, 110(5): 1221-1227

Georgiadis, C.; Preece, R.; Nickolay, L.; **Etuk, A**.; Petrova, A.; Ladon, D.; Danyi, A.; Humphryes-Kirilov, N.; Ajetunmobi, A.; Kim, D.; Kim, J.S. and Qasim, W. Long Terminal Repeat CRISPR-CAR-Coupled "Universal" T Cells Mediate Potent Anti-leukemic Effects. *Molecular. Therapy* 2018, *26*: 1215–1227

Admiraal R, Jol-van der Zijde CM, Furtado Silva JM, Knibbe CAJ, Lankester AC, Boelens JJ, Hale G, Adams S, **Etuk A**, Veys P, van Kesteren C and Bredius RGM "Population pharmacokinetics of alemtuzumab (Campath) in paediatric haematopoietic cell transplantation: towards individualised dosing to improve outcome". *Clinical Pharmacokinetics* 2018 (Submitted)

Contents

Table of figures

Table of tables

List of Abbreviations

°C	Degrees Celsius
aa	Amino acid
ACT	Adoptive cell therapy
ADC	Antibody drug conjugate
ADCC	Antibody-dependent cellular cytotoxicity
ALL	Acute lymphoblastic leukaemia
AML	Acute myeloid leukaemia
ANOVA	Analysis of variance
APC	Antigen presenting cell
arbU	Arbitrary units
ATCC	American Type Culture Collection
ATP	Adenosine tri-phosphate
BAFFR	Receptor for B cell-activating factor
BCR	B-cell receptor
BCR-ABL	Breakpoint cluster region-Abelson
BFA	Brefeldin A
BiTE	Bi-specific T-cell engager
CAA	Cancer-associated antigen
CAR	Chimeric antigen receptor
CD	Cluster of differentiation
cDC	Conventional dendritic cell
CDR	Complementarity determining region
CEA	Carcino-embryonic antigen
CFSE	Carboxyfluorescein succinimidyl ester
CLL	Chronic lymphoid leukaemia
CML	Chronic myeloid Leukaemia
^{CMV}T-cell	CMV-specific $CD8^+$ T-cell(s)
CRC	Colorectal cancer
CS	Cytokine storm
CTL	Cytotoxic T lymphocyte
DAMP	Damage associated molecular pattern

DC	Dendritic cell(s)
DCD1	Dendritic cell differentiation medium I
DCD2	Dendritic cell differentiation medium II
DCM1	Dendritic cell maturation medium I
DCM2	Dendritic cell maturation medium II
DMEM	Dulbecco's Modified Eagles Medium
DNA	Deoxyribonucleic acid
DNAM-I	DNAX accessory molecule-I
DRIPs	Incomplete translation products
EBV	Epstein-Barr virus
EGF	Epidermal growth factor
EGFR	Epidermal growth factor receptor
^{EGFR}T-cell	EGFR-specific $CD8^+$ T-cell(s)
^{EGFR}T-cell	EGFR peptide-loaded dendritic cell(s)
ELISpot	Enzyme-linked immunospot
ER	Endoplasmic reticulum
FAB	French-American-British
FAb	Fragment antigen binding
FACS	Fluorescence activated cell sorting
Fc	Fragment crystallisable
FDA	Food and drug administration
FO	Follicular
FuT	Fucosyltransferase
Fv	Fragment variable
G-CHOP	GA101GE plus cyclophosphamide, doxorubicin, vincristine and prednisone
GE	Glyco-engineered
GFP	Green fluorescence protein
GlcNAc	Bisecting N-acetylglucosamine
GMCSF	Granulocyte macrophage colony-stimulating factor
Gy	Grays
HC	Heavy chain
HER	Human epidermal growth factor receptor

HLA	Human leukocyte antigen
HNSCC	Head and neck squamous cell carcinoma
ICS	Intracellular cytokine staining
iDC	Immature dendritic cell(s)
IFN	Interferon
Ig	Immunoglobulin
IGF-1R	Insulin-like growth factor-1 receptor
IL	Interleukin
INO	Inotuzumab ozogamicin
ITAM	Immunoreceptor tyrosine activating motif
ITIM	Immunoreceptor tyrosine inhibitory motif
KCL	King's College London
KIR	Killer-cell immunoglobulin-like receptor
KO	Knockout
KRAS	Kirsten rat sarcoma
LAC	Leukocyte activation cocktail
LAMP-I	Lysosomal-associated membrane protein I
LC	Light chain
LPS	Lipopolysaccharide
LSC	Leukaemic stem cell
mAb	Monoclonal antibody
MABEL	Minimum anticipated biological effect level
MAC	Membrane attack complex
MACS	Magnetic activated cell sorting
MAGE	Melanoma antigen
MAMP	Microbe-associated molecular pattern
mDC	Mature dendritic cell(s)
^{MelanA}DC	MelanA peptide-loaded dendritic cell(s)
^{MelanA}T-cell	MelanA-specific $CD8^+$ T-cell(s)
MFI	Median fluorescence intensity
MHC	Major histocompatibility complex
MICA/B	Major histocompatibility complex class-I related chains A/B

moDC	Monocyte-derived dendritic cell(s)
MRD	Minimal residual disease
MUC-1	Mucin-1
MuLV	Murine leukaemia virus
MZ	Marginal zone
NCR	Natural cytotoxicity receptor
NFκB	Nuclear factor kappa B
NHL	Non-Hodgkin lymphoma
NHS-BT	National Health Service Blood and Transplant
NK	Natural killer
NKG2A	Natural killer group II, member A
NKG2D	Natural killer group II, member D
NSCLC	Non-small cell lung cancer
ORR	Overall response rate
OS	Overall survival
PAMP	Pathogen-associated molecular pattern
PBMC	Peripheral blood mononuclear cell
PBS	Phosphate buffered saline
PCR	Polymerase chain reaction
PD1	Programmed cell death protein I
pDC	Plasmacytoid DC
pDC	Plasmacytoid dendritic cell
PDL1	Programmed cell death ligand I
PEG	Polyethylene glycol
PFS	Progression free survival
PGE_2	Prostaglandin E2
PI	Propidium iodide
PK	Pharmacokinetic
PMA	Phorbol 12-myristate 13-acetate
PTM	Post translational modification
RAG	Recombination-activating gene
R-CHOP	Rituximab plus cyclophosphamide, doxorubicin, vincristine and prednisone

Ref.	Reference
RIC	Reduced intensity conditioning
RPM	Revolutions per minute
RPMI	Roswell Park Memorial Institute^{1640} Medium
RT	Room temperature
SNP	Single nucleotide polymorphism
TA	Tumour antigen
TAP	Transporter associated with antigen processing 1
TCR	T-cell receptor
TGFβ	Transforming growth factor beta
TLR	Toll-like receptor
TNFα	Tumour necrosis factor alpha
Treg	T-regulatory cell
Tu	PCI-15B cell line
VDJ	Variable, Diversity, Joining
WHO	World Health Organisation
WT	Wild type
WT1	Wilm's tumour I
β_2M	Beta-2 microglubulin

Chapter 1. Introduction

1.1. Tumour immunology

Cancer is the result of abnormal, uncontrolled proliferation and differentiation of cells. The multistep process by which normal cells are progressively transformed to malignancy is now known to require the sequential acquisition of mutations that arise as a consequence of damage to the genome. This damage can be inherited, or induced by carcinogens, radiation, chronic inflammation or viruses [1]. Proto-oncogenes and tumour-suppressor genes are normal genes that control crucial functions such as cell division and survival. As genetic alterations accumulate in these genes, cells acquire a succession of abilities, defined by Hanahan and Weinberg as the hallmarks of cancer. They include the ability to sustain proliferative signalling, evade growth suppression, resist cell death, enable replicative immortality, induce angiogenesis, activate invasion/metastasis and (most recently acknowledged) evade immune destruction [2].

The antigenic changes in malignant cells that are created by individual mutations during transformation can be subtle. In addition, the majority of antigens expressed by human cancer cells are non-mutated self-antigens also expressed in normal cells [1]. Crucially, the immune system must discriminate between self and non-self in order to prevent auto-immunity. Self-tolerance is acquired and maintained by a combination of central [3] and peripheral [4] education mechanisms. Transformed malignant cells that do not appear overtly foreign to the immune system are therefore ineffective at triggering immune responses. However, tumours are genetically unstable and continue to acquire mutations. Although increased virulence and immune escape can occur as a consequence of tumour evolution, this genome instability can also lead to aberrant expression of self-proteins and creation of new antigenic potentialities [1].

1.1.1. Cancer immunosurveillance

The mechanisms of tumour progression and tumour rejection are key concepts in the study of tumour immunology. A body of evidence exists indicating that components of the immune system are involved in controlling primary tumour development. This concept was first proposed by Paul Erlich in 1909. He suggested that “aberrante Keime” or mutant cells arise continuously and were it not for host defence mechanisms, cancer would occur at an enormous frequency (“in einer ungeheurer Frekvenz”) [5]. At the time, so little was known about the composition and function of

the immune system that it was simply not possible to assess the validity of this theory. More than 50 years later the idea of immune control of cancer resurfaced, fuelled by an enhanced understanding of the immune system. The suggestion of an anti-tumour immune response, formally re-introduced by Macfarlane Burnet [6] in 1957 and echoed shortly after by Lewis Thomas [7], was later referred to as 'cancer immunosurveillance' [8, 9]. Burnet and Thomas speculated that lymphocytes acted as sentinels, continuously recognising and eliminating nascent transformed cells to prevent manifestation of neoplasms. However, despite earlier demonstration of the existence of tumour antigens [10], subsequent studies by Stutman provided little support for the theory of cancer immunosurveillance. Of particular note were experiments showing that CBA/H strain nude mice did not form more carcinogen-induced tumours than their wild-type (WT) counterparts, nor did they show a shortened tumour latency period. Nude mice or immunocompetent mice (heterozygous for the nude mutation) were injected subcutaneously at birth with 0.1mg of the chemical carcinogen methylcholanthrene (MCA) and monitored for tumour incidence. After 120 days, 5 of 27 nude mice formed tumours at the injection site, with a mean time to tumour appearance of 90 days. Of the control immunocompetent mice, 7 of 39 formed tumours, with a mean time to appearance of 95 days [11]. The similarity between nude and immunocompetent mice was maintained in subsequent experiments employing different doses of carcinogen in mice of different ages [12] and even when the observation period was extended to 420 days [13]. At least one other group corroborated these results [14]. Stutman additionally showed that there were no significant differences in the incidence of spontaneous non-viral tumour formation between nude and wild-type mice [15]. These findings were supported by the work of Rygaard and Povlsen who studied nearly 11,000 mice over a period of 3-7 months and showed no differences in spontaneous tumour formation [16].

Based on these findings, the theory of cancer immunosurveillance resisted widespread acceptance, however, it is now clear that there were a number of caveats to these experiments. First, MCA requires biotransformation from its pro-form to its carcinogenic form via the aryl hydrocarbon hydroxylase enzyme pathway. The CBA/H mouse strain used in the Stutman studies expresses an isoform of the enzyme with high specific activity, thus these mice may have been more sensitive to MCA-induced tumour formation than other inbred mouse strains [17]. Second, although Rygaard and Povlsen corroborated Stutman's results using large numbers of nude mice, it is now considered that their monitoring periods of 3-7 months may have been too short to

observe spontaneous tumour formation when considering fully functional intrinsic tumour suppressor systems (such as p53) [18]. Third, the nude mouse was considered immunologically deficient due to congenital absence of the thymus. Importantly, it is now clear that nude mice are not completely immunocompromised. Although they possess fewer T cells than wild-type mice, they have detectable populations of functional T-cell receptor αβ-bearing (TCR- αβ) lymphocytes [19, 20], B cells and natural killer (NK) cells, which are not thymus dependent [21].

Two key findings in the mid 1990s renewed enthusiasm for the concept of cancer immunosurveillance. First, it was discovered that endogenously derived interferon gamma (IFNγ) protected C57BL/6 host mice against the growth of transplanted tumours and the formation of chemically induced tumours [22]. Second, it was observed that mice lacking perforin (C57BL/6 perforin$^{-/-}$) were more prone to spontaneous and chemically induced tumours than their wild type counterparts [23]. The secretion of perforin and IFNγ are characteristics of natural killer (NK) cells and cytotoxic T-lymphocytes (CTL) [24], respectively important in mediating lymphocyte-dependent killing of tumour cells and activating auxiliary immune cells (discussed in section 1.4 onwards). Notably, perforin mutations have been documented in lymphoma patients [25].

Evidence both supporting and opposing the principals of cancer immunosurveillance began to emerge. The logical prediction from these renaissance findings was that immunodeficient or immunosuppressed humans should show greater cancer incidence. Indeed, early studies of individuals with primary immunodeficiencies [26] and immunosuppressed transplant patients [27] showed significantly higher relative risk of developing cancer. An approximate 4-fold increase in the incidence of *de novo* malignant melanoma has been reported after organ transplantation [28]. When 608 University of Pittsburgh cardiac transplant patients were assessed for the occurrence of neoplasia over a 13-year period, the prevalence of lung tumours was 25-fold higher than in the general population [29]. Additionally, the follow up of nearly 6000 Nordic renal transplant patients showed higher standardised cancer incidence ratios for malignant melanomas and ureter, kidney, bladder, colon, lung and endocrine tumours, compared to the general population [30].

Thus, individuals with immune deficits have a higher probability of developing cancers with no known viral aetiology, however the majority of tumours in the immune-compromised are virus-associated, and are linked to infection with Epstein-Barr virus, human herpes virus and human

papilloma virus [27, 31]. Associations between different bacteria and higher incidence of various tumours have also been described, including Helicobacter pylori [32] and chlamydia [33]; which fostered speculation that cancer immunosurveillance targeted transforming agents but not tumours *per se*. It is now well established that the induction of inflammation by bacterial and viral infections increases cancer risk. This may, in part, be due to the anti-inflammatory reactions of antigen-presenting cells, which release anti-inflammatory cytokines such as IL-10 and transforming growth factor-β (TGF-β) that inhibit effector-cell activation [34]. Regulatory T cells (Tregs) are also presumed to act mostly in a pro-tumorigenic fashion through suppression of anti-tumour immune responses [35]. Also, despite the protective role of IFNγ demonstrated in mouse experiments, treatment with IFNγ had no benefit for patients with different tumour types [36, 37, 38].

1.1.2. Cancer immunoediting

The concept of cancer immunosurveillance evolved into the theory of 'cancer immunoediting' after Schreiber and colleagues summarised that the immune system can exert both tumour-inhibitory and tumour-promoting effects [39]. Cancer immunoediting, illustrated in Figure 1.1, occurs in three sequential phases: elimination, equilibrium, and escape. Elimination, a refined view of cancer immunosurveillance, considers that innate and adaptive immunity work together to detect and destroy transformed cells long before they become clinically apparent. However, tumour cell variants that are not completely eliminated reach an equilibrium phase. In equilibrium, adaptive immunity constrains growth of clinically undetectable tumour cells but edits their immunogenicity; iteratively selecting for variants with poor immunogenicity and resistance to immune cell elimination. If the functional dormancy of equilibrium tumour cells is broken, the cells progress to the escape phase, during which edited tumours with reduced immunogenicity begin to grow progressively in an immunologically unrestrained manner. An immunosuppressive microenvironment is established, and the tumour eventually becomes clinically significant [40, 41]. A key theme in the cancer immunoediting process is that tumour cells express antigens that distinguish them from their non-transformed counterparts. Tumour antigens (TA) expressed by tumours but poorly expressed or absent in healthy somatic tissue thus permit tumour recognition and eventual destruction by immune cells.

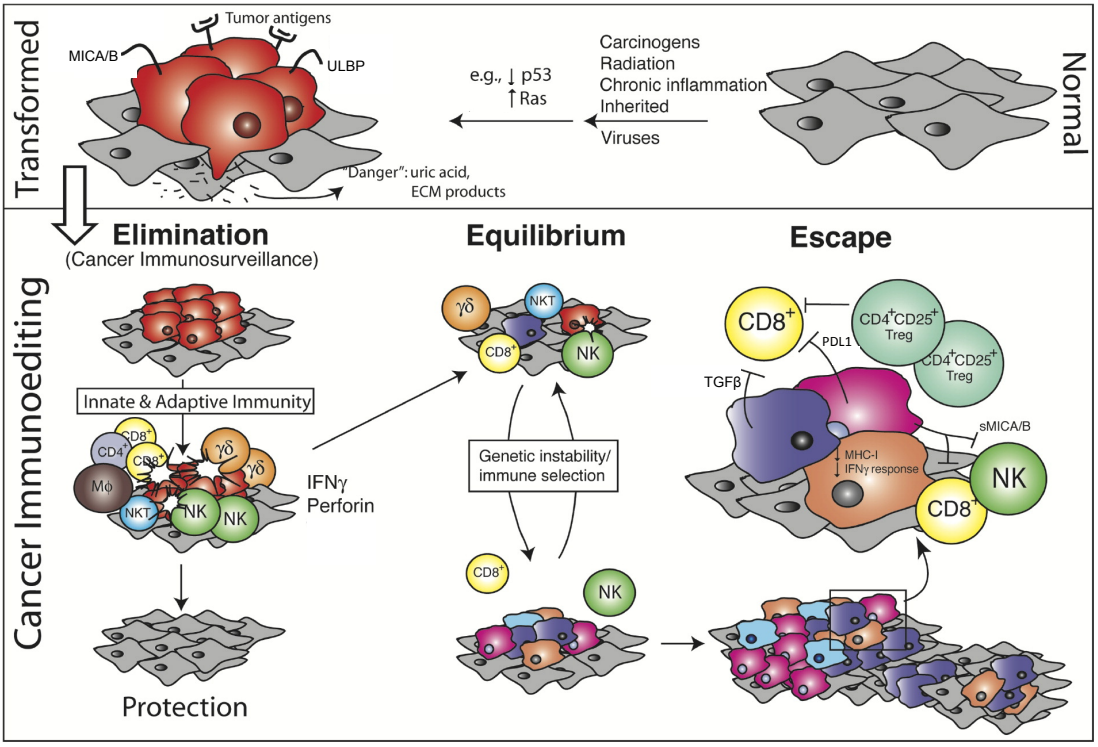

Figure 1.1. The theory of cancer immunoediting
Adapted from Dunn *et al* (2004) [42]

1.2. Classification of tumour antigens

Some TA can be derived from exogenous foreign sources, such as the proteins involved in viral structure. The oncogenic human papillomaviruses (HPV) have been well-studied because individuals are commonly exposed to these viruses and additionally they have been implicated as co-factors in the pathogenesis of many cancers, including cervical cancer [43] and some forms of head and neck squamous cell carcinoma (HNSCC) [44]. In 1991, van der Bruggen *et al* defined the first endogenous human TA in melanoma patients, melanoma antigen I (MAGE-I). MAGE-I was found to be exclusively expressed in melanoma cells and CTL raised from their melanoma patient were shown to specifically lyse autologous tumour, providing strong evidence of tumour recognition by the immune system [45]. Ground breaking work by Ron Levy and colleagues was to follow, demonstrating the induction of immune responses in patients with B-cell lymphoma, against the surface-immunoglobulin idiotype expressed by their tumours. The tumours of patients with measurable disease regressed completely and these studies opened the field of monoclonal antibody therapy for B-cell malignancies [46]. Since then, hundreds of TA have been discovered

and characterised (documented by Vigneron *et al* [47]). Most TA can be distinctly classified based on their aetiology as follows:

1.2.1. Cancer testes antigens and embryonic antigens

Cancer testes (CT) antigens are present in germ-line cells and tumours, but absent from other somatic tissues. Of the CT antigens, the aforementioned MAGE family are the best-defined [48]. Embryonic antigens are expressed during early development but not post-natally; of which carcinoembryonic antigen (CEA) is best defined [49, 50].

1.2.2. Post-translational modification

Some TA are subject to post-translational modification (PTM) that can cause conformational changes or form new antigen epitopes; of which mucin-I (MUC-1) is a well-studied example. MUC-I is preferentially expressed on epithelial tumours but is hypoglycosylated in breast tumours, exposing regions of the MUC-I protein backbone that can be differentially recognised by antibodies [51].

1.2.3. Mutated antigens (point mutations and chromosome abnormalities)

These can be borne of point mutations, such as the range of mutations documented in the notorious p53 tumour suppressor [52]; or fusion proteins that result in tumour-specific neoantigens, such as the breakpoint cluster region-abelson (BCR-ABL) tyrosine kinase protein created by reciprocal chromosomal translocation, seen in patients with chronic myeloid leukaemia (CML) [53, 54].

1.2.4. Overexpressed or aberrantly expressed antigens

These antigens are expressed at low levels on healthy tissue but significantly overexpressed on tumour cells; which may expose cryptic or subdominant epitopes [55]. One putative example and a major focus within this study is the epidermal growth factor receptor (EGFR) discussed further in section 1.11.

1.3. Tumour elimination: the interaction between innate and adaptive effector cells

Virtually every known cell type of the immune system is represented in the tumour microenvironment [56]. The immune response to tumour cells can typically be divided into innate and adaptive components. Upon encounter with malignant cells, innate immune responses occur rapidly, within hours; but are non-specific [57]. These early innate anti-tumour responses are mediated by NK cells, invariant NK T cells (iNKT cells) [58] and γδ T cells [59]. Several studies have demonstrated tumour infiltration of the aforementioned effector cell types, endowed with the capacity to directly kill tumour cells *in vitro* [60, 61, 62, 63]. However, the functional significance and complex interactions between tumour infiltrating effector cells are still being fully elucidated.

Although adaptive responses may, in contrast take days to develop, this route of resistance efficiently targets individual antigens [57]. With the help of NK cells and dendritic cells (DC) the adaptive response to tumours is driven by T cells and B cells and relies on somatic gene rearrangements to provide highly specific target recognition and long-term "memory" defence against subsequent encounters with the same antigen [60, 61, 64, 65]. Thus the key to tumour elimination is the interplay between immune system effector cells, rather than the activity of one element alone. The immune cells, interactions and tumour types that influence this study are discussed further.

1.4. Natural killer cells

Natural killer (NK) cells are large granular lymphocytes that were serendipitously identified in 1973 during the assessment of tumour directed cytotoxicity. The observation that NK cells were able to kill aberrant cells in the absence of antigen specific recognition later redefined them as sentinels of innate immunity, endowed with both cytotoxic and cytokine-producing functions [66, 67].

Consistent with their role in immune surveillance, NK cells are widespread throughout lymphoid and non-lymphoid tissues, but represent a minor fraction of total lymphocytes from 2% to 18% in the peripheral blood of healthy human adults [68].

1.4.1. NK-cell subsets

Distinct NK-cell subsets have been defined in mice and humans based on phenotypic, functional and anatomical features. Human NK cells are classically identified by expression of the surface

marker CD56, absence of the lineage markers CD3 and CD19 and lack of T and B cell antigen receptors. Two major NK subsets exist in humans, distinguished primarily by their levels of CD56 expression: $CD56^{dim}$ NK cells are mature, make up approximately 90% of the NK cells in peripheral blood, and predominantly mediate cytotoxic responses. In contrast, $CD56^{bright}$ cells are a more immature form, constituting approximately 10% of total NK cells, and considered primarily as cytokine producers that play a limited role in cytolytic responses [68].

1.4.2. NK-cell receptors

NK cells express a variety of activating and inhibitory receptors, respectively characterised by the presence of an immunoreceptor tyrosine activating motif (ITAM) or an immunoreceptor tyrosine inhibitory motif (ITIM) in their cytosolic domains. These receptors finely regulate NK cell activation; a process that relies on integration and amplification of multiple signalling pathways [69]. NK cell receptors and their functional influence are summarised in Figure 1.2. Notable examples of NK-cell activating receptors discussed in this study include FcγRIIIa (CD16), KLRK1 (NKG2D) a lectin-like receptor and the activating co-receptor molecules DNAM-I and NKp30.

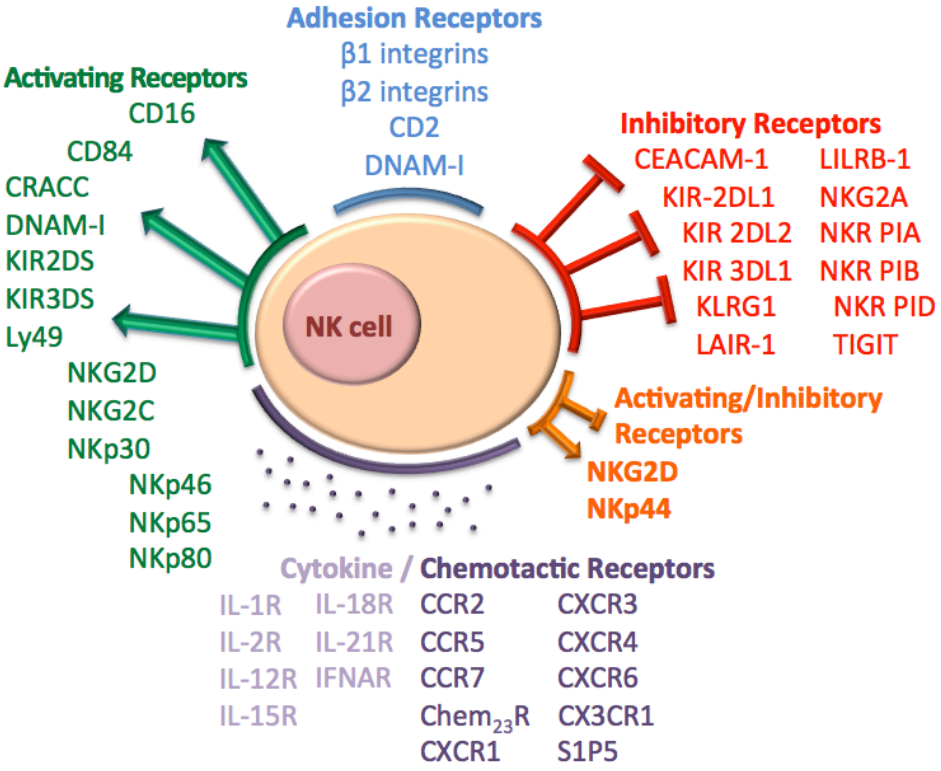

Figure 1.2. Schematic representation of NK-cell receptors and their functional influence

1.4.3. NK-cell killing: antibody dependent cellular cytotoxicity

The NK-cell killing mechanism that is the primary focus of this report is known as antibody-dependent cellular cytotoxicity (ADCC). B cells can produce antibodies, proteins such as immunoglobulin G (IgG) that can bind to the surface of tumour cells and to the CD16 receptor on NK cells; forming an immunological synapse (IS) that activates NK cells. Perforin proteins and serine proteases known as granzymes are sequestered in small preformed granules in the cytoplasm of NK cells. Upon NK-cell activation, these granules are released through specialised secretory vesicles, in close proximity to the tumour target cell. The perforin forms transient porous aqueous channels in the tumour cell membrane, through which granzymes diffuse into the cytosol; triggering caspase activation pathways and leading to programmed cell death or apoptosis [24]. Importantly, apoptotic tumour particulate provides a source of TA for DC [70]. NK cells activated by ADCC upregulate lymphocyte activation markers such as CD69 and are able to secrete large amounts of immunomodulatory soluble factors, such as the cytokines IFNγ and TNFα [71, 72, 73, 74]. After detaching, NK cells can rapidly attack and "serial kill" up to 10 cells within a 6-hour period [75]. Notably, a common single nucleotide polymorphism (SNP) has been defined in exon 4 of the CD16 Ig-like domain (559G>T: rs396991). This SNP results in a valine/phenylalanine substitution at position 158 (V158F) that affects the affinity of CD16 for IgG. It has been described that the 158V variant increases CD16 affinity for IgG compared to the 158F variant [76].

1.4.4. NK-cell killing: "missing self"

The alternative mechanism by which NK cells kill involves lack of engagement of NK-cell inhibitory receptors. The ability shown by NK cells to spare normal tissues but not transformed cells was affectionately termed the "missing self hypothesis" and is mediated by natural cytotoxicity receptors (NCR) such as NKG2A and the majority of killer-cell Ig-like receptors (KIRs) bearing an immunoreceptor tyrosine inhibitory motif (ITIM) in their long cytoplasmic tails[a]. Major histocompatibility (MHC)-absence activates the NK cells and culminates in the same cytotoxic granule release as described for ADCC. This natural cytotoxic capacity is augmented in the presence of interleukin (IL)-2, IL-12 and IL-18, the latter two synergistically [71].

[a] Notable exceptions being KIR2DS and KIR3DS, whose short tails have ITAMs in their transmembrane portions.

1.5. Dendritic cells

The term dendritic cell (DC) was first coined by Ralph Steinman to describe a small subset of murine splenic cells exhibiting a peculiar tree-like morphology (derived from the Greek word 'dendron' meaning tree) [77]. DC have now been characterised with increasing precision. They can be found in virtually all tissues, although have a tropism for environments, such as lymphoid organs, the skin and both external and internal mucosae, where antigens are concentrated and most likely to be encountered [78]. The immunostimulatory potential of DC is not limited to the elicitation of cellular immune responses, but also impacts humoral and innate immunity [79].

1.5.1. Immature DC

DC differentiate from common myeloid bone marrow progenitors. At an immature stage of development, they express low levels of co-stimulatory molecules such as CD80 and CD86 (B7.1 and B7.2) and CD40, but are very efficient at engulfing extracellular material. Importantly, in the absence of appropriate maturation stimuli, immature DC (iDC) present antigens to T cells in the context of inhibitory signals, hence contributing to peripheral tolerance [80], which relies on both deletion of antigen specific T-cell clones and expansion of $CD4^+CD25^+FOXP3^+$ regulatory T cells (Tregs) [81, 82, 83].

1.5.2. Mature DC

Several stimuli can induce the maturation of iDC, including damage-associated molecular patterns (DAMPs), microbe/pathogen-associated molecular patterns (MAMPs/PAMPs) and a plethora of cytokines and chemokines including IFNγ, tumour necrosis factor alpha (TNFα), IL-6, IL-1beta (IL-1β), prostaglandin E2 (PGE_2), polyinosinic-polycytidylic acid (poly I:C) and lipopolysaccharide (LPS) [84]. Mature DC (mDC) upregulate expression of major histocompatibility complex class I (MHC-I) and class II (MHC-II) molecules at their cell surface and secrete high levels of chemokines and cytokines (notably IL-12) [85, 86]. In contrast to their immature counterparts, mDC exhibit a limited ability to engulf antigens, but attain the ability to migrate to lymph nodes due to upregulation of lymph node homing chemokine receptors such as CCR7; as well as efficiently present and cross present antigen [87].

Many groups have studied the minimal requirements for induction of T-cell effector function in the context of antigen presentation. Notably, in 1999, Mescher and colleagues did so using a simple system of beads conjugated with MHC and antigen at different densities to provide signal 1; and a

panel of membrane co-stimulatory molecules including CD80 and CD86 to provide signal 2 [88]. In line with the co-stimulatory concept proposed by Lafferty [89], they were able to show that signals 1 and 2 were sufficient for naïve $CD8^+$ T cell proliferation and cytokine production. However, for cytotoxic effector function, a third signal, IL-12, was required [88, 90]. DC maturation can be primarily defined by secretion of IL-12 and upregulation of the CD80/CD86, co-stimulatory molecules that provide the essential signals required for T-cell activation. This affords mDC highly efficient triggering of adaptive immune responses, to an extent exceeding all other professional antigen-presenting cells (APCs) including B cells and macrophages. Crucially, because of their IL-12 production, DC are the only APC capable of stimulating $CD8^+$ naïve T cells [91].

1.5.3. DC subsets

There are several subsets of DC[b] that are morphologically, phenotypically and functionally distinct in addition to residing in the various anatomical locations. DC in human peripheral blood comprise three types: conventional or classical DC (cDC): $CD1c^+$ ($BDCA\text{-}1^+$) and $CD141^+$ ($BDCA\text{-}3^+$) myeloid DC; $CD303^+$ plasmacytoid DC (pDC) and 'slanDC' [92, 93]. To illustrate DC diversity by example: human $CD14^+$ dermal DC produce high levels of IL-12, thus promoting the differentiation of naïve B cells into antibody-producing plasma cells. Circulating $CD141^+$ human DC are highly efficient at cross-presentation, and are required for optimal responses to foreign antigens and TA**.** As the most abundant subset in peripheral blood, pDC, defined by their resemblance to plasma cells, constitute a morphologically peculiar subset of DC that produce high levels of type I IFN upon viral infection, yielding robust T-helper I (Th1) immune responses. This ability is shared by cDC, but pDC are endowed with a superior ability to detect DAMPs and MAMPs because they express a large panel of pattern recognition receptors, including several members of the toll-like receptor (TLR) family [94]. DC subsets, receptors and anatomical locations are summarised in Figure 1.3.

[b] DC subsets are abbreviated according to international convention on nomenclature [61].

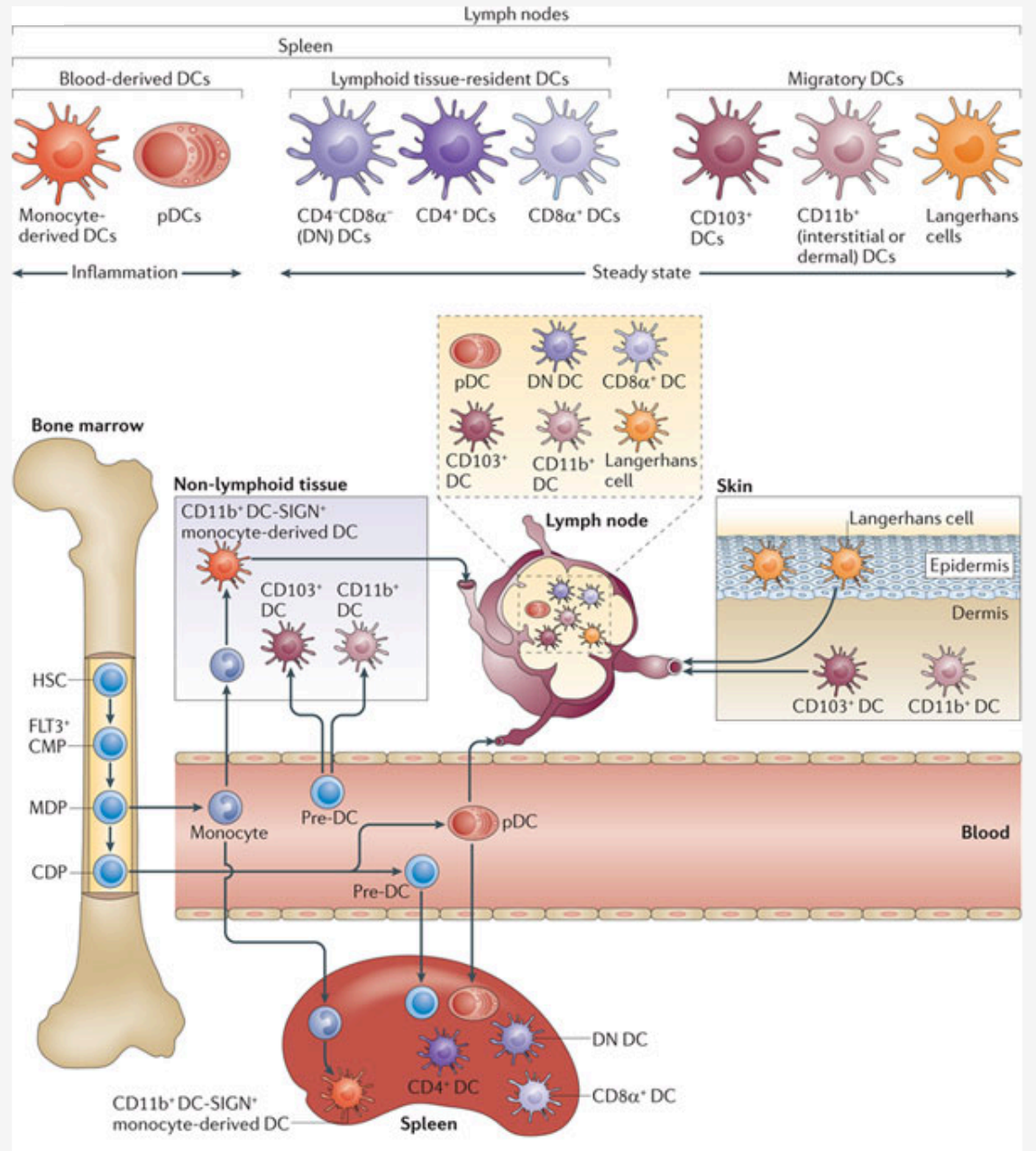

Figure 1.3. DC subsets, receptors and anatomical Locations
Adapted from Belz and Nutt (2012) [95]

1.6. NK:DC crosstalk

NK cells and DC occupy a functional niche at the interface between innate and adaptive immunity, able to influence both non-specific innate responses and antigen-specific adaptive responses as part of a complex crosstalk between NK cells, DC and T cells.

1.6.1. NK-cell induced activation and maturation of DC

NK cells enhance the immunostimulatory function of DC [71, 96, 97]. Activated NK cells promote the differentiation and maturation of iDC as indicated by the upregulation of costimulatory molecules such as CD80, CD83 and CD86 on the surface of DC. This NK-cell-mediated DC maturation effect is dependent on direct cell-to-cell contact between NK cells and DC, involving engagement of NK-cell membrane associated activating receptors NKp30 (also known as NCR3) and DNAM-I (also known as CD226); and on the release of IFNγ and TNFα [71, 72, 73, 74, 98, 99]. Activated NK cells also markedly increase IL-12 secretion by DC as well as TNFα release by DC to perpetuate DC maturation in an autocrine manner [98]. In addition, activated NK cells are able to improve DC ability to stimulate both T-cell proliferation and IFNγ production by $CD8^+$ T cells as well as differentiation of naïve $CD4^+$ T cells into IFNγ producing Th1 cells [71, 73].

1.6.2. NK-cell regulation of DC

NK cells also play a crucial role in DC homeostasis. In peripheral tissues, iDC continuously sample the environment for antigens, whilst expressing low levels of MHC and co-stimulatory molecules. In this steady state, iDC are highly susceptible to lysis by autologous activated NK cells, but become resistant upon maturation. It is suggested that NK-cell-mediated removal of iDC prevents induction of regulatory T cells at sites of inflammation [72].

1.6.3. DC activation of NK cells

DC also play a crucial reciprocal role in the activation of NK cells. Mature DC can efficiently promote NK-cell proliferation and enhance the cytotoxic capacity of NK cells [72], in addition to modulating NK-cell cytokine production. DC mediated IFNγ production from NK cells is facilitated by the release of IL-12 and IL-15 by DC and is accompanied by increased expression of the activation marker CD69 on the surface of NK cells [71, 73, 98]. This again occurs in a contact dependent manner, the importance of which was highlighted by Fernandez *et al* (1999) in the very

first study of NK:DC crosstalk [100]. The bi-directional crosstalk between NK cells and DC demands further scrutiny because of its important role in shaping the immune response. The reciprocal activating interaction between NK cells and DC is illustrated in Figure 1.4.

1.7. T cells

T cells are effector lymphocytes that play a central role in adaptive immunity. T cells are borne of haematopoietic precursors that vacate the bone marrow and migrate to the thymus; from which the 'T' in their name is derived. As early T-cell precursors, these thymic immigrants do not express the CD3/T-cell receptor (TCR) complex and since they also lack CD4 or CD8 surface molecules are termed "double negative" (DN). Within the thymus T cells first undergo TCR-β gene segment rearrangement to express a pre-TCR. The process of variable, diversity and joining (VDJ) recombination is initiated by the recombination-activating gene (RAG) enzymes RAG-1 and RAG-2. This is followed by rearrangement of the TCR-α gene segment to eventually generate and express a diverse repertoire of αβTCRs [101].

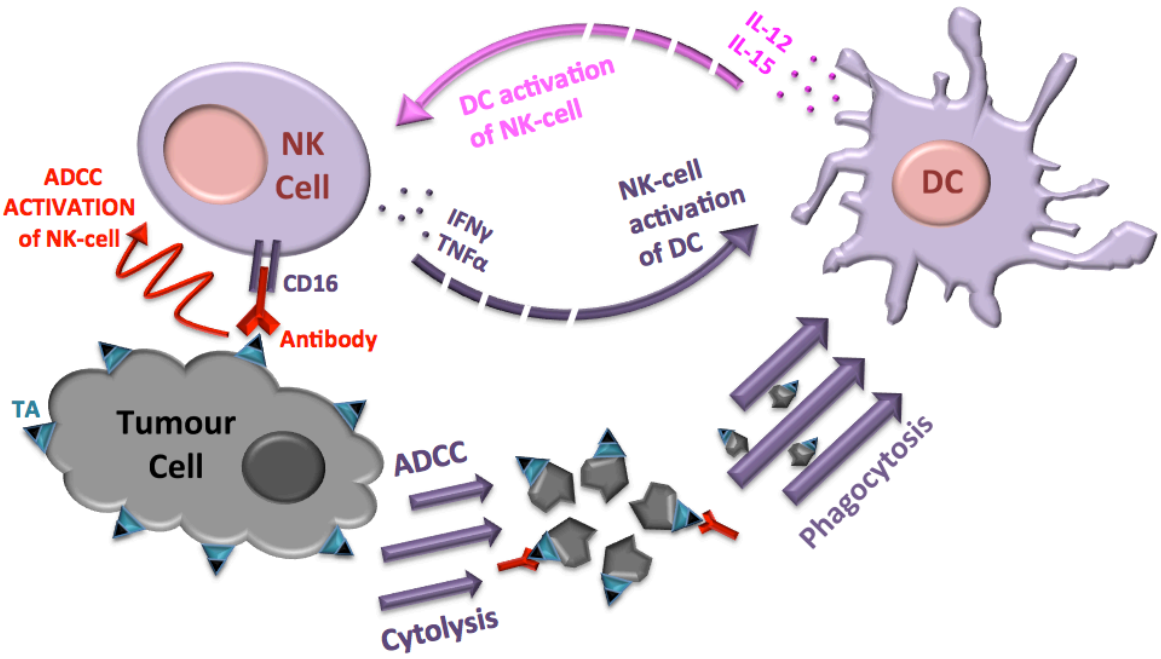

Figure 1.4. Schematic representation of the reciprocal activation between NK cells and DC

1.7.1. Thymic selection

The pre-TCR of a developing DN T-cell interacts with cortical epithelial cells. DN T cells which fail to express an appropriate pre-TCR die in the thymic cortex due to the lack of signalling. Those with successful interactions with self-MHC become CD4 and CD8 double positive (DP) and constitute the largest subpopulation in the thymus. During development of DP T cells, pre-TCR signalling leads to rearrangement of the TCR-α chain gene segments and consequently the expression of a mature αβTCR. Approximately 90% of the $CD4^+CD8^+TCR\alpha\beta^+$ T cells do not recognise self-MHC and die by neglect within the cortex. The surviving T cells migrate from the thymic cortex into the medulla of the thymus, where they interact with DC. $CD4^+CD8^+TCR\alpha\beta^+$ T cells that respond with appropriate low affinity binding to self-antigen presented on MHC-II molecules differentiate into $CD4^+$ single positive T cells, while those that bind with low affinity to self-antigen presented by MHC-I differentiate into $CD8^+$ single positive; a process known as positive selection. Apoptosis is triggered in T cells that bind with high affinity to self-peptide/MHC complexes; a process known as negative selection. T cells with appropriate TCRs exit the thymus to circulate in the periphery as naïve T cells, yet to encounter their cognate antigen. This stringent selection in the thymus (a state of central tolerance), results in deletion of over 95% of DP T cells prior to peripheral release, minimising the potential for auto-reactivity [101, 102].

1.7.2. Antigen presentation to T cells

APC are critical regulators of immunity that continuously survey their microenvironment, uptake antigenic material, then process proteins and present the resulting peptide fragments to antigen-specific T cells in the context of MHC molecules. The capture of exogenous matter occurs via receptor-mediated endocytosis, pinocytosis and phagocytosis mechanisms. The mechanism of uptake determines the intracellular compartment to which antigen is delivered and may determine the type of T-cell epitopes generated [103].

An area of focus in this report will be DC-mediated phagocytosis, defined as the engulfment of large particulate antigens. Many studies have demonstrated that DC can ingest apoptotic tumour particulate [104, 105, 106], such as that generated by NK-cell mediated ADCC. Actin remodelling allows for the formation of a cup like structure around the particle that eventually closes to form a phagosome. While trafficking through the endosome the phagosome becomes increasingly acidic due to delivery of H^+ into its lumen. The phagosome becomes fused to enzyme-rich lysosomes and matures into a phagolysosome, leading to particle degradation. Although still poorly

understood, it is thought that some pathogens, including tumour cells, have evolved mechanisms to alter or impair the schedule of lysosomal degradation. Consequently, the ultimate fate of an ingested particle, i.e. its presentation, can differ, even within the same cell type [103].

1.7.3. MHC antigen presentation pathways

The process of antigen presentation requires a series of protein and organelle interactions that occur via two distinct pathways: MHC-I and MHC-II. MHC-II molecules are constitutively expressed on DC, macrophages and B cells, who, as a result, are often referred to as 'professional' antigen presenting cells (APC). These cells are specialised to present antigens internalized from the extracellular space to $CD4^+$ T cells [107]. Conversely, intracellular/endogenous antigens encountered in the cytoplasm, nucleus and mitochondria are mainly channelled to the MHC-I processing pathway. Peptides derived by cytosolic proteolysis of such antigens are translocated into the endoplasmic reticulum (ER), where they encounter and may assemble with newly synthesized MHC-I molecules (expressed by virtually all cell types). The MHC-I pathway is responsible for the recruitment and activation of $CD8^+$ T cells [103, 107]. Cross-presentation by MHC-I is a distinct process in which antigens from phagocytosed particles and extracellular soluble proteins are internalized, bound by MHC-I and presented to $CD8^+$ T cells. The cross presentation of exogenous antigen, such as that derived from apoptotic tumour particulate, is essential for effective anti-tumour immunity and is a process restricted to specific DC subsets *in vivo* [103, 107] (discussed in section 1.7.7).

1.7.4. MHC restriction

Human MHC molecules are known as human leukocyte antigens (HLA) and are encoded by highly polymorphic genes, giving rise to the many different HLA proteins that distinguish individuals. T cells interact with both the HLA molecule and the bound peptide and are specific for peptides presented by autologous HLA molecules (self HLA-restriction) [108].

1.7.5. MHC-II

MHC-II molecules comprise two polymorphic integral membrane chains, α and β, both encoded within the MHC. Association of new synthesised α and β chains with invariant chain (also called Ii or CD74) in the ER facilitates MHC-II assembly and ER exit, and blocks the peptide binding site to

prevent binding of endogenous peptides. Ii also directs transport of MHC-II complexes to the endosomal pathway [107, 109].

Ii is degraded by resident proteases within late endosomal MHC-II-containing compartments (MIIC), leaving only a fragment of Ii known as CLIP occupying the MHC-II peptide-binding site. Simultaneously, internalized exogenous proteins are also degraded by endosomal resident proteases, generating peptide MHC-II ligands. The structure of the MHC-II peptide-binding site accommodates peptide fragments typically 12-25 amino acids (aa) in length. Peptide exchange via CLIP dissociation and subsequent peptide binding to the MHC-II peptide binding site is facilitated by the MIIC-resident protein HLA-DM. Stable MHC-II:peptide complexes are then transported to the cell surface where they are presented to stimulate $CD4^+$ T cells that express an appropriate TCR specific for the MHC-II:peptide complex [107, 109].

Peptide loading onto newly synthesised MHC-II molecules can occur in multiple compartments of the endosomal pathway although this is primarily in an HLA-DM dependant manner and in late endosomal MIICs. By contrast, internalized MHC-II αβ dimers from the cell surface can be 'reloaded' with peptides within the early endosomal system [107, 109].

1.7.6. MHC-I

MHC-I molecules assemble in the ER and comprise two chains: the polymorphic α or heavy chain and the non-polymorphic β2 microglobulin (β2m) light chain. ER export can only happen when assembly is complete, reliant on the binding of a peptide in the MHC-I peptide binding groove. These MHC-I binding peptides are usually 8-9 aa long, precursors of which are generated in the cytosol. The peptides are derived from ubiquitinated proteins undergoing degradation as part of cell protein recycling, incomplete translation products (DRIPs) that are partially degraded by the proteasome, and other misfolded proteins or retrotranslocated proteins from the ER cleaved by the proteasome or other cytosolic proteases [107, 110].

Dedicated adenosine tri-phosphate (ATP)-dependent transporter associated with antigen processing (TAP)-1/2 proteins translocate these peptides into the lumen of the ER. They are then trimmed at their N-termini by ER proteases called ERAAPs and transferred from TAP onto folding MHC-I, facilitated by a 'loading complex'. Once assembled, the MHC-I/β2m/peptide complexes are exported from the ER via the classical secretory pathway and are expressed at the cell surface. The loading of endogenously produced peptides onto MHC-I molecules plays a critical

role in the killing of transformed or virally infected cells because of the interaction between MHC-I and the TCR of $CD8^+$ T cells [107, 110].

1.7.7. Cross presentation by MHC-I

Although some viruses can infect DC directly and generate MHC-I peptide ligands using this classical pathway, in many cases DC are not infected and therefore the antigens cannot be expressed by the DC themselves. However, DC can phagocytose antigens derived from other cells and cross-present peptides derived from these antigens on their own MHC-I. This pathway is particularly important in the context of anti-tumour immunity. Tumour cells are poor APC because they lack co-stimulatory molecules [111, 112] and can secrete immunosuppressive factors (discussed further in section 1.9.2) [113]. They therefore require lysis, for example via NK-cell-mediated ADCC, and uptake of tumour-cell particulate by professional APC for presentation of TA to T cells. This pathway is illustrated in Figure 1.5. Two main intracellular models for cross-presentation have been proposed, and are referred to as the 'cytosolic' and 'vacuolar' pathways [107, 110].

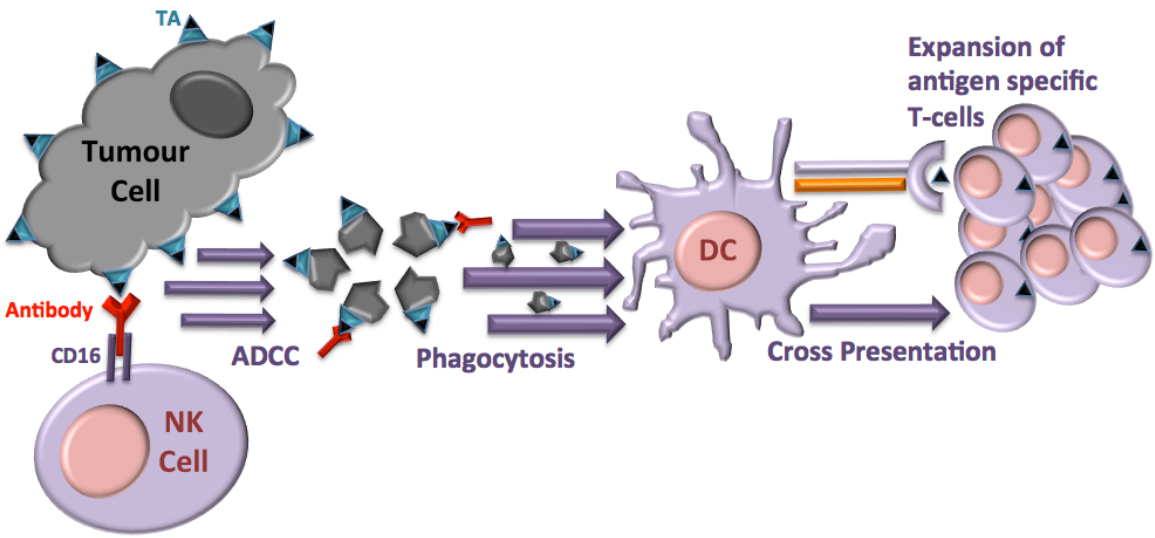

Figure 1.5. Schematic representation of cross presentation in the context of ADCC and anti-tumour immunity

1.7.7.1. Cross presentation: the cytosolic pathway

The cytosolic pathway provides a means by which DC can present peptides from internalized antigens that were present endogenously in other cell types, and thus stimulate relevant $CD8^+$ T cells. After partial degradation in endosomes, exogenous-derived proteins are exported to the cytosol and processed by the proteasome in the same way as endogenous MHC-I processing. These exogenous proteasome-processed peptides are then loaded onto MHC-I molecules in the ER following TAP-dependent uptake [107, 110].

1.7.7.2. Cross presentation: the vacuolar pathway

In the vacuolar pathway, the peptides that bind MHC-I are derived from internalized exogenous proteins that were processed directly in endosomes and phagosomes. MHC-I molecules access endocytic compartments via recycling from the cell surface, and bind peptides independently of proteasomal degradation, TAP transporters and the MHC-I loading complex [107, 110].

1.7.8. T-cell activation

Like NK cells, T-cell activation is a multistep process. The first signal is received when the TCR binds its cognate peptide:MHC complex. T cells express several co-stimulatory receptors through which they receive their subsequent activation signals including CD28 and CTLA-4. Notably, CD28 is the only co-stimulatory receptor constitutively expressed by naïve T cells. These receptors engage the ligands CD80 and CD86 (collectively known as B7), which are expressed on APC. The second signal licenses mature T cells to respond to antigen fully (proliferation, cytokine secretion and cytotoxicity), while in naïve T cells the second signal allows proliferation and cytokine secretion, with a third signal, provided by IL-12 or IL-1β, enabling cytotoxicity [88, 90]. Without secondary and subsequent signals, T cells become anergic and more difficult to activate in future. Self-peptides are not usually presented with appropriate co-stimulation, thus this multi-step activation process prevents inappropriate responses to self.

Upon appropriate activation, T cells will upregulate activation markers such as CD69 and CD137. In addition, expression of the inhibitory receptor CTLA-4 is also upregulated on activated T cells. CTLA-4 has a higher affinity for the B7 ligands it shares with CD28 and this serves as an immune checkpoint mechanism to down-modulate T-cell activation [114] (discussed further in section 1.10.1.2).

1.8. B cells

B cells are a class of lymphocyte involved in the humoral arm of the adaptive immune response. B cells function as professional APC (as discussed in section 1.7.3) with cytokine secretion capabilities, but their primary role is the expression/secretion of immunoglobulin (Ig) proteins (antibodies).

1.8.1. B-cell development

B cells originate from common lymphoid progenitors in the bone marrow, and their development into mature functional cells occurs in several stages [115]. RAG-1 and RAG-2 initiate the recombination of the Ig heavy-chain (HC) VDJ gene segments in pro-B cells. Pro-B cells represent the earliest committed stage of B-cell development, which occurs in an IL-7 dependent manner [116]. This is followed by recombination of the light chain (LC) VJ genes in pre-B cells. Binding of μHC proteins with the λ5 and VpreB surrogate LC[c] proteins leads to surface expression of the pre-B cell receptor (pre-BCR) on large pre-B cells. The pre-BCR initiates proliferation, maturation and survival signals *via* Igα and Igβ signaling subunits. Down-regulation of pre-BCR expression permits entry into the resting small pre B-cell stage. Resting small pre-B cells cease cell cycle progression and begin the recombination process again, leading to rearrangement of the LC proteins. LC proteins associate with μHC proteins to form the mature B-cell receptor (BCR). This is expressed on immature B cells as stable IgM and alternative splicing permits co-production of IgD. Acquisition of a functional BCR comprising a HC and LC combination distinguishes immature B cells from their pre-B cell precursors [117].

1.8.2. B-cell selection and transition

Immature B cells first undergo selection in the bone marrow (central tolerance) and subsequently exit into the periphery where they sustain additional selection (peripheral tolerance) prior to becoming functional B cells capable of responding to antigen. If the BCR can bind strongly to self-antigen, then the B-cell will endure one of three fates: receptor editing to produce a non-autoreactive BCR, anergy to prevent peripheral activation or clonal deletion via apoptosis. This is the first key checkpoint in B-cell development [115].

[c] The 'surrogate' light chain is an immunoglobulin light chain-like molecule

Much of the data reported for human B cell differentiation has been extrapolated from mouse studies and the corresponding processes in humans remain incompletely defined [115, 118]. As such discrepancies in definitions of transitional B cells are often encountered when the literature is reviewed as a whole [119]. Broadly, it is believed that after selection, as they migrate from the bone marrow and enter the periphery, immature B cells undergo three transitional phases: T1, T2 and T3. These phases have discrete phenotypes characterised by analysis of cell-surface markers such as IgM, IgD, CD5, CD9, CD10, CD19, CD20, CD21, CD24, CD34 and CD38. Recent bone marrow emigrants are considered T1 B cells, primarily characterised as $CD5^{HIGH}$ $CD10^{+}$ $CD21^{LOW}$ IgM^{HIGH}. In the spleen, T1 B cells transition to T2 B cells of a $CD5^{HIGH}CD10^{+}CD21^{HIGH}IgM^{HIGH}$ phenotype. T2 B cells can either progress to a T3 phase, exhibiting a $CD5^{LOW}CD10^{-}$ $CD21^{HIGH}IgM^{LOW}$ phenotype (now thought to represent primarily self-reactive anergic B cells), or eventually differentiate into naïve follicular (FO) B cells or marginal-zone (MZ) B cells. This fate is dependent on self antigen-mediated activation of the BCR, Notch2, the receptor for B cell-activating factor (BAFFR) and the canonical nuclear factor-κB (NFκB) pathway, as well as signals involved in the migration and anatomical retention of MZ B cells [119]. MZ B cells migrate to a new location in the spleen, where they are physically retained. A newly differentiated MZ B-cell also acquires the ability to self-renew, with an unlimited lifespan [120].

1.8.3. B-cell activation

Immunocompetent naïve FO B cells re-circulate through the lymphatic system and peripheral tissues until they encounter an antigen and are activated. B-cell activation requires two distinct signals. The first activation signal occurs when antigen is bound to the BCR. The second activation signal occurs via either thymus-dependent or thymus-independent mechanisms (T-dependent and T-independent respectively) [121, 122]. Most B-cell responses to antigen are T-dependent and require the close interaction of B cells with $CD4^{+}$ T cells specific for the same antigen. The antigen is internalised by B-cell receptor-mediated endocytosis, digested, complexed with MHC-II molecules on the B-cell surface and subsequently presented to T cells, inducing their activation. The activated T cells then provide a second activation signal to the B cell, which can occur through a variety of proteins such as CD40L. Alternatively, there are a few types of antigens that can directly provide the co-stimulatory signal for B cells (T-independent), including some bacterial cell wall components such as LPS, or antigens containing highly repetitious elements such as bacterial flagellin. Once activated, B cells proliferate and form specialized structures

called germinal centres (GC) where they differentiate into memory B cells or plasma B cells. Following differentiation into plasma cells, additional T-cell derived signals result in somatic hypermutation, which can for example, switch the class of antibody produced by the B-cell from IgM to IgG. Additionally, the B cells undergo affinity maturation, producing antibodies with increased affinity for antigen. With repeated exposure to the same antigen, B cells will produce antibodies of several log-fold greater affinity than in a primary response [115]. Once released into the blood and lymph, these antibodies bind and opsonise target antigens, initiating their neutralization or destruction via ADCC (discussed in section 1.4.3) and complement-dependent cytotoxicity (CDC). The basic stages of human B-cell development are summarized in Figure 1.6.

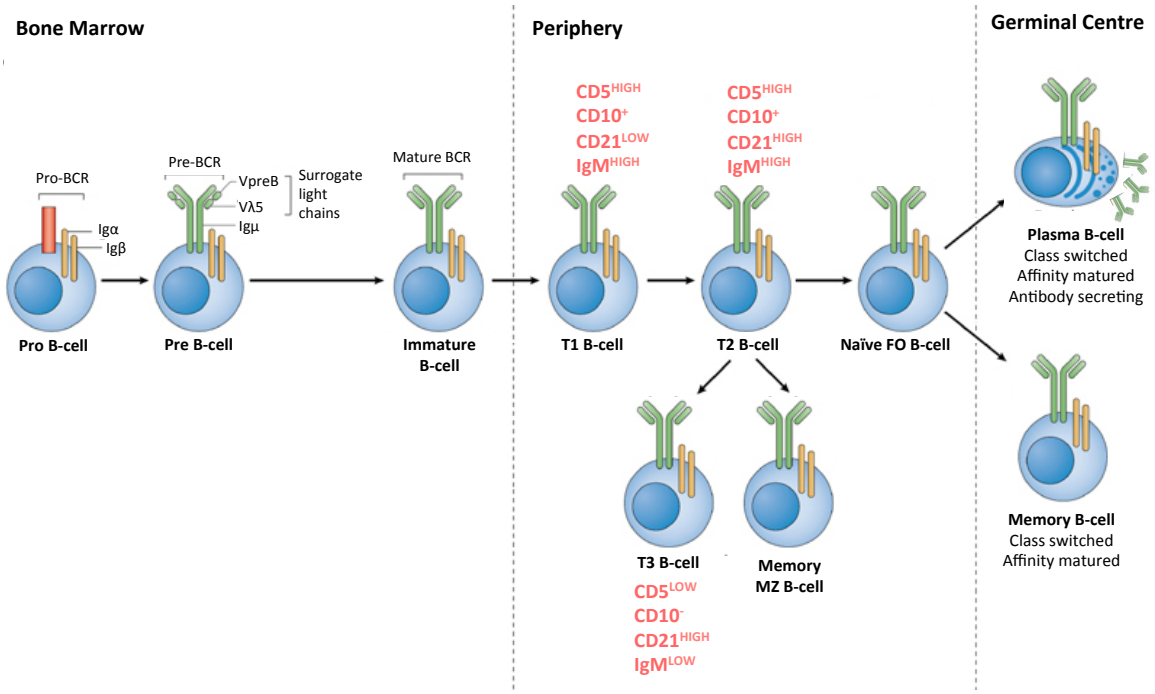

Figure 1.6. Schematic representation of the basic stages of human B-cell development
Adapted from Cambier *et al* (2007) [123]

1.8.4. Immunoglobulin

The fundamental 'Y'-shaped structure of an antibody Ig molecule can be divided into three sections: two arm-like antigen-binding fragment (FAb) regions and a stem-like fragment crystallisable (Fc) region. The FAb contains a variable domain (Fv) incorporating complementarity-determining regions (CDRs) that bind to cognate antigens [124]. The Fc fragment provides a binding site for endogenous Fc receptors on the surface of lymphocytes. An intact

single Ig molecule comprises two identical copies of an inner heavy chain, and two identical copies of an outer light chain. Heavy chains are composed of two successive regions: variable (V_H) and constant (C_H). There are five classes of Ig - IgA, IgD, IgE, IgG and IgM; distinguished by the type of heavy chain they contain (α-chains, δ-chains, ε-chains, γ-chains and μ-chains respectively). The α, δ and γ heavy chains have a constant region composed of three tandem Ig domains (denoted C_H1, C_H2, C_H3) and a hinge segment for added flexibility; while ε and μ heavy chains have a constant region composed of four domains (denoted C_H1, C_H2, C_H3, C_H4). Polypeptide variation in the heavy chains allows each immunoglobulin class to function in a different type of immune response or during a different stage of immune defence. The amino acid sequences that confer these functional differences are located mainly within the Fc region. Some immunoglobulins are able to form multimers through linkage of their Fc domains via a J chain. IgM for example is a pentamer of five identical Ig monomers and therefore has a high valency due to the number of arms available to bind antigen.

Light chains can be classified as either kappa (κ) or lambda (λ) based on small differences in polypeptide sequence. A given Ig has either κ light chains or λ light chains, never one of each. No functional difference has been found between antibodies having κ or λ light chains, and either type of light chain may be found in any of the five major classes of Ig. Light chains are composed of two successive regions: variable (V_L) and constant (C_L) [124].

1.8.5. IgG

IgG is the most abundant protein in human serum and a major focus in this study. IgG can be further divided into subclasses 1, 2, 3 or 4 (denoted IgG_1, IgG_2, IgG_3 or IgG_4). Although closely related glycoproteins, the major differences between the subclasses are the length of the hinge region, amino acid composition, and the numbers of disulfide bridges between the two heavy chains, all of which have implications for FcγR binding, effector functions, and pharmacokinetic properties. For example, compared to IgG_2, IgG_1 has two fewer inter-heavy chain di-sulfide bonds and an extra 3 aa residues most proximal to the hinge region in the C_H2 domain of the Fc portion.

The Fc portion contains a largely overlapping binding site for FcγRIIIa receptors on innate effector cells. The aforementioned substitutions here are responsible for a subtle but important change of quaternary structure in the Fc, resulting in a more exposed FcγRIIIa binding-site in IgG_1. Thus, in

contrast to IgG_1, IgG_2 mAbs are devoid or severely limited in their ability to induce NK cell-mediated ADCC [124, 125]. The subtle differences between IgG_1 and IgG_2 is illustrated in Figure 1.7.

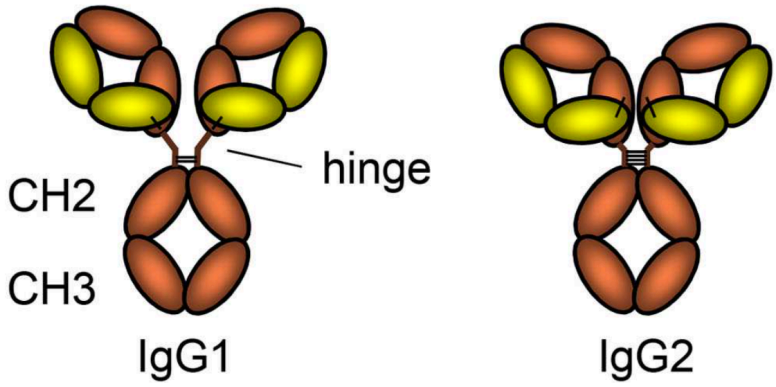

Figure 1.7. Illustrating the subtle difference between IgG_1 and IgG_2
Adapted from Vidarsson *et al*, 2014 [124]. The schematic depicts the difference in heavy and light chain linkage, hinge length, and the number of disulfide bridges connecting the two heavy chains between the IgG_1 and IgG_2 subclasses.

1.8.5.1. IgG in cancer

Natural IgG recognises defined cell surface structures, predominantly oligosaccharides, which are expressed in larger quantities in a tissue-specific manner during fetal differentiation but are also expressed on tumour cells. Tumour-reactive natural IgG can be found in a small percentage of healthy blood donors [126] and increased concentrations have also been detected in the peripheral blood of acute lymphoblastic leukaemia (ALL) patients [127]. Natural IgG may not only have a direct cytotoxic effect on intact tumour cells, but also a bystander effect during a humoral anti-tumour response as they can recognize modified cell surface structures arising during the necrotic processes that accompany tumourigenesis. Natural IgG can also help to attract other immune cells to sites of inflammation, particularly those bearing CD16 receptors that can potentiate the destruction of cancer cells via ADCC or antibody dependent cellular phagocytosis (ADCP): NK cells, monocytes, macrophages, neutrophils, eosinophils and DC [128].

In addition, IgG_1 and IgG_3 are potent activators of the classical complement pathway. The binding of two or more IgG molecules to the surface of tumour cells leads to high-affinity binding of C1q to the Fc domain, followed by activation of C1r enzymatic activity and subsequent activation of downstream complement proteins. The result of this cascade is the formation of pores facilitated by the membrane attack complex (MAC) on the tumour-cell surface, resulting in tumour-cell lysis.

The production of the highly chemotactic complement molecules C3a and C5a also leads to the recruitment and activation of immune effector cells, such as macrophages, neutrophils, basophils, mast cells and eosinophils [129].

1.9. Tumour evasion of immune cell recognition

Despite the growing knowledge of both TA and immune cell interactions in cancer, tumours can utilize a variety of mechanisms to evade the immune system. Immune cells are frequently suppressed in cancer patients, the mechanisms of which can be categorised as follows:

1.9.1. Modified expression of ligands on tumour cells

Evidence for downregulation of the stress molecule major histocompatibility complex class I chain-related peptide A (MICA) by tumour cells has been reported. MICA is one of the ligands for the NKG2D receptor expressed on NK cells, thus downregulation markedly reduces tumour susceptibility to NK-cell mediated lysis [130]. It has also been shown that the expression of Fas ligand (FASL/CD95L) on tumours can induce apoptosis of intratumoural T cells [131]; and that tumour cells expressing programmed cell death ligand-1 also known as B7 homolog-1 (PD-L1/B7.H1) can downregulate active tumour immunity *in vivo* by limiting antigen-specific T-cell proliferation [132].

1.9.2. Secretion of inhibitory ligands by tumour cells

Secretion of inhibitory ligands like MICA as an exosome (cell derived vesicles [133]) or soluble ligand (sMICA) effectively engages the NK-cell activating receptor NKG2D away from the tumour cell, preventing target cell recognition or causing "mis-firing" [113, 134, 135]. Meanwhile, other studies demonstrate that the tumour release of immunosuppressive cytokines such as transforming growth factor beta (TGFβ) downregulate tumour directed NK-cell cytotoxicity in cancer patients [135, 136] and that supernatants derived from *in vitro* cultures of tumour cells adversely affect T-cell activation/proliferation by inhibiting transcription factors such as NF-κβ [137].

1.9.3. Altered expression of "self"

The well-documented disappearance or reduction in the expression of TA and downregulation of MHC and other molecules associated with processing and presentation can alter the quantity and

profile of MHC-I epitopes presented at the cell surface, and has major implications for CTL antigen recognition (comprehensively reviewed by Garrido *et al*, 2010). While complete loss of MHC expression would render tumour cells susceptible to NK-cell mediated lysis, intermediate levels have been shown to confer resistance to T-cell and NK-cell killing, supporting the notion that thresholds of expression are required for lymphocyte activation. Proteins involved with antigen processing and loading share a degree of co-regulation with MHC; thus, changes in MHC expression are often accompanied by altered expression of antigen presentation pathway co-factors such as TAP and β2m [138]. Conversely, MHC-I upregulation has been described in some tumour types, mechanistically providing a strong inhibition signal for NK cells [139].

A major challenge in cancer therapy is to design means to either prevent these impairment mechanisms or find ways to circumvent them. Thus harnessing the immune system for therapeutic benefit in cancer has been an attractive long-term goal in oncology.

1.10. Harnessing the power of immune effector cells: immunotherapy

Improved understanding of TA, the means by which tumours avoid immune detection and the role of the immune system have led to the identification of novel therapeutic targets in cancer. Immunotherapy is designed to take advantage of the unique properties of the immune system: specificity, adaptability, and memory; to destroy tumours and maintain remission. The significant breakthroughs are detailed as follows:

1.10.1. Therapeutic antibodies

In 1975, Kohler and Milstein developed ground-breaking monoclonal antibody (mAb) technology that provided the possibility of creating antibodies as a class of therapeutics. Antibodies can be purified from the serum of immunised animals, where the antigen of interest stimulates B cells to produce a diverse range of antibodies specific to that antigen. The large numbers of antibodies produced have different specificities and epitope affinities and are known as polyclonal antibodies. Kohler and Milstein were able to fuse immortal heteromyeloma cells with B cells, using polyethylene glycol (PEG) to break down cell membranes and allow mixing of the genetic material from both cell types. The result was a hybridoma - an immortal cell line with the ability to produce antibodies. As the hybridoma was a product of the fusion of one heteromyeloma cell with one B-

cell, the culture supernatant only contained antibodies to one specific epitope, which, when purified, were called monoclonal antibodies [140].

1.10.1.1. Anti-TA monoclonal antibodies

Anti-TA mAbs are a principal focus in this study and represent an attractive "off the shelf" therapy in cancer. Anti-TA mAbs have maintained their popularity and success due to an increased understanding of anti-tumour immunity and intense pharmaceutical company investment (estimated to be in the order of £100 billion over the next four years) [141, 142]. Antibodies remain the fastest growing class of biotherapeutics. Currently, there are over 70 mAbs approved for clinical use; targeting various TA and antigens in other therapeutic areas such as infection, autoimmunity, allergy, inflammation and cardiovascular disease. Notably, expiration of patents on mAb products has allowed for the generation of biosimilars - near identical copies of original mAbs synthesised by different companies. Approved biosimilars are often produced and sold at substantially reduced cost compared to their reference products [143]. In 2017, 50 mAbs entered clinical trial, of which 28 had a primary indication for cancer therapy [144]. The cancer therapeutic mAbs that are approved for clinical use by the United States Food and Drug Administration (FDA) are listed in Table 1.1.

Table 1.1. Cancer therapeutic mAbs approved for clinical use by the FDA

Mechanism of Action	Brand Name	International Non-proprietary Name	Target	Type	First Approved Indications
Check point inhibitors	Yervoy	Ipilimumab	CTLA-4	Human IgGl	Advanced melanoma
	Opdivo	Nivolumab	PD1	Human IgG4	Advanced melanoma
	Keytruda	Pembrolizumab	PD1	Humanized IgG4	Refractory melanoma
	Bavencio	Avelumab	PDL1	Human IgGl	Merkle cell carcinoma
	Imfinzi	Durvalumab	PDL1	Human IgGl	Bladder cancer
	Tencentriq	Atezolizumab	PDL1	Humanized IgG1	Bladder cancer
Antibody-drug conjugate	Adcetris	Brentuximab vedotin	CD30	Chimeric IgGl	Refractory HL, refractory relapse sALCL
	Mylotarg	Gemtuzumab ozogamicin	CD33	Humanized IgGl	Acute myeloid leukaemia
	Besponsa	Inotuzumab ozogamicin	CD22	Humanized IgGl	Relapsed or refractory CD22+ non-Hodgkin lymphoma
	Kadcyla	Trastuzumab emtansine	HER2	Humanized IgGl	Her2+ breast cancer

Targeted radiotherapy	Zevalin	Ibritumomab-tiuxetan Y90	CD20	Murine IgGl	Non-Hodgkin lymphoma
	Bexxar	Tositumomab-iiodine-131	CD20	Murine IgG2	Non-Hodgkin lymphoma
	ProstaScint	Capromab penetide	PSMA	Murine IgGl	Prostate cancer
Targeted therapy ligation/ADCC/ CDC	Campath	Alemtuzumab	CD52	Human IgGl	B-cell chronic lymphocytic leukaemia
	Avastin	Bevacizumab	VEGF	Humanized IgGl	CRC, NSCLC-squamous, renal cancer
	Erbitux	Cetuximab	EGFR	Chimeric IgGl	HNSCC, Kras- CRC
	Darzalex	Daratumumab	CD38		Multiple Myeloma
	Portrazza	Necitumumab	EGFR	Human IgGl	NSCLC
	Gazyva	Obinutuzumab	CD20	Humanized IgGl	CLL Follicular lymphoma
	Arzerra	Ofatumumab	CD20	Human IgGl	B-cell chronic lymphocytic leukaemia
	Vectibix	Panitumumab	EGFR	Human IgG2	Metastatic colorectal carcinoma
	Perjeta	Pertuzumab	HER2	Humanized IgGl	Her2+ breast cancer
	Cyramza	Ramucirumab	VEGFR2	Human IgGl	Gastric cancer
	Rituxan	Rituximab	CD20	Chimeric IgGl	Non-Hodgkin lymphoma
	Herceptin	Trastuzumab	HER2	Humanized IgGl	Her2+ breast cancer
	Lartruvo	Olaratumab	PDGFRa	Human IgGl	Soft tissue sarcoma
	Unituxin	Dinituximab	GD2	Chimeric IgGl	Neuroblastoma
	Blincyto	Blinatumomab	CD3/CD19	BiTE	Pre-B ALL
	Empliciti	Elotuzumab	SLAMF7 (CD319)	Humanized IgGl	Multiple Myeloma
	Perjata	Pertuzumab	HER2	Humanized IgGl	Metastatic breast cancer

These mAbs can be characterised as murine, chimeric, humanised or human, qualified by the extent of human sequences present within the mAb, as illustrated in Figure 1.8. Murine mAbs are derived entirely from mouse sources. Chimeric mAbs are constructed with V_H and V_L regions derived from a mouse source and constant regions derived from a human source. Humanized mAbs are derived predominantly from a human source except for their CDRs, which are murine. Human mAbs are derived entirely from human sources [145].

There are a number of ways to achieve mAb chimerism and humanization. The use of mice genetically engineered to carry humanised Ig genes or engrafted with a human immune system is a means to obtain and immortalise clones that produce either fully human Ig or Ig variable domains associated with customised human-like constant regions [146]. Mouse free processes have also been sought that allow the insertion or substitution of portions of the Ig molecule such as CDRs into a human scaffold. These systems take advantage of the fact that mAb production can be achieved using recombinant DNA to create constructs for expression in mammalian cell culture systems [147]. In addition, these mAbs can be any of the IgG_1, IgG_2, IgG_3 or IgG_4 subclasses discussed in section 1.8.5.

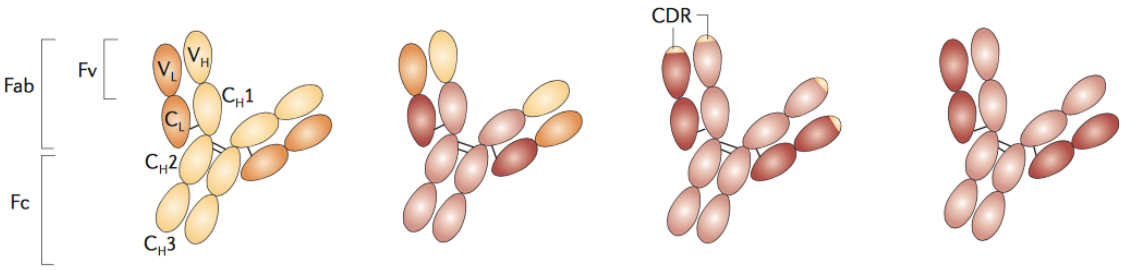

Type of mAb	Murine	Chimeric	Humanized	Human
	Ibritumomab tiuxetan (CD20); IgG1κ*	Cetuximab (EGFR); IgG1κ	Trastuzumab (ERBB2); IgG1κ	Panitumumab (EGFR); IgG2
	Tositumomab-I^{131} (CD20); IgG2aλ*	Rituximab (CD20); IgG1κ	Bevacizumab (VEGF); IgG1	
			Alemtuzumab (CD52); IgG1κ	
			Gemtuzumab ozogamicin (CD33); IgG4κ*	

Figure 1.8. The classification of mAbs by type: murine, chimeric, humanised and human.
Adapted from Imai and Takaoka (2006) [145]

1.10.1.2. Immune checkpoint inhibitors

Immune checkpoints refer to any of the ligand:receptor interactions involved in maintaining self-tolerance and modulating the amplitude and duration of peripheral immune responses in order to minimize collateral damage; particularly in the context of TA-specific T cells. A strong body of evidence suggests that tumours can manipulate these pathways as a means to resist immune cell control, which gave rise to a class of therapeutics designed to inhibit these ligand:receptor interactions. The first to achieve FDA approval was based on the research initiated by Leach *et al*

[148]. The anti-CTLA-4 mAb: ipilimumab (Yervoy®) prevents the down-modulation of T-cell activation [149]. Another well-studied immune checkpoint interaction, highlighting the broad and diverse targeting opportunities for these inhibitors; is between the receptor programmed cell death protein 1 (PD1) and the PD-L1 ligand frequently expressed on tumour cells. The major role of PD1 is to limit the activity of T cells in peripheral tissues during inflammatory responses. Phase I and II clinical trials of anti-PD1 mAbs are currently ongoing [150, 151].

1.10.1.3. Bi-specific antibodies

Bi-specific T-cell engagers or BiTEs are recombinant fusion proteins comprising two single chain mAbs with different specificities that can target two antigens simultaneously; typically a TA and an activating moiety present on effector cells, such as CD3. BiTE constructs have been shown to induce strong proliferation and activation of T cells independent of MHC-restriction. A CD3/CD19 BiTE called blinatumomab has demonstrated potent anti-leukaemia and anti-lymphoma activity at low doses [152], prompting the clinical trial of other BiTE combinations such as CD33/CD3 for AML [153] and EGFR/CD3 for solid tumours [154].

1.10.1.4. Antibody-drug conjugates

An antibody-drug conjugate (ADC) is composed of an antibody (typically a TA-specific mAb), a biologically active cytotoxic drug and a linker that attaches the two. The toxic payload is delivered directly into the tumour cell when the antibody is absorbed via receptor-mediated endocytosis, then trafficked to and degraded in the lysosome. Many payloads have been attached to mAbs, including radioisotopes, protein toxins, laser-activated nanoparticles and small molecule drugs, via chemical motifs such as disulfide bonds, non-cleavable thioethers and, more commonly, cleavable peptides [155]. The ADC inotuzumab ozogamicin (INO) comprises an anti-CD22 mAb conjugated to the cytotoxic agent *N*-acetyl-γ-calicheamicin via an acetyl butyrate linker. In a phase II clinical trial, INO demonstrated significant efficacy against $CD22^{+}$ refractory and relapsed ALL. A 57% overall response rate (ORR) was observed in a cohort of 49 patients treated with INO as a single agent [156]. To date, over 30 INO clinical trials have been initiated, 13 of which are currently recruiting [157].

1.10.2. Adoptive T-cell therapy

In adoptive cell therapy (ACT), T cells isolated from patient PBMC or TILs isolated from primary tumours are expanded *in vitro,* (with or without genetic engineering to augment function) and then re-infused into the patient in order to enhance anti-tumour responses. An early study by Rosenberg and colleagues was the first demonstration that ACT using autologous TILs could mediate objective regression of cancer in patients with metastatic melanoma. Patients with metastatic melanoma were treated with ex-vivo expanded TILs and IL2. In patients who had not previously been treated with IL2, 60% (9 of 15) showed cancer regression. 40% (2 of 5) of patients in whom previous IL2 therapy had failed also showed regression. This was sustained for up to 13 months [158]. In another recent phase II study, ACT using EBV-specific CTL in combination with chemotherapy showed promising results, with a 2-year OS of 62.9% [159].

1.10.3. DC vaccines

Accumulating preclinical evidence suggests that numeric or functional defects in specific DC subsets can facilitate tumour growth, tumour progression and chemoresistance [78]. Corroborating this notion, elevated levels of tumour infiltrating mDC have been associated with improved clinical outcomes in cohorts of patients affected by a variety of solid tumours, whereas the accumulation of intra-tumoural tolerogenic DC has been indicated as a poor prognostic factor in multiple clinical settings [160]. Thus, for the last 20 years, strategies have been devised for harnessing the immunotherapeutic potential of DC in the treatment of malignant conditions, which, based on the underlying mechanistic principle, can be categorised into four major groups [78]:

1. *In vivo* DC loading with TA [161]
2. DC-derived exosomes [162]
3. Reinfusion of B7.IL-12 transduced DC [163]
4. Reinfusion of *ex vivo* TA loaded DC:
    - Via exposure of iDC to autologous cancer cell lysates [164, 165]
    - Via incubation of iDC with recombinant TA [166]
    - Via transfection of DC with TA-coding RNA [167] or TA expression vectors [168]
    - Via creation of ‘dendritomes’ - fusions of DC with inactivated cancer cells [169]

The apogee of these efforts was reached in 2010, when the FDA approved use of Sipuleucel-T (Provenge®) in patients with asymptomatic or minimally symptomatic metastatic castration-refractory prostate cancer. Provenge® is a DC-enriched autologous cell preparation expanded *ex vivo* in the presence of a prostate acid phosphatase/granulocyte macrophage colony-stimulating factor (PAP/GMCSF) fusion protein [170].

1.10.4. Enhancing the antigen presenting potential of tumour cells

Acute myeloid leukaemia (AML) cells express high levels of MHC-II (and in some cases MHC-I) but lack CD80, the co-stimulatory molecule that provides the essential second signal required for lymphocyte activation, making them poor APC. In addition, the preponderance of AML is associated with impaired NK cell activity [171, 172]. In 2009, Ingram *et al* showed that lenti-viral transduction of AML cells to express CD80 in conjunction with the stimulatory cytokine IL2 promoted *in vitro* NK-cell activation, NK-cell cytolytic activity and increased $CD8^+$ CTL frequency and function [172, 173] which importantly showed cytotoxic activity towards autologous unmodified AML cells [173]. The immunotherapeutic potential of CD80/IL2 transduced AML cells is currently being evaluated in a phase I clinical trial at King's College Hospital.

Treatment of AML cells with TLR agonists such as the synthetic TLR7/TLR8 ligand R-848 (Resiquimod) promotes increased MHC expression and thus the antigen presentation potential of AML cells. R-848 treatment also increased AML cell production of IL-6, IL1β and TNFα; cytokines known to induce DC maturation; and induced CD80 upregulation by APC [174] while the pharmacological agent 5-aza-2'-deoxycytidine (decitabine) has been shown to upregulate CD80 in cancer cells directly and stimulate tumour-specific T-cell responses [175].

1.10.5. Chimeric antigen receptor-mediated therapy

Chimeric antigen receptor (CAR)-redirected T cells (colloquially referred to as CARs) are the result of genetic modification of T cells to stably express artificial surface immune receptors, conferring novel antigen specificities. Early versions fused single-chain variable fragments (scFv) derived from monoclonal antibodies, to the CD3-zeta transmembrane and endodomain. The introduction of 2^{nd} and 3^{rd} generation CAR T cells, incorporating co-stimulatory signalling elements in their transmembrane portions, have shown considerable promise and many CAR T-cell clinical trials are currently ongoing in both haematological and solid malignancies [176]. CAR-

mediated immunotherapy has a number of advantages over some of the aforementioned immunotherapy approaches insofar as:

1. CARs recognize native, unprocessed antigens, thus bypassing autologous HLA restriction and its regulation.
2. Although CARs are mainly expressed on autologous patient-derived T cells they are not limited to T cells. Indeed, several groups have already successfully retargeted monocytes [177], γδ T cells [178] and NK cells [179] amongst others.
3. In contrast to conventional αβ TCR, CARs can recognize non-protein targets such as carbohydrates and glycolipids [176].

Recently, Zah and colleagues presented work using a novel bi-specific CAR. This was the first demonstration that a bi-specific CAR could prevent antigen escape in an *in vivo* xenograft model [180]. Furthermore, 2015 saw the world first use of a "universal" CAR T-cell redirected to CD19 (uCART19) in an 11-month-old girl with high-risk $CD19^+$ ALL. The uCART19 were manufactured from a third-party healthy donor and genome edited using transcription activator-like effector nucleases (TALEN™) to simultaneously inactivate two genes. The knockout of the TCRα gene eliminated TCR expression and abrogated the potential for donor-mediated graft-versus-host disease (GvHD) while knockout of the CD52 gene made the donor T cells resistant to the lymphodepleting agent alemtuzumab, commonly used in the conditioning regimen for bone marrow transplantation. Infusion of the uCART19s induced molecular remission where all other treatments had failed [181] and have since been used in a second infant ALL case [182]. This novel strategy, using a frozen preparation of mismatched donor T cells represents another 'off the shelf' therapy, and provides a considerable reduction in production cost when compared to autologous patient-derived preparations. Despite the exciting promise of CAR T cells, this therapy is only at the experimental stage. Notably a different CAR would be required for different target epitopes and the cost for a single infusion of CAR T cells is estimated to exceed that of the annual cost of an equivalent mAb therapy. CAR T cells continue to show poor efficacy in the control of solid tumours. Additionally, a major limitation in the use of CAR T-cell therapy is its potential to induce cytokine storm (CS), the rapid and massive release of cytokines from CAR T cells into the periphery. Although manageable and reversible with the administration of steroids and IL-receptor antagonists, in some cases the precipitous drops in blood pressure, swelling and high fevers that

result from CS can lead to life threatening multiple organ failure. More research is needed before CAR T-cell therapy becomes a routine option in cancer treatment [183].

1.11. EGFR$^+$ cancers

EGFR (also known as ErbB-1 or HER1) is a tyrosine kinase receptor of the HER family, affecting cell adhesion, cell survival and cell proliferation. The binding of EGFR specific endogenous ligands such as epidermal growth factor (EGF) or transforming growth factor alpha (TGFα) induces receptor dimerisation, transphosphorylation of the kinase domains with subsequent activation of two major signalling cascades: Ras/Raf/MEK/MAPK and PI3K/Akt/mTOR. These pathways trigger numerous oncogenic processes such as cell survival, proliferation, angiogenesis, tumourigenesis and inhibition of apoptosis [184]. The overexpression of EGFR is correlated to poor prognosis and has been characterised in 80-100% of head and neck squamous cell carcinomas (HNSCC) [185], 40-80% of non small cell lung carcinomas (NSCLC) [186] and 50-80% of colorectal carcinomas (CRC) [187].

In CRC, a modest increase in average survival can be achieved with current chemo-therapeutic strategies, yielding 10-12 months with single agent 5-Fluorouracil and increasing to 16-20 months upon addition of oxaliplatin and irinotecan when compared to 6 months with palliative care alone. When administered as a first line treatment, combination chemotherapy can substantially improve response rates from 31% to 56%, median PFS from 6.5 to 9 months and median OS from 14.5 to 21.4 months [188, 189, 190, 191, 192, 193, 194, 195, 196, 197]. Although encouraging, much remains to be achieved in CRC therapy.

1.11.1. Anti-EGFR mAbs in the treatment of EGFR$^+$ cancer

The expression of EGFR on malignant cells can reach $2x10^6$ million receptors per cell, compared to 40,000-100,000 receptors on normal cells [198]. This significant difference makes targeted EGFR therapies potentially very effective and less toxic than traditional chemotherapy. The mAbs panitumumAb and cetuximAb bind to the extracellular domain of the human EGFR with approximately 5 to 10 fold higher affinity than its natural ligands. They block ligand binding, resulting in inhibition of receptor function and blocking of downstream survival signals; and can also induce the internalisation and downregulation of EGFR [199]. However, the benefit of anti-

EGFR mAbs can be bypassed by gain-of-function mutations in Kirsten rat sarcoma viral oncogene homolog (KRAS), a signalling molecule downstream of EGFR [200, 201, 202, 203]. In patients with KRAS-mutant tumours, the proliferative signal is constitutively active and therefore unaffected by receptor blockade [204].

While panitumumAb is human IgG_2 class, cetuximab is a chimeric antibody of IgG_1 class, with demonstrable improvements over panitumumab in terms of NK-cell recruitment for ADCC [205]. Cetuximab (marketed by Merck, trade name Erbitux®) is still the only targeted agent that has been approved for the treatment of HNSCC by the regulatory agencies of the US and Europe. In addition cetuximab is approved for use in metastatic NSCLC, KRAS wild type (WT) CRC in combination with chemotherapy, and as a 3rd and 4th line single agent therapy in CRC patients who are intolerant to irinotecan or who have failed oxaliplatin- and irinotecan-based therapy [199].

1.11.2. MAbs: why the lack of therapeutic efficacy?

For dose escalation studies and early phase clinical trials, new drugs are typically tested alone, with efficacy compared to the standard level of care. Upon reaching phase II, immunotherapies can be combined with conventional radiotherapy/chemotherapy as per standard clinical conditions. As a single agent, TA-targeted mAbs such as cetuximab offer only modest response rates. A study by Pessino *et al* treated 39 chemotherapy naïve CRC patients with cetuximab as a first line monotherapy. According to WHO definitions, one patient showed a complete response, with no detectable cancer after a median 8-weeks treatment and three showed a partial response (≥ 50% reduction in measurable tumour). This represented an ORR of 10% [206] with a HNSCC/NSCLC study showing that the response rate rises only moderately to 15% upon combination of cetuximab with cisplatin-based chemotherapy [207]. Indeed, as of November 2015, the NHS removed cetuximab from its list of funding approved 3rd and 4th line single agents [208].

Although predicting clinical efficacy is multifactorial and may not be explicable by one factor *per se*, the CD16 polymorphism, described in section 1.4.3, has been implicated in influencing the clinical outcome of mAb therapy. Mechanistically, this polymorphism modulates the affinity of CD16 for IgG_1 antibodies, consequently affecting the potency of ADCC [209]. The F/F allelic variant of CD16 has been correlated with poor clinical responses to cetuximAb, the rationale being that the lower affinity conferred by this genotype may reduce the clearance of antigen:antibody

immune complexes (ICs) [210]. The efficacy of cetuximAb is therefore limited by patient genotype, but could still be useful in a personalised medicine setting with pre-selection of patients predisposed to respond. Notably, the finding of a link between Fc receptor affinity and ADCC efficiency is important because it leads to the prediction that enhancements of mAb affinity for Fc receptors may result in significant therapeutic benefit.

1.12. Anti-EGFR mAb enhancements: glyco-engineering

Standard mAbs can be further optimised for greater therapeutic potential. One approach to increase the binding between Fc receptors and mAbs is to manipulate protein glycosylation, which is known to affect protein-protein interactions. Pioneering work demonstrated that antibodies lacking fucose residues in their Fc domain show greatly increased affinity for CD16, ultimately resulting in ADCC amplification [211, 212, 213].

1.12.1. Protein glycosylation

Glycosylation is an enzymatic modification that results in the addition of sugar moieties to specific amino acids. It is a critical function of the biosynthetic-secretory pathway in the ER and Golgi apparatus and approximately half of all proteins expressed in a cell undergo glycosylation - including ligands, surface receptors and secreted proteins. Protein glycosylation exerts multiple functions within the cell that are not necessarily dependent on the detailed 3-dimensional structure of the glycan, but rather their bulk. Glycans can alter the behaviour of proteins, for example by covering antigenic sites; protecting them from proteolysis; or making them more soluble, simply because they are large and hydrophilic [214].

The molecular events of glycosylation include ligation of monosaccharides, transfer of sugars between substrates and the trimming of sugars from the glycan structure. Unlike other cell processes such as transcription or translation, glycosylation is non-templated, and as such it is possible that not all of these steps occur during every glycosylation event. The pathway relies on a host of enzymes such as glycosyltransferases (Gtf) and glycosidases that respectively add or remove sugars in a stepwise fashion, to generate the glycoproteins. Each glycosidase shows specificity for removing a particular sugar e.g., mannosidase. Since enzyme activity varies by cell type and intracellular compartment, a single cell can provide heterogeneous glycosylation patterns that differ by up to 30%. Almost every aspect of this process can be modified, including:

the site of glycosidic linkage, glycan composition; glycan length (short- or long-chain) and glycan structure (branched or unbranched chains). Therefore, glycosylation increases the diversity of the proteome to a level unmatched by any other post-translational modification (be it phosphorylation, ubiquitination, nitrosylation, methylation, acetylation, lipidation and proteolysis) [215].

Five classes of glycans are produced, which are classified as follows based on the nature of the sugar-peptide bond and the oligosaccharide attached:

N-linked	Glycan binds to the nitrogen (amino group) of asparagine (Asn or N) within the ER
O-linked	Monosaccharides bind to the hydroxyl group of serine, threonine, tyrosine, hydroxylyseine or hydroxyproline side chains, or to oxygens on lipids in the ER, Golgi, cytosol and nucleus
C-linked	Mannose binds to carbon (indole ring) of tryptophan
Glypiation	Glycan core links a phospholipid and a protein (GPI anchoring)
Phospho-glycosylation	Glycan binds to serine via phosphodiester bond

The most common class and therefore the emphasis of this study, is N-linked; which accounts for 90% of glycosylation and can occur both co-translationally (where the glycan is attached to the nascent protein during translation and transport into the ER) and as a post-translational modification [216].

N-glycosylation can be categorised into three initial stages - precursor glycan assembly; attachment; and subsequent trimming - which occur identically for all N-glycosylated proteins. The diversity previously described manifests during the final stage - maturation in the Golgi complex. Oligosaccharides attached to proteins via N-glycosidic linkages are derived from a 14-sugar precursor molecule comprised of N-acetylglucosamine (GlcNAc), mannose (Man) and glucose (Glc). These sugars are added consecutively via a polyisoprenoid lipid carrier called dolichol, which is embedded in the ER membrane [217, 218]. Glycans are covalently bound to the carboxamido nitrogen on asparagine (Asn or N) residues, from which the “N” nomenclature is derived. Notably, not all Asn residues with consensus sequence are glycosylated. Protein synthesis occurs in the direction N- to C-terminus and the growing polypeptide is transported into the ER in the same orientation that it is synthesised. Since protein folding occurs soon after ER

entry, the consensus sequences for glycan transfer become less accessible, thus more N-terminal than C-terminal Asn residues are glycosylated.

The oligosaccharides are then trimmed via glycosidase hydrolysis, until correctly folded. In higher eukaryotes, the glycan structure for all properly folded glycoproteins that proceed to the Golgi is Man6-5GlcNAc2 [219]. In the Golgi, the enzymes that mediate glycan processing are segregated into distinct cisternae to ensure that glycosylation occurs in a step-wise fashion. Further step-wise sugar addition and removal yields a common core oligosaccharide, to which multiple Gtfs add different sugars to generate two other forms - highly variable complex oligosaccharides and high mannose oligosaccharides. The crystal structure of IgG_1 and the common core oligosaccharide that binds IgG_1 at position N297 is depicted in Figure 1.9.

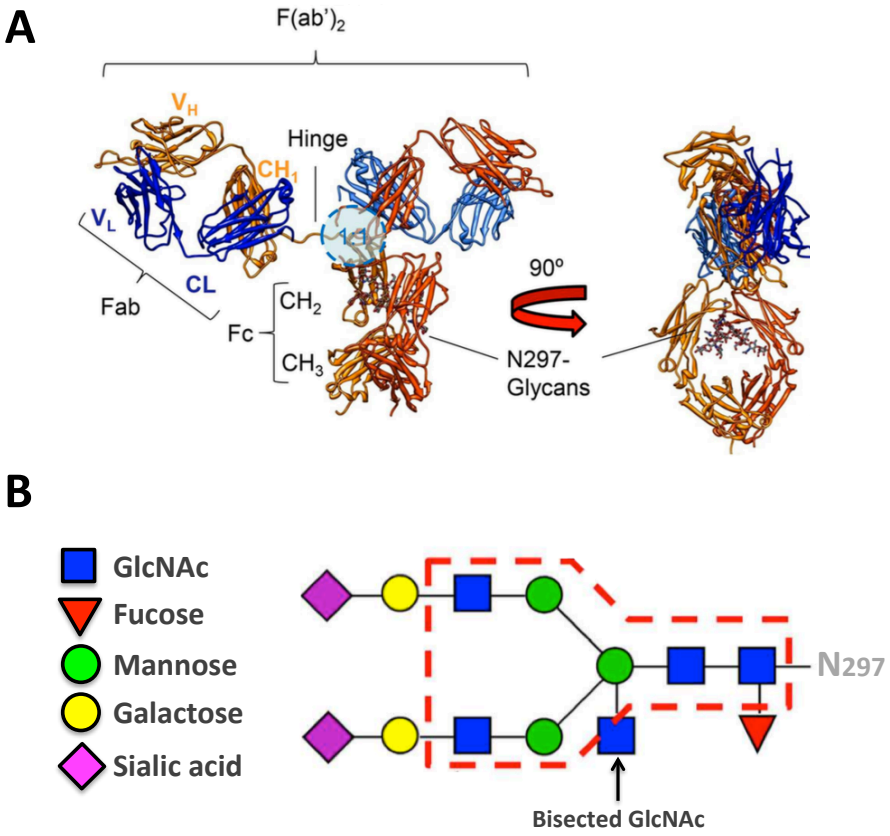

Figure 1.9. Illustrating the crystal structure of IgG_1 and the core structure of N-linked glycan found at position 297
Adapted from Vidarsson *et al*, 2014 [124]. **A.** The crystal structure of an human IgG_1 molecule. The flexibility of the two FAb fragments with respect to the Fc tail and each other is demonstrated when viewed from two different angles. The position where the FcγR binds IgG asymmetrically in a 1:1 configuration is indicated by the blue circle (lower hinge, upper C_H2) on the left, and the N-linked glycan at position 297 is shown on the right attached to each heavy chain. **B.** The N-linked glycan at position 297 attached to each of the heavy chains is shown in A. This glycan can be found as a core oligosaccharide structure (indicated by the red dashed line) that is common to all IgG found in humans and rodents, but can be found with either addition of bisecting N-acetylglucosamine (GlcNAc), one or two galactose, one or two sialic acid residues and a fucose.

1.12.2. Fucosylation

6-deoxy-L-galactose (fucose) is a common component of many N-linked glycans produced in mammalian cells [124]. Fucose is added to the core glycan structure of IgG in the late stages of glycan biosynthesis by Golgi-resident fucosyltransferase (FuT) enzymes. A total of 13 FuT have been identified in the human genome, which catalyse the transfer of a fucose residue from Guanosine 5′-diphospho-β-L-fucose to an acceptor substrate; however, FuT8 is the only FuT that transfers fucose via an α1,6-linkage to the innermost N-acetylglucosamine on N-linked glycans for core fucosylation [216]. The position of the fucose residue on N-linked glycans is illustrated in Figure 1.9.

1.12.3. Glyco-engineering and afucosylation

It is long established that core fucosylation of IgG-Fc affects binding to FcγRIIIa; where non-fucosylated antibodies bind to FcγRIIIa with significantly higher affinity (5-50 fold), translating into a significantly greater magnitude of ADCC and phagocytosis of targets by these antibodies [220, 221]. GlycoMab technology, created by Glycart Biotechnology and acquired by Roche, was developed for the glyco-engineering (GE) of human proteins to express complex N-glycosylation modifications [222]. Glycart first utilised their technology in Chinese hamster ovary (CHO) cells. Umana *et al* transfected CHO cells to produce: i) an anti-neuroblastoma chimeric IgG1 mAb called chCE7 and ii) tetracycline-regulated expression of (1,4)-*N*-acetylglucosaminyltransferase III (GnTIII). GnTIII catalyzes the formation of a bisecting GlcNAc by attaching a GlcNAc to the β-linked mannose of the trimannosyl core of N-glycans (position illustrated in Figure 1.9). It was shown that overexpression of GnTIII in CHO cells was able to reduce Fc core fucosylation and inhibit further processing due to substrate competition and steric hindrance. Roche also evaluated the overexpression of a series of Golgi resident enzymes in combination with GnTIII and showed that overexpression of GnTIII and Golgi α-mannosidase II resulted in the highest level of bisecting and afucosylated glycans on IgG antibodies [221, 223].

Glycoprotein identification and quantitation was performed before and after enzymatic cleavage using mass spectrometry (which required protein enrichment, multidimensional separation by liquid chromatography, tandem MALDI-TOF mass spectrometry and subsequent bioinformatics analysis). Approximately 70% of chCE7 Fc regions bore bisecting and afucosylated glycans after

glyco-engineering, and importantly, the process of glyco-engineering did not alter the binding affinity of chCE7 for human neuroblastoma cells when compared to non-GE and parental mAb [221]. This technology was used to create the GE-mAbs imgatuzumab and GA101GE. Their WT equivalents were created in the same model, but with the administration of tetracycline to inhibit GnTIII function (thereby removing inhibition of FuT8); or in unmodified CHO cells [212, 221].

1.12.4. Other methods of glyco-engineering

CHO Lec13 cells are deficient in endogenous GDP-mannose 4,6-dehydratase (GMD), an enzyme responsible for catalysing de novo GDP-fucose biosynthesis. As a result CHO Lec13 are naturally defective in GDP-fucose formation 61. Shields *et al* exploited this property of Lec13 cells for the production of afucosylated antibodies [220]. However subsequent studies showed that single clones isolated from Lec13 cells displayed a wide range of fucosylation; with the majority producing 50–70% fucosylated antibody under confluent culture conditions [224].

Another strategy to produce afucosylated antibodies involves inactivating the FuT8 gene. Yamane-Ohnuki *et al* targeted the FuT8 gene in an anti-CD20 antibody-producing CHO DG44 cell line, using sequential homologous recombination [225]. Both FuT8 alleles were knocked out from the FuT8 genomic region in the resultant cell line. $FuT8^{-/-}$ CHO were shown to express completely afucosylated antibodies, and elicited a two-fold increase in ADCC compared to the same antibody produced in parental cells. $FuT8^{-/-}$ CHO also demonstrated similar growth kinetics and productivity compared to the parental cell line when cultures were scaled up to 1L bioreactors [225]. FuT8 gene has also been targeted for inactivation using the zinc finger nucleases [226] or small interfering RNA (siRNA) [227]. Respectively, this led to the production of 100% and 60% afucosylated antibodies.

1.12.5. The impact of afucosylation on FcγRs

Defucosylated forms of human IgG are observed as a natural component of normal human serum [228], as such there is little concern regarding their intrinsic immunogenicity and the control of core fucosylation of therapeutic mAbs is now widely recognised as being of great importance regarding Fcγ receptor biology. The family of Fcγ receptors are broadly characterized into three groups: FcγRI (CD64), FcγRII (CD32) and CD16. Differences exist between the groups of receptors, particularly in their structure, function, and affinity for IgG. CD64, CD32a and CD16 are ITAM containing activating receptors that induce effector activities in innate cells such as macrophages

and NK cells. CD32b harbours an ITIM thus fundamentally acts as an inhibitory receptor [229]. Signalling through CD32b induces inhibitory signals that decrease the activation:inhibition (A:I) ratio and bring the cells further from the threshold level required for activation [230].

Importantly, the oligosaccharide structure of Fcγ receptors is also found to contribute to the binding of afucosylated antibody [212]. The structural basis for the high ADCC observed with afucosylated mAbs is that the fucose located at the core Asn297 on IgG_1 Fc blocks the interaction of the carbohydrate located at Asn162 on FcγRIIIa [213]. Afucosylated mAbs thus exhibit higher affinity selectively for FcγRIIIa (and the FcγRIIIb expressed exclusively on neutrophils [230]) since the other Fcγ receptors are not glycosylated at that location [212, 213]. Detailed X-ray crystallography studies of the Fc:FcγRIIIa complex confirmed this model. Ferrara *et al* showed that an increased number of newly formed hydrogen bonds and van der Waals contacts coupled with a unique type of carbohydrate:carbohydrate interaction likely contribute to the increased binding affinity observed between afucosylated Fc and the Asn162 on FcγRIIIa [212]. Fc galactosylation and sialylation also modulate IgG_1 interaction with FcγRIIIa, but to a significantly lesser extent than afucosylation [231].

The binding of human IgG_1 antibodies to C1q and CD64 does not change irrespective of the core fucosylation, although afucosylated human IgG_1 shows a slight increase in binding for FcγRIIa and FcγRIIb [220, 231].

1.12.6. The benefits of glyco-engineering: GA201GE (Imgatuzumab)

Importantly, glyco-engineering improves the therapeutic potential of mAbs in both low (158F) and high (158V) affinity variants of CD16 [205, 232]. Gerdes *et al* measured killing of the $EGFR^+$ human tumour cell line A431 by variants of the human NK cell line NK-92 expressing either the V158 (high affinity) or F158 (low affinity) CD16 genotype in the presence of cetuximAb or the novel humanised IgG_1 glyco-engineered mAb imgatuzumab (also known as RG7160). With high affinity CD16 expressing NK-92 at an effector to target (E:T) ratio of 3:1, imgatuzumab was approximately 2-fold more efficacious at inducing ADCC than the same concentration of cetuximAb. This increased dramatically to 35-fold when low affinity CD16 expressing NK-92 cells were used. Notably, in the presence of physiologic concentrations of competing nonspecific total human IgG, imgatuzumab continued to promote substantial ADCC-mediated killing, whereas the ADCC activity of cetuximAb was virtually abolished. Superior imgatuzumab activity was also

demonstrated for survival in a KRAS mutant mouse xenograft model. Furthermore, GE-mAbs exhibit enhanced ability to induce monocyte/macrophage mediated phagocytosis and cytotoxicity [233]. Thus, to summarise, novel drugs such as imgatuzumab are efficacious, irrespective of patient genotype and additionally irrespective of KRAS status, and as such would not require selection of patients who are most likely to benefit [205].

1.12.7. Imgatuzumab in clinical trials

For ADCC-based immunotherapy to be effective, it is essential that pivotal immune effector cells are present and have sufficient functional capacity; however, chemotherapy induced leukopenia may negatively impact on the immunotherapeutic efficacy of mAbs. Understanding whether ADCC-eliciting antibodies retain effectiveness when combined with chemotherapy is a vital requirement in the development of novel therapeutic strategies against cancer. The importance of which is illustrated by recent findings calling into question the clinical efficacy of cetuximab when combined with oxaliplatin-based chemotherapy [195]. Therefore an examination of the use of imgatuzumab in cancer patients formed the basis of a clinical trial collaboration between King's College London and Roche Glycart AG. The analytical service conducted at King's involved *in vitro* studies of NK-cell cytotoxic responses in metastatic CRC, HNSCC and non-small cell lung cancer (NSCLC) patients. Early trial objectives included:

- Generation of a longitudinal serum cytokine profile throughout the course of treatment using a multiplex immunodetection assay (LUMINEX – Invitrogen, Paisley UK)
- Monitoring of patient immune cell populations to include enumeration of T cells (with $CD4^+$/$CD8^+$ subsets), B cells and NK cells
- Detailed examination of patient NK cell phenotype
- Assessment of patient CD16 genotype
- Analysis of cytotoxic capacity of patient NK cells against $EGFR^+$ and $EGFR^-$ tumour cell lines

1.12.7.1. Ethical approval

The clinical studies were conducted in accordance with Good Clinical Practice guidelines and the Declaration of Helsinki. All patients provided written consent, and local independent ethics committee approval was obtained (comments detailed in Roche-Glycart investigator brochures:

WP21748, BO21495, BP22350, BP22349, BP25438 and summarised by Paz-Ares *et al*, 2011 [234]). Information sheets provided to patients for informed consent included details of sample frequency, sample storage and sample access. In addition information sheets detailed the use of samples for *in vitro* immunophenotyping and *in vitro* functional assessments, with potential assessment of the development of adaptive immune responses in patients of suitable HLA type (comments detailed in Roche-Glycart investigator brochures).

1.12.8. *In vitro* assessment of imgatuzumab

As a major trial objective, the potential of mAbs to elicit NK-cell mediated ADCC *in vitro* was assessed via a degranulation assay. Lysosomal-associated membrane protein I (LAMP-I more commonly referred to as CD107a) is a vesicle-associated protein that is transiently displayed on the surface of an NK cell when it degranulates, thus serving as a measure of NK-cell cytotoxic capacity [235]. The assay was conducted as follows: in the presence or absence of therapeutic mAbs, patient peripheral blood mononuclear cells (PBMC) were co-incubated with two tumour target cell lines - A431 or K562. A431 cells were derived from the vulval carcinoma of an 85-year-old female and express a very high level of EGFR [236], thus serving as a realistic model for the tumour type of trial participants and a means to assess CD16-dependent responses. K562 is an undifferentiated erythroleukaemic, BCR:ABL fusion gene positive (Philadelphia$^+$) cell line that was derived from a 53-year-old female CML patient in blast crisis [237]. Importantly, K562 cells are devoid of MHC-I and thus serve as a classical target for CD16-independent NK cell killing. K562 served as a positive control for NK-cell cytotoxicity and flow cytometry was used to detect and quantify CD107a$^+$ positive NK cells as a measure of degranulation and, by inference, cytotoxicity.

One of the earliest trial protocols involved assessment of metastatic CRC patient PBMC before, during and after oxaliplatin/irinotecan-based chemotherapy. It was found that patient NK cell frequencies were preserved and NK cells retained their CD16 expression and ability to mount an imgatuzumab-mediated ADCC response; regardless of their therapeutic stage (no statistical differences compared to age-matched healthy controls), as illustrated in Figure 1.10. These results, published by Oppeneheim *et al*, were a promising indication that immunotherapeutic approaches exploiting ADCC in cancer patients may be viable, despite the lymphopenia induced by chemotherapy [238]. Phase I and II clinical trials were subsequently undertaken to assess the combination of imgatuzumab with chemotherapy in multiple tumour types, often compared to cetuximab with chemotherapy as the standard treatment care.

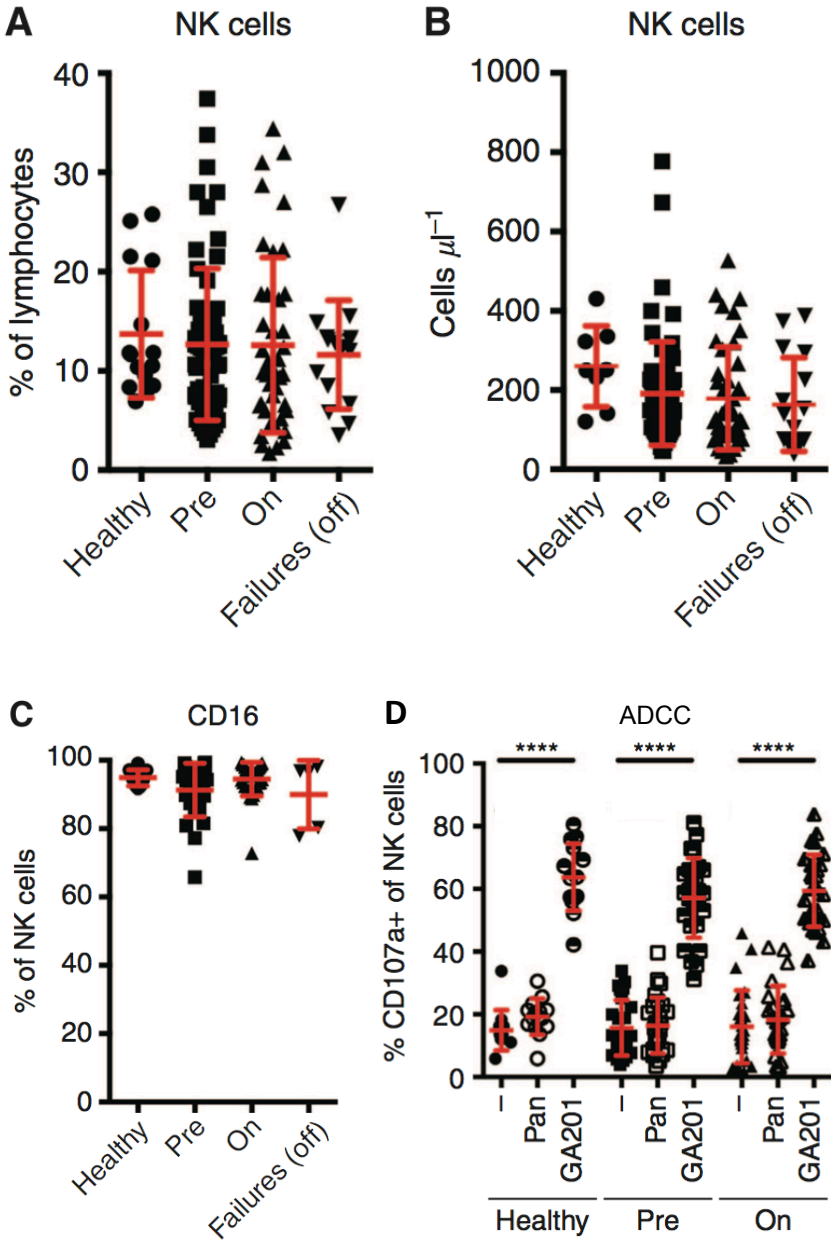

Figure 1.10. NK-cell frequency, counts and function in PBMC of CRC clinical trial patients
Adapted from Oppenheim *et al* 2014 [238]. (A) Frequency in lymphocytes (B) absolute counts of $CD3^{-}CD56/CD16^{+}$ NK cells (C) Percentage of $CD16^{+}$ in $CD3^{-}CD56^{+}$ NK cells (D) Percentage of $CD107a^{+}$ NK cells in cohorts: patients at presentation with metastatic disease, on active chemotherapy and second line chemotherapy failures (off). Mean and standard deviation are shown in red. Patient cohorts were contrasted to an age matched healthy control group. ****p <0.0001, with no significant differences in any of the other parameters examined.

1.13. Experimental assessment of NK:DC:T-cell crosstalk

In the context of cancer immunotherapy, an adaptive T-cell mediated immune response is advantageous because of specificity for TA and the persistent memory that is essential for long-term immunosurveillance. It is therefore important to evaluate whether ADCC mediated by NK cells and induced by mAbs such as imgatuzumab has the potential to promote adaptive immunity. Co-incubation of tumour target cells, NK cells and DC in the presence of TA-directed mAbs is a means of building upon the CD107a assay discussed in section 1.12.4 and assessing NK:DC crosstalk, antigen cross presentation and T-cell immunity *in vitro*. In 2002, Dhodhapkar *et al* reported that antisyndecan-I mAb coating of myeloma cells promoted cross presentation of TA to T cells by DC, in a series of *in vitro* co-culture experiments [239]. In 2011, the group led by Robert L Ferris, extended these studies to the EGFR and ADCC setting by incubating the $EGFR^{+}$HLA-$A*02^{-}$ HNSCC cell line PCI-15B (Tu) with cetuximab, NK cells and HLA-$A*02^{+}$ DC. In addition to showing that NK cells activated by ADCC induced DC maturation, they assessed the IFNγ production of EGFR specific HLA-A*02 restricted $CD8^{+}$ T cells exposed to DC that had been co-cultured with NK cells and tumour cells. They established that NK-cell killing mediated by cetuximab promoted cross presentation of EGFR peptides by DC [96]. The Ferris group is, to date, the only group to present evidence that cetuximab mediated ADCC activation of NK cells promotes DC cross-presentation of antigens to T cells. They also noted that the frequency of EGFR specific T cells was significantly increased in cetuximab treated versus cetuximab naïve patients. This is important for two reasons: first it suggests that associated enhancement of adaptive immunity with mAb treatment may contribute to a clinical response. Second it confirms the clinical response by providing evidence for detectible EGFR-specific T cells, in agreement with a previous study by Schuler *et al* (2011) [240].

1.13.1. T-cell immunity: intra- and inter-molecular epitope spreading

Typically, a T-cell response to an antigenic protein is focused on one or two epitopes within the protein, which are termed dominant. Immunodominance occurs in part because of the individual HLA-type peptide binding preferences detailed in section 1.7.4, but also because of any marked bias in the processing or presentation of a protein. If, for example, the conformation or tertiary structure of an antigen dictates that some parts of the protein are more easily accessible than others, then these parts will be preferentially targeted for antigen processing. The diversification

of epitope specificity from the initial focused dominant epitope to subdominant epitopes within the protein was first described in an autoimmunity setting by Lehman *et al* as an example of intra-molecular epitope spreading; and can occur for the same reasons as dominant epitopes [241, 242]. Interestingly, intra-epitope spreading has been seen in cases of clinical responders to peptide vaccines in clinical trials involving patients with melanoma [243].

Furthermore, when the targeting of a TA such as EGFR induces NK cell-mediated lysis of tumour cells, other antigens such as carcino-embryonic antigen (CEA), present in lysis particulates are also phagocytosed by DC and presented to T cells. This is known as inter-epitope spreading. The EGFR targeting experiments by the Ferris group showed that the DC matured by anti-EGFR mAb-activated NK cells not only enhance cross-presentation to EGFR specific CD8+ T cells but also cross-present another antigen, melanoma antigen III (MAGE-3) to $CD8^{+}$ T cells in HNSCC patients [97]. The concept of epitope spreading is illustrated in Figure 1.11.

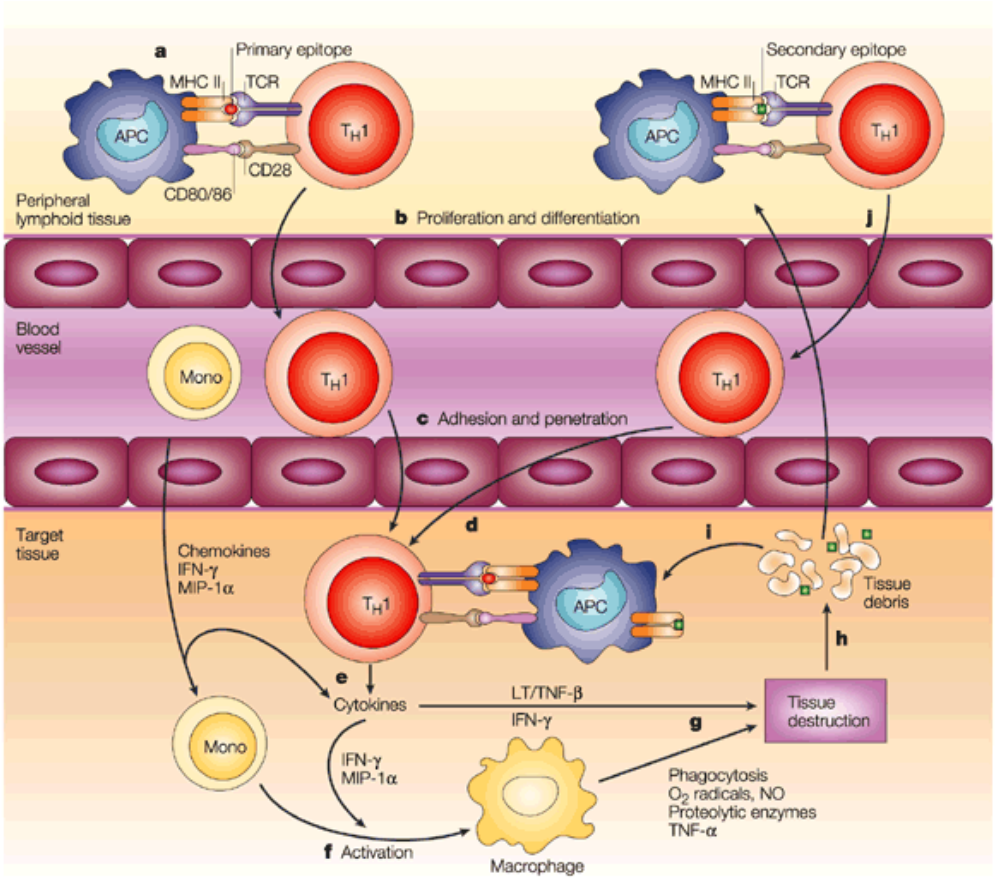

Figure 1.11. Schematic representation of the concept of epitope spreading
Adapted from Vanderlugt and Miller, 2012 [244]

The anti-EGFR mAbs used in this study are detailed in Table 1.2.

Table 1.2. Details of the anti-EGFR mAbs used in this study

mAb	Type	Parental mAb CDR	Target Epitope	Framework	Manufacture
Panitumumab (Vectibix®)	Human IgG2	Clone E7.6.3 (derived from A431 cells)	**EGFR ECD-3** 386-391	Human CDRs Human V_H and V_L Human C regions	Transgenic mouse strains created by introducing human Ig genes into mice engineered to lack functional mouse Ig genes. XenoMouse then immunized with A431 cells [245].
Cetuximab (Erbitux®)	Chimeric IgG1	M225 (mouse)	**EGFR ECD-3** 408-468	Murine CDRs Murine V_H and V_L Human C regions	BALB/c mice immunised with A431 [246]. RNA from hybridomas used to make chimeric gene constructs comprising M225 variable regions and human constant regions (designated IMC-C225); subsequently transfected into CHO cells for mAb production [247].
Imgatuzumab (GA201, RO5083945, RG7160)	Humanised IgG1	ICR62 (rat)	**EGFR ECD-3** Unmapped*	Rat CDRs Human V_H and V_L Human C regions	CBH/cbi rats immunised with MDA-MB.468 breast cancer cells producing clone ICR62 [248]. Humanised gene construct synthesised [249]. CHO cells transfected to produce both mAb and GnTIII enzyme to catalyse afucosylation [205, 221].

Table Key
ECD - extracellular domain
CDR - complementarity determining region
V_H - variable heavy chain
V_L - variable light chain
Ig - Immunoglobulin

* Imgatuzumab epitope not specifically mapped, however documented distinct from cetuximab and panitumumab [205].

1.14. CD20^{+} cancers

CD20 is selectively expressed on the surface of both normal and malignant B cells, but absent on plasma B cells. Although much has been learned about its structure, its function is still poorly characterised and its natural ligand unknown. CD20 is a small transmembrane protein with multiple hydrophobic regions that confer the remarkable ability to pass through the cell membrane four times. The N- and C-termini located in the cytoplasm are serine and threonine rich, housing multiple consensus sequences for phosphorylation. Only a small portion of the molecule is exposed at the cell surface and it is currently suggested that CD20 regulates transmembrane Ca^{2+} conductance and initiates intracellular signals that modulate cell growth and differentiation [250].

The distinct stages of B-cell development have been associated with B-cell malignancies. Chromosomal translocations and gene mutations are frequently involved in these neoplasms, and additional genetic aberrations such as hyperploidy and aneuploidy are also important contributors to the disease phenotypes. B-cell acute lymphocytic leukaemias (B-ALLs) arising from pre-B cells usually involve the BCR–ABL translocation or mutations affecting one or more of the following genes: runt-related transcription factor 1 (RUNX1), pre-B cell leukaemia homeobox 1 (PBX1), mixed-lineage leukaemia (MLL), protein tyrosine phosphatase non-receptor type 11 (PTPN11) and RAS. These transforming events do not affect resting small pre-B cells which undergo light-chain gene rearrangement, but rather the rapidly proliferating large pre-B cells[d].

The diversity of GC-derived lymphomas parallels the diversity of this dynamic compartment. Follicular lymphoma, diffuse large B cell lymphoma (DLBCL) and Burkitt's lymphoma are all derived from GC B cells. Multiple myeloma (MM) is a GC-derived plasma cell malignancy that is dependent on stromal cell contact and cytokines such as IL-6. Thus MM persists in the bone marrow. In some types of B-cell malignancy there is evidence that continual BCR signalling is required for malignant-cell survival and progression [251, 252].

---

[d] Several types of lymphoma arise from differentiated subsets of mature B cells in the secondary lymphoid organs. B-cell chronic lymphocytic leukaemia (B-CLL) is an indolent malignancy and an unmutated type of B-CLL is derived from mature CD5-positive B cells. Mantle cell lymphomas (MCL) arise from differentiated subsets of mature B cells in the secondary lymphoid organs. Splenic marginal zone lymphoma (SMZL) and mucosa-associated lymphoid tissue (MALT) lymphoma are indolent malignancies derived from marginal zone B cells [197].

1.14.1. Anti-CD20 mAbs in the treatment of CD20^{+} cancers

Since expression of the CD20 glycoprotein is tightly restricted to the surface of B-cells it is therefore a favoured target for therapy in malignant lymphoma and other B-cell malignancies [253]. In 1997, the anti-CD20 IgG-I chimeric mAb rituximab was approved for use in non-Hodgkin lymphoma (NHL) and demonstrated promising clinical activity. However, early trials in chronic lymphocytic leukaemia (CLL) showed only a modest 12% ORR with rituximAb as a single agent. This ORR dramatically increased to 95% with rituximab in combination with standard fludarabine and cyclophosphamide chemotherapy, findings that eventually revolutionised CLL treatment [254]. Despite these impressive statistics, some CLL patients fail to respond to rituximab therapy, and relapse rates are high in those who do initially respond to treatment [253]. The F/F allelic variant of CD16 has been correlated with poor clinical responses to rituximAb [255], thus, strategies to enhance efficacy of anti-CD20 mAb therapy have been sought.

1.14.2. Anti-CD20 mAb enhancements: Obinutuzumab (GA101GE)

Obinutuzumab (GA101GE) is a glyco-engineered anti-CD20 mAb with superior efficacy to rituximab in terms of CD16 affinity and NK-cell mediated ADCC [232, 253], that has recently received US approval as a first line CLL treatment in combination with the chemotherapeutic agent chlorambucil [233]. Anti-CD20 mAbs have been classified into two subtypes based on antigen-binding properties and mechanism of action. Type I mAbs like rituximab elicit CDC activation and redistribute CD20 into membrane lipid rafts. Type II mAbs like obinutuzumab do not stabilise CD20 redistribution, and have minimal CDC potential. However, they exhibit direct tumoural effects and increased ADCC. GA101GE was approved for use by the European Medical Association (EMA) based on the results of the CLL11 clinical trial (reported by Goede *et al*) [256]. The study was designed to compare the efficacy of GA101GE plus chlorambucil to rituximab plus chlorambucil or chlorambucil alone in CLL patients with significant co-morbidities. Although both mAbs showed significant increases in PFS and OS, the inclusion of GA101GE yielded a significant increase in PFS when compared to rituximab [256]. Notably however, despite promising preclinical activity; subsequent studies in DLBCL patients did not support the findings of the CLL11 study [257, 258]. Vitolo *et al* reported that there were no significant differences in PFS for patients administered GA101GE plus cyclophosphamide, doxorubicin, vincristine, and prednisone (G-CHOP) or rituximab plus CHOP (R-CHOP). This was despite patients receiving GA101GE at higher doses than rituximab (1000mg and 375mg/m^2 respectively - i.v. every 21 days for 8

cycles), and receiving two additional infusions of GA101GE on days 8 and 15 of cycle 1, that were not included in the rituximab treatment arm [258, 259]. This disparity provides further rationale for investigating the underlying immune cell mechanisms involved in sustained tumour clearance in a wide variety of $CD20^+$ tumour types.

The anti-CD20 mAbs used in this study are detailed in Table 1.3.

Table 1.3. Details of the anti-CD20 mAbs used in this study

mAb	Type	Parental mAb CDR	Target Epitope	Framework	Manufacture
Rituximab (mAbThera, Rituxan)	Chimeric IgG1	2B8 (mouse)	CD20 Large EC loop 168-175	Murine CDRs Murine V_H and V_L Human C regions	BALB/c mice immunised with human lymphoblastoid cell line SB-2 (derived from 11 year old boy with lymphosarcoma) [260]. RNA from hybridomas used to make chimeric gene constructs comprising 2B8 variable regions and human constant regions (designated IDEC-2B8); subsequently transfected into CHO cells for antibody production [261].
Obinutuzumab (GA101GE, Gazyva®, Gazyvaro®)	Humanised IgG1	B-Ly1 (mouse)	CD20 Large EC loop 172-178	Murine CDRs Human V_H and V_L Human C regions	Immunised BALB/c mice produce clone B-Ly1 [262]. Humanised gene construct synthesised [249]. CHO cells transfected to produce both mAb and GnTIII enzyme to catalyse afucosylation [221, 232].
GA101WT	Humanised IgG1	B-Ly1 (mouse)	CD20 Large EC loop 172-178	Murine CDRs Human V_H and V_L Human C regions	Immunised BALB/c mice produce clone B-Ly1 [262]. Humanised gene construct synthesised [249]. CHO cells transfected to produce mAb [232].

Table Key
EC - extracellular
CDR - complementarity determining region
V_H - variable heavy chain
V_L - variable light chain
Ig - Immunoglubulin

1.15. Hypothesis, specific aims and experimental model

Previous studies have shown therapeutic mAbs that mediate ADCC can also promote the NK:DC cross-talk that stimulates TA-specific $CD8^+$ T cell immunity [97, 263]. GE mAbs have been developed that exhibit enhanced ADCC compared with conventional therapeutic mAbs [205, 232]. In this study, the potential for GE mAbs to promote anti-tumour adaptive cellular immunity was assessed and compared with conventional therapeutic mAbs.

1.15.1. Hypothesis

GE-mAbs induce NK-cell activity that promotes DC to phagocytose TA, undergo maturation and cross present TA to TA-specific $CD8^+$ T cells.

1.15.2. Study aims

The hypothesis was tested by addressing the following research questions:

1. Does GE-mAb-mediated ADCC induce NK-cell activation and function associated with promoting adaptive cellular immunity?
2. Are GE-mAbs able to induce DC phagocytosis of TA and promote DC maturation?
3. Do GE-mAbs promote DC cross presentation of TA to TA-specific $CD8^+$ T cells?

1.15.3. Experimental model

Interactions between tumour cells and highly purified (>90%) NK cells, DC and $CD8^+$ T cells in the presence of unmodified or GE-mAbs were assessed using the *in vitro* co-culture model illustrated in Figure 1.12. To study cross presentation, HLA-A*02$^-$ tumour cells were used with HLA-A*02$^+$ NK cells, DC and $CD8^+$ T cells. NK-cell mediated lysis of tumour cells will release particulate antigen for uptake by DC and presentation of HLA-A*02-restricted peptides to HLA-A*02$^+$ TA-specific $CD8^+$ T cells. The HLA mismatch between tumour cells and $CD8^+$ T cells allows for the assessment of cross presentation of TA by DC to HLA-A*02 restricted T cells because the HLA-A*02$^-$ tumour cells cannot be directly recognised by the HLA-A*02$^+$ T cells.

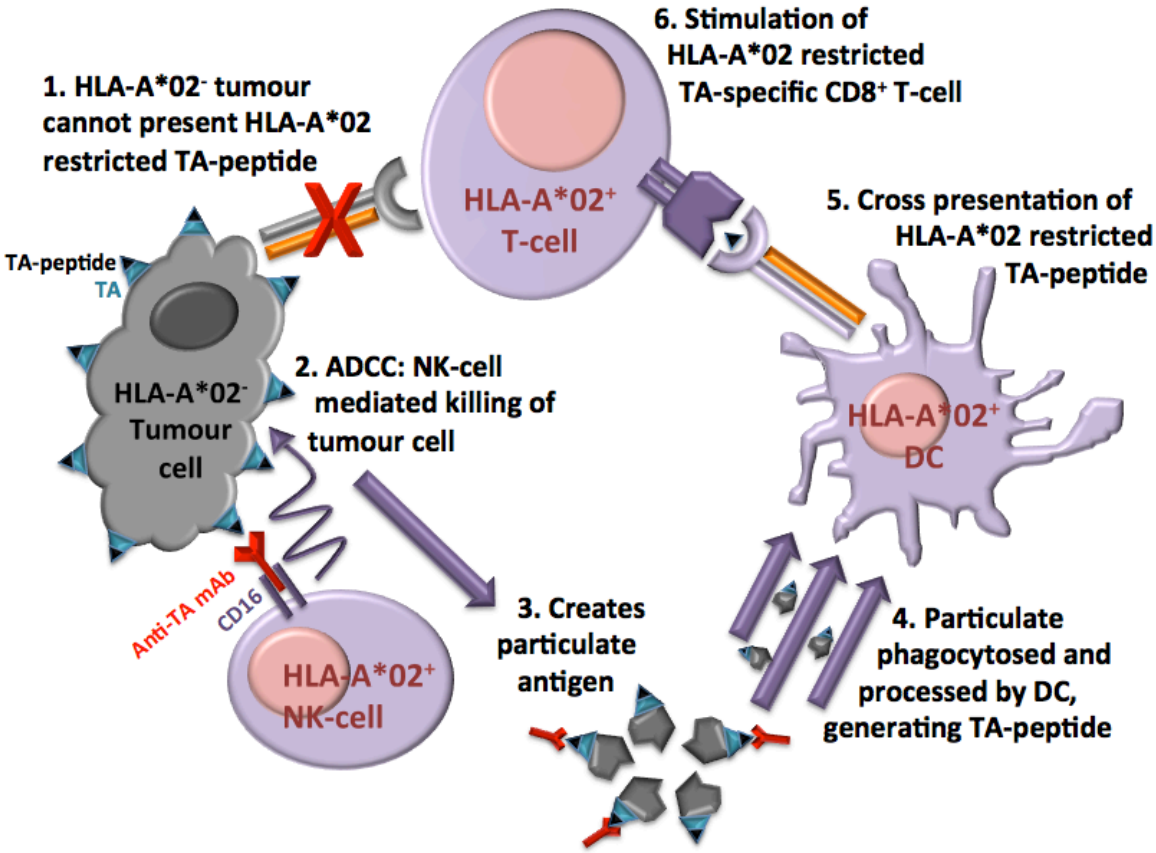

Figure 1.12. Schematic representation of experimental model
Used to evaluate interactions between tumour cells, NK cells, DC and $CD8^+$ T cells, in the presence of unmodified or GE-mAbs

Chapter 2. Materials and Methods

The products and reagents used in this study are detailed in Table 2.1 with supplier information indicated. When combinations of reagents were used to make a solution (w/v or v/v), the composition has been described and an abbreviated name for the composition is used thereafter.

2.1. Products and reagents

2.1.1. Media, buffers and solutions

Complete DMEM: comprised Dulbecco's Modified Eagle Medium supplemented with 10% heat inactivated foetal bovine serum (FBS), 100IU/ml penicillin and 100mg/ml streptomycin (PS).

Complete RPMI: comprised Roswell Park Memorial Institute^{1640} (RPMI) Medium supplemented with 10% heat inactivated FBS and PS.

Complete RPMI and complete DMEM were 0.22μM filtered before use.

Cytokines: were reconstituted according to manufacturer instructions, diluted to working concentrations and frozen at -20°C in single use aliquots.

DAPI solution: comprised PBS^{+} supplemented with 0.25μg/ml 4',6-diamidino-2-phenylindole, dihydrochloride (DAPI).

DC Differentiation Medium I (DCD_1): comprised complete RPMI supplemented with 1000IU/ml IL-4 and 1000IU/ml GMCSF.

DC Differentiation Medium II (DCD_2): comprised CellGro DC Medium supplemented with 1% "Off The Clot" human AB serum (hAB); 10ng/ml IL-4 and 800IU/ml GMCSF.

DC Differentiation Medium III (DCD_3): comprised CellGro supplemented with 1% hAB; 10ng/ml IL-4 and 1600IU/ml GMCSF. DCD_2/D_3 were as described by Wolfl and Greenberg (2014) [264].

DC Maturation Medium I (DCM_1): comprised complete RPMI supplemented with 10ng/ml IL-1β; 1000IU/ml IL-6; 1μg/ml PGE_2 and 10ng/ml TNFα. Adapted from protocols stipulated by Dauer *et al* [265].

DC Maturation Medium II (DCM_2): comprised complete RPMI supplemented with 25ng/ml IL-1β; 25ng/ml Poly I:C; 5500IU/ml TNFα; 1000IU/ml IFNγ and 3000IU/ml IFNα as described by López-Albaitero *et al* [266].

DC Maturation Medium III (DCM_3): comprised CellGro supplemented with 1% hAB; 10ng/ml LPS and 100IU/ml IFNγ as described by Wolfl and Greenberg (2014) [264].

Fluorescence Activated Cell Sorting (FACS) Buffer: comprised PBS^+ supplemented with 2.5% FBS and 0.1% (w/v) sodium azide (NaN_3).

Lysogen broth (LB) agar plates: comprised 20g/L LB agar in dH_2O, supplemented with 30µg/ml kanamycin.

LB Medium: comprised 15g/L LB agar, 10g/L sodium chloride ($NaCL_2$), 5g/L yeast and 10g/L tryptone in deionised water (dH_2O).

Magnetic Activated Cell Sorting (MACS) Buffer: comprised PBS^+, 2mM ethylenediaminetetraacetic acid (EDTA) and 0.5% bovine serum albumin (BSA) was kindly donated by King's College London (KCL - London, UK) tissue bank staff.

NK-cell Recovery Medium (NKRM): comprised complete RPMI supplemented with 50IU/ml IL-2

PBS^+ and **PBS^-:** Phosphate Buffered Saline with or without 1mM calcium chloride ($CaCl^2$) and magnesium chloride ($MgCl^2$) supplementation.

Peptides: were reconstituted in dimethyl sulfoxide (DMSO) to a stock concentration of 20mg/ml. Stock and working dilutions were frozen at -20°C in single use aliquots.

pHrodo Red Succinimydyl Ester (pHrodo-SE): was reconstituted in DMSO to a stock concentration of 1mg/ml and frozen at -20°C in single use aliquots.

T-cell Recovery Medium (TcRM): comprised CellGro supplemented with 5% hAB; 5ng/ml IL-7.

T-cell Stimulation Medium - Day Zero ($TcSM_0$): comprised CellGro supplemented with 5% hAB and 30ng/ml IL-21.

T-cell Stimulation Medium - I ($TcSM_1$): comprised CellGro supplemented with 5% hAB and 5ng/ml IL-7 and IL-15.

T-cell Stimulation Medium - II ($TcSM_2$): comprised CellGro supplemented with 5% hAB and 10ng/ml IL-7 and IL-15.

TcRM, $TcSM_0$, $TcSM_1$ and $TcSM_2$ were as described by Wolfl and Greenberg (2014) [264]

T-cell Stimulation Medium - III ($TcSM_3$): comprised X-Vivo15 medium supplemented with 5ng/ml IL7

T-cell Stimulation Medium - III ($TcSM_4$): comprised X-Vivo15 medium supplemented with 10ng/ml IL-2 and IL7

Triton Solution (0.1%): comprised PBS^+ supplemented with 0.1% Triton X-100.

Trypsinisation Buffer: comprised 10x Trypsin/EDTA diluted 1:9 in PBS^- to give a 1x Trypsin/EDTA solution.

Table 2.1. Summary of products and reagents used in this study

	Product	Catalogue No.	Supplier
Reagents	"Off the Clot" Human AB serum	ACCM-112-HIS	SeraLab, UK
	10x Tris-Acetate-EDTA (TAE) Buffer	T9650	Sigma-Aldrich - Dorset, UK
	6x Loading Dye	R0611	ThermoFisher - Paisley, UK
	Agarose Powder	A5304	Sigma-Aldrich - Dorset, UK
	BD Cytofix	554655	BD Biosciences - Oxford, UK
	BD Cytoperm	554723	BD Biosciences - Oxford, UK
	Brefeldin	B5936	Sigma-Aldrich - Dorset, UK
	CellGro DC Medium	0020801-0500	CellGenix - Germany
	CompBeadPLUS	560497	BD Biosciences - Oxford, UK
	CST Beads	642412	BD Biosciences - Oxford, UK
	DAPI	40835	CellSignallingTechnology - UK
	Dulbecco's Modified Eagle Medium	D5796	Sigma-Aldrich - Dorset, UK
	Dulbecco's Phosphate Buffered Saline with$^{Ca/Mg}$	D8662	Sigma-Aldrich - Dorset, UK
	Dulbecco's Phosphate Buffered Saline without$^{Ca/Mg}$	D8537	Sigma-Aldrich - Dorset, UK
	Ethidium Bromide	E1510	Sigma-Aldrich - Dorset, UK
	Ficoll-Paque PLUS	17-1440-03	GE Healthcare - UK
	Goat Anti-Rabbit AF647 2°	ab150083	AbCam - Cambridge, UK
	Heat Inactivated Foetal Bovine Serum (FBS)	10500-064	Gibco, London, UK
	Ionomycin	I0634	Sigma-Aldrich - Dorset, UK
	Kanamycin	K1377	Sigma-Aldrich - Dorset, UK
	LB Agar	A5306	Sigma-Aldrich - Dorset, UK
	Leukocyte Activation Cocktail (LAC)	550583	BD Biosciences - Oxford, UK
	Lipopolysaccharide (LPS)	L4391-1MG	Sigma-Aldrich - Dorset, UK
	Monensin	M5273	Sigma-Aldrich - Dorset, UK
	Mounting Medium	345789	Merck Millipore - UK
	Nuclease Free Water	AM9938	ThermoFisher - Paisley, UK
	O'gene Ruler DNA ladder	SM0333	ThermoFisher - Paisley, UK
	Penicillin-Streptomycin	P4333	Sigma-Aldrich - Dorset, UK
	PGE_2	TOCRIS 2296	R&D, London, UK
	pHrodo Red Succinimidyl Ester	P36600	ThermoFisher - Paisley, UK
	Plasmocin	ant-mpt	Source Bioscience - UK
	PMA	P8139	Sigma-Aldrich - Dorset, UK
	Polyinosinic:polycytidylic acid (Poly:IC)	P9582	Sigma-Aldrich - Dorset, UK
	Puromycin	sc-108071	SantaCruz Bio - Germany
	Rabbit Anti-MelanA 1°	ab51061	AbCam - Cambridge, UK
	Roswell Park Memorial Institute^{1640} Medium (RPMI)	R8758	Sigma-Aldrich - Dorset, UK
	Super Optimal Broth with Catabolite Repression (SOC)	15544-034	ThermoFisher - Paisley, UK
	Synth-a-Freeze Cryopreservation Medium	A12542-01	Gibco, London, UK
	TaqMan Genotyping MasterMix	4371353	ThermoFisher - Paisley, UK
	Total Immunoglobulin G (IgG)	I4506	Sigma-Aldrich - Dorset, UK
	Trypan Blue	T8154	Sigma-Aldrich - Dorset, UK
	Trypsin-EDTA 10x Solution	T4174	Sigma-Aldrich - Dorset, UK
	UltraComp antibody capture beads	01-2222-42	eBioscience - Wycombe, UK
	X-Vivo 15 Medium	LZBE04-418F	Lonza, UK
	Yeast	288620	BD Biosciences - Oxford, UK
Kits	Apoptosis Inducer Set	BV-K121-9	Caltag Medsystems - UK
	Dead Cell Removal kit	130-090-101	Miltenyi Biotec - Surrey, UK
	DNA Blood Mini Kit	51104	Qiagen - Manchester, UK
	DNA Maxi-Prep Kit	12662	
	EZ-PCR Mycoplasma Test Kit	20-700-20	Biological Industries, Israel
	FITC Annexin V Apoptosis Detection Kit with PI	640914	BioLegend - London, UK
	Human CD45RO+ Cell Isolation Kit	130-046-001	Miltenyi Biotec - Surrey, UK
	Human CD57+ Cell Isolation Kit	130-092-073	Miltenyi Biotec - Surrey, UK
	Human CD8+ T-cell Isolation Kit	130-094-156	Miltenyi Biotec - Surrey, UK
	Human Monocyte Isolation Kit II	130-091-153	Miltenyi Biotec - Surrey, UK
	Human NK-cell Isolation Kit	130-092-657	Miltenyi Biotec - Surrey, UK
	K2 Transfection Kit	T060-8.0	Biontex - Munich, Germany
	TaqMan SNP Genotyping Assay: rs396991	4351379	Thermofisher - Paisley, UK
Therapeutic monoclonal antibodies	Cetuximab GA101-WT Imgatuzumab (GA201GE) Obinutuzumab (GA101GE) Panitumumab Rituximab		Provided by Roche-Glycart Basel, Switzerland

Fluorochrome-conjugated antibodies (mouse anti-human)	CD107a APC	328620	BioLegend - London, UK
	CD11c FITC	301604	BioLegend - London, UK
	CD11c PerCP/Cy5.5	301624	BioLegend - London, UK
	CD137 APC	309810	BioLegend - London, UK
	CD14 PB	301828	BioLegend - London, UK
	CD16 APC-H7	560195	BD Biosciences - Oxford, UK
	CD19 PB	302232	BioLegend - London, UK
	CD20 PB	302328	BioLegend - London, UK
	CD20 PE	302305	BioLegend - London, UK
	CD3 PE/Cy7	317334	BioLegend - London, UK
	CD4 APC	317416	BioLegend - London, UK
	CD56 PB	304629	BioLegend - London, UK
	CD56 PE	318306	BioLegend - London, UK
	CD69 FITC	310904	BioLegend - London, UK
	CD71 APC/Cy7	334110	BioLegend - London, UK
	CD8 PerCP/Cy5.5	344710	BioLegend - London, UK
	CD80 PE	305208	BioLegend - London, UK
	CD83 PECy7	305326	BioLegend - London, UK
	CD86 APC	305412	BioLegend - London, UK
	EGFR PE	352903	BioLegend - London, UK
	HLA-A2 PE	343306	BioLegend - London, UK
	HLA-DR FITC	307604	BioLegend - London, UK
	IFNγ FITC	506518	BD Biosciences - Oxford, UK
	TNFα AF700	56-7349-42	eBioscience - Wycombe, UK
Viability dyes	Live/Dead Aqua	L34957	Invitrogen, Paisley, UK
	Live/Dead Zombie Violet	423113	BioLegend - London, UK
MHC multimers	CD20 Pentamer-PE	F1056-2A-G	ProImmune - Oxford, UK
	CMV Pentamer-PE	F008-2B-G	ProImmune - Oxford, UK
	EGFR Pentamers-PE	F2A-G CUSTOM	ProImmune - Oxford, UK
	Flu Pentamer-PE	F007-2A-G	ProImmune - Oxford, UK
	MelanA Dextramer-PE	WB2162-PE	Immudex - Denmark
Peptides	CD20 Peptide	PC0AF-G-	ProImmune - Oxford, UK
	CMV Peptide	aa sequence*	ProImmune - Oxford, UK
	EGFR Peptides		ProImmune - Oxford, UK
	Flu Peptide		ProImmune - Oxford, UK
	MelanA Peptide		ProImmune - Oxford, UK
Cytokines (recombinant human)	GMCSF	300-03	Peprotech, London UK
	IFNα	300-02A	Peprotech, London UK
	IFNγ	300-02	Peprotech, London UK
	IL-1β	200-01B	Peprotech, London UK
	IL-2	200-02	Peprotech, London UK
	IL-4	200-04	Peprotech, London UK
	IL-6	200-06	Peprotech, London UK
	IL-7	200-07	Peprotech, London UK
	IL-15	200-15	Peprotech, London UK
	IL-21	200-21	Peprotech, London UK
	TNFα	130-094-017	Miltenyi Biotech - Surrey, UK
Cell lines	A431	CRL-1555	ATCC/LGC - Teddington, UK
	H1299 (WT and $EGFR^{LOW/MEDIUM/HIGH}$)	-	Donated
	JY	-	Donated
	K562	CCL-243	ATCC/LGC - Teddington, UK
	SK-MEL-30	ACC-151	DSMZ - Germany
	T2	-	Donated
Consumables	1.5ml Microfuge Tubes	616201	Greiner Bio - Stonehouse, UK
	75cm^2 Tissue Culture Treated Flask	315361	Greiner Bio - Stonehouse, UK
	96-well V-bottomed Plates	651101	Greiner Bio - Stonehouse, UK
	LD MACS Column	130-042-901	Miltenyi Biotech - Surrey, UK
	LS MACS Column	130-042-401	Miltenyi Biotech - Surrey, UK
	MicroAmp Fast Plates	4346907	ThermoFisher - Paisley, UK
	MicroAmp Optical Adhesive Film	4360954	ThermoFisher - Paisley, UK

TABLE KEY

1°	Primary antibody	**FITC**	Fluorescein isothiocyanate
2°	Secondary antibody	**GMCSF**	Granulocyte macrophage colony-stimulating factor
AF	Alexa fluor	**H7**	Cyanine7 analogue
APC	Allophycocyanin	**IF**	Interferon
BV421	Brilliant violet 421	**IL**	Interleukin
Ca/Mg	Calcium/Magnesium	**PB**	Pacific blue
CD	Cluster of differentiation	**PE**	R-phycoerythrin
Cy7	Cyanine 7	**PerCP/Cy5.5**	Peridinin-chlorophyll/cyanine 5.5
DAPI	4',6-diamidino-2-phenylindole	**TNF**	Tumour necrosis factor
EDTA	Ethylenediaminetetraacetic acid		

*Peptide aa sequences detailed in Table 2.5

2.1.2. Therapeutic mAbs

The mAbs and stock concentrations detailed in Table 2.2 were provided by Roche Glycart (Basel, Switzerland). Concentrations were determined by measuring absorbance at 280nm (A_{280}) on a NanoDrop spectrophotometer (ThermoFisher) utilising calculated antibody-specific extinction coefficients [267, 268]. The average of three readings is displayed for stock and diluted samples.

Table 2.2. Summary details of mAbs used in this study

mAb	Stock concentration	A_{280} Pre dilution	A_{280} Diluted: 1:2	A_{280} Diluted: 1mg/ml	Manufacturer /Distributor
Panitumumab (Vectibix®)	10mg/ml	10.34	5.16	1.02	Amgen Inc
Cetuximab (Erbitux®)	4mg/ml	4.24	2.21	1.01	Merck
Imgatuzumab (GA201, RO5083945, RG7160)	25mg/ml	25.81	12.83	0.99	Roche Glycart AG
Rituximab (mAbThera, Rituxan)	10mg/ml	10.04	5.00	1.04	Hoffmann-La Roche
GA101WT	8mg/ml	8.45	4.29	1.03	Roche Glycart AG
Obinutuzumab (GA101GE, Gazyva®, Gazyvaro®)	25mg/ml	25.97	12.85	0.99	Roche Glycart AG

2.2. Cell lines

All cell lines were handled aseptically in containment level two microbiological safety cabinets and grown in standard vented 75cm^2 tissue culture treated flasks. Cells were incubated at 37°C in 5% carbon dioxide (CO_2). Supplier details can be found in Table 2.1 and specific cell culture requirements are described below.

2.2.1. A431

A431 cells were derived from the vulval carcinoma of an 85-year-old female [236]. The cells expressed very high levels of EGFR (confirmed by flow cytometry, see Figure 3.2). Cells were maintained in either complete DMEM or complete RPMI, with a minimum of 2 passages per week when cells reached approximately 80% confluence. As an adherent cell line, A431 required trypsinisation to obtain a cell suspension. Briefly, A431 cells were washed twice in PBS$^-$ and incubated with 5ml trypsinisation buffer for 10-15 minutes at 37°C; with regular checks to determine adherent status. When all cells were in suspension, trypsinisation buffer was neutralised with an equal volume of complete RPMI, centrifuged at 300g_{max} for 5 minutes and resuspended in appropriate medium to be counted and reseeded at desired concentration.

2.2.2. H1299

H1299 cells were derived from the NSCLC lymph node metastasis of a 43 year old male patient [269] and were confirmed as expressing HLA-A*02 by flow cytometry. As an adherent cell line, H1299 required trypsinisation to obtain a cell suspension, as described for A431. H1299 cells that had been transfected to express various levels of EGFR were kindly provided by Professor Mahvash Tavassoli (KCL - London, UK) and are hereafter referred to as H1299^{LOW}, H1299^{MEDIUM} and H1299^{HIGH}.

2.2.3. JY

JY is an Epstein–Barr virus (EBV) transformed B cell lymphoblastoid cell line, first characterised by Terhorst *et al* as expressing CD20, HLA-A*02:01 and class-II HLA-DR [270] and known to form aggregates in suspension culture. JY cells were kindly donated by Dr Linda Barber (KCL - London, UK) and maintained in suspension culture in complete RPMI, with a minimum of 2 passages per week at a cell density approximately 10 times greater than initial seeding density (or

when medium was spent). Before use in assays, dead cells were removed from JY cultures as described in section 2.18.

2.2.4. K562

K562 is an undifferentiated human erythroleukaemic, BCR:ABL fusion gene positive (Philadelphia$^+$) cell line, derived from a 53-year-old female chronic myeloid leukaemia (CML) patient in blast crisis [237]. Importantly, the cells are devoid of MHC-I and thus served as a classical target for NK cells. It is well established that K562 cells are highly sensitive to NK-cell killing [271]. K562 were maintained in suspension culture in complete RPMI, with a minimum of 2 passages per week at a cell density approximately 10 times greater than initial seeding density (or when medium was spent).

2.2.5. SK-MEL-30

SK-MEL-30 is a melanoma cell line reported to exhibit medium to high levels of the MelanA transcript and protein [272], and additionally characterised by Letsch *et al* as expressing HLA-A*02 [273] (MelanA protein and HLA-A*02 expression was confirmed by flow cytometry). Cells were maintained in complete RPMI, with a minimum of 2 passages per week when cells reached approximately 80% confluence. As an adherent cell line, SK-MEL-30 required trypsinisation to obtain a cell suspension, as described for A431.

2.2.6. T2

T2 cells were derived from the EBV transformed B-cell lymphoblastoid cell line 721.174 [274, 275]. The cells are deficient in TAP and therefore unable to transport endogenous processed peptides generated in the cytosol to the site of MHC-I loading in the ER. Consequently T2 MHC-I cannot present peptides derived from cytosolic antigens and therefore MHC-I is not stably expressed at the cell surface. The HLA-A*02:01 molecules expressed by T2 cells can be stabilised by culture with exogenous provision of HLA-A*02:01 restricted peptide, and is used as an assay to assess peptide binding. T2 cells were kindly donated by Dr Linda Barber (KCL - London, UK) and maintained in suspension culture in complete RPMI, with a minimum of 2 passages per week at a cell density approximately 10 times greater than initial seeding density (or when medium was spent).

2.3. Mycoplasma testing

Cell lines were tested monthly for mycoplasma contamination or more frequently when necessary. The procedure involved polymerase chain reaction (PCR) amplification of genus and species-specific mycoplasmal 16S ribosomal RNA sequences naturally present in high copy numbers in contaminated cultures [276]. The PCR reaction was set up according to the protocol provided within the EZ-PCR Mycoplasma Test Kit (Biological Industries, Israel). Briefly, 5mls of supernatant was removed from confluent cell cultures and centrifuged at $300g_{max}$ for 5 minutes to pellet any cellular debris. 1ml of the resulting supernatant was transferred to a sterile 1.5ml capped microfuge tube and centrifuged at $16,500g_{max}$ for 10 minutes, to sediment mycoplasma. After carefully decanting the supernatant, the micro-pellet was resuspended in 25µl of the Sample Buffer Solution provided and heated to 95°C for 3 minutes. Reaction mixtures were then prepared in PCR tubes according to Table 2.2 and the PCR was performed in a Veriti® Thermal Cycler (Applied Biosystems - Paisley, UK) according to the conditions detailed in Table 2.3. Substituting the sample with either template DNA provided in the kit or fresh culture medium served as a positive or negative control respectively.

Table 2.3. EZ-PCR mycoplasma test reaction mixture preparation

Reagent	**Volume (µl)**
Molecular Biology Grade H_20	17.5
Reaction Mix	5
Test Sample	2.5
Total Volume	**25µl**

Table 2.4. EZ-PCR mycoplasma test thermal cycling conditions

Temperature (°C)	**Time (seconds)**	**Cycles**
94	30	1
94	30	35
60	120	
72	60	
94	30	1
60	120	1
72	300	1
4	∞	∞

2.4. Agarose gel electrophoresis

Electrophoresis was used to separate PCR amplified products in an agarose gel for determination of molecular weight by subsequent comparison to a standardized DNA ladder. The agarose gel was made by adding agarose powder to 1x Tris Acetate-EDTA (TAE) buffer at 2% w/v. The agarose was carefully dissolved in a microwave with intermittent power and stirred until transparent and free of bubbles. After cooling to a temperature of approximately 50°C, 6µl of ethidium bromide (10mg/ml stock) was added per 100ml of solution. The gel was then poured into a casting tray with a comb inserted to create wells, and left to solidify for approximately 30 minutes. With comb removed, the gel and casting tray were placed into a gel rig and completely immersed in 1x TAE buffer. 10µl of O'Gene Ruler DNA Ladder (New England Biolabs, USA) was added to the first and last wells to enable fragment size determination and subsequently, the gel was loaded with a mixture containing 10µl of the PCR product and 2µl of 6x loading dye. A steady current of 100 volts was then applied to the gel for 1 hour. To enable fragment band comparison, the gel was carefully removed from the rig and casting tray and placed upon an ultra violet (UV) light box (UVP GelDoc-IT, UVP, Cambridge, UK). The gel was then photographed using the associated Polaroid camera. Mycoplasma contamination in samples was indicated by the presence of a PCR product with the same molecular weight as the positive control.

2.5. Elimination of mycoplasma from cell cultures

Cultures identified as positive for mycoplasma contamination and easily replaceable were immediately discarded. When cultures were irreplaceable, cells underwent a decontamination treatment regimen using the bactericidal agent Plasmocin^{TM} and a protocol adapted from Uphoff *et al*, 2012 [277]. Cells were cultured in a standard 75cm^3 tissue culture treated flask in complete RPMI supplemented with 25µg/ml Plasmocin^{TM}. Cells were seeded to reach 90% confluence within 2-3 days, with fresh treatment medium added at each passage. After a minimum of 14 days, treatment was removed and cells were cultured in RPMI supplemented with 10% (v/v) 0.22uM filtered, heat inactivated FBS without P/S. After at least 7 days growth in the absence of antibiotics, confluent culture supernatant was re-tested for mycoplasma contamination as described in sections 2.3 and 2.4.

2.6. Peripheral blood mononuclear cells

Peripheral blood leukophoresis, obtained as described by Dietz *et al* [278] was purchased from National Health Service Blood and Transplant (NHS-BT) in the form of anonymised leukocyte reduction chambers (hereafter referred to as leukocyte cones). Cells were recovered aseptically in a laminar hood (class II microbiological safety cabinets), as described by Néron *et al* [279] and peripheral blood mononuclear cells (PBMC) were isolated from the leukophoresis product by Ficoll-Paque density gradient centrifugation. Leukocyte cones were swabbed with 70% ethanol and contents were drained into sterile 50ml tubes. Cones were flushed with 20ml PBS^+, the eluate made to 35ml final volume with PBS^+ to give an approximate 1:3 dilution of the leukophoresis product, and then gently inverted to mix. A sterile 50ml tube containing 15ml of Ficoll-Paque (previously warmed to room temperature) was prepared and the diluted leukophoresis product was carefully layered onto the gradient. Tubes were centrifuged at $1000g_{max}$ with rapid acceleration and slow deceleration (no brake applied) for 20 minutes at room temperature (RT). Upon completion of centrifugation cycle, the clearly visible white PBMC layer (resembling a thick carpet of cells) was collected into a new sterile 50ml tube, topped up to 50ml with PBS^+ and washed twice, first at $250g_{max}$ for 10 minutes at RT and subsequently at $200g_{max}$ for 10 minutes at RT to facilitate platelet removal. Cells were resuspended in RPMI supplemented with P/S, and live cells counted via trypan blue exclusion. 10^5 live cells were removed to screen for expression of HLA-A*02 as described in section 2.18. Remaining cells were pelleted and cryopreserved in 1ml chilled synth-a-freeze freezing medium per $5x10^7$ live PBMC, with 1ml aliquoted to labelled cryovials and stored in a -80°C freezer within a chilled Nalgene (Nunc International, Hereford, UK) temperature controlled freezing vessel containing isopropanol. After 24 hours, the frozen vials were transferred to -196°C gaseous phase liquid nitrogen storage in our cryostore facility. Cells were retrieved from the cryostore on dry ice, thawed quickly at 37°C and added to prospective assay medium, drop-wise initially then at a quicker rate for counting and washing immediately prior to use.

2.7. Cell isolations

2.7.1. NK cells

The human NK-cell population was isolated from PBMC by negative selection via Miltenyi magnetic activated cell sorting (MACS) according to the protocol supplied within the NK-cell

Isolation Kit. Briefly, after collection of PBMC by centrifugation at $300g_{max}$ for 5 minutes, the cell pellet was resuspended in MACS buffer (40µl per 10^7 cells) and a cocktail of biotin-conjugated mAbs were added to label all non-NK cells (10µl per 10^7 cells). After a 5 minute incubation at 4°C, microbeads conjugated to anti-biotin mAbs were added (20µl per 10^7 cells) and incubated for a further 10 minutes at 4°C. This solution was made up to 1ml with MACS buffer and applied to a pre-washed LS MACS column. Non-NK cells were retained on the column and the eluted fraction, containing the negatively selected NK cells, was collected. Eluted NK cells were counted and 10^5 apportioned for isolated NK "time zero" phenotyping and purity assessment. The remainder were centrifuged at $300g_{max}$ for 5 minutes and resuspended at a concentration of 10^6 NK cells per ml in NKRM. NK cells were recovered for a minimum of 4 hours before use in subsequent processes.

2.7.2. Monocytes

2.7.2.1. Monocytes: MACS

The human monocyte population was isolated from PBMC by negative selection via Miltenyi MACS, according to the protocol supplied within Monocyte Isolation Kit II. Briefly, after collection of PBMC by centrifugation at $300g_{max}$ for 5 minutes, the cell pellet was resuspended in MACS buffer (30µl per 10^7 cells). An FcR blocking reagent was added and then a cocktail of biotin-conjugated mAbs to label all non-monocytes (both 10µl per 10^7 cells). After a 10 minute incubation at 4°C, microbeads conjugated to anti-biotin mAbs were added (20µl per 10^7 cells) and incubated for a further 15 minutes at 4°C. Cells were then washed once in 2mls of MACS buffer; the pellet was resuspended in 1ml MACS buffer and then applied to a pre-washed LS MACS column. Non-monocytes were retained on the column and the eluted fraction, containing the negatively selected monocytes, was collected on ice. Eluted monocytes were counted and 10^5 apportioned for isolated monocyte phenotyping and purity assessment. The remainder were centrifuged at $300g_{max}$ for 5 minutes and resuspended in appropriate media for subsequent processes.

2.7.2.2. Monocytes: plastic adherence

PBMC were plastic adhered in tissue culture treated 6-well plates for two hours. The cells were suspended in 2ml RPMI at concentrations of $1.18x10^6$-$1.98x10^6$ cells per cm^2. This cell seeding range was determined during several years of research and development for the Rayne Cell Therapy Suite (RCTS) adaptation of the Northwest Biotherapeutics DCVax®-L protocol

(unpublished commercial data). After 2 hours, non-adherent cells were gently washed thrice with 1ml of warm complete RPMI and either discarded in the case of isolated monocytes or frozen for later use as a source of NK cells. The remaining adherent monocytes were resuspended in appropriate media for subsequent processes.

2.7.3. $CD8^+$ T cells

The human $CD8^+$ T-cell population was isolated from PBMC by negative selection via Miltenyi MACS according to the protocol supplied within the $CD8^+$ T-cell Isolation Kit. Briefly, after collection of PBMC by centrifugation at $300g_{max}$ for 5 minutes, the cell pellet was resuspended in MACS buffer (40µl per 10^7 cells) and a cocktail of biotin-conjugated mAbs were added to label all non-$CD8^+$ T cells (10µl per 10^7 cells). After a 5 minute incubation at 4°C, microbeads conjugated to anti-biotin mAbs were added (20µl per 10^7 cells) and incubated for a further 10 minutes at 4°C. This solution was made up to 1ml with MACS buffer and applied to a pre-washed LS MACS column. Non-$CD8^+$ T cells were retained on the column and the eluted fraction, containing the, negatively selected $CD8^+$ T cells, was collected. Eluted $CD8^+$ T cells were counted and 10^5 apportioned to assess purity. The remainder were centrifuged at $300g_{max}$ for 5 minutes and resuspended in appropriate medium for subsequent processes.

2.7.4. Naïve $CD8^+$ T cells

To purify a human naïve T-cell population, $CD8^+$ T cells were first isolated from PBMC by negative selection as described above, then subsequently depleted of $CD45RO^+$ and $CD57^+$ T cells via Miltenyi MACS positive selection. $CD8^+$ T cells that express CD57 and/or CD45RO were thus removed from the isolated $CD8^+$ T-cell population to leave the naïve population. The procedure was performed as follows: after $CD8^+$ T-cell isolation, cells were counted and collected by centrifugation at $300g_{max}$ for 5 minutes. The cell pellet was resuspended in MACS buffer (40µl per 10^7 cells) and a cocktail of microbead-conjugated mAbs were added to label $CD57^+$ and $CD45RO^+$ cells (20µl each per 10^7 cells). After a 15 minute incubation at 4°C the solution was made up to 1ml with MACS buffer and applied to a pre-washed LD MACS column. $CD57^+$ and $CD45RO^+$ cells were retained on the column and the eluted fraction, containing the negatively selected naïve T-cells, was collected. The eluted naïve T cells were counted and 10^5 apportioned to assess purity. The remainder were centrifuged at $300g_{max}$ for 5 minutes and resuspended at a

concentration of $3x10^6$ naïve T cells per ml in TcRM. Naïve T cells were recovered overnight before use in subsequent processes.

2.7.5. Dead cell removal

In the culture of adherent cell lines, dead cells are identified as those that float and therefore were easily removed with PBS^- washes prior to trypsinisation. As this was not possible with suspension cells, dead cells were removed via Miltenyi MACS according to the protocol supplied within the Dead Cell Removal Kit. Briefly, after collection of cells by centrifugation at $300g_{max}$ for 5 minutes, the cell pellet was directly resuspended in dead cell removal microbeads (100µl per 10^7 cells). After a 15-minute incubation at RT, the solution was made up to 1ml with dead-cell binding buffer and applied to a pre-washed LS MACS column. Dead cells were retained on the column and the eluted fraction, containing negatively selected viable cells, was collected. Eluted viable cells were counted using the trypan blue exclusion method to determine viability, then subsequently centrifuged at $300g_{max}$ for 5 minutes and resuspended in appropriate medium for subsequent processes.

2.8. MoDC preparation

The protocol for generation of moDC underwent a series of refinements. The final optimised procedure is described below. For standard “slow” DC preparation in 6-well plates, $5x10^6$ isolated monocytes were incubated in 2ml DCD_1 medium. After 3 days, a further 2ml of DCD_1 was added. After 6 days of differentiation, iDCs were either harvested or matured for use in subsequent processes. Harvesting was performed by vigorous trituration, first in incubation media and then with cold PBS to remove any remaining adherent cells. Cells were counted, 10^5 cells were allocated for time zero phenotyping as described in section 2.18, and remaining cells were washed in complete RPMI and resuspended in relevant medium for subsequent processes. Maturation was induced by addition of DCM_1 or DCM_2 media for a further two days. At day 8, mDC were harvested as previously described for iDC. For ‘fast’ DC, the duration of monocyte differentiation ranged from 1-3 days in total to yield iDC and the subsequent maturation step ranged from 1-2 days in total.

2.9. *In vitro* expansion of antigen specific $CD8^+$ T cells

The HLA-A*02:01 restricted peptides and their concentrations used for *in vitro* stimulation of T cells are detailed in Table 2.5. All T cells were cultured at 37°C in 5% CO_2.

Table 2.5. HLA-A*02:01 Restricted Peptides Used for *In Vitro* T-cell Expansion

Antigen	Peptide Designation	aa Sequence	Concentration (μg/ml)
CD20	$CD20_{188-196}$	SLFLGILSV	10
CMV pp65 Protein	$CMVpp65_{495-504}$	NLVPMVATV	50
EGFR	$EGFR_{479-488}$	KLFGTSGQKT	10
	$EGFR_{1138-1147}$	YLNTVQPTCV	5
Influenza A Matrix Protein-I	$Flu\text{-}A_{58-66}$	GILGFVFTL	50
MelanA Protein	$MelanA_{26-35}$ (A27L)*	ELAGIGILTV	2.5

* Heteroclytic peptide analogue with increased binding affinity for HLA-A*02 [280, 281].

2.9.1. In vitro expansion of HLA-A*02:01-restricted antigen-specific $CD8^+$ T cells from the naïve repertoire in healthy donors

Several protocols have been described for *in vitro* expansion of antigen specific $CD8^+$ T cells from the naïve population. All involve the following steps: selection of APC; APC antigen loading; selection, prime and re-stimulation of responder T cells; and screening for antigen specificity. The protocols vary greatly in terms of media, cytokine use, cell ratios and duration of stimulation (as summarised in Table 2.6). The final optimised procedure used in this study is described.

Table 2.6. Summary of previously published TA-specific naïve CD8$^+$ T-cell *in vitro* expansion protocols

Reference	Summary				Peptide Loading				Stimulation and Culture				Restimulation and Screening			
	Antigen	Peptide	Donor	Max Specificity	APC	Media	Cytokines	APC : Peptide (Time)	Irradiation	Responders	Media	Cytokines	Responder : APC	Restim	Schedule	Multimer	Functional test
Andrade Filho *et al* (2010)	$EGFR_{853-861}$	ITDFGLAKL	Healthy	0.45% Tetramer$^+$	Day 8 mDC	AIM-V	**iDC:** IL4, GMCSF **mDC:** IL1β, PGE_2, IL6, TNFα	10^6 : 10ug/ml (4 hours)	50 Gy	Isolated $CD8^+$ Tcells	IMDM	IL2, IL7	10:1	2	Weekly restim, screen day 21	Tetramer	IFNγ ELISPOT
			$Patient_{HNSCC}$	0.65% Tetramer$^+$													
Ho *et al* (2006)	$WT1_{126-134}$	RMFPNAPYL	Healthy	2.86% Tetramer$^+$	Day 2 mDC	CellGro	**iDC:** IL4, GMCSF **mDC:** IL1β, PGE_2, IL6, TNFα	? : 10uM (2-4 hours)	32 Gy	Isolated $CD8^+$ Tcells	CellGro	IL2, IL7	5:1	1	PBMC Restim day 10, screen day 18	Tetramer	^{51}Cr release
Wolfl and Greenberg (2014)	Melan-A_{26-35}	ELAGIGILTV (A27L)	Healthy	47.6% Dextramer$^+$	Day 4 mDC	CellGro	**iDC:** IL4, GMCSF **mDC:** IFNγ, LPS	10^6 : 2.5ug/ml (overnight)	30 Gy	Isolated Naïve Tcells	CellGro	IL7, IL15, IL21	4:1	-	Screen days 10-12	Dextramer	Activated Caspase 3
	$STEAP1_{292-300}$	MLAVFLPIV (I293L)	Healthy	13.3% Dextramer$^+$													
	$gp100_{209-217}$	IMDQVPFSV (T210M)	Healthy	6.5% Dextramer$^+$													
Schuler *et al* (2011)	$EGFR_{479-488}$	KLFGTSGQKT	Healthy	0% Pentamer$^+$	Day 6 iDC	AIM-V	**iDC:** IL4, GMCSF	$2x10^6$: 10ug/ml (45 minutes)	-	PBMC	X-Vivo 15	IL2, IL7	10:3	3	Weekly restim, screen day 28	Pentamer Tetramer	IFNγ ELISPOT
			$Patient_{HNSCC}$	0.01% Pentamer$^+$													
	$EGFR_{1138-1147}$	YLNTVQPTCV	Healthy	0% Tetramer$^+$													
			$Patient_{HNSCC}$	0.06% Tetramer$^+$													
Grübe *et al* (2004)	$CD20_{188-196}$	SLFLGILSV	Healthy	13% SI ≥2	CD40-B Cells	"CM"	-	? : 50ug/ml (2 hours)	75 Gy	Isolated $CD8^+$ Tcells	"CM"	IL2, IL7	4:1	3	Weekly restim, screen day 28	-	IFNγ mRNA
			$Patient_{CLL}$	19% SI ≥2													
Bae *et al* (2005)	$CD20_{188-196}$	SLFLGILSV	Healthy	Significant IFNγ release with malignant Bcell stimulation	Day 10 mDC	RPMI	**iDC:** IL4, GMCSF **mDC:** IFNα, TNFα	? : 100ug/ml (2 hours)	10 Gy	Isolated $CD3^+$ Tcells	AIM-V	IL2	20:1	2	Weekly restim, screen day 21	-	^{51}Cr release IFNγ ELISA Tcell proliferation
Kleihauer *et al* (2001)	$CMVpp65_{495-504}$	NLVPMVATV	Healthy	78% Tetramer$^+$	Day 7 mDC	RP10	**iDC:** IL4, GMCSF **mDC:** TNFα	$5x10^5$: 50ug/ml (2 hours)	30 Gy	PBMC	αMEM	IL2	6:1	3-6	Weekly restim, screen 7 days post stim	Tetramer	Europium release

Purified $CD8^+$ naïve T cells from HLA-$A*02^+$ healthy donors were stimulated with autologous, peptide-pulsed DC. iDC were incubated for 16 hours in DCM_3 supplemented with peptides at 2.5 µg/ml (v/v). The peptide pulsed DC were then washed once with CellGro and resuspended at a concentration of $5x10^5$/ml in $TcSM_0$. Recovered $CD8^+$ naive T cells were resuspended in $TcSM_0$ at a concentration of $2x10^6$. Equal volumes of the T-cell and DC suspensions were combined to give a final T-cell:DC ratio of 4:1 and 2ml of this suspension was added to multiple wells of a 24-well plate on day zero and incubated. On day 3, 500µl of $TcSM_1$ was added to each well. On day 6, T cells were harvested by gentle trituration, leaving behind the majority of adherent DC. Contents were transferred to 12 well plates, where a further 1ml of $TcSM_1$ was added. On day 8, wells were again harvested as described on day 6. Contents were transferred to 6-well plates where a further 2ml of $TcSM_2$ was added. Peptide-stimulated T cells were harvested on days 10-12 and screened for antigen specificity via MHC-multimer staining (as described in section 2.18.3) prior to cryopreservation. Frozen antigen specific T cells were thawed and added directly to co-culture assays as required.

2.9.2. *In vitro* expansion of HLA-A*02:01-restricted $CD8^+$ T cells from cancer patients

A single *in vitro* stimulation was employed, using a protocol adapted from the study by Andrade Filho *et al* [282], because cell numbers from patient samples were limited. Thawed patient cells were allocated at $2x10^6$ PBMC per well (24 well plate) for each condition, in the presence of IL7 at a final concentration of 10ng/ml. Peptides were added to respective wells at a final concentration of 5-10µg/ml. IL-2 was added to a final concentration of 25U/ml on days 3 and 6. On day 10, cultures were harvested and screened for antigen specificity.

For samples with very low cell numbers, a pool of peptides was used in a single culture instead of multiple cultures testing individual peptides. When pools were used, peptide concentrations were adjusted so that high affinity binders were present at lower concentrations than low affinity binders to ensure that all peptides were present at equivalent densities.

2.9.3. HLA-A*02:01 peptide binding assay using T2 cells

In order to assess the relative binding capacity of peptides to HLA-A*02:01, $5x10^5$ T2 cells were cultured for 18 hours in complete RPMI with various concentrations of the peptides (0.1 - 20 µg/ml). T2 cells were then screened for surface expression of HLA-A*02 by flow cytometry as

described (section 2.18.1). The HLA-A*02 binding scores were calculated using median fluorescence intensity (MFI) as follows:

$$T2\ Binding\ Score = \frac{MFI\ [T2 + Peptide]}{MFI\ [T2\ Alone]}$$

The T2 binding scores were used to adjust the concentration of individual peptides so that all peptides were likely to be presented by HLA-A*02 at equivalent densities when peptide pools were used to stimulate T cells.

2.10. Genomic DNA extraction

Total genomic DNA was extracted from either whole blood (WB) or PBMC samples using the QIAamp DNA Blood Mini Kit (Qiagen - Manchester, UK) according to the manufacturer's protocol. Briefly, 200µl of whole blood or PBMC suspension containing 10^6-10^7 cells was lysed in the presence of a protease to release the cell contents and remove protein contamination. The DNA was then bound to the silica membrane of the mini column via centrifugation in the presence of the organic solvent ethanol and high concentrations of chaotropic salt. The salt dehydrates the negatively charged DNA and decreases the negative surface charge density of the silica, thereby permitting binding by reducing electrostatic repulsion. Remaining contaminants and enzyme inhibitors were removed via two wash steps and the DNA was then eluted in a low salt TE buffer. The process of solid phase DNA extraction has been described in detail by Vandeventer *et al* (2012) [283].

2.11. DNA quantification and purity assessment

DNA concentration and purity was assessed using a NanoDrop spectrophotometer (Thermo Scientific, UK). DNA absorbs UV light at 260 and 280 nanometres (nm), while proteins containing aromatic amino acids absorb UV light at 280 nm. Pure DNA has an A260/A280 ratio of 1.8 or greater indicating that the preparation is relatively free from protein contamination. DNA that is contaminated with protein has an A260/A280 ratio lower than 1.8. At a concentration of 1mg/ml and with a 1cm path length, double stranded DNA (dsDNA) has an absorption at 260nm of 50 units, that can be used to determine DNA concentration.

2.12. CD16 genotyping

A real-time PCR based approach was employed for CD16 genotyping. The assay utilised allele specific probes that have a fluorophore and a quencher linked to the 5' and 3' ends respectively. When the probe is intact, the quencher remains in close proximity to the fluorophore, eliminating its signal. However, when the probe binds to DNA it is degraded by the 5'-nuclease activity of Taq polymerase, thereby separating the fluorophore from the quencher molecule and generating a detectable signal [284]. The assay was conducted according to the protocol supplied with the TaqMan SNP Genotyping Assay C__25815666_10 corresponding to SNP id: rs396991 (Invitrogen - Paisley, UK). Briefly, genomic DNA was isolated as described in section 2.10 and diluted to a concentration of 0.555µg/ml. Reaction mixtures were then prepared in fast PCR reaction plates according to Table 2.7 The PCR was performed using a StepOnePlus™ real-time-PCR unit (Applied Biosystems - Paisley, UK) according to the thermal cycling conditions detailed in Table 2.8. Substituting the test sample with molecular biology grade water served as a negative "no target" control (ran in triplicate) and samples of known genotype were included as positive controls in each run. Donor CD16 genotypes and HLA-A*02 status are summarised in Table 2.9.

Table 2.7. Preparation of TaqMan genotyping reaction mix

Reagent	Volume (µl)
Genotyping Mix	0.5
TaqMan Master Mix	5
Test Sample	4.5*
Total Volume	**10µl**

***Volume corresponds to 2.5ng DNA**
(Low starting concentration reduced accumulation of primer dimer by-products)

Table 2.8. TaqMan genotyping thermal cycling conditions

Temperature (°C)	Time (seconds)	Cycles
95	600	1
92	15	40
60	60	
4	∞	∞

Table 2.9. Donor CD16 genotype and HLA-A*02 status

Donor	HLA-A*02 Status	CD16 Genotype
LC44	Negative	V/F
LC45	POSITIVE	F/F
LC46	Negative	F/F
LC47	Negative	V/V
LC48	Negative	V/F
LC49	Negative	V/V
LC53	Negative	F/F
LC54	POSITIVE	V/V
LC55	POSITIVE	V/V
LC56	Negative	F/F
LC60	Negative	F/F
LC63	Negative	V/F
LC64	Negative	V/F
LC65	POSITIVE	V/F
LC67	POSITIVE	V/F
LC94	Negative	V/F
LC96	POSITIVE	F/F
LC97	POSITIVE	F/F

Donor	HLA-A*02 Status	CD16 Genotype
LC98	POSITIVE	F/F
LC99	Negative	F/F
LC100	POSITIVE	V/F
LC101	Negative	F/F
LC102	POSITIVE	V/F
LC103	POSITIVE	V/F
LC104	Negative	V/F
LC105	POSITIVE	V/F
LC116	POSITIVE	V/F
LC117	POSITIVE	V/F
LC118	POSITIVE	F/F
LC119	Negative	F/F
LC120	POSITIVE	F/F
LC121	Negative	F/F
LC122	Negative	F/F
LC123	POSITIVE	F/F
LC124	Negative	V/F
	Total Donors	**35**

2.13. Plasmid expression vectors

Variants of the A431 and H1299 cell lines expressing MelanA protein (hereafter referred to as A431$^{\mathbf{MelanA}}$ and H1299$^{\mathbf{MelanA}}$) were produced by transfection with a plasmid expression vector encoding MelanA. The plasmid comprised the full length MelanA gene fused to green fluorescence protein (GFP) gene via a short, inert DNA sequence encoding a self-cleaving peptide known as a P2A (described in detail by Kim *et al*, 2011 [285]). In addition to the MelanA/GFP fusion gene insert, the plasmid also contained a cytomegalovirus (CMV) promoter for driving expression MelanA/GFP, a puromycin resistance gene placed downstream of an internal ribosome entry site (IRES) and a prokaryotic kanamycin resistance gene. The "MelanA" plasmid, descriptively named CMV-**MelanA.P2A.eGFP**-IRES-Puro was 6515 nucleotide base pairs (bp) in length and produced A431$^{\mathrm{MelanA}}$ and H1299$^{\mathbf{MelanA}}$ transfected cells. Expression of the puromycin resistance gene was used to select transfected cells. GFP expression by transfected cells was used as an indirect measure of likely expression of MelanA. A "Control" plasmid with an insert containing the P2A and GFP DNA sequences but no MelanA gene was also synthesised (6164 bp in length) and designated CMV-**P2A.eGFP**-IRES-Puro; producing A431$^{\mathbf{CTRL}}$ and H1299$^{\mathbf{CTRL}}$ transfected cells. Dr David Darling and Dr Richard Beswick (KCL - London, UK) kindly helped with advice for vector design and codon optimisation. Insert DNA was synthesised and cloned into the NcoI/XbaI restriction sites of the ready-made OG317 vector by Oxford Genetics (Oxford, UK). The DNA sequences of the plasmid expression vectors can be found in the appendix (Chapter 7) and the plasmids and their restriction sites are depicted in Figure 2.1.

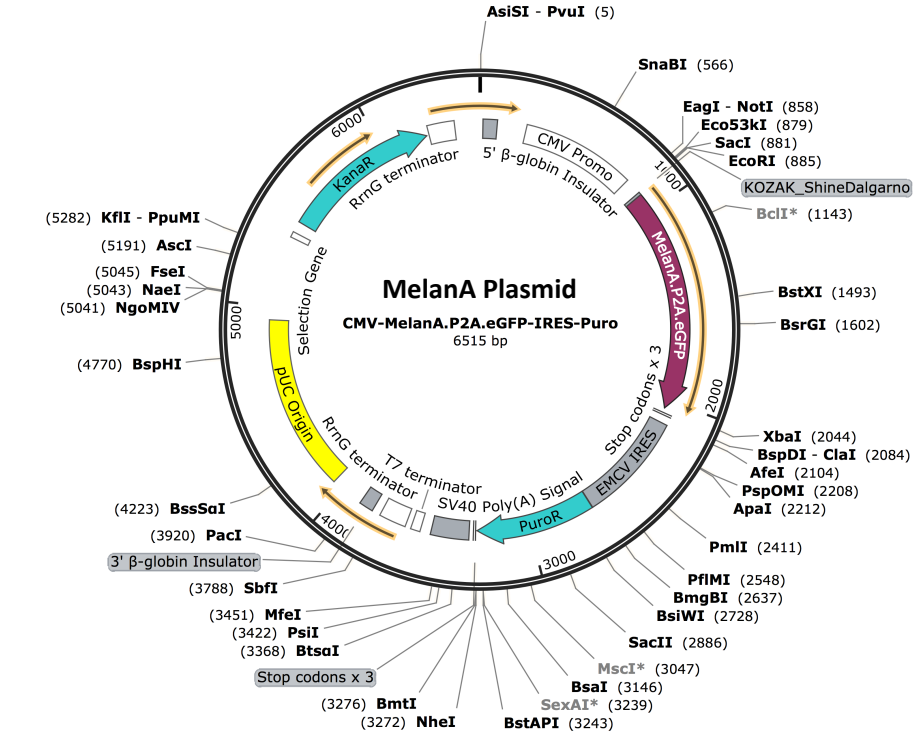

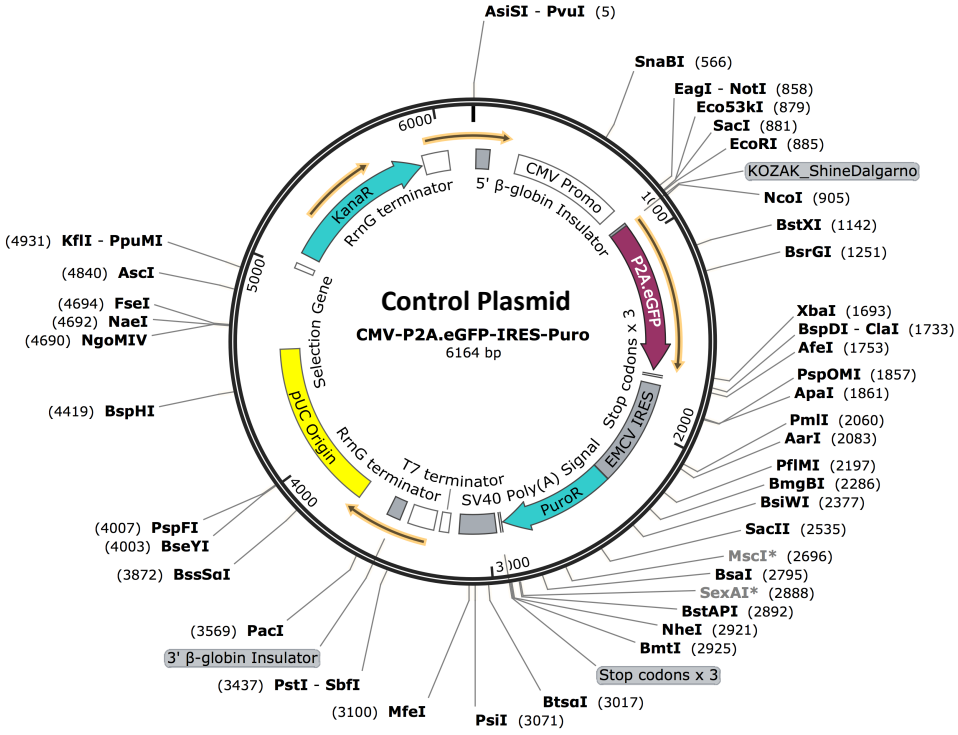

Figure 2.1. Schematic representation of plasmid expression vectors
Produced using SnapGeneViewer Software, version 2.82 (GSL Biotech LLC | Chicago, USA - 2016)

2.14. E. coli transformation and maxi-prep

E. coli C2988J DH5α cells were purchased from New England Biolabs (NEB - Hitchin, UK) and stored at -80°C. The $CaCl_2$ treatment of these bacterial cells produces competent cells that will uptake DNA after a heat shock [286]. To transform a 50µl suspension of C2988J, cells were thawed on ice in a sterile 1.5ml capped microfuge tube and inoculated with 200pg of plasmid DNA. After a 30 minute incubation on ice, the mixture was heated for 1 minute at 42°C to disrupt the bacterial cell membrane, allowing the DNA to enter. The mixture was then placed back on ice. After a minimum of 1 minute, to allow for retention of the plasmids inside the bacteria, 950µl of super optimal broth with catabolite repression (SOC) medium was added to the transformed bacteria. The tube was then placed horizontally in a shaking incubator (Cole-Parmer, UK) for 1 hour at 37°C and 225 revolutions per minute (rpm). Each transformation mixture was then centrifuged at $500g_{max}$. The pellet was resuspend in residual SOC medium and this volume was spread on pre-warmed LB agar plates, then incubated overnight at 37°C.

The following day, 1-3 well-spaced single, kanamycin resistant bacterial colonies were selected for expansion in sterile 500ml flasks containing 200ml LB medium supplemented with 30µg/ml kanamycin. Flasks were placed in a shaking incubator overnight at 37°C and 225rpm. Plasmid DNA was isolated using the QIAamp HiSpeed Plasmid Maxi Kit with a protocol similar to the genomic DNA extraction described in section 2.10 but scaled up for a larger column. Plasmid DNA was subsequently quantified and purity checked as described section 2.11.

2.15. Tumour cell transfection

Transfection is the process by which genetic material is introduced into cells [287]. Tumour cells were transfected with plasmid DNA using the Biontex K2 transfection system according to the manufacturer's protocol. Briefly, A431 or H1299 cells were seeded in complete RPMI in multiple wells of a 6-well plate. Cells were monitored until an optimum confluence of 70-80% was achieved with the cells in exponential growth phase (typically seen the day after seeding). Media was then removed and replaced with 2ml of complete RPMI supplemented with 9µl/ml K2 multiplier reagent for a minimum of 2 hours pre-transfection. Plasmid DNA and K2 transfection reagent were combined for 20 minutes in serum/antibiotic free RPMI at a ratio of 0.5µg/µl respectively in order to form lipid complexes. This "lipoplex" mixture was then applied to the pre-treated cells and gently swilled. After 24 hours, transfection medium was replaced with fresh

complete RPMI. After 48 hours, cells were either exposed to puromycin or harvested for subsequent processes. Puromycin was administered in complete RPMI at a pre-determined killing concentration for each cell line, enabling enrichment of transfected puromycin resistant cells and removal of untransfected cells. Harvested cells were sorted by FACS based on GFP^{HIGH} expression and subsequently screened for intracellular expression of MelanA or used in co-culture assays.

2.16. Co-culture assays

Final optimised procedures are described below with any refinements detailed in the results section. All assays were conducted in V-bottomed plates in complete RPMI with a 200µl total volume. Cultures were incubated at 37°C in 5% CO_2.

2.16.1. NK-cell activation

This assay was designed to measure ADCC activation of NK cells in the presence of therapeutic mAbs and as such comprised two cell types, tumour cells and NK cells as illustrated in Figure 3.1. Recovered NK cells ($2.5x10^4$) were incubated with viable tumour cells at a 1:1 ratio in the presence or absence of mAbs at various concentrations. NK cells alone for the duration of the assay served as a negative control and 10ng/ml PMA with 1µg/ml ionomycin (PMA/Ionomycin) was used to activate NK cells for a positive control. After 6-18 hours of co-culture, cells were washed with 200µl PBS^+, pelleted by centrifugation at $300g_{max}$ for 5 minutes and phenotyped as described in section 2.18.

When intracellular cytokine staining (ICS) was performed, CD107a antibody was added for the duration of the incubation at 5µl per well. After one hour, the protein transport inhibitor brefeldin A (BFA) was added to a final concentration of 10µg/ml and incubated for a further 5 hours. BFA blocked intracellular protein transport such that cytokines accumulated in the rough ER to a level detectable by intracellular staining, as described by Nylander and Kalies [288]. NK cells alone for the duration of the assay served as a negative control and NK cells activated with 1µl/well leukocyte activation cocktail (LAC) were used as a positive control. LAC contains the phorbol ester phorbol 12-myristate 13-acetate (PMA), a calcium ionophore (Ionomycin) and the protein transport inhibitor BD GolgiPlug™ (BFA) and provides mitogenic stimulation that bypasses receptor-mediated activation.

2.16.2. Tumour cell apoptosis

This assay was designed to measure the induction of tumour cell apoptosis and as such comprised two cell types, tumour cells and NK cells as illustrated in Figure 3.1. Recovered NK cells ($2.5x10^4$) were incubated with either mAbs alone at various concentrations or at a 1:1 ratio with viable JY cells plus mAbs at various concentrations. Some assays were performed in the presence of physiologic concentrations of total IgG (5µg/ml). JY cells alone for the duration of the assay served as a negative control and a (v/v) combination of Actinomycin D (10µM), Camptothecin (2µM), Cycloheximide (0.1mM), Dexamethasone (10µM) and Etoposide (0.1mM) were used to induce JY apoptosis for a positive control (provided in the CalTag apoptosis Inducer set). After incubation intervals of 3, 6 and 9 hours, cells were pelleted by centrifugation at $300g_{max}$ for 5 minutes and phenotyped as described in section 2.18.4.

2.16.3. NK:DC crosstalk

This assay was designed to measure the effect of ADCC activated NK cells on iDC and thus comprised three cell types, tumour cells, NK cells and iDC as illustrated in Figure 4.5. Recovered NK cells were incubated with autologous iDC and allogeneic tumour cell lines at a 1:1:1 ratio in the presence or absence of mAbs at various concentrations. 'iDC alone' and 'iDC with tumour cells plus mAb' for the duration of the assay served as negative controls. DC matured with DCM_1 medium served as a positive control. After co-culture durations of 18-48 hours, cells were phenotyped as described in section 2.18.

2.16.4. T-cell activation: cross presentation of tumour antigen to $CD8^+$ T cells

This assay was designed to generate tumour antigen by ADCC activated NK-cell lysis of tumour cells and assess cross presentation by DC to TA-specific T cells, based on measurement of T-cell activation. The assay utilised HLA-A*02^- $A431^{MelanA}$ as the tumour antigen source and autologous HLA-A*02^+ recovered NK cells, DC and ^{MelanA}T cells, incubated at 1:1:1:4 ratio for 18 hours, as depicted in Figure 5.7. ^{MelanA}T cells alone for the duration of the assay served as an unstimulated negative control. ^{MelanA}T cells incubated with EGFR peptide pulsed DC served as an irrelevant stimulus negative control. ^{MelanA}T cells incubated with ^{MelanA}DC, SK-MEL-30 or PMA/Ionomycin served as positive controls.

2.17. Phagocytosis assay

This assay was designed to assess the uptake by DC of tumour-cell derived particulate antigen generated by apoptosis of tumour cells. The assay exploited the properties of pHrodo-SE, a pH-sensitive fluorescent dye that enables detection of engulfed apoptotic cells due to increased post-phagocytic light emission [289].

2.17.1. Labelling of apoptotic tumour cells with pHrodo-SE

After removal of dead cells, viable JY were resuspended at 10^6 cells/ml in either complete RPMI or complete RPMI supplemented with 10µg/ml GA101-GE to induce apoptosis. After 16 hours, cells were washed twice with PBS^-, pelleted by centrifugation at $300g_{max}$ for 5 minutes and resuspended in PBS^- at 10^6 cells/ml. pHrodo-SE was added to a final concentration of 1µg/ml. After incubation for 30 minutes in the dark at RT cells were washed twice with complete RPMI and resuspended at $0.5x10^6$ cells/ml in complete RPMI.

2.17.2. Uptake of tumour cell particulate by DC

Harvested iDC were resuspended at $0.5x10^6$ cells/ml in complete RPMI and incubated with pHrodo-SE labelled viable or apoptotic JY cells at 1:1 ratio for 1, 2 or 3 hours in a 96 well V-bottomed plate in a 200µl total volume and protected from light. After incubation, cells were washed and resuspended in 100µl FACS buffer with 5µl of CD11c FITC added to each well to label DC. After incubation for 30 minutes at 4°C, cells were washed with PBS^+, pelleted by centrifugation at $300g_{max}$ for 5 minutes and resuspended in 125µl PBS^+.

2.17.3. Slide preparation

The cell suspension was applied to the chamber of an assembled cell concentrator (Thermofisher Scientific - Basingstoke, UK), illustrated in Figure 2.2. The concentrator was placed in the Statspin Cytofuge® II (Beckman Coulter - High Wycombe, UK) and centrifuged at $55g_{max}$ for 5 minutes [290]. The supernatant was then aspirated and after washing gently with 200µl PBS^+, cells were fixed to the slide by adding 200µl of 3% formaldehyde solution to the central chamber at RT, protected from light. After 15 minutes, formaldehyde was aspirated, the slide was washed gently with 200µl PBS^+ and the cells were then permeabilised with 0.1% triton solution. After 5 minutes, the triton was aspirated, cells were washed and 150µl of DAPI solution was added to the central chamber at RT, protected from light. After a further 5 minutes, slides were washed with 200µl PBS^+ and

coverslips were applied with mounting media. The labelled slides were immediately refrigerated and visualised by microscopy within 72 hours.

The Statspin Cytofuge® II, cell concentrators, mounting media, triton and DAPI solutions were kindly provided by Dr Alan Ramsey (KCL - London, UK).

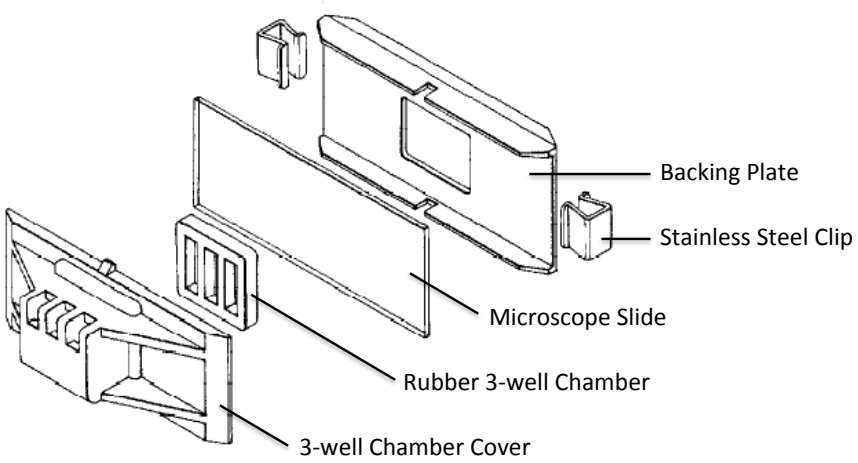

Figure 2.2. Cell concentrator apparatus
Adapted from Kelley *et al* (1997) [291]

2.17.4. Fluorescent microscopy

Internalisation of tumour-cell particulate was visualised using the Nikon A1R confocal microscope at the KCL Nikon Imaging Centre (NIC – London, UK). All images were captured at 60x magnification (oil immersion objective) with a display resolution of 1024 pixels or greater, and where 10 or more DC occupied the focal plane. Three images were taken per slide. Files were saved in nd2 format and analysis performed using the NIS elements viewer, version 4.0 (Nikon Instruments - Europe) and ImageJ (National Institutes of Health - Maryland, USA). The percentage of DC showing phagocytic activity was calculated as follows:

$$\frac{\text{Number of DC containing } \geq 1 \text{ phagocyte(s)}}{\text{Total number of DC in focal plane}} \text{ x } 100$$

A colleague also independently performed the analysis to verify results.

2.18. Phenotyping of cells

Phenotyping was typically performed in a 96 well V-bottomed plate protected from light, using $2.5x10^4$-$1x10^6$ cells labelled with fluorochrome-conjugated antibodies at titrated or manufacturer-recommended concentrations. Phenotyping antibody cocktails are detailed in Table 2.10 and labelling protocols are described below.

2.18.1. Cell surface staining

Cells were washed in 200µl PBS^+ to remove serum, pelleted by centrifugation at $300g_{max}$ for 5 minutes and stained with a fixable viability dye (diluted in 100µl PBS^+) for 20 minutes at 4°C. Without washing, cells were then counter stained with a phenotyping antibody cocktail at 4°C. After a further 30 minutes, cells were pelleted by centrifugation at $300g_{max}$ for 5 minutes, washed in 200µl PBS^+, and pelleted. Cells were resuspended in 100-300µl PBS^+ and transferred to round-bottom 12x75mm polystyrene test tubes for immediate analysis by flow cytometry. If analysed at a later time, cells were fixed in 100-300µl 1% PFA and refrigerated at 4°C. Fixed cells were analysed within 72 hours.

2.18.2. Intracellular staining

If required, cells were first stained for surface markers (as described above), then washed and fixed in 100µl BD cytofix solution at 4°C. After 20 minutes, 100µl PBS^+ was added before centrifugation at $300g_{max}$ for 5 minutes. Cell pellets were resuspended in 100µl of 1x BD cytoperm solution at 4°C. After 20 minutes, 100µl 1x BD cytoperm solution was added before centrifugation at $300g_{max}$ for 5 minutes. Cell pellets were then resuspended in either an intracellular cytokine staining (ICS) antibody cocktail or with primary then secondary antibody cocktails, for 30 minutes at 4°C. Cells were subsequently washed in 200µl PBS^+, resuspended in either PBS^+ or 1% PFA and transferred to tubes for analysis.

2.18.3. MHC multimer staining

Cells were incubated at RT with 10µl of pentamer in 50µl FACS buffer. After 10 minutes, cells were centrifuged at $300g_{max}$ for 5 minutes, washed with 200µl PBS^+ and surface staining performed as described section 2.18.1. The wash step was omitted in the case of dextramer staining.

Table 2.10. Phenotyping: fluorochrome-conjugated antibody cocktails

	Antibody	Clone	Volume per test[e] (µl)
NK-cell activation	CD69 FITC	L78	2
	CD16 APC-H7	3G8	0.5
	Live/Dead Aqua[f]	-	0.1
	CD56 PE	HCD56	2
	CD3 PECy7	SK7	2
NK-cell activation ICS[g]	IFNγ FITC	4S.B3	5
	TNFα AF700	MAb11	5
	CD107a APC	H4A3	5
	CD16 APC-H7	3G8	0.5
	CD3 PB	UCHT1	2
	Live/Dead Aqua	-	0.1
	CD56 PE	HCD56	2
DC maturation	HLA-DR FITC	L243	10
	CD11c PerCPeFluor710	3.9	15
	CD86 APC	2331(FUN-1)	20
	Live/Dead Aqua	-	0.1
	CD80 PE	L307.4	20
	CD83 PECy7	HB15e	7.5
T-cell activation	CD69 FITC	L78	5
	CD8 PerCP/Cy5.5	RPAT8	5
	CD137 APC	4B4-1	5
	CD71 APC-Cy7	CY1G4	5
	Live/Dead Violet	-	0.1
	Multimer PE	-	10
	CD3 PECy7	SK7	5
T-cell activation ICS	IFNγ FITC	4S.B3	5
	CD8 PerCP/Cy5.5	RPAT8	5
	Live/Dead Violet	-	0.1
	Multimer PE	-	10
	CD3 PECy7	SK7	5
Apoptosis	CD20 PB	2H7	5
	Annexin V FITC	-	5
	PI	-	10
	Binding Buffer	-	80
Post transfection confirmation	1° - Rabbit Anti-MelanA (Unconjugated)	EP1422Y	0.2[h]
	2° - Goat anti Rabbit AF647	-	0.2[h]
Other phenotyping	HLA-A*02 PE	BB7.2	5
	EGFR PE	AY13	5
	CD20 PE	2H7	5

[e] Volumes per test were determined by titration
[f] Live/Dead viability dye diluted 1:1000 in PBS. 100µl of this solution added to cells.
[g] Intracellular cytokines screened after fixative/permeation step. Detailed in section 2.18.2.
[h] 1:1000 dilution of 2mg/ml stock solution in 1x Perm Buffer. 100µl of this solution added to cells.

2.18.4. Apoptosis assay staining

Pelleted cells were resuspended at RT in 100µl of apoptosis phenotyping antibody cocktail. Experimental samples were numbered in the order they were to be analysed by flow cytometry, stained chronologically at one-minute intervals and immediately transferred to tubes. When all 20 samples had been stained, analysis was performed chronologically at one-minute intervals. This ensured that each sample was exposed to propidium iodide (PI) for the same length of time (20 minutes).

2.19. Flow cytometry

Flow cytometry was used to assess and quantify expression of cell surface and intracellular markers. Flow cytometry was also used to sort and retrieve cells, based on marker expression. Analysis was performed using either a BD FACSCantoII™, BD LSRFortessa™ or BD FACSAria™ flow cytometer with associated FACSDiva™ software, version 6.0 or above (BD Biosciences, Oxford, UK).

2.19.1. Instrument setup

Mahnke and Roederer (2007) provide comprehensive guidance on cytometry instrument set-up and experimental validation, which was followed closely [292]. Cytometer Setup and Tracking beads (CST - BD Biosciences, UK) were run once a week to monitor instrument performance. Automated compensation was conducted using either UltraComp or CompBeadPLUS antibody capture beads with the purpose of establishing corrections for the spectral overlaps in fluorochrome combinations. The compensation beads were labelled with the same fluorochrome-conjugated antibody used for experimental samples. The positive signal for the compensation sample was always at least as bright as the corresponding signal for the fluorochrome in the test sample. At least 10,000 live cells were acquired for phenotyping. Raw data files were exported and analysed using FlowJo cytometric analytical software (TreeStar Inc. Ashland, OR), version 9.6.4 or above.

2.19.2. Controls for analysis

In a widely cited article, Maecker and Trotter (2006) detail considerations for the control of background fluorescence in flow cytometry [293]. They present a set of recommendations that

enable users to develop optimized cell labelling protocols that minimize background and maximize the ability to reliably distinguish between positive and negative cell populations. Of their crucial criteria, foremost was the inclusion of viability dyes, which are essential for removing dead cells that will non-specifically uptake antibodies and auto-fluoresce.

They suggest that fluorescence minus-one (FMO) controls are more relevant than isotype controls for gating cells in the context of data spread due to the multiple fluorochromes in a phenotyping panel [293]. FMOs are samples that are stained with all antibody conjugates present in test samples, except one. The channel of the omitted antibody is the one for which the FMO provides a gating control (as illustrated in figures 3.6, 3.7 and 4.8).

Maecker and Trotter were careful to state that the best control for a marker stimulated *in vitro* is an unstimulated control sample, stained with the same antibodies as the test sample. They emphasised that an unstimulated control is far more relevant and appropriate than an isotype or FMO control and advised that measurements of positivity or upregulation should always be relative to these. Their recommendations were echoed and adopted by McLaughlin *et al*, who sought to formulate consensus guidelines for FACS analysis of clinical samples across multiple instruments [294]. As such, FMOs were included in all preliminary studies and viability dyes and unstimulated or unactivated reference samples were included in all experiments.

2.20. Statistical analysis

A professional statistician, Dr Alessandra Bisquera (KCL - London, UK) was consulted regarding statistical analysis. All data were analysed and plotted using GraphPad Prism® software, version 5 (GraphPad Software - California, USA). No assumptions were made about the distribution of data. Significance was calculated using the non-parametric Wilcoxon signed-rank test when considering two paired parameters. For comparison of three or more paired parameters, overall significance was first evaluated via Friedman's analysis of variance (ANOVA) with Dunn's multiple comparison post-hoc [295]. As is appropriate for data that is ranked and non-Gaussian, data are presented with the median and interquartile range [296]. Two-tailed P values <0.05 were considered significant.

Chapter 3. Results I: Glyco-engineered monoclonal antibodies induce NK-cell activation and function associated with promoting adaptive cellular immunity

3.1. Introduction

Previous studies have reported that GE-mAbs possess enhanced ability to induce ADCC. Gerdes *et al* (2013) showed that imgatuzumab exhibits superior *in vitro* ADCC activity compared to cetuximab. The increased ADDC translated into superior *in vivo* anti-tumour activity that was evaluated using a human tumour xenograft mouse model [205]. Similarly, Mössner *et al* (2010) showed that GA101GE has augmented *in vitro* ADCC activity relative to rituximab [232]. These studies suggest that GE-mAbs may be more effective than antibodies with already proven clinical benefit.

A property of GE-mAbs that has not yet been assessed is their ability to promote anti-tumour cellular immunity. To this end, the first stage of this study aimed to determine whether GE-mAbs activate NK cells and induce functions necessary for stimulation of adaptive immunity. This required establishing the two-cell *in vitro* co-culture model depicted in Figure 3.1. The model was designed with potential to add other cell types in mind, so that subsequent analyses could be undertaken to assess the ability of GE-mAb-activated NK cells to promote DC maturation and cross presentation of antigen to TA-specific $CD8^+$ T cells. The previous *in vitro* studies of GE-mAb ADCC activity were performed using the human NK-cell line NK-92 [205] or human PBMC [232] as effectors, with a primary focus on measurement of tumour cell death. No evaluation of NK-cell activation or function, other than lytic activity, was performed. In this study, purified primary NK cells from healthy donors were used and a flow-cytometry based readout developed to assess NK-cell activity based on expression of the activation marker CD69, downregulation of CD16, degranulation (CD107a) and production of TNFα and IFNγ. This combination of markers has previously been used by the Ferris laboratory to study activation of NK cells by cetuximab and subsequent influence on anti-tumour cellular immunity [263].

The objective of the studies described in this chapter was to assess whether GE-mAbs induce activation of NK cells and functions required for promotion of adaptive cellular immunity. Previous studies of GE-mAbs have compared their efficacy with clinically utilised mAbs at equivalent concentrations, with the rationale that a more efficacious drug could potentially replace the current standard of care [205, 232, 238, 263, 297]. In keeping with this precedent, imgatuzumab was compared with the clinically utilised anti-EGFR mAb cetuximab at equivalent concentrations, and GA101GE was compared with the clinically utilised anti-CD20 mAb rituximab. These comparator mAbs, however, have different epitope specificities to the GE-mAbs. Therefore, to assess any impact of the GE modification *per se* on efficacy, GA101GE was compared to the unmodified counterpart GA101WT, that is otherwise identical.

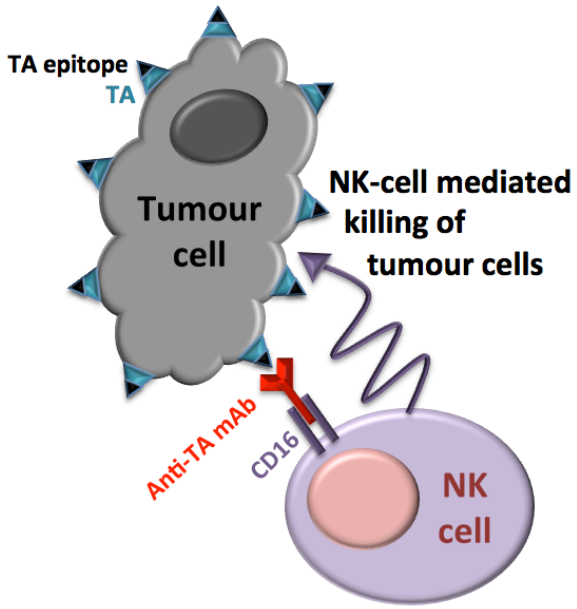

Figure 3.1. Schematic representation of two-cell *in vitro* co-culture model to assess NK-cell activation and function

3.2. *In vitro* assessment of NK-cell activation: co-culture components with anti-EGFR mAbs

3.2.1. EGFR$^+$ tumour cell line: A431

EGFR is typically overexpressed in solid tumours of epithelial origin. The A431 cell line was chosen for use in the EGFR *in vitro* model due to pathophysiological similarities with epithelial carcinomas and because other groups have previously reported successful use of A431 cells to

study anti-EGFR mAbs [205, 238]. Surface expression of EGFR by A431 cells was confirmed by flow cytometry, with the JY B-cell line used as a negative control. Results are shown in Figure 3.2.

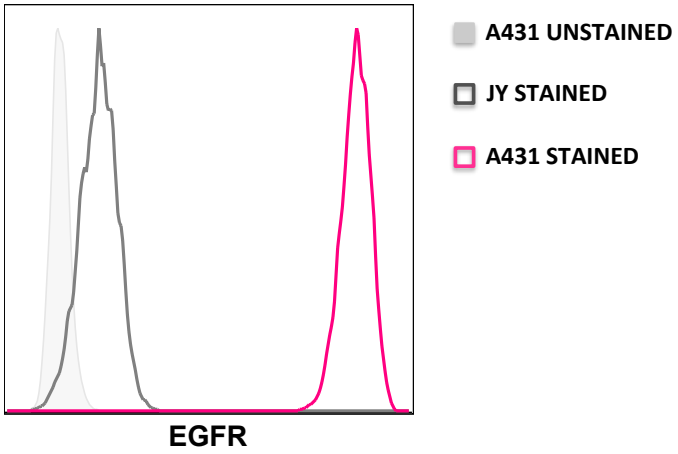

Figure 3.2. The tumour cell line A431 expresses high levels of EGFR
10^5 A431 cells and JY cells (negative control) were stained with anti-EGFR PE-labelled antibody.

3.2.2. NK cells

NK cells were isolated from healthy donor PBMC by negative selection using antibody conjugated magnetic microbeads. Previous studies have used CD16 as a biomarker for potential clinical response to therapeutic mAbs and correlated CD16 genotype with prognosis [209, 210, 255]. Therefore, PBMC from 35 healthy donors were screened for the FCRγIIIa polymorphism (V158F) that yields the low (F/F) and high (V/V) affinity variants of CD16, in order to correlate CD16 genotype with level of NK-cell activation. Genotypes were present at the frequencies indicated in Table 3.1.

Table 3.1. CD16 Genotype Frequencies

Genotype	Frequency (%)
V/V (High)	11.1
V/F	41.7
F/F (Low)	47.2

3.2.3. NK-cell phenotyping and gating strategy

The NK-cell phenotyping panel was designed to achieve clear segregation of NK cells within a mixed population and to include markers for phenotypic identification of NK cells and measurement of NK-cell activation. Markers of NK-cell activation were selected based on use in previously published studies. The most frequent indicators of NK-cell activation used are upregulated expression of the secreted cytokines IFNγ and TNFα, and the surface markers CD69 and CD107a [71, 172], and reduced surface expression of CD16 [298].

The sequential NK-cell gating strategy is illustrated in Figure 3.3. After exclusion of doublets, debris and dead cells, lymphocytes were separated into quadrants containing permutations of $CD3^{-/+}$ and $CD56^{-/+}$ cells.

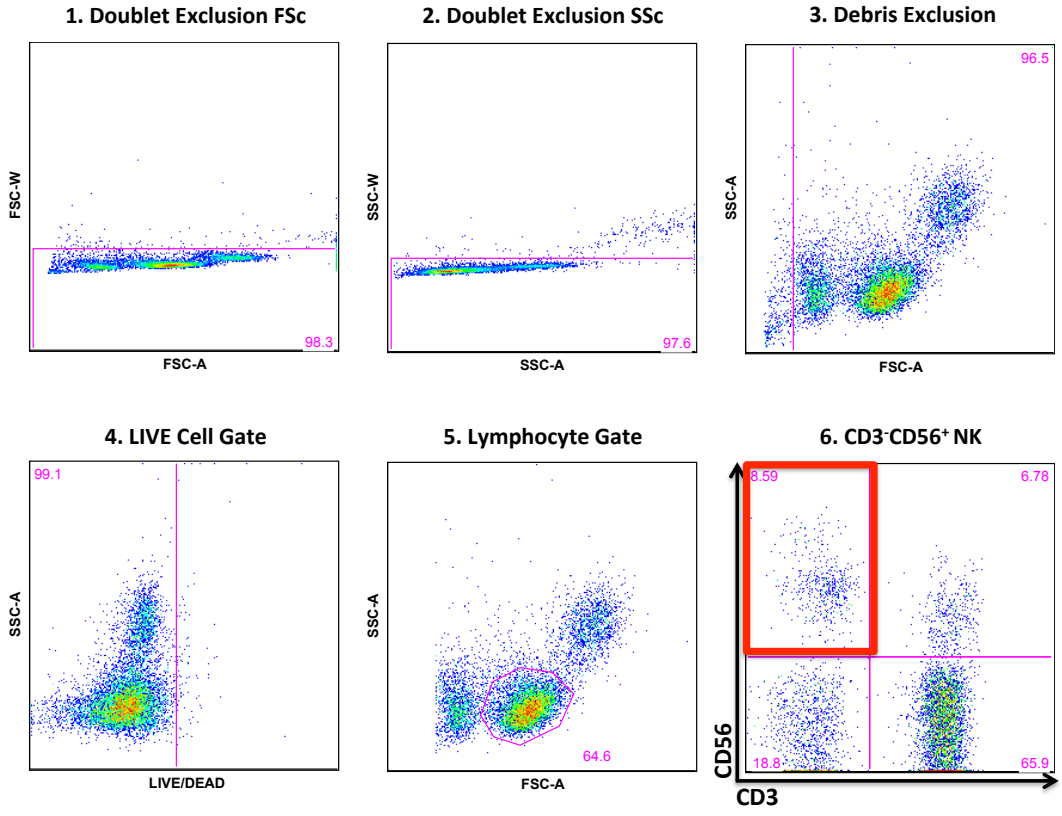

Figure 3.3. NK-cell gating within mixed populations
10^5 PBMC were analysed and NK cells were identified according to the strategy illustrated above. Sequential gating achieved exclusion of doublets, debris and dead cells. Lymphocytes were separated into quadrants containing all permutations of CD3-/+ and CD56-/+ cells and NK cells were identified as the $CD3^-CD56^+$ population.

The co-culture model was ultimately to be used for assessment of NK:DC crosstalk. Therefore, NK cells were purified from PBMC via Miltenyi MACS because it was important that no other effector lymphocytes were present. Negative selection was chosen to minimise any engagement of NK-cell surface receptors that could lead to NK-cell activation. For ten independent experiments, the average NK-cell isolation purity was 97.1% +/- 1.1% standard deviation (sd). Figure 3.4 depicts a representative example of NK cells isolated from PBMC at 98% purity.

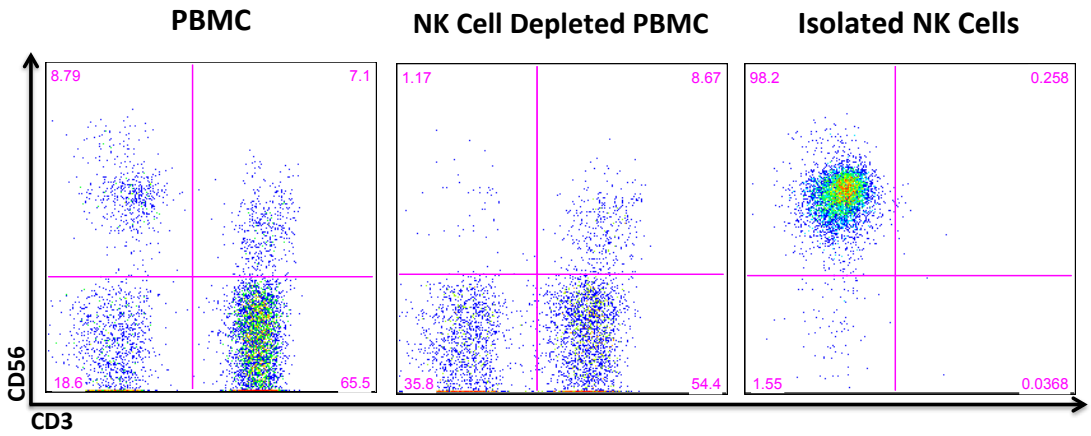

Figure 3.4. NK-cell isolation from PBMC
Identification of $CD3^{-}CD56^{+}$ NK cells within mixed PBMC population and after MACS isolation. In the left-hand plot NK cells can be seen as a percentage of PBMC, in the middle plot these NK cells have been removed from PBMC and the right hand plot depicts isolated NK cells at 98% purity.

Purified NK cells were stimulated for 6 hours with PMA/Ionomycin to demonstrate that they were capable of activation and function. The most informative NK-cell markers are summarised in Table 3.2. The markers NKp44, NKG2D and HLA-DR were also evaluated, but showed only modest modulation after stimulation. This was consistent with previously published work [299] and therefore these markers were not included in the NK-cell activation marker panel used in this study.

Table 3.2. NK-cell activation markers

Activation marker	Modulation of marker upon NK-cell activation	Reference
CD16	Downregulation	[298], [299]
CD69	Upregulation	[71], [73], [300], [299]
CD107a	Upregulation	[172], [301]
IFNγ	Upregulation	[71], [73], [96]
TNFα	Upregulation	[74]

Figure 3.5 depicts the expression of these activation markers on unstimulated NK cells (panel A) and stimulated NK cells (panel B), with a histogram overlay for comparison of fluorescence (panel C). As described in section 2.19, FMO controls were used to define background fluorescence for each of the NK-cell activation markers and the FMO gating strategy is illustrated in Figures 3.6 and 3.7. Gates were set using the FMO boundaries defined for each of the NK-cell activation markers.

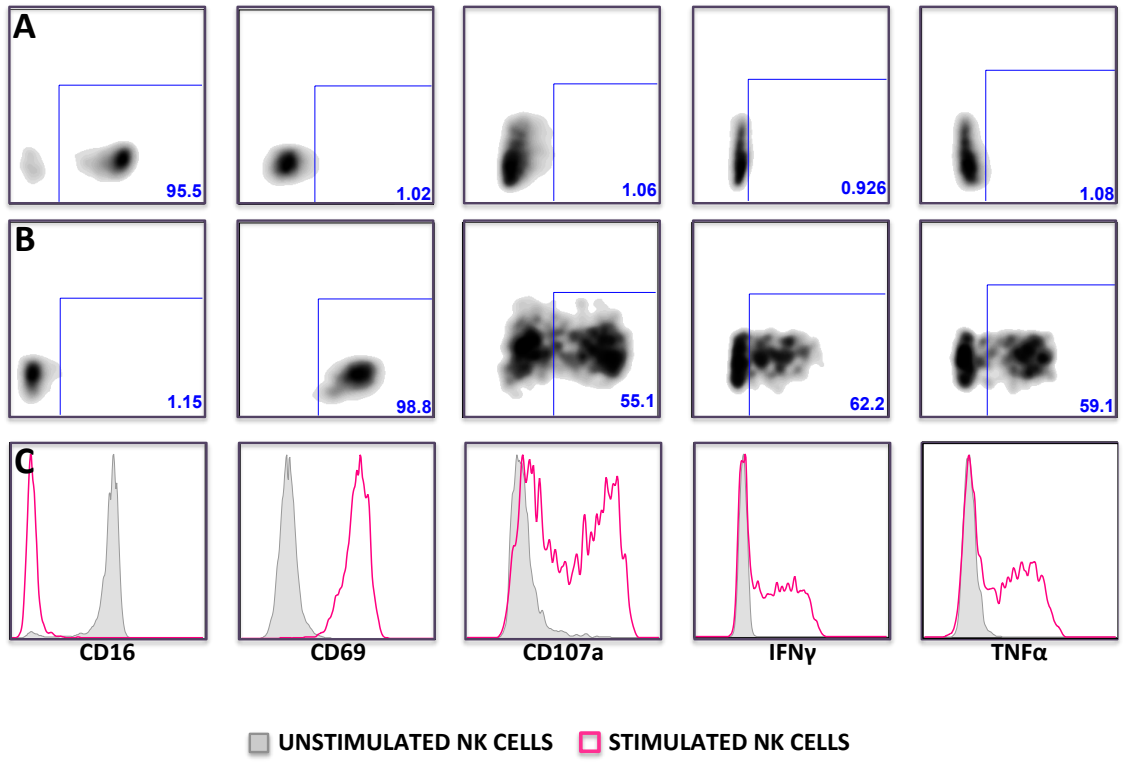

Figure 3.5. Assessment of NK-cell activation
10^5 isolated NK cells were incubated for 6 hours in the presence or absence of PMA/ionomycin. Panel A: unstimulated NK cells were gated to determine the baseline percentage of cells expressing activation markers; these gates were then applied to stimulated NK cells (panel B) to determine the change in percentage expression. Panel C displays these changes as histogram overlays.

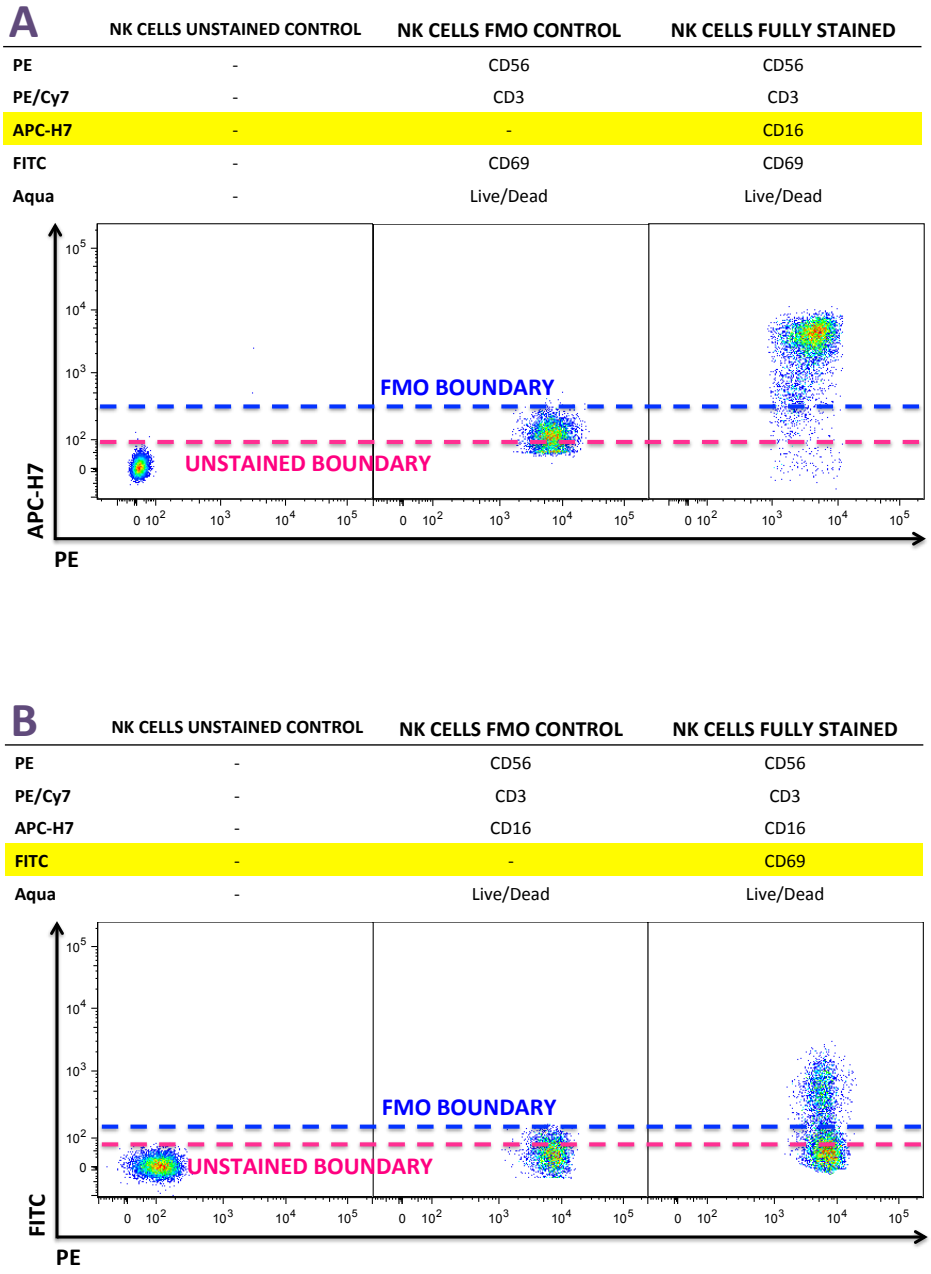

Figure 3.6. Illustration of the FMO control gating strategy used to assess CD16 and CD69 expression on NK cells
FMO controls were used to identify and gate NK cells in the context of data spread due to the multiple fluorochromes. Compensation was correctly set using single stained controls and 10^5 activated NK cells were stained as shown with all fluorochrome-conjugated antibodies except CD16-APC-H7 (panel A) or CD69-FITC (panel B). Gating boundaries were determined for FMO stained NK cells (dotted blue line). Unstained NK-cell gating boundaries are also shown (dotted pink line). Representative example of n=3 independent experiments.

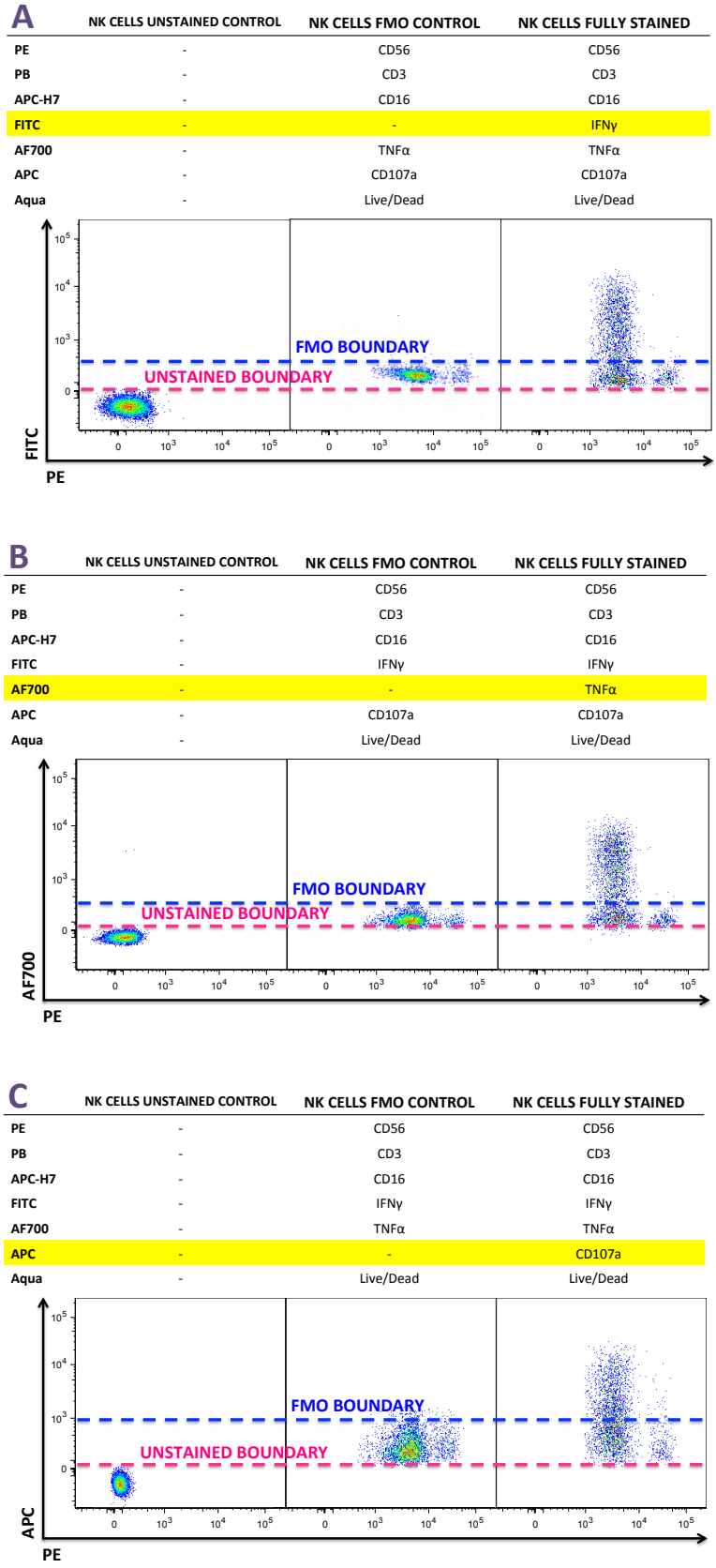

Figure 3.7. Illustration of the FMO control gating strategy used to assess IFNγ, TNFα, CD107a expression on NK cells
FMO controls were used to identify and gate NK cells in the context of data spread due to the multiple fluorochromes. Compensation was correctly set using single stained controls and 10^5 activated NK cells were stained as shown with all fluorochrome-conjugated antibodies except IFNγ-FITC (panel A), TNFα-AF700 (panel B) or CD107a-APC (panel C). Gating boundaries were determined for FMO stained NK cells (dotted blue line). Unstained NK-cell gating boundaries are also shown (dotted pink line). Representative example of n=2 independent experiments.

3.3. *In vitro* assessment of NK-cell activation: preliminary co-cultures with anti-EGFR mAbs

To assess ADCC-mediated activation, NK cells were incubated with A431 tumour target cells at 1:1 ratio, with or without anti-EGFR mAbs at 10µg/ml. Preliminary co-cultures were performed for 48 hours and utilised NK cells immediately after MACS isolation. The cell ratio, assay duration and mAb concentrations were based on studies previously reported by the Ferris laboratory [97, 240]. Cell numbers were based on those used for the clinical trial *in vitro* studies of patient samples, discussed in section 1.12.4 and these studies had also used mAbs at a concentration of 10µg/ml. Notably each of the cell types used in the co-cultures had individual preparation requirements. The conditions used for the preliminary co-cultures are summarised in Table 3.3.

Table 3.3. NK-cell activation: conditions used for preliminary co-cultures with anti-EGFR mAbs

Condition	Preparation Notes	Medium
NK-cell	MACS negatively selected NK cells (Straight *ex vivo* - NO recovery)	-
A431 tumour cell	Seeded night before assay	DMEM (with 2% hAB) [a]
Assay details	96-well flat bottom	RPMI (with 2% hAB) [a]
Assay duration	48 hours [b]	
Cell ratio | Cell number	(1:1 ratio) [b] | 10^5 of each cell type [c]	
mAb concentration	10µg/ml [d]	

[a] 2%v/v hAB serum was used instead of 10% FBS, to minimise potential for xenoactivation of NK cells
[b] Assay duration and cell ratio based on studies reported by the Ferris laboratory
[c] Cell number adapted from those used in previous clinical trials
[d] mAb concentration based on studies reported by the Ferris laboratory and previous clinical trials

3.3.1. Positive and negative controls for assessment of NK-cell activation

NK cells stimulated with PMA/Ionomycin were used as a positive control for NK-cell activation compared to freshly isolated NK cells; and are referred to in figures as [NK POSITIVE CONTROL] and [NK TIME ZERO] respectively. As a negative control, NK cells alone for the duration of the assay were included to assess the level of spontaneous NK-cell activation; referred to in figures as [NK NEGATIVE CONTROL]

3.3.2. Preliminary results showed high levels of spontaneous NK-cell activation

Results presented in Figure 3.8 show that all NK cells in the negative control exhibited substantial downregulation of CD16 and upregulated expression of CD69 compared to NK cells at time zero, indicative of spontaneous activation. When the two-cell co-culture was conducted in the presence of imgatuzumab (10µg/ml), the modulation of NK-cell activation markers did not surpass the high spontaneous activation observed in the negative control.

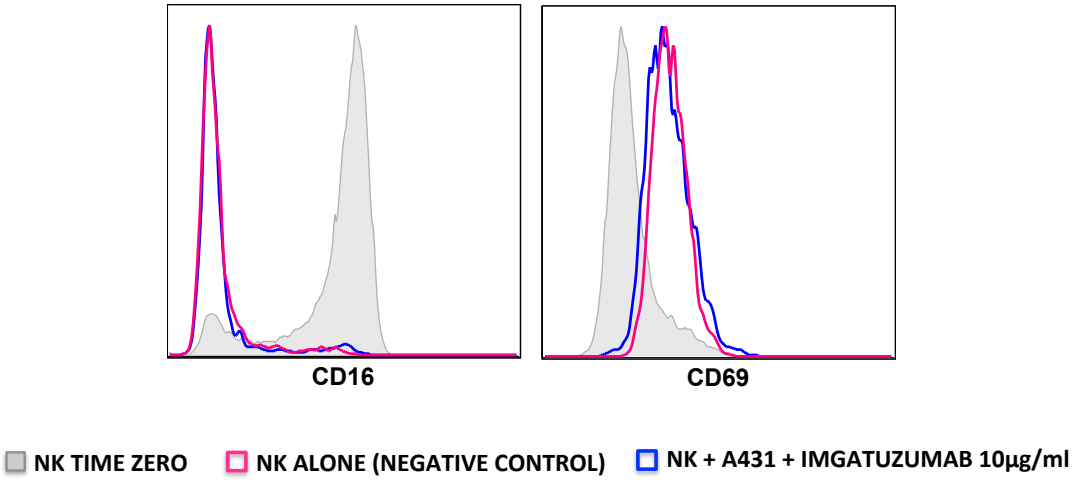

Figure 3.8. Preliminary co-culture results show high levels of spontaneous NK-cell activation
10^5 freshly isolated NK cells were screened for the expression of CD16 and CD69 at time zero (solid grey peak) and compared to NK cells incubated for 48 hours either alone (pink peak) or at 1:1 ratio with A431 tumour cells in the presence of 10µg/ml imgatuzumab (blue peak). Representative example of 2 independent experiments

3.4. *In vitro* assessment of NK-cell activation: optimisation of co-cultures with anti-EGFR mAbs to reduce spontaneous NK-cell activation

A series of assay refinements were undertaken to reduce spontaneous activation of NK cells. Optimisation of the two-cell co-culture was undertaken in conjunction with the three-cell co-culture optimisation described in Chapter 4 (section 4.6). The refinements relevant to NK-cell activation are detailed as follows:

3.4.1. NK-cell recovery prior to co-culture

There is a precedent in published literature to use NK cells after a period of recovery in low dose IL-2. This has been shown to improve NK-cell viability and also to induce uniformly higher expression levels of CD56 and CD16 when compared to non-recovered NK cells (comprehensively examined by Bryceson *et al*, 2006) [302]. In light of this, an NK-cell recovery period was introduced, comprising 16-hour incubation in complete RPMI supplemented with 50U/ml IL-2. The decision to recover the NK cells and the IL-2 concentration was also based on our previous experience of analysing samples from clinical trial patients that showed recovery of viable NK cells for use in functional assays was improved by incubation of thawed PBMC in 50U/ml IL-2 for 16 hours prior to assay. Recovering NK cells prior to use in co-culture achieved a reduction in spontaneous NK-cell activation as illustrated in Figure 3.9.

3.4.2. Media standardisation and removal of human AB serum

Although inclusion of 2% v/v hAB serum was the initial choice to avoid xenoactivation of effector cells, it came to light that hAB serum contains a high concentration of TGFβ (personal communication from Professor Giovanna Lombardi, KCL); an immunosuppressive cytokine known to negatively affect NK-cell function [136]. Additionally, it was observed that A431 cells contracted in size and lost their typical uniform monolayer when grown in DMEM supplemented with 2% hAB serum. Therefore, the media used in all cell preparations was standardised so that cells were not subjected to the shock and potential stimulatory effects of a media change when combined for co-culture. The *in vitro* maintenance of the A431 cell line and recovery of NK cells were all performed in complete RPMI (with relevant supplementation) and this media standardisation achieved a reduction in spontaneous NK-cell activation as illustrated in Figure 3.9.

3.4.3. Shorter co-culture durations and reduction of cell numbers

The 48-hour co-culture duration was reduced to 18 hours for assessment of surface activation markers and 6 hours for assessment of functional activation markers. The shorter intervals were sufficient to detect NK-cell activation with a lower level of spontaneous activation, as illustrated in Figure 3.9 A, in addition to a reduction in NK-cell death (3.9 B). Cell numbers were decreased from 10^5 of each type to $2.5x10^4$ of each type while the co-culture volume, mAb concentration and 1:1 cell ratio were maintained. The lower cell numbers allowed for more economical use of limited

donor material, without undue compromise to the flow cytometry results obtained (data from a minimum of 10,000 events was always collected). The cumulative effect of refinements detailed in sections 3.4.1 - 3.4.3 substantially reduced spontaneous NK-cell activation as illustrated in Figure 3.9, compared to results shown Figure 3.8.

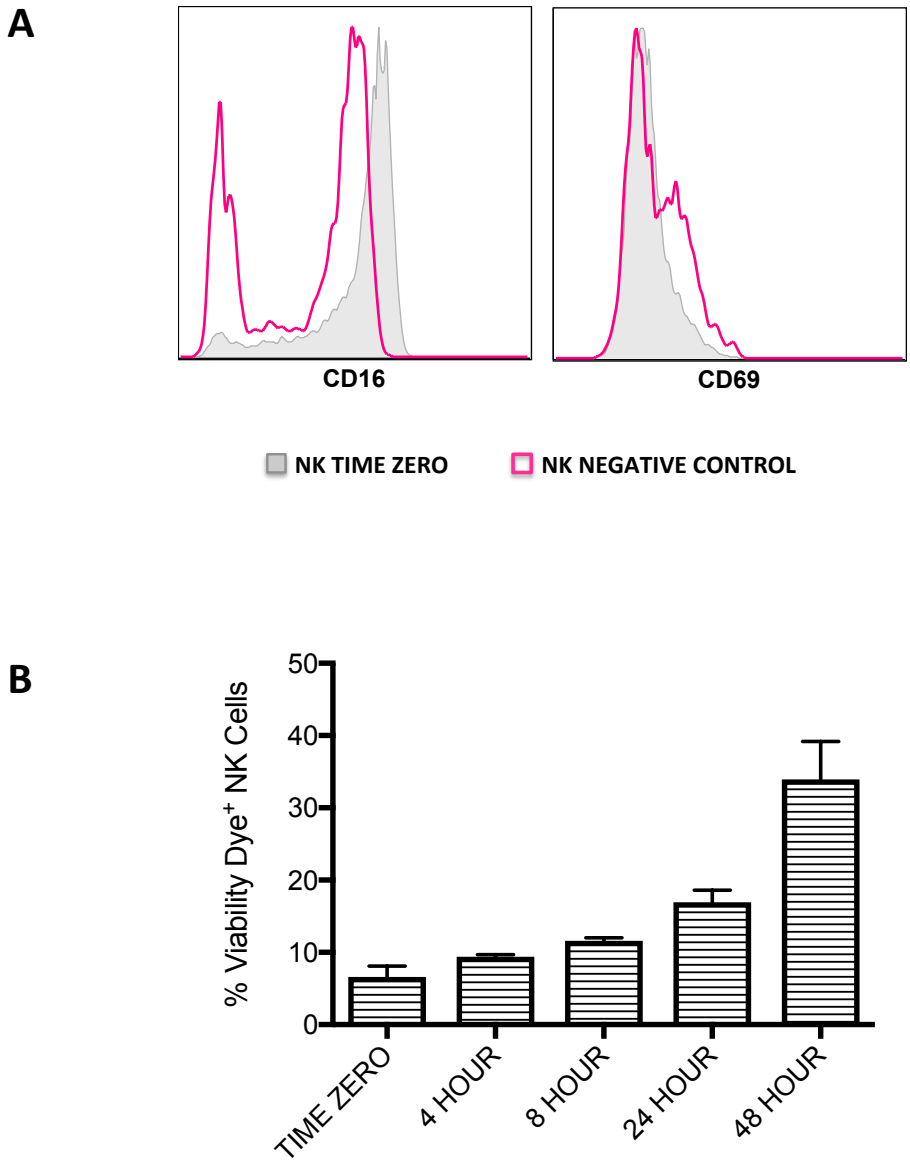

Figure 3.9. Optimisation of two-cell co-cultures with anti-EGFR mAbs: NK-cell recovery, media standardisation and decreased co-culture duration substantially reduce spontaneous NK-cell activation
A) $2.5x10^4$ recovered NK cells were screened for the expression of CD16 and CD69 at time zero (solid grey peak) and compared to the NK-cell negative control condition (pink peak) after 18 hours of co-culture. Representative example of two independent experiments. **B)** $2.5x10^4$ recovered NK cells were incubated at 1:1 ratio with A431 tumour cells for the indicated durations. A generous FACS analysis gate was set to capture live and intact dead intact cells. $CD3^-CD56^+$ NK cells were screened for expression of live/dead viability dye and compared to NK cells at time zero. Error bars represent 2 independent experiments (n=2).

3.4.4. Imgatuzumab induces activation of NK cells

Using the optimised two-cell co-culture assay, the abilities of imgatuzumab and cetuximab to activate NK cells were assessed. The results are displayed in Figure 3.10 and show the expression of the NK-cell activation marker CD69 induced by the anti-EGFR mAbs at a range of concentrations between 10µg/ml and 0.1ng/ml, relative to the NK-cell negative control. Imgatuzumab was found to induce expression of CD69 by NK cells. Cetuximab also induced NK-cell activation, consistent with other previously published reports [96, 97, 263]. At mAb concentrations of 100ng/ml and above, imgatuzumab and cetuximab induced similar levels of CD69 expression by NK cells. Notably, imgatuzumab activated NK cells to a greater extent than cetuximab at the lower concentrations of 10ng/ml and 1ng/ml. An objective during development and evaluation of therapeutic mAbs is to determine the minimum effective dose, often referred to as the minimum anticipated biological effect level (MABEL), because use of the lowest efficacious dose may help to mitigate toxicity [303, 304]. Thus, the lower concentrations of 10ng/ml and 1ng/ml were used hereafter.

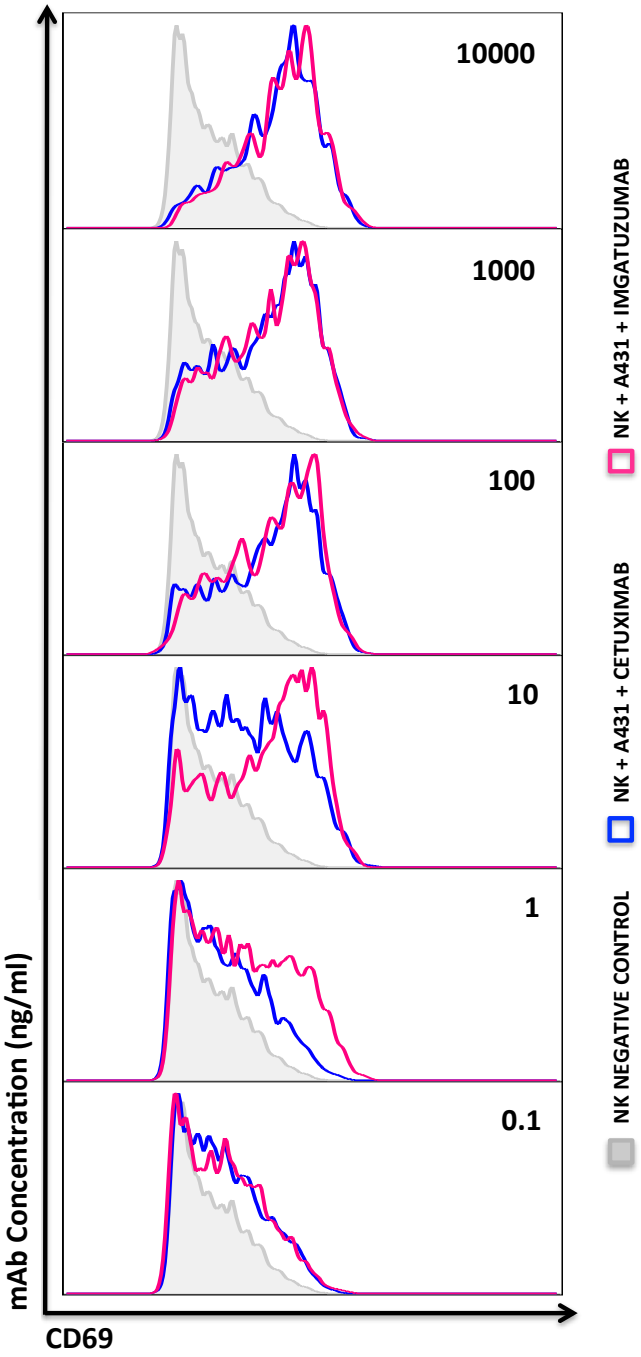

Figure 3.10. Imgatuzumab induces expression of the activation marker CD69 by NK cells and to a greater extent than cetuximab at the lower mAb concentrations

$2.5x10^4$ recovered NK cells were incubated either alone or at 1:1 ratio with A431 tumour cells in the presence or absence of mAbs at 0.1, 1, 10, 100, 1,000 and 10,000ng/ml. After 18 hours of co-culture, NK cells were screened for expression of the activation marker CD69 and compared to the negative control. Results are representative of two independent experiments.

Table 3.4. Optimised conditions used for NK-cell activation in two-cell co-cultures

Condition	Preparation Notes	Medium [a]
NK-cell	Negatively selected NK cells isolated by magnetic cell separation and recovered for 16 hours	NKRM
A431 tumour cell	Seeded 4 hours before assay	Complete RPMI
Assay details	96-well v-bottom	Complete RPMI
Assay duration	18 hours	
Cell ratio | Cell number	(1:1 ratio) | $2.5x10^4$ of each cell type	
mAb concentration	10ng/ml and 1ng/ml	

[a] All medium varieties comprised complete RPMI, with relevant supplementation

3.5. Comparison of NK-cell activation and function induced by the anti-EGFR mAbs imgatuzumab or cetuximab

3.5.1. Imgatuzumab promotes changes in expression of NK-cell surface activation markers to a greater extent than cetuximab at low mAb concentrations

Using the optimised two-cell co-culture conditions summarised in Table 3.4, NK cells isolated from 6 healthy donors were incubated with A431 cells in the presence of the anti-EGFR mAbs at equivalent concentrations, followed by measurement of expression of the surface activation markers CD16 and CD69. These experiments included an important negative control condition of NK cells incubated with A431 without mAb to assess the potential for allogeneic activation of NK cells by the HLA class I mismatched A431 cells. North *et al* demonstrated that allogeneic tumour cells could activate NK cells. These tumour-activated NK (TANK) cells displayed levels of NCR killing akin to those observed with IL2 activated NK cells [299]. In light of this, positive activation gates were set using the allogeneic control and applied to all other conditions. The only difference between the allogeneic control and the test conditions was the presence of mAb, and therefore represents a more appropriate negative control than NK cells alone. This gating strategy ensured that activation reported was above any potential allogeneic activation (although none was seen in experiments reported here).

Results are presented in Figure 3.11. CD16 expression by NK cells was significantly downregulated by imgatuzumab, but not by cetuximab. The median frequency of $CD16^+$ NK cells was 77.5% for NK cells co-cultured with A431, 75.5% for NK cells co-cultured with A431 plus the

negative control IgG_2 mAb panitumumab at 1ng/ml and similarly 71.4% for NK cells co-cultured with A431 plus cetuximab at 1ng/ml (Figure 3.11 A). In contrast, imgatuzumab at 1ng/ml induced a 2.6-fold reduction of $CD16^+$ NK cells to 30.3% ($p < 0.05$). The NK cells that remained $CD16^+$ in the co-culture containing imgatuzumab expressed significantly lower levels of CD16 compared to expression levels on $CD16^+$ NK cells in the co-culture containing cetuximab ($p < 0.05$) (Figure 3.11 B).

CD69 expression by NK cells was significantly upregulated by imgatuzumab, but not by cetuximab. The median frequency of $CD69^+$ NK cells was 1.1% for NK cells co-cultured with A431, 10.9% for NK cells co-cultured with A431 plus panitumumab at 1ng/ml and 10.5% for NK cells co-cultured with A431 plus cetuximab at 1ng/ml (Figure 3.11 C). In contrast, imgatuzumab induced a 32-fold increase of $CD69^+$ NK cells to 34.9% ($p < 0.05$). The NK cells that became $CD69^+$ in the co-culture containing imgatuzumab expressed a significantly higher intensity of CD69 compared to expression levels on $CD69^+$ NK cells in the co-culture containing cetuximab ($p < 0.05$) (Figure 3.11 D).

The mAbs were also tested at 10ng/ml and a similar trend was observed for both NK-cell surface activation markers (Figure 3.11). Although this was not significant for the frequencies of $CD16^+$ and $CD69^+$ NK cells, the NK cells that became $CD69^+$ in the presence of 10ng/ml imgatuzumab compared to cetuximab expressed a significantly higher intensity of CD69 ($p < 0.05$). These results show that imgatuzumab promoted downregulation of CD16 and increased expression of CD69 by NK cells at low mAb concentrations, whereas cetuximab did not consistently activate NK cells at low concentrations. The mAbs used in these experiments had been quantified via spectrophotometry (Table 2.2, Materials and Methods) to ensure differences observed could be attributed to properties of the mAbs and not concentration differences.

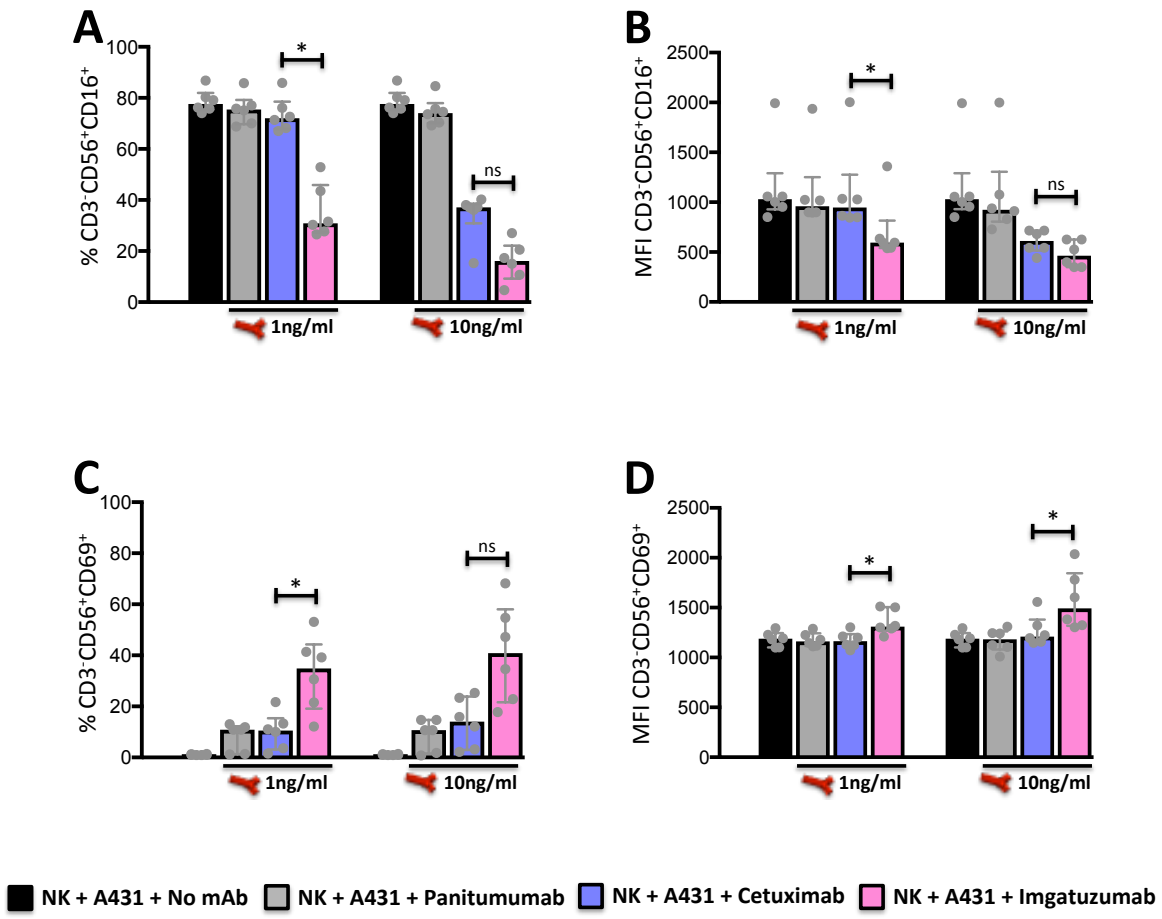

Figure 3.11. Imgatuzumab promotes changes in expression of NK-cell surface activation markers to a significantly greater extent than cetuximab at equivalent concentration

$2.5x10^4$ recovered NK cells were incubated at 1:1 ratio with A431 tumour target cells in the presence or absence of panitumumab, cetuximab or imgatuzumab (1ng/ml and 10ng/ml). Cells were co-cultured for 18 hours. Graphs depict $CD3^-CD56^+CD16^+$ NK-cell frequency (A) and MFI (B) and $CD3^-CD56^+CD69^+$ NK-cell frequency (C) and MFI (D), with median and interquartile range for 6 independent experiments (n=6). *p <0.05 **p <0.005 (Friedman's ANOVA, with Dunn's multiple comparison post hoc).

3.5.2. Imgatuzumab promotes changes in expression of NK-cell surface activation markers to a greater extent than cetuximab when target cells express low levels of EGFR

Expression of EGFR by primary tumours is heterogeneous and at lower levels than the A431 cell line, which expresses uniformly high levels of EGFR [305]. Therefore, it was important to assess the impact of EGFR cell surface expression on mAb mediated NK-cell activation. Assays were performed using the transfected H1299 cell line from which three ΔEGFR stable sub-lines were selected that expressed a range EGFR levels, designated $EGFR^{LOW}$, $EGFR^{MEDIUM}$ and $EGFR^{HIGH}$, as depicted in Figure 3.12. 6-hour assays were conducted using mAbs at 10ng/ml; probing expression of NK-cell surface activation markers CD16 and CD69. The use of isogenic transfected cells meant that any variation in induced NK-cell activation was likely the result of differences in sub-line EGFR expression level, rather than differences in cell type.

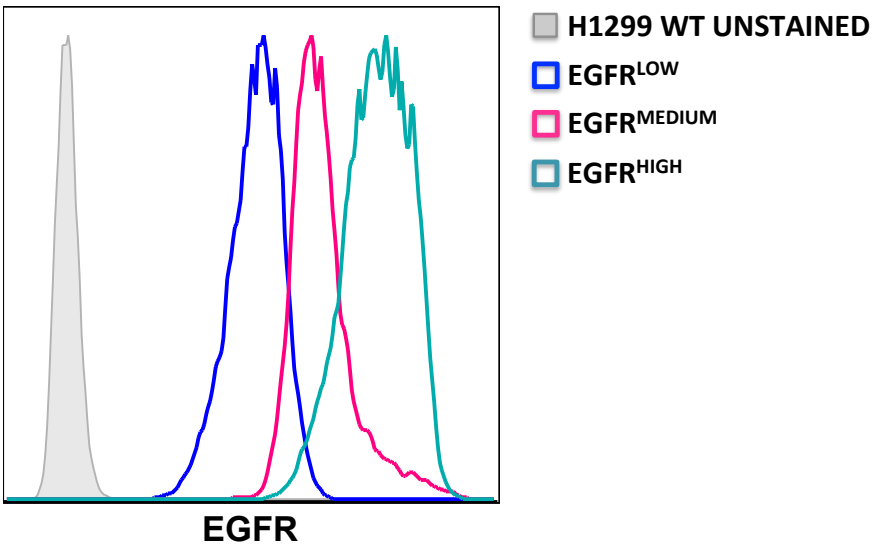

Figure 3.12. Tumour target cells with low, medium and high EGFR expression levels
Surface EGFR expression levels on the H1299 cell line, and the H1299 transfected ΔEGFR sub-lines: $EGFR^{LOW}$, $EGFR^{MEDIUM}$ and $EGFR^{HIGH}$ were assessed by flow cytometry. Representative example of 2 independent experiments.

These experiments included the negative control conditions of NK cells incubated with $EGFR^{LOW}$, $EGFR^{MEDIUM}$ or $EGFR^{HIGH}$ without mAb, to assess the potential for allogeneic activation of NK cells by the HLA class I mismatched ΔEGFR cells and the gating strategy ensured that activation reported was above any potential allogeneic activation. Results are presented in Figure 3.13. In

these experiments, cetuximab exhibited some ability to promote NK-cell activation, but imgatuzumab was superior at all target cell EGFR expression levels.

The median frequency of $CD16^{+}$ NK cells was 72.6% for NK cells co-cultured with $EGFR^{LOW}$ target cells alone and similarly 67.6% for NK cells co-cultured with $EGFR^{LOW}$ plus panitumumab. The $CD16^{+}$ frequency decreased to 47.4% for NK cells co-cultured with $EGFR^{LOW}$ plus cetuximab, but decreased furthermore to 28.4% in the presence of imgatuzumab ($p < 0.05$). This represented a median 1.5- and 2.6-fold decrease in CD16 expression induced by cetuximab and imgatuzumab respectively, relative to the control. Although the same trend was observed using $EGFR^{MEDIUM}$ and $EGFR^{HIGH}$ target cells, these results were not significant, as illustrated in Figure 3.13 A. The median fold change in activation marker expression compared to control is summarised in Table 3.5.

The median frequency of $CD69^{+}$ NK cells was 1.1% when co-cultured with $EGFR^{LOW}$ target cells alone and similarly 1% when co-cultured with $EGFR^{LOW}$ plus panitumumab. The $CD69^{+}$ frequency increased to 9.4% for NK cells co-cultured with $EGFR^{LOW}$ plus cetuximab, but increased furthermore to 11.6% in the presence of imgatuzumab ($p < 0.05$). This represented a median 8.5 and 10.5-fold increase in the CD69 expression induced by cetuximab and imgatuzumab respectively, relative to the control. Like CD16, this finding was not observed with the use of $EGFR^{MEDIUM}$ and $EGFR^{HIGH}$ target cells. There were no statistical differences between the cetuximab or imgatuzumab induced $CD69^{+}$ NK-cell frequencies as illustrated in Figure 3.13 B, nor the median fold change as summarised in Table 3.5.

Of note, higher levels of EGFR expression by target cells correlated with greater NK-cell activation. For imgatuzumab, the median fold change in $CD16^{+}$ NK-cell frequency rose from 2.6 to 5.2 when using $EGFR^{LOW}$ and $EGFR^{HIGH}$ target cells respectively and the median fold change in $CD69^{+}$ NK-cell frequency rose from 10.5 to 15.1 when using $EGFR^{LOW}$ and $EGFR^{HIGH}$ target cells respectively. Since the mAb concentration was kept constant across all EGFR intensities it is reasonable to assert that the level of NK-cell activation is also dependent on antigen density, a finding previously reported by Derer *et al* [306].

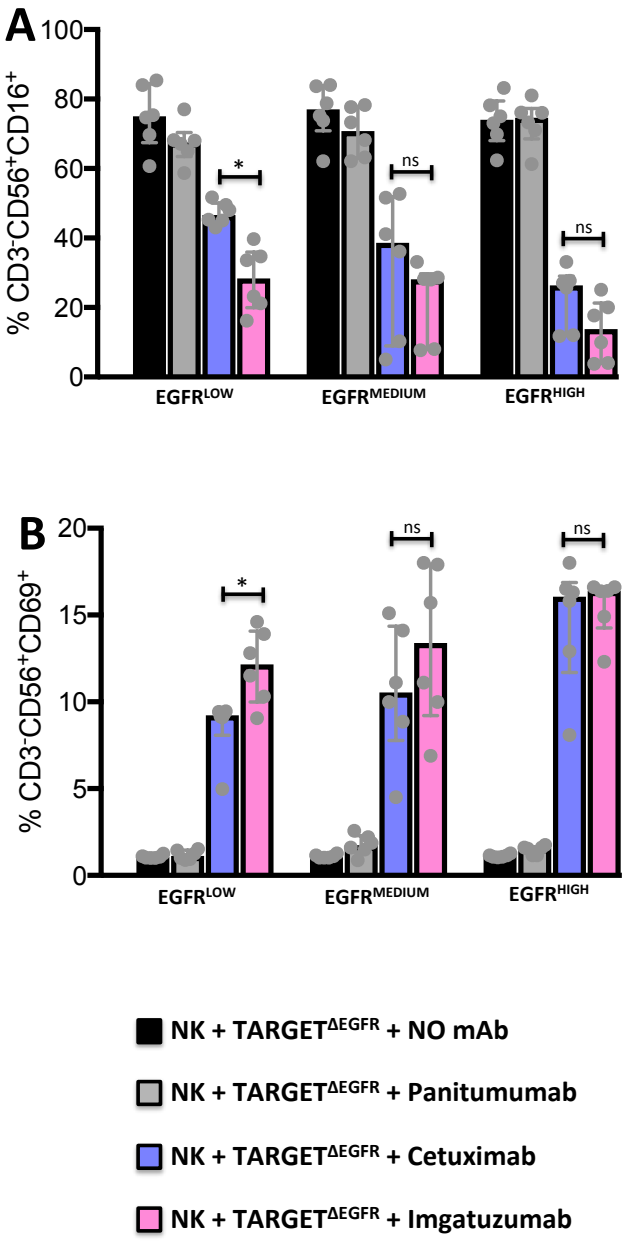

Figure 3.13. Imgatuzumab promotes changes in expression of NK-cell surface activation markers to a significantly greater extent than cetuximab at low EGFR antigen expression levels

$2.5x10^4$ recovered NK cells were incubated at 1:1 ratio with $EGFR^{LOW}$, $EGFR^{MEDIUM}$ or $EGFR^{HIGH}$ tumour target cells in the presence or absence of panitumumab, cetuximab or imgatuzumab (10ng/ml). Cells were co-cultured for 6 hours. Graphs depict (A) $\%CD16^+$ and (B) %CD69+ NK cells, with median and interquartile range for 6 independent experiments (n=6). *p <0.05 (Friedman's ANOVA, with Dunn's multiple comparison post hoc).

Table 3.5. Median fold change in expression of NK-cell surface activation markers in the presence of ΔEGFR cell lines and anti-EGFR mAbs

Median fold change vs. control	$EGFR^{LOW}$			$EGFR^{MEDIUM}$			$EGFR^{HIGH}$		
	PAN	CETUX	IMGAT	PAN	CETUX	IMGAT	PAN	CETUX	IMGAT
%CD16+	1.1	1.5	2.6*	1.1	2.1	2.6	0.99	2.7	5.2
%CD69+	0.91	8.5	10.5*	1.4	10.1	10.6	1.5	15	15.1

Abbreviations: PAN - Panitumumab | CETUX - Cetuximab | IMGAT - Imgatuzumab
Significantly greater fold change compared to cetuximab *p <0.05

It was intended that all experiments conducted with A431 would be reproduced with H1299 cells. Unfortunately this was not possible as H1299 clones became infected with mycoplasma and attempts to rescue were unsuccessful.

3.5.3. Imgatuzumab promotes NK-cell function to a greater extent than cetuximab

Comparison of the promotion of NK-cell function by imgatuzumab and cetuximab anti-EGFR mAbs was performed using NK cells isolated from 7 healthy donors. Recovered NK cells were incubated with A431 cells in the presence of mAbs at 10ng/ml for 6 hours, followed by measurement of NK-cell function based on expression of CD107a and production of IFNγ and TNFα. These experiments included the condition of NK cells incubated with A431 without mAbs, to control for potential allogeneic NK-cell activation. The results are presented in Figure 3.14. For all NK-cell function markers, no NK-cell activation was detected in the test condition of NK cells incubated with A431 and panitumumab, consistent with the limited ability of the IgG_2 mAb to recruit NK cells for ADCC (the effector recruitment capabilities of antibody isotypes is reviewed by Vidarsson *et al* [124]). Incubation of NK cells with K562 cells increased the frequency of $CD107a^+$, $IFN\gamma^+$, $TNF\alpha^+$ and $IFN\gamma^+TNF\alpha^+$ NK cells to medians of 20.8%, 6.1%, 7.3% and 4.2% respectively, consistent with NK-cell activation induced by CD16-independent killing mechanisms.

Comparison of median percentage positive showed that imgatuzumab consistently mediated significantly greater NK-cell functional activity than cetuximab ($p < 0.05$). The median $CD107a^+$ NK-cell frequency increased significantly from 30.2% in the presence of cetuximAb to 46.8% with

imgatuzumab. Similarly, the median IFNγ$^+$ frequency rose significantly from 9.2% to 16.8%, TNFα$^+$ from 9.4% to 15% and IFNγ$^+$TNFα$^+$ from 3.1% to 6.3%. The superiority observed with imgatuzumab was reproducible for all donors across all markers of NK-cell function assessed.

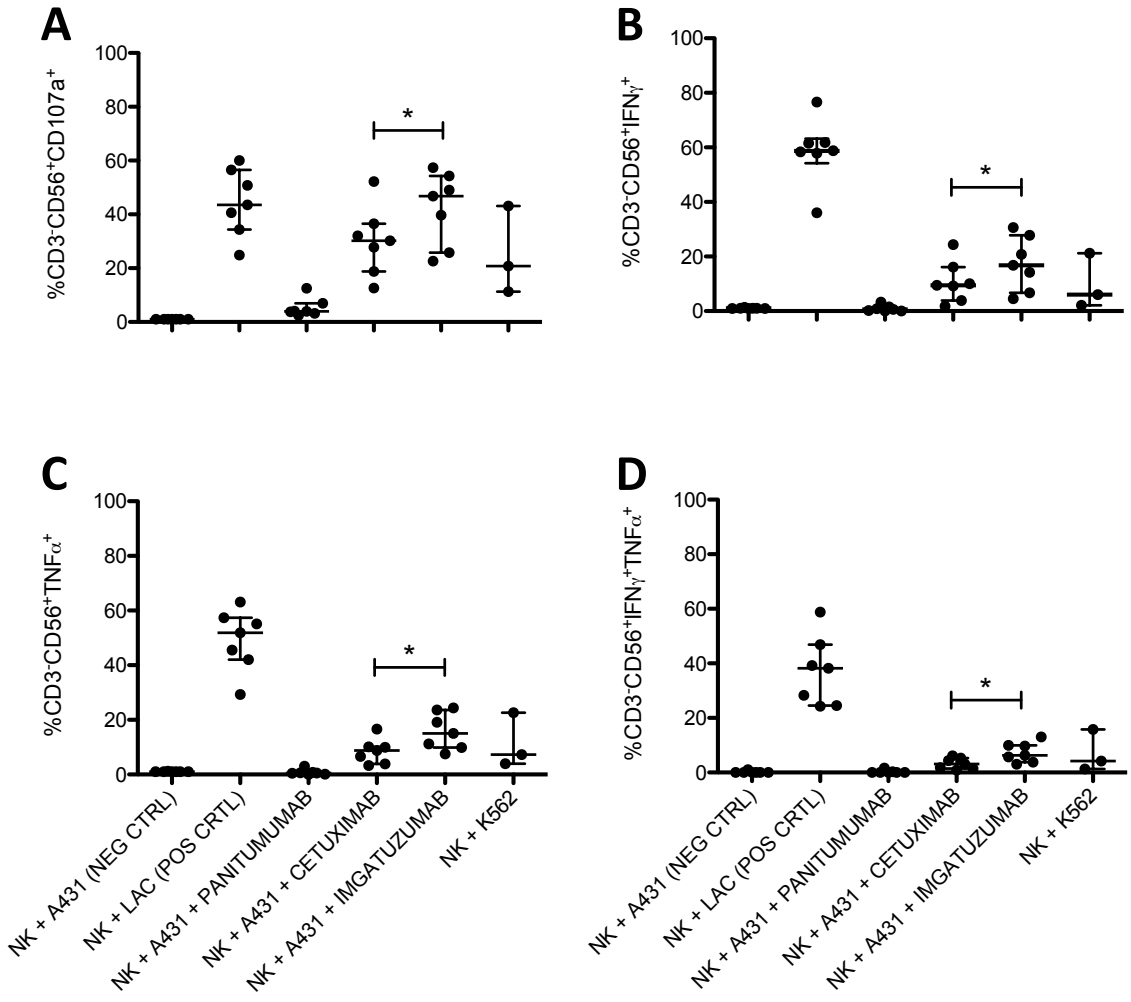

Figure 3.14. Imgatuzumab promotes NK-cell function to a significantly greater extent than cetuximab at equivalent concentration

2.5x10^4 recovered NK cells were incubated at 1:1 ratio with either K562 or A431 tumour target cells in the presence or absence of panitumumAb, cetuximab or imgatuzumab (10ng/ml). Cells were co-cultured for 6 hours with addition of BFA after 1 hour. Graphs depict frequency of CD3$^-$CD56$^+$ NK cells that are (A) CD107a$^+$, (B) IFNγ$^+$, (C) TNFα$^+$ and (D) IFNγ$^+$TNFα$^+$, with median and interquartile range for 7 independent experiments (n=7). *p<0.05 (Wilcoxon signed rank test).

3.5.4. Imgatuzumab promotes NK-cell function to a greater extent than cetuximab in the context of all CD16 genotypes

The V158F FCγRIIIa (CD16) polymorphism encoding V/V high affinity homozygotes has previously been correlated with improved survival in cetuximab-treated HNSCC patients when compared to F/F low affinity homozygotes [97]. The NK-cell function experiment described in section 1.5.3 included donors with all possible CD16 genotypes. In Figure 3.15, these results have been segregated according to donor CD16 genotype (CD16 low affinity (F/F), high affinity (V/V) and heterozygote (V/F) donors). At equivalent concentration, imgatuzumab promoted better NK-cell functional activity than cetuximab, specifically using NK cells from donors that were homozygous for the low affinity CD16 genotype. Unfortunately the cohort of NK-cell donors used in the genotyping evaluation was too small to allow statistical comparison between genotypes (n=7).

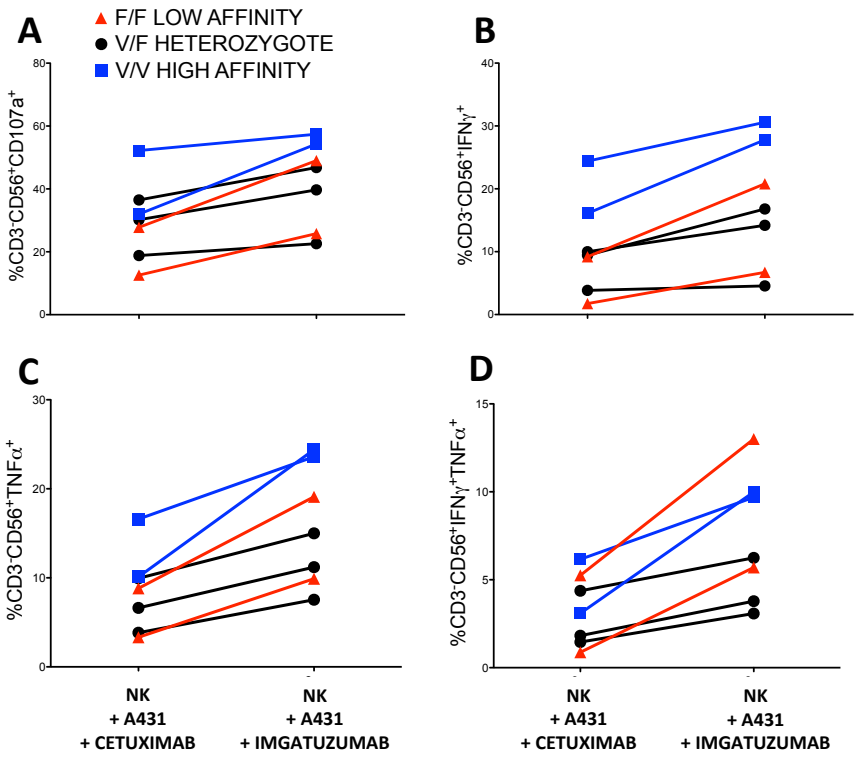

Figure 3.15. Imgatuzumab promotes NK-cell function to a greater extent than cetuximab in the context of all CD16 genotypes

$2.5x10^4$ recovered NK cells were incubated at 1:1 ratio with A431 tumour target cells in the presence of cetuximab or imgatuzumab (10ng/ml). Cells were co-cultured for 6 hours with addition of BFA after 1 hour. Graphs depict frequency of $CD3^-CD56^+$ NK cells that are (A) $CD107a^+$, (B) $IFN\gamma^+$, (C) $TNF\alpha^+$ and (D) $IFN\gamma^+TNF\alpha^+$, with median for 7 independent experiments (n=7). CD16 low affinity (F/F), high affinity (V/V) and heterozygote (V/F) donors are highlighted in red, blue and black respectively.

3.6. Comparison of NK-cell activation and function induced by the glyco-engineered anti-CD20 mAb GA101GE or unmodified equivalent GA101WT

The ability of a GE-mAb to induce NK-cell activity and function was also assessed for the antibody target CD20, which is exploited for the treatment of B-cell malignancies. Both the GE-modified anti-CD20 drug obinituzumab (GA101GE) and the unmodified wild type counterpart GA101WT were available for study, enabling evaluation of the impact of the GE-modification *per se*. In keeping with the precedent to compare efficacy of GE-mAbs to clinically utilised mAbs set by previously reported studies [205, 232, 238, 263, 297], the widely used anti-CD20 therapeutic mAb rituximab was also studied.

The material transfer agreement between Roche Glycart and King's College London for use of GA101GE and GA101WT was only obtained towards the end of the research project. Therefore, due to limited time, it was not possible to perform all the two-cell *in vitro* co-culture experiments to evaluate NK-cell activity and function that were previously undertaken with the anti-EGFR mAbs.

3.6.1. $CD20^+$ tumour cell line: JY

The TA CD20 is a surface marker expressed by B cells. The Epstein-Barr virus immortalised lymphoblastoid B-cell line JY was used in the CD20 *in vitro* model. Surface expression of CD20 by JY cells was confirmed by flow cytometry, with the A431 cell line used as a negative control. Results are shown in Figure 3.16.

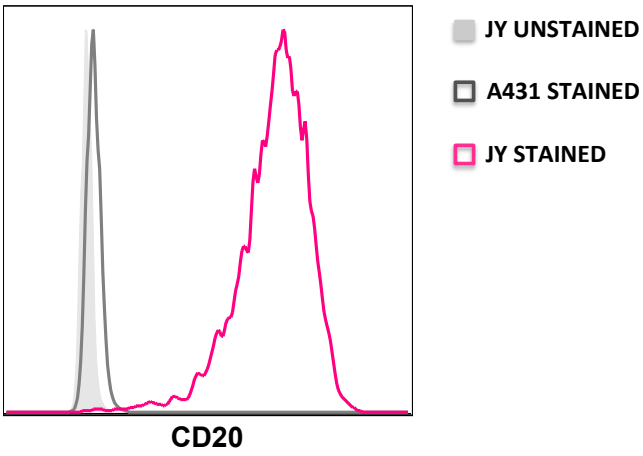

Figure 3.16. Tumour cell line JY expresses high levels of CD20
10^5 JY cells and A431 cells (negative control) were stained with anti-CD20 PE-labelled antibody and assessed by flow cytometry.

3.6.2. GA101GE promotes changes in expression of NK-cell surface activation markers to a greater extent than GA101WT

The two-cell, 18-hour co-culture assay was performed to assess NK-cell activation in the presence of the anti-CD20 mAbs rituximab, GA101WT and GA101GE, using $CD20^+$ JY tumour target cells co-cultured with recovered NK cells isolated from 6 healthy donors. The mAbs were tested at concentrations of 10ng/ml and 1ng/ml. Experiments included the negative control condition of NK cells incubated with JY only, to assess the potential for allogeneic activation of NK cells by the HLA class I mismatched JY cells. Gates set using the JY allogeneic control were applied to all other conditions, ensuring that reported activation was above any potential allogeneic activation.

Results displayed in Figure 3.17 show that the glyco-engineered mAb GA101GE promoted changes in expression of NK-cell surface markers indicative of activation. Moreover, GA101GE induced changes to a significantly greater extent than GA101WT at both concentrations tested, indicating that the GE modification enhances activity. The median percentage of $CD16^+$ NK cells was reduced to 53.3% with GA101GE compared to 73% with GA101WT at 1ng/ml; 2.7% and 64% respectively at 10ng/ml ($p < 0.05$). Also, the remaining $CD16^+$ NK cells had significantly lower levels of CD16 expression with GA101GE compared to GA101WT at both concentrations ($p < 0.05$). The median percentage of NK cells expressing the activation marker CD69 was

significantly increased to 23.2% with GA101GE compared to 6.1% with GA101WT at 1ng/ml; 42.8% and 22.7% respectively at 10ng/ml. However, the induced $CD69^+$ NK cells attained similar levels of expression at both concentrations. Notably the median percentage of $CD69^+$ NK cells was significantly higher with 10ng/ml GA101GE (42.8%) compared to 1ng/ml GA101GE (23.2%). The increase in mAb concentration correlated with the increase in NK-cell activation, suggesting that the level of activation induced by ADCC is also dependent on mAb concentration; supporting previous findings by Derer *et al* [306]. Additionally, at the lower concentration of 1ng/ml, a significantly greater level of activation was induced with GA101GE compared to GA101WT for both activation markers ($p < 0.05$). The mAbs used in these experiments had been quantified by spectrophotometry (Table 2.2) to ensure differences observed could be attributed to properties of the mAbs, not differences in concentration. Rituximab promoted little or no change in expression of NK-cell surface activation markers at the concentrations tested.

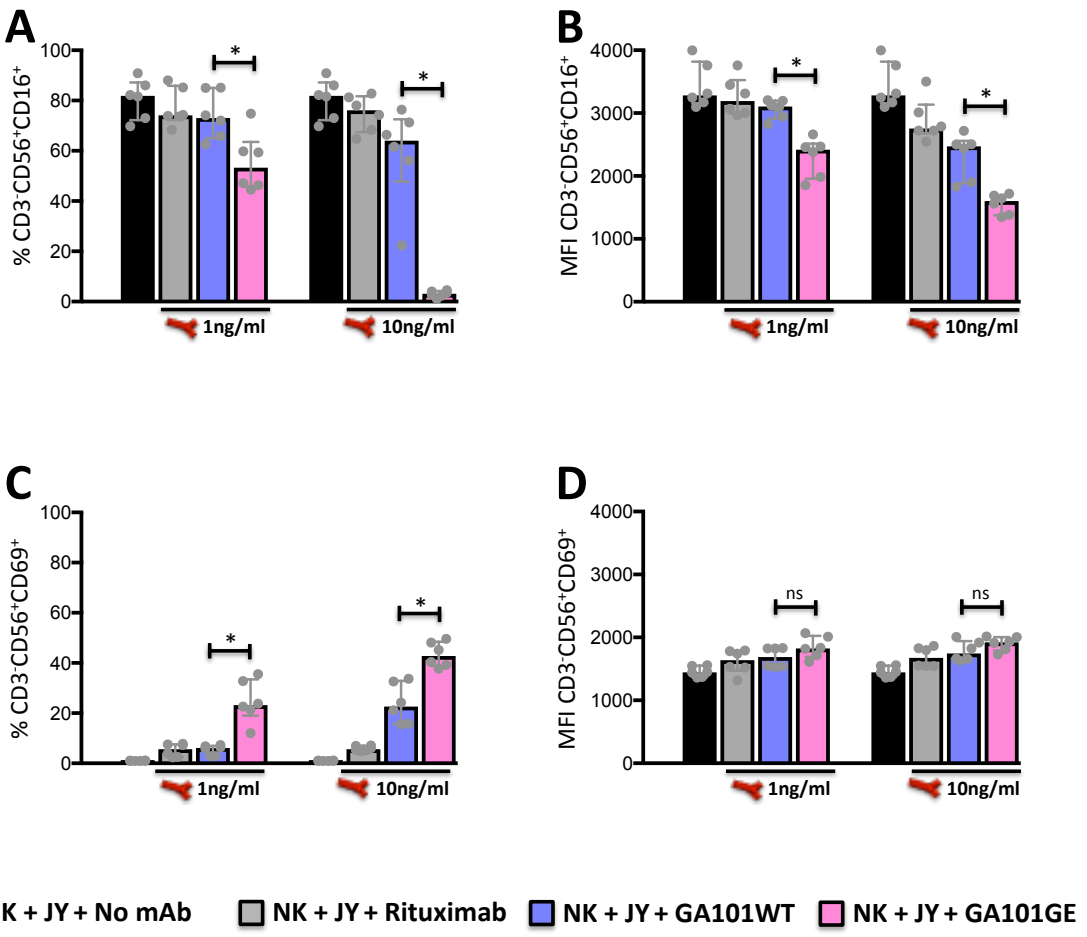

Figure 3.17. GA101GE promotes changes in expression of NK-cell surface activation markers to a significantly greater extent than GA101WT at equivalent concentration

$2.5x10^4$ recovered NK cells were incubated at 1:1 ratio with JY tumour target cells in the presence or absence of rituximab, GA101WT or GA101GE (1ng/ml and 10ng/ml). Cells were co-cultured for 18 hours. Graphs depict $CD3^-CD56^+CD16^+$ NK-cell frequency (A) and MFI (B) and $CD3^-CD56^+CD69^+$ NK-cell frequency (C) and MFI (D), with median and interquartile range for 6 independent experiments (n=6). *p <0.05 (Friedman's ANOVA, with Dunn's multiple comparison post hoc).

3.6.3. GA101GE promotes NK-cell function to a greater extent than GA101WT

Comparison of the promotion of NK-cell function by GA101GE and GA101WT anti-CD20 mAbs was performed using NK cells isolated from 8 healthy donors. Recovered NK cells were incubated with JY cells in the presence of mAbs at 10ng/ml for 6 hours, followed by measurement of NK-cell function based on expression of CD107a and production of IFNγ and TNFα. These experiments included the condition of NK cells incubated with JY without mAbs, to control for potential allogeneic NK-cell activation.

The results presented in Figure 3.18 show that GA101GE consistently mediated significantly greater NK-cell functional activity than GA101WT ($p < 0.05$). The median $CD107a^+$ NK-cell frequency increased significantly from 20.4% in the presence of GA101WT to 35.5% with GA101GE. Similarly, the median $IFN\gamma^+$ frequency rose significantly from 20.7% to 46.5%, $TNF\alpha^+$ from 14.4% to 29.8% and $IFN\gamma^+TNF\alpha^+$ from 15.9% to 32.2%. Rituximab did not promote NK-cell function at the concentrations tested. The superiority observed with GA101GE over GA101WT was reproducible for NK cells from all donors across all markers of NK-cell function assessed. These findings indicate that the GE modification significantly improves the ability of the mAb to promote NK-cell function.

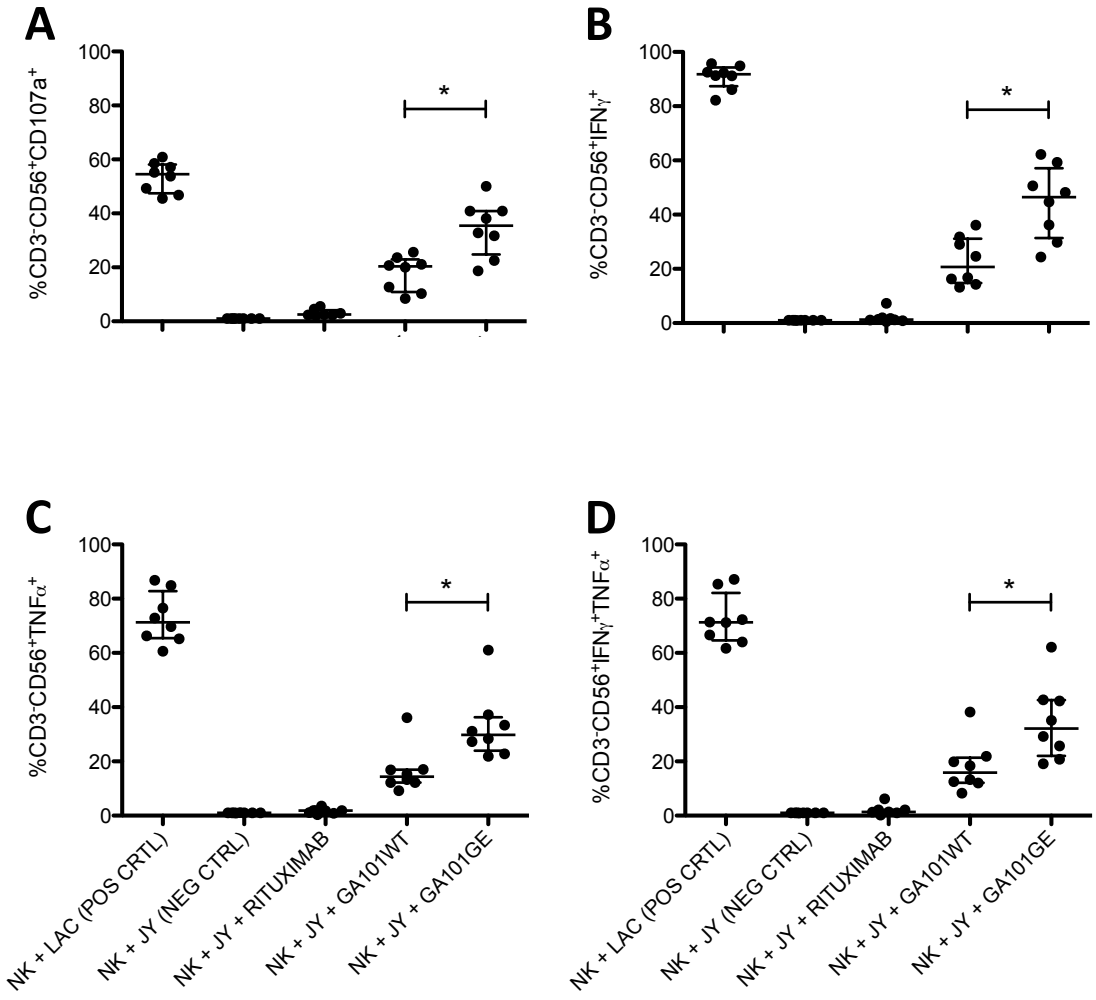

Figure 3.18. GA101GE promotes NK-cell function to a significantly greater extent than GA101WT at equivalent concentration

$2.5x10^4$ recovered NK cells were incubated at 1:1 ratio with JY tumour target cells in the presence or absence of rituximab, GA101WT or GA101GE (10ng/ml). Cells were co-cultured for 6 hours with addition of BFA after 1 hour. Graphs depict frequency of $CD3^-CD56^+$ NK cells that are (A) $CD107a^+$, (B) $IFN\gamma^+$, (C) $TNF\alpha^+$ and (D) $IFN\gamma^+TNF\alpha^+$, with median and interquartile range (n=8). *$p<0.05$ (Wilcoxon signed rank test).

3.6.4. GA101GE promotes tumour cell apoptosis to a greater extent than GA101WT

Stimulation of TA-specific $CD8^+$ T cell immunity as a consequence of ADCC activity by mAbs requires that they induce apoptotic death of tumour cells, thereby releasing TA for phagocytosis by DC. The next step, therefore, was to assess whether the NK-cell activity induced by GE-mAbs resulted in apoptosis of tumour cells.

Apoptotic cells undergo multiple microcellular rearrangements including cellular condensation, redistribution of specific organelles into peripheral membrane protrusions or "blebs" and the exposure of apoptosis-specific structures on the cell membrane such as, phosphotidyl serine (PS) [307, 308]. AnnexinV is an intracellular protein that binds to PS with high affinity and can be used as a sensitive marker to identify early apoptotic cells that possess PS on the cell surface. Early apoptotic cells exclude viability dyes such as propidium iodide (PI) whilst the loss of membrane integrity observed in late-stage apoptotic and necrotic cells allows passage of these dyes into the nucleus where they bind DNA. The combination of a viability dye such as PI and annexin V can be used to identify early apoptotic and late apoptotic/necrotic populations. Viable cells are considered $AnnexinV^-PI^-$; early apoptotic cells are $AnnexinV^+PI^-$; and late apoptotic/necrotic cells are $AnnexinV^+PI^+$. A single observation of double positive cells is not sufficient to conclude apoptosis as the mode of cell death, rather, when apoptosis is measured over time or over a range of drug killing concentrations, the cells can be tracked through the three stages [308, 309, 310].

Induction of apoptotic cell death was measured in the anti-CD20 mAb setting using the JY tumour cell line. The activity of GA101GE was assessed and compared to the unmodified GA101WT to evaluate any impact of the GE-modification *per se*. The anti-CD20 therapeutic mAb rituximab was also studied. An assessment of target cell apoptosis induction using the anti-EGFR mAbs could not be performed because the $EGFR^+$ tumour cell line A431 is adherent, requiring trypsinisation that made the cells permeable to PI. Recovered NK cells from 4-6 healthy donors were incubated with JY tumour cells for 3, 6 and 9 hours in the presence of the anti-CD20 mAbs at 10ng/ml, 100ng/ml and 1000ng/ml. The three-hour assay was also conducted in the presence of physiologic concentrations of competing non-specific total human IgG (5mg/ml) as this was used for some of the GE-mAb mediated tumour killing assays reported by Gerdes *et al* [205].

The gating strategy employed to analyse the apoptosis assay data is illustrated in Figure 3.19.

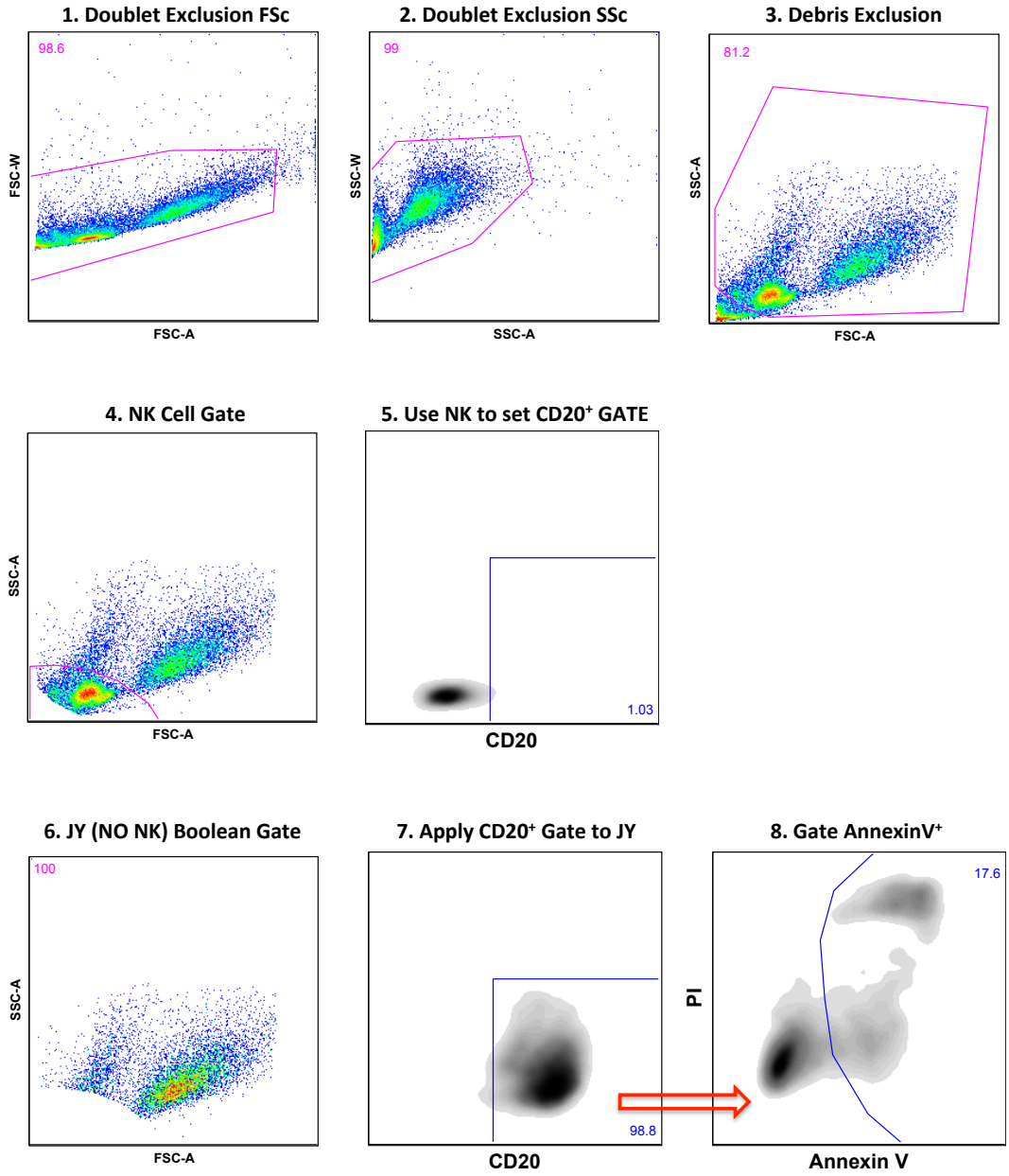

Figure 3.19. Apoptosis assay gating strategy
$2.5x10^4$ live JY cells were incubated either alone or at 1:1 ratio with recovered NK cells in the presence or absence of anti-CD20 mAbs and apoptotic death of JY cells was evaluated based on Annexin V and PI staining. Sequential gating achieved exclusion of doublets and debris. NK cells were identifiable as a small $CD20^-$ population as shown in plots 4 and 5 and excluded from the JY population via Boolean gating as shown in plot 6. The $CD20^+$ gate, set using $CD20^-$ NK cells was applied to the JY population, clearly displaying dead and viable cells distinguishable by FSc. This population was then assessed for Annexin V and PI staining. Representative example shown.

As negative controls, JY cells were incubated alone without mAbs to assess spontaneous apoptosis (Figure 3.20A), or in the presence of NK cells (1:1 ratio) without mAbs, to assess apoptosis induced by NK-cell allorecognition of JY cells (Figure 3.20B). As a positive control, JY cells were exposed to a combination of apoptosis inducing agents - 10μM actinomycin D, 2μM camptothecin, 100μM cycloheximide, 10μM dexamethasone and 100μM etoposide (Figure 3.20C).

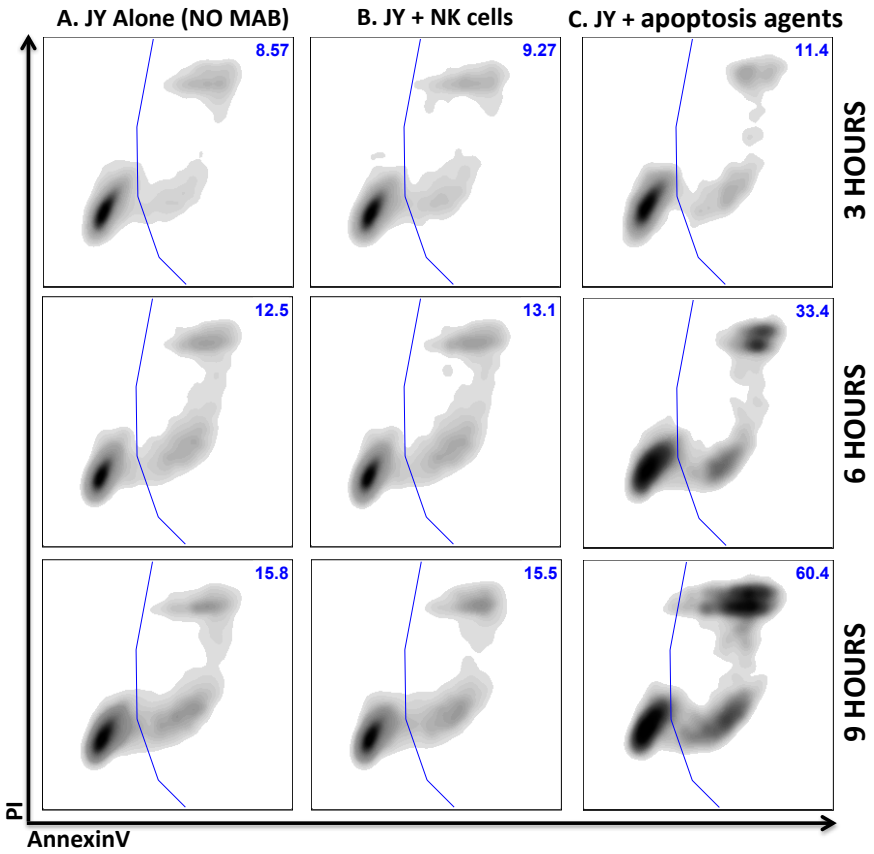

Figure 3.20. Apoptosis assay: negative and positive controls
$2.5x10^4$ live JY cells were incubated either alone, at 1:1 ratio with recovered NK cells or in the presence of apoptosis inducing agents. Apoptotic death of JY cells was evaluated based on Annexin V and PI staining. Representative example shown.

Results presented in Figure 3.21 show that the glyco-engineered mAb was able to promote NK-cell mediated apoptotic tumour cell death. Moreover, GA101GE promoted apoptosis to a greater extent than unmodified GA101WT, with significant differences observed using mAbs at a concentration of 10ng/ml (Figure 3.21 A) and at the 3-hour incubation time (Figure 3.21 B). Under these assay conditions, the median frequency of $AnnexinV^+$ JY cells was significantly higher for

GA101GE (22.6%) compared to GA101WT (16.1%, p <0.05). GA101GE was 1.4-fold more efficacious at inducing apoptosis than GA101WT at the same concentration. Rituximab only promoted apoptosis of tumour cells at the higher mAb concentrations (100ng/ml and 1µg/ml) and was less efficacious than GA101WT and GA101GE (Figure 3.21 A).

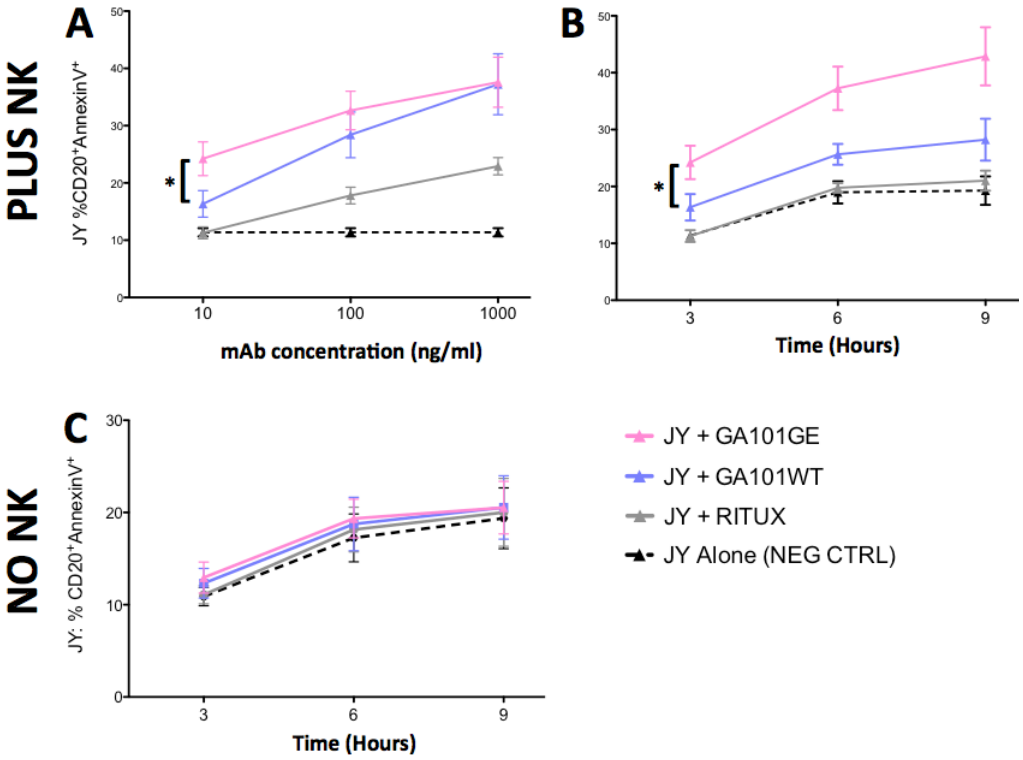

Figure 3.21. GA101GE promotes apoptotic tumour-cell death to a significantly greater extent than GA101WT
$2.5x10^4$ live JY cells were cultured with anti-CD20 mAbs: rituximab, GA101WT or GA101GE in the presence (PLUS NK) or absence (NO NK) of recovered NK cells at 1:1 ratio. **(A)** Cells were incubated for 3 hours with mAbs at concentration of 10ng/ml, 100ng/ml and 1000ng/ml. **(B and C)** Cells were incubated for durations of 3, 6 or 9 hours with mAbs at a concentration of 10ng/ml. Graphs display frequency $CD20^+AnnexinV^+$ JY cells, with median and interquartile range for minimum n=4. *p <0.05 (Friedman's ANOVA, with Dunn's multiple comparison post hoc). No other statistically significant differences were observed.

Previous studies have reported that the dimerization of CD20 induced by antibody binding is sufficient to induce apoptosis, in the absence of ADCC [297, 311, 312] (reviewed by Deans *et al*, 2002 [313]). Therefore, JY cells were incubated with mAbs at 10ng/ml in the absence of NK cells to assess CD20 ligation-mediated apoptosis. JY cells alone served as a negative control to assess spontaneous apoptosis. Results are displayed in Figure 3.21 C. Spontaneous apoptosis of JY cells occurred with a median of 11% at 3 hours rising to 15% at 6 hours and 17% by 9 hours. The presence of mAbs at 10ng/ml did not increase the level of tumour-cell apoptosis significantly

above spontaneous apoptosis; suggesting that at a concentration of 10ng/ml mAbs alone were not inducing apoptosis in assays reported in this study.

The significantly enhanced efficacy of GA101GE was maintained when apoptosis of tumour cells was assessed in the presence of physiologic concentrations of competing nonspecific total human IgG (5mg/ml). The results presented in Figure 3.22 show that presence of competing IgG reduced mAb-mediated apoptosis of JY cells, but GA101GE still induced a significantly higher percentage of apoptotic JY cells (median 17.3%) compared to GA101WT (median 13.7% - p <0.05).

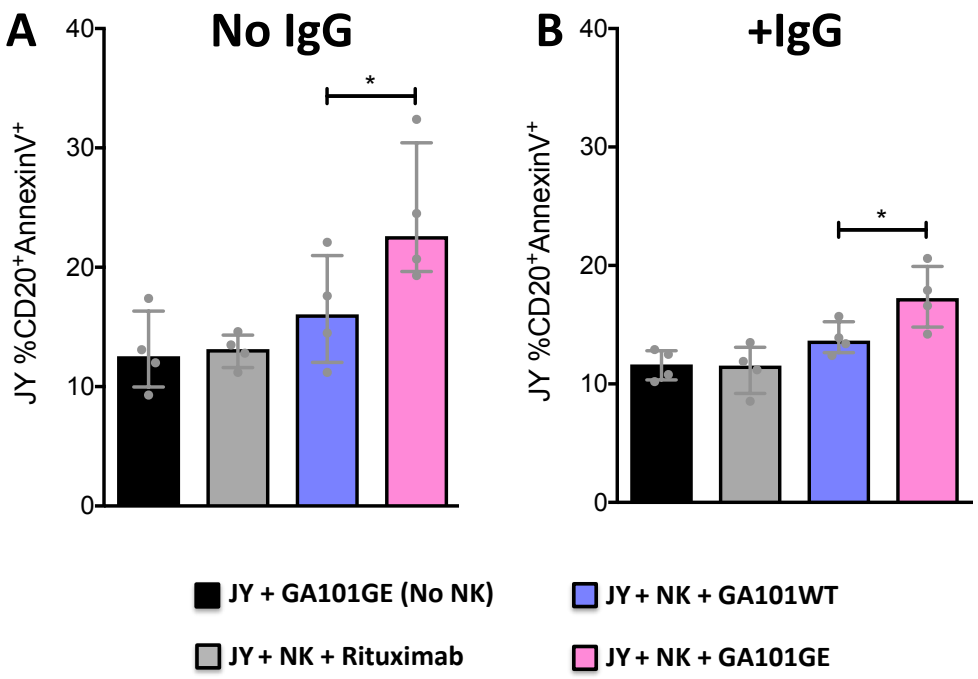

Figure 3.22. GA101GE promotes apoptotic cell death to a significantly greater extent than GA101WT in the presence of physiologically relevant concentrations of competing IgG
$2.5x10^4$ live JY cells were cultured at 1:1 ratio with recovered NK cells in the presence or absence of anti-CD20 mAbs: rituximab, GA101WT or GA101GE (10ng/ml). Cells were incubated for 3 hours without **(A)** or with physiologic concentration of competing human IgG **(B)**. Graphs display frequency $CD20^+AnnexinV^+$ JY cells, with median and interquartile range for n=4. *p <0.05 (Friedman's ANOVA, with Dunn's multiple comparison post hoc).

3.7. Discussion

The results presented in this chapter demonstrated that GE mAbs induced the NK-cell activation and NK-cell function associated with adaptive cellular immunity. This is the first report to describe the cytokine and surface marker phenotype of primary NK cells activated by GE-mAb-mediated ADCC. Previous studies have used NK cell lines as effectors [205], and assessed ability to lyse tumour cells but did not evaluate NK-cell activation and function associated with promoting anti-tumour adaptive cellular immunity [205, 232, 297]. In keeping with the precedent set by these previous studies, GE mAbs were compared to clinically utilised mAbs at equivalent concentrations, and shown to promote NK-cell activity to a greater extent at low mAb concentrations.

3.7.1. GE-mAbs induce NK-cell activation and functions associated with stimulation of adaptive immunity

Activation of NK cells by GE-mAbs was detected in the context of several different parameters of NK-cell activity. ADCC-mediated killing of target cells by NK cells can be inferred by measuring downregulation of CD16 that occurs after binding of IgG_1 [298]. The GE-mAbs consistently induced downregulation of CD16 on NK cells, indicating the ability to promote NK-cell killing of tumour cells. GE-mAbs also induced increased cell surface expression of CD69. CD69 is an early activation marker that is now considered to be a NCR, following observations that it can initiate lytic activity [314].

Assessment of NK-cell activity by measurement of the functional parameters CD107a, IFNγ and TNFα also showed the GE-mAbs induced functional activity. CD107a is expressed on lysosomal intra-cellular membranes. Presence on the cell surface is indicative of degranulation, and thus represents another measure of NK-cell killing activity. Evidence of enhanced production of cytokines in the presence of GE-mAbs is important because cytokines promote activity of other immune cells, such as DC [74, 301]. Assessment of the ability of GE-mAbs to promote DC function will be described in the next chapter. Notably, the GE-mAbs increased the frequency of polyfunctional NK cells producing both IFNγ and TNFα. Effector cells that produce multiple cytokines are associated with more effective immune responses than single cytokine producers [315, 316].

3.7.2. Imgatuzumab significantly enhances NK-cell activation compared to cetuximab

When compared with cetuximab, imgatuzumab was found to promote modulation of CD16 and CD69, to a significantly greater extent than cetuximab; including when tumour antigen expression was low. The finding that a imgatuzumab has significantly better ability to promote NK-cell killing at lower antigen densities is important because heterogeneity of tumour antigen expression is observed, and studies have cited low antigen expression and downregulation of tumour antigen post treatment as reasons for lack of mAb efficacy [305, 317]. The augmented performance of a GE-mAb at low antigen density does, however, warrant caution. In the case of TA such as EGFR, a protein expressed at low levels on healthy cells and abnormally high levels on tumour cells, a GE-mAb may have the potential to cause killing of normal healthy cells. This so called 'on-target' but 'off-tumour' reactivity could have life threatening consequences.

Imgatuzumab-activated NK cells upregulated CD107, IFNγ and TNFα to a significantly greater extent than cetuximab-activated NK cells. The rationale for glyco-engineering a therapeutic IgG_1 mAb is to circumvent the impact of CD16 genotype on functional efficacy. Although the number of donors was insufficient for statistical analysis of each CD16 genotype, imgatuzumab promoted superior NK-cell functional activity compared to cetuximab across all functional activation markers and for all donors, irrespective of genotype and importantly in the most challenging setting of low affinity. Extending the study to include sufficient donors for statistical analysis of each CD16 genotype is a future consideration.

Statistically significant differences between imgatuzumab and cetuximab were observed at low concentrations (1ng/ml and 10ng/ml), and often when imgatuzumab showed activity but cetuximab was close to background. These results support the findings of Gerdes *et al,* who measured cell cytotoxicity by quantifying lactose dehydrogenase activity released from damaged/dying cells [205] and observed that imgatuzumab exhibited superior *in vitro* ADCC when compared with cetuximab. Gerdes *et al* titrated mAbs from 1µg/ml to 0.01ng/ml in a number of their experiments with A431 or A549 adenocarcinoma cells [205] and 10ng/ml was often the earliest point at which differences were seen between cetuximab and imgatuzumab.

In this study, NK-cell activity was indistinguishable at higher mAb concentrations. This observation suggests that GE mAbs may have better potential for activity within the tumour milieu where mAb concentrations are likely to be much lower than circulating levels in plasma [318, 319, 320]. Pharmacokinetic studies of patients treated with GE and non-GE mAbs have reported the mean peak plasma concentration post single-dose infusion to be around 10µg/ml (personal communication from Roche-Glycart and cited elsewhere for cetuximab as ~200ng/ml based on standard 400mg/m^2 [321]). By inference, the 1-10ng/ml concentration at which NK-cell activation efficacy differed between the imgatuzumab and cetuximab may approximate to the physiologically relevant concentration of mAb within tumour lesions.

Undertaking a functional comparison between imgatuzumab and cetuximab calls for caution before drawing any conclusions. The binding site of imgatuzumab differs from cetuximab (see Table 1.2). Consequently, the superiority of imgatuzumab could also be due to fundamental differences in its interactions with the binding site on the EGFR ECD, such as binding orientation and membrane proximity. Rigorous comparison, with the objective to identify which variation is responsible for which experimental effect would require step-wise assessment, that is, the use of GE-cetuximab, such as that created by Yi *et al* [322] for direct comparison with non-GE cetuximab; and the use of GE and non-GE imgatuzumab to evaluate the contribution of glyco-engineering, then comparison of equivalent mAb forms to evaluate the benefit of the binding epitope.

Gerdes *et al* determined the mAb concentration that inhibited the binding of EGF to EGFR by half (IC_{50}) for cetuximab and imgatuzumab and both mAbs inhibited EGF binding with an IC_{50} of ~0.33nmol/L [205]. Treating at equivalent EGF-binding concentrations such as IC_{50}, or at equivalent binding affinity are further strategies to normalise each of the mAbs used in this study and should be considered in future.

3.7.3. GA101GE induces NK-cell activation to a greater extent than GA101WT

The epitope limitations mentioned for the anti-EGFR mAb comparisons also apply to the comparison of rituximab and GA101GE in the anti-CD20 mAb context; although the inclusion of GA101WT has addressed this. Roche Glycart have previously reported that their WT- and GE-mAbs showed identical antigen binding and pharmacokinetic (PK) properties to their parental mAbs; and reason that this is because there are no potential N-linked glycosylation sites within

their variable regions [205, 221]. This finding that the altered FcγR binding affinity in afucosylated mAbs does not alter PK compared to fucosylated mAbs is supported by at least one other study [323], using FuT8-KO glyco-engineering. Therefore comparing GA101WT and GA101GE allowed conclusions to be drawn on the effect of glyco-engineering *per se*, because these mAbs bind identical antigen epitopes.

GA101GE was found to promote the modulation of CD16, CD69, CD107, IFNγ and TNFα to a significantly greater extent than GA101WT. Thus, under the conditions described in this study, glyco-engineering can enhance NK-cell activation, which has the potential to benefit individuals of both low (158F) and high (158V) affinity CD16 genotype [205, 232].

3.7.4. GA101GE promotes apoptotic tumour-cell death to a significantly greater extent than GA101WT

Given one objective of this study was to assess whether GE-mAbs are able to induce adaptive immunity, a key assessment of the NK-cell activity promoted by GE-mAbs was measurement of the tumour cell apoptosis induced. Blebbing associated with apoptosis is a potent 'eat me' signal for DC that facilitates cell clearance and crucially could provide DC with tumour antigen for presentation to T cells [70].

It is well established that destruction of tumour cells by apoptosis is essential for tumour-cell phagocytosis by DC, and that tumour particulate with a higher percentage of apoptotic material is preferentially phagocytosed compared to necrotic remnants with a lower proportion of apoptotic material [70, 106, 324, 325, 326]. The GE-mAb-mediated apoptosis of tumour cells therefore generates apoptotic tumour particulate that could potentially be ingested by DC.

When compared at equivalent concentration, GA101GE was shown to promote a significantly higher frequency of NK-cell mediated apoptosis of tumour cells in the same timeframe as GA101WT. This effect was maintained in the presence of physiologic concentrations of non-specific total IgG. Faster induction of apoptosis is important for two reasons. First, the length of time that the immune synapse between an NK-cell and its target remains stable can potentially be as short as 45 minutes before the NK-cell disassociates to continue serial killing [327]. Second, DC actively ingest exogenous material, a process which has been shown to occur within 6 minutes for

some phagocytes [328]. Therefore, by inference, GE-mAbs might augment DC phagocytosis of tumour particulate compared to unmodified mAbs.

The choice to use the $EGFR^+$ A431 cell line was justified by its use in previous studies as representative of epithelial carcinomas [205, 238]. Significant differences between imgatuzumab and cetuximab were also seen with an alternative $EGFR^+$ cell line H1299, providing some evidence for wider applicability. However, because of the delay in receiving the anti-CD20 mAbs, these experiments were conducted with only one $CD20^+$ cell line, JY. Interpretation of results using JY may be problematic for the following reasons:

1. JY cells characterised by RNA-seq analysis have been reported to express murine leukaemia virus (MuLV) antigens, which Lin *et al* suggested are potentially immunogenic and a source of experimental variation [329]. The authors were however careful to indicate that the cells they tested were donated 20 years prior to their analysis, undergoing multiple rounds of freeze thawing. They analysed a further 3 $CD20^+$ cell lines subsequently purchased from ATCC and compared them in parallel to their donated stocks. The purchased cells were $MuLV^-$ negative, therefore implicating laboratory contamination as the most likely mechanism of infection [329]. Although NK cells did not appear alloreactive to JY cells in this study, this is nevertheless a cautionary note on fully characterising investigative cell lines; which, other than screening for surface expression of the antigen of interest and HLA-type, was not done in this study.

2. In addition, JY cells may represent an aggressive subtype of DLBCL-like EBV-driven lymphoproliferative disease, in which rituximab has limited efficacy (personal communication with Professor Christopher Fegan, Cardiff University). This may explain why experimental results with rituximab and JY were essentially negative or close to background. The demonstration that GA101GE-induced NK-cell activation exceeded both GA101WT and rituximab in many JY experiments suggests that GA101GE has potential to be efficacious even in a wider variety of B-cell malignancies including those that are rituximab refractory. Notably this *in vitro* result contradicts the initial clinical observations of the GOYA DLBCL study described in section 1.14.2, which saw no statistical differences in the efficacy of GA101GE compared to rituximab [258]. This discord suggests that JY cells may not be suitable for *in vitro* $CD20^+$ tumour modelling, possibly because their uniformly high CD20 expression does not reflect the heterogeneity of CD20

expression between and within different lymphoma subtypes as determined by flow cytometry [330], thus cannot predict the heterogeneity of a clinical response. Interestingly, subsequent reanalysis of GOYA study data by the original investigators identified a new molecular subgroup of DLBCL referred to as "strong- germinal center B-cell" (GCB) in almost 25% of patients. This distinct subgroup was identifiable by gene expression profiling and characterised by mutations that are also commonly identified in FO-lymphoma patients. Strikingly, in the strong-GCB subgroup, treatment with G-CHOP conferred substantial clinical benefit over R-CHOP, with PFS of 88% and 66% respectively [331]. Thus the retrospective GOYA data analysis showed some agreement with the *in vitro* results obtained for JY in this study, but mostly served to highlight and reiterate that JY cells may represent a distinct rituximab refractory niche. It would be invaluable if PFS in the strong-GCB subgroup could be further categorised or correlated with other prognostic markers such as CD20 expression. This may help to identify panels of representative cell lines upon which pre-clinical work could be modelled.

3. Furthermore, although the GA101GE results detailed in this chapter were significant, related studies of anti-CD20 targeted therapies have presented data with more widely used $CD20^+$ cell lines such as Daudi [317, 332] and Raji [232, 253, 297, 317] (both derived from Burkitt's lymphoma). Ideally, both established cell lines and recently harvested primary tumour cells should be used to reproduce these experiments, to enable comparisons with previous work and to demonstrate wider applicability and clinical relevance.

Investigation of the effect of GE-mAbs on DC will be described in the following chapter.

Chapter 4. Results II: Glyco-engineered monoclonal antibodies induce DC phagocytosis of tumour antigen and promote DC maturation

4.1. Introduction

Results presented in the previous chapter demonstrated that GE-mAbs are able to induce the NK-cell functions required for stimulation of adaptive cellular immunity. In this chapter, analysis of the cross-talk of GE-mAb-activated NK cells with DC is described.

The next steps required for priming of TA-specific $CD8^+$ T cells are that tumour particulate generated by apoptotic tumour cell death induced by GE-mAbs is phagocytosed by DC and that NK-cell activity induces maturation of DC. Tumour particulate taken up by DC is processed to generate TA for cross-presentation to $CD8^+$ T cells. DC maturation is characterised by the upregulation of co-stimulatory molecules which provide the essential second signal for activation, differentiation and proliferation of $CD8^+$ T cells. The GE-mAb-activated NK cells were shown to produce IFNγ and TNFα that could potentially induce DC maturation. Furthermore, results presented in Figures 3.14 and 3.18 showed that GE-mAbs promote production of IFNγ and TNFα by NK cells to a significantly greater extent than non-GE mAbs at equivalent concentrations. Therefore, by inference, GE-mAbs may induce DC maturation more than unmodified mAbs.

Visualisation by *in vitro* fluorescence microscopy of the ability of GE-mAbs to enhance monocyte/macrophage and neutrophil-mediated phagocytosis of tumour cells has been reported previously [233, 333]. Using a similar approach, GE-mAb-dependent phagocytosis by DC was evaluated.

The Ferris laboratory has shown that cetuximab-activated NK cells induce DC maturation [96, 97, 263]. In this study, the ability of GE-mAb-activated NK cells to induce maturation of iDC was explored. Comparisons with clinically utilised mAbs at equivalent concentrations were performed, in keeping with the precedent to compare efficacy of GE-mAbs to current standard of care set by previously reported studies [205, 232, 238, 263, 297]. To assess any impact of the GE modification *per se* on efficacy,

where possible GA101GE was compared to the unmodified counterpart GA101WT that is otherwise identical.

The objectives of the studies described in this chapter were to assess whether tumour particulate generated by GE-mAb activity is phagocytosed by DC and if GE-mAb-activated NK cells promote DC maturation.

4.2. Phagocytosis of tumour particulate by DC

The phagocytosis of tumour-derived material was examined by co-culture of iDC with apoptotic tumour cells. Phagocytosis of tumour particulate by DC was assessed in the context of the anti-CD20 mAb *in vitro* co-culture model using JY tumour cells that are grown in suspension. Experiments in the context of anti-EGFR mAbs were not performed because the trypsinisation required for the adherent tumour cell line A431 before co-culture caused some background apoptosis, likely due to the increased permeability of A431 cell membranes after this process.

Detection of DC phagocytosis *in vitro* requires high concentrations of apoptotic material. The enhanced ability of GA101GE to induce apoptosis compared to GA101WT was only evident at a concentration of 10ng/ml, however less than 45% of tumour cells underwent apoptosis at these low concentrations (Figure 3.21 A and B) and the amount of material generated with 10ng/ml GA101GE was insufficient to detect phagocytosis of apoptotic tumour particulate by DC above background in this study[i]. At the high mAb concentrations required to induce sufficient apoptosis of tumour cells for detection, it has been reported previously that anti-CD20 mAb alone induces high levels of tumour-cell apoptosis due to dimerization of CD20 stimulating apoptosis, in the absence of ADCC [297, 311, 312] (reviewed by Deans *et al*, 2002 [313]). The phenomenon of CD20 ligation-mediated apoptosis by mAb alone was exploited to assess whether phagocytosis of tumour particulate by DC could occur in the *in vitro* co-culture model used in this study.

[i] Triplicates screened:
n=3 independent experiments with GA101GE at 10ng/ml
n=2 independent experiments with rituximab at 10ng/ml

4.2.1. Assay conditions for assessment of phagocytosis

The assay used was based on a protocol described by Miksa *et al* (2009) that exploited the properties of pHrodoRed-SE to label cells after apoptosis induction. This pH-sensitive dye fluoresces with brighter intensity in acidic environments such as in the DC phagosome and enabled detection of engulfed material due to increased post-phagocytic light emission [289]. Miksa and colleagues induced apoptosis in thymocytes by pre-treating with dexamethasone, labelled the apoptotic cells with pHrodoRed-SE and subsequently monitored phagocytosis of the thymocytes by monocytes using microscopy. In this study, JY tumour cells were pre-treated with 10µg/ml GA101GE for 16 hours to induce high levels of apoptosis, then labelled with pHrodoRed-SE prior to addition of iDC for 1-3 hours at 1:1 ratio, followed by counterstaining and visualisation by microscopy.

4.2.2. Microscopy: phagocytosis visualisation strategy

The visualisation strategy employed gave the clearest discrimination of phagocytosed particles. The top three panels in Figure 4.1 display iDC labelled with CD11c FITC (green), JY tumour particulate labelled with pHrodoRed-SE (red) and a merged image of the same area (left to right). The merged image in the bottom right panel incorporated the DAPI nuclear stain (blue) to identify intact DC. The enlarged slices view illustrates discrimination of tumour particulate that had been engulfed by the DC, with phagocytosis indicated by co-localisation and yellowing, compared to a situation where tumour particulate is attached to a DC, but not inside the cell. Figures 4.2 and 4.3 show 3-dimensional (3D) volume views of internalised tumour particulate (small and large respectively).

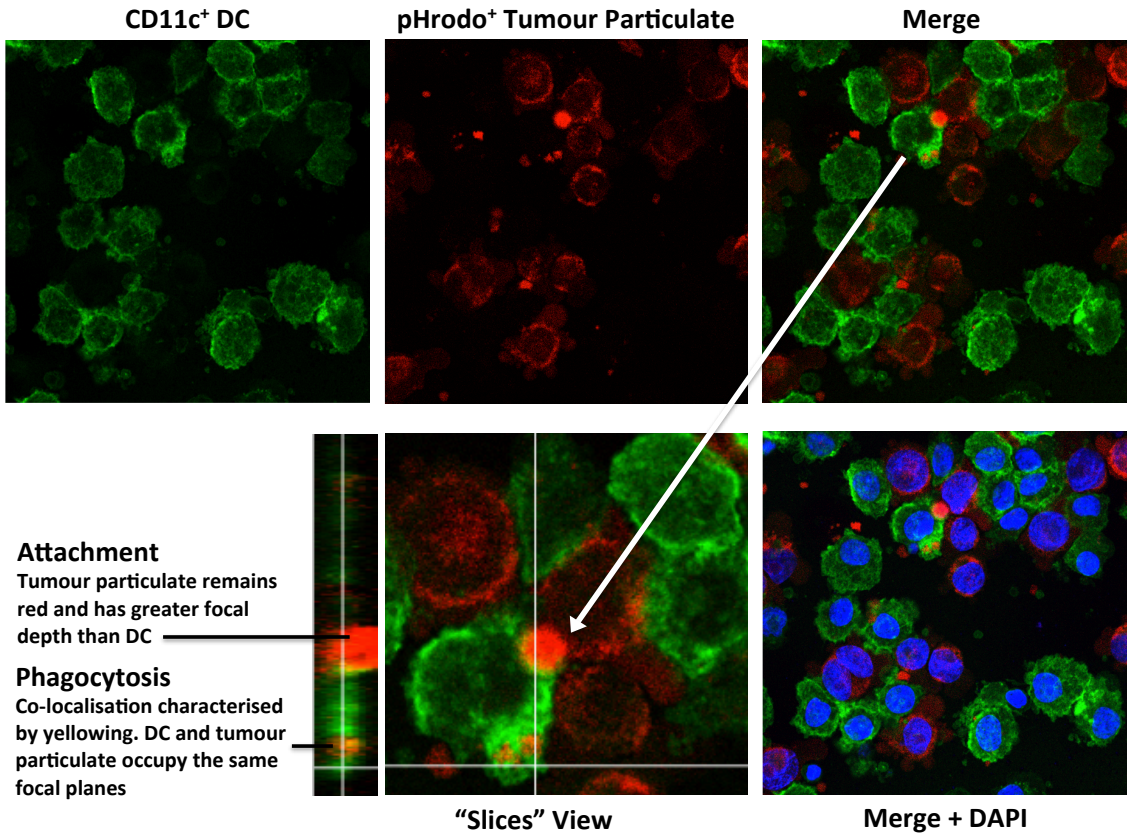

Figure 4.1. Phagocytosis of apoptotic tumour particulate by iDC
$5x10^4$ $CD11c^+$ iDC were incubated at 1:1 ratio with pHrodo labelled JY tumour cells that had been pre-treated with GA101GA (10µg/ml). After 1-3 hours, microscopy slides were prepared as described in section 2.17.3. Clockwise from top left: iDC (green), JY tumour cells (red), merged image of same area, merged image with DAPI, enlarged slices view showing tumour particulate phagocytosis or attachment. Representative example of n=4 (in triplicate).

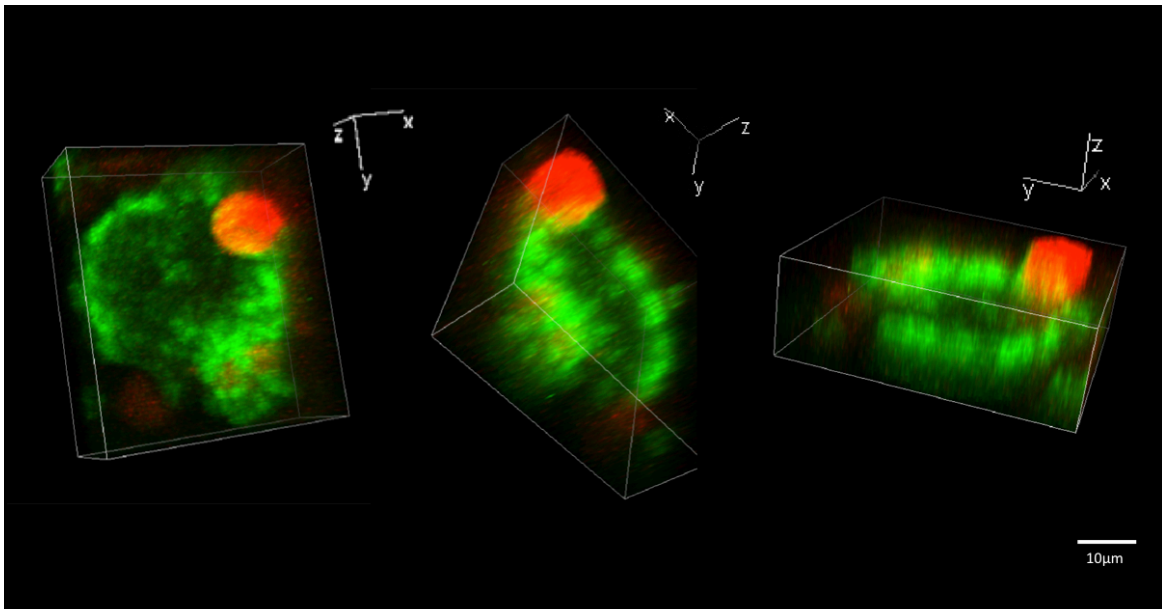

Figure 4.2. Phagocytosis of small tumour particulate by DC (3D volume view)
An alternative 3D view of the sliced DC depicted in Figure 4.1 above
Representative example of n=4 (in triplicate)

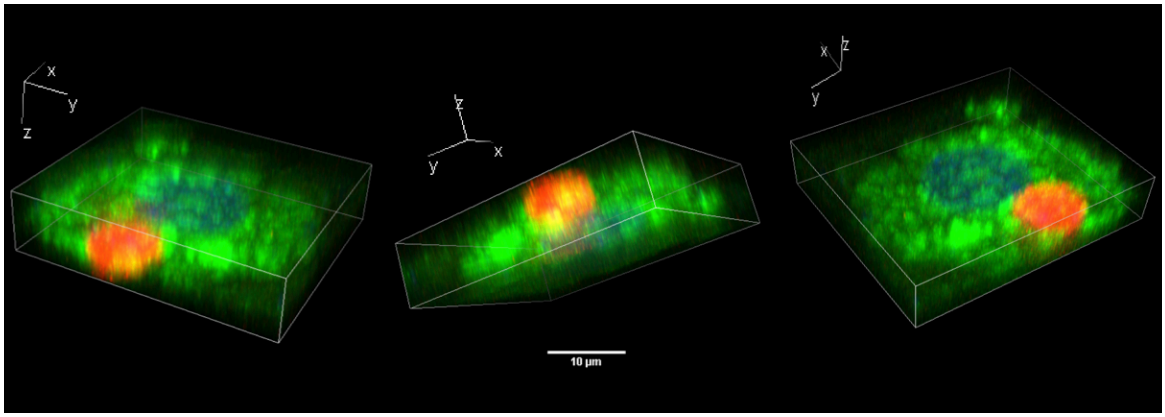

Figure 4.3. Phagocytosis of large tumour particulate by DC (3D volume view)
3D image of a DC with large internalised tumour particulate, large dendrite and nucleus visible.
Representative example of n=4 (in triplicate)

4.2.3. Tumour particulate produced by GA101GE treatment is phagocytosed by DC

Using the visualisation strategy detailed in section 4.2.2, the percentage of pHrodoRed^{+} DC was measured and the results are displayed in Figure 4.4. The assays were performed using iDC from four different healthy donors and each condition was tested in triplicate. For two of the donors, slides were also prepared at time zero for each condition to confirm that the process of slide preparation *per se* did not produce false positives. No pHrodoRed^{+} DC were observed at time zero. A low percentage of pHrodoRed^{+} DC was observed after culture with untreated JY cells, rising from a median of 0.7% at 1 hour, to 0.9% at 2 hours, and 1.6% at 3 hours. This was possibly due to the death of some JY cells as a result of manipulation during assay set up, and subsequent phagocytosis by DC. The median percentage of pHrodoRed^{+} DC in GA101GE pre-treated JY cells was 12.9%, 15.1% and 14.5% at 1, 2 and 3 hours respectively. The difference compared to untreated control JY cells was significant after a 2-hour incubation (*p <0.05) and trends were evident at 1 and 3 hours. The results obtained demonstrate that tumour particulate generated by GA101GE-mediated apoptosis was phagocytosed by DC. This indicates that a pre-requisite step for assessment of TA processing by DC and cross presentation to T cells does occur in the context of the i*n vitro* co-culture model to be used for these studies.

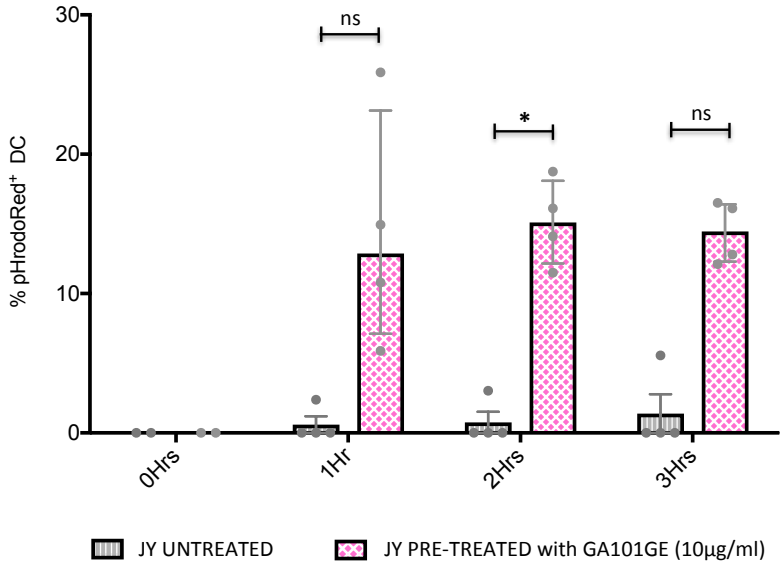

Figure 4.4. Phagocytosis of tumour particulate by DC is significantly increased after pre-treatment with GA101GE
$5x10^4$ iDC were incubated at 1:1 ratio with JY tumour cells that had previously been treated with GA101GE overnight (10µg/ml) or untreated overnight. After 0-3 hours, microscopy slides were prepared and the percentage of pHrodoRed$^+$ DC was calculated. Graph depicts frequency as % pHrodoRed$^+$ DC, with median and interquartile range for n=4 (triplicate average). *p <0.05 (Friedman's ANOVA, with Dunn's multiple comparison post hoc).

4.3. *In vitro* assessment of DC maturation

The ability of GE-mAb-activated NK cells to promote DC maturation was explored by adding purified DC to the *in vitro* co-culture model that was used to assess NK-cell activation. Monocytes for DC generation were isolated from the same donor as the NK cells. iDC were incubated with NK cells and tumour target cells at 1:1:1 ratio in the presence of mAbs. The three-cell *in vitro* co-culture model used to evaluate DC maturation is illustrated in Figure 4.5.

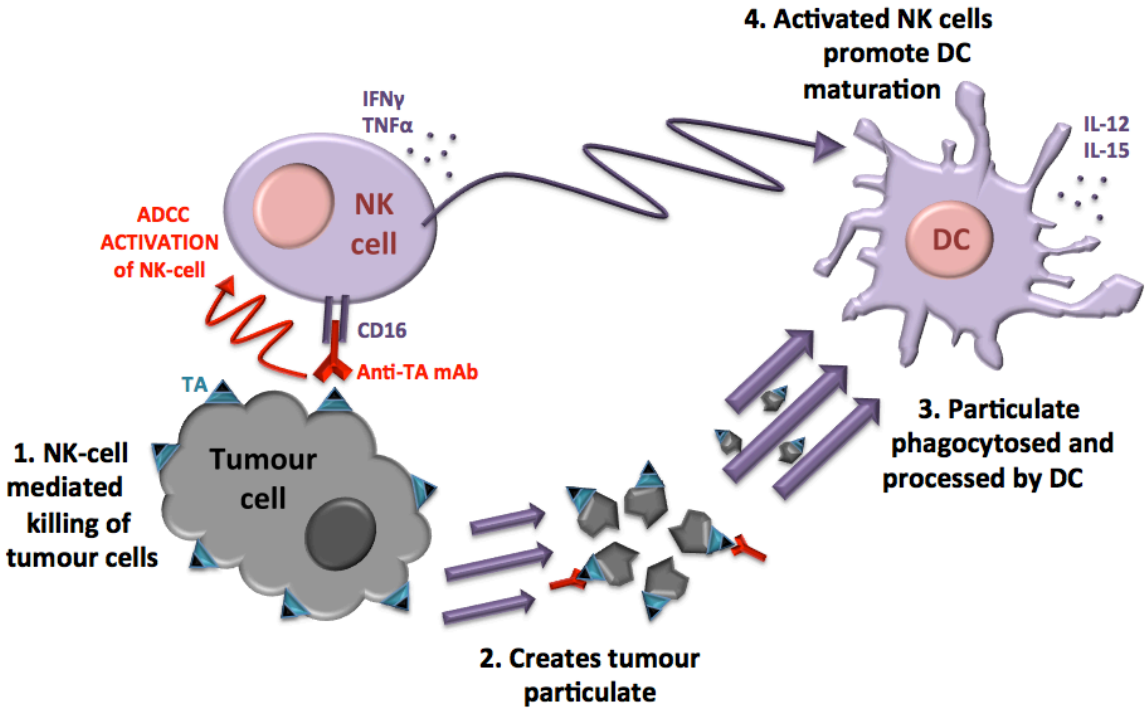

Figure 4.5. Schematic representation of the three-cell *in vitro* co-culture to assess DC maturation

4.4. *In vitro* assessment of DC maturation: purified DC

It was important to obtain a pure population of DC for assessment of NK:DC crosstalk in the absence of other cell types. There are approximately 13-37 DC per µl in the peripheral blood of healthy adults, and numbers can be significantly reduced during infection and chronic disease. Thus DC constitute a maximum of just 0.5% of circulating white blood cells (WBC) [334]. In addition, fresh purified DC isolates lack the characteristic morphology, phenotype, and immunostimulatory function of cDC [93].

4.4.1. Monocyte-derived DC

Because of the low frequency and heterogeneity of DC in peripheral blood, monocyte derived DC (moDC) generated *ex vivo* are often utilised in functional studies. There are many methods for *in vitro* moDC generation, which are comprehensively reviewed by Castiello *et al* [84]. In essence, *in vitro* generation of moDC is a four-step process requiring:

1. PBMC collection via apheresis
2. Monocyte selection via elutriation, plastic adherence or magnetic bead isolation
3. Differentiation from $CD14^+$ monocytes to iDC, typically in the presence of:

- serum (either human AB or FBS)

- various concentrations of IL-4 and GMCSF

4. Subsequent maturation of iDC, typically using cytokine cocktail combinations

The protocols reviewed by Castiello *et al* had minor differences in step 3, related to the duration of differentiation; but differed most appreciably at step 4, in terms of duration of maturation, maturation agent used, and maturation agent concentration. The most frequently used moDC maturation protocols are summarised in Table 4.1.

Table 4.1. Frequently Used moDC Maturation Protocols
Adapted from Castiello *et al* 2011 [84]

Protocol	Time for maturation	Protocol	Time for maturation
LPS (100 μg/ml)	2 days	TNF-α (1,100 U/ml),	
LPS (100 ng/ml)	2 days	PGE2 (1 μg/ml)	
LPS (10 ng/ml)	1 day	IL-1β (10 ng/ml),	2 days
LPS (100 ng/ml)	n/a	IL-6 (1,000 IU/ml),	
LPS (1 μg/ml)	16 h	TNFα (10 ng/ml),	
LPS (100 ng/ml)	2 days	PGE2 (1 μm/ml)	
CD40L (undefined)	2 days	IL-1β (25 ng/ml),	2 days
CD40L (undefined)	n/a	IFN-α (3,000 IU/ml),	
CD40L (1 μg/ml)	1 day	IFN-γ (1,000 IU/ml),	
TNF-α (50 ng/ml)	2 days	TNF-α (50 ng/ml),	
TNF-α (10 ng/ml)	7 days	poly (I:C) (20 ng/ml)	
TNF-α (10 ng/ml)	1 days	IL-1β (10 ng/ml),	n/a
TNF-α (1,000 U/ml)	2 days	IL-6 (1,000 U/ml),	
TNF-α (5 ng/ml)	1 day	TNF-α (10 ng/ml),	
IFNα (1,000 U/ml)	8 h	PGE2 (1 μm/ml)	
IFN-γ (1,000 U/ml)	2 days	LPS (100 mg/ml),	1 day
IL-1β (1,870 U/ml),	3 days	IFN-γ (1,000 IU/ml)	
IL-6 (1,000 U/ml),			

4.4.2. Generation of monocyte-derived iDC and mDC

iDC were generated as described in materials and methods (section 2.8); requiring 6-8 day differentiation of monocytes to iDC in the presence of IL-4 and GMCSF. For the subsequent 1-2 day step yielding mDC, two maturation cocktails were examined. The first utilised a standard, more widely used cytokine combination comprising complete RPMI supplemented with proinflammatory mediators IL-1β (10ng/ml), IL-6 (1000IU/ml), PGE_2 (1μg/ml), and TNFα (10ng/ml) adapted from Dauer *et al* [265]. This cocktail is widely referred to as TIP but designated DCM_1 in this study. The second cocktail, DCM_2, utilised a cytokine combination cited by the Ferris group as

producing DC with the most efficient cross presentation ability. DCM_2 comprised complete RPMI supplemented with 25ng/ml IL-1β, 25ng/ml Poly I:C, 5500IU/ml TNFα, 1000IU/ml IFNγ and 3000IU/ml IFNα [266].

4.4.3. DC phenotyping and gating strategy

The DC phenotyping panel and gating strategy was developed to achieve clear segregation of DC within a mixed population co-culture. The sequential gating strategy for DC is illustrated in Figure 4.6, where DC were identified as $CD11c^+HLA\text{-}DR^+$ after exclusion of all other cell populations. The DC phenotyping panel also included markers to measure DC maturation. These were selected based on studies previously published that demonstrated surface expression of the markers CD80, CD83, CD86 and HLA-DR is upregulated upon iDC maturation; with results typically reported as a fold increase in median fluorescence intensity (MFI) and/or visually displayed as multiple peak overlays [73, 97, 335]. Morphology of the monocyte derived iDC and mDC produced is shown in Figure 4.7 A, with DCM_1 mDC appearing much less adherent than DCM_2 mDC. The corresponding $CD11c^+HLA\text{-}DR^+$ phenotype is shown below in Figure 4.7 B. Surface maturation marker expression on iDC was compared to mDC using superimposed histograms. A representative example of expression of DC maturation markers CD80, CD83, CD86 and HLA-DR by iDC and both versions of mDC is shown in Figure 4.7 C. DCM_1 mDC were chosen as a positive control for DC maturation because upregulation of the maturation markers was higher and as they were much less adherent than DCM_2 mDC, they did not require extensive trituration to harvest. As described in section 2.19, FMO controls were used to define background fluorescence for each of the DC maturation markers and the FMO gating strategy is illustrated in Figure 4.8. Gates were set using the FMO boundaries defined for each of the DC maturation markers and all measurements were relative to this.

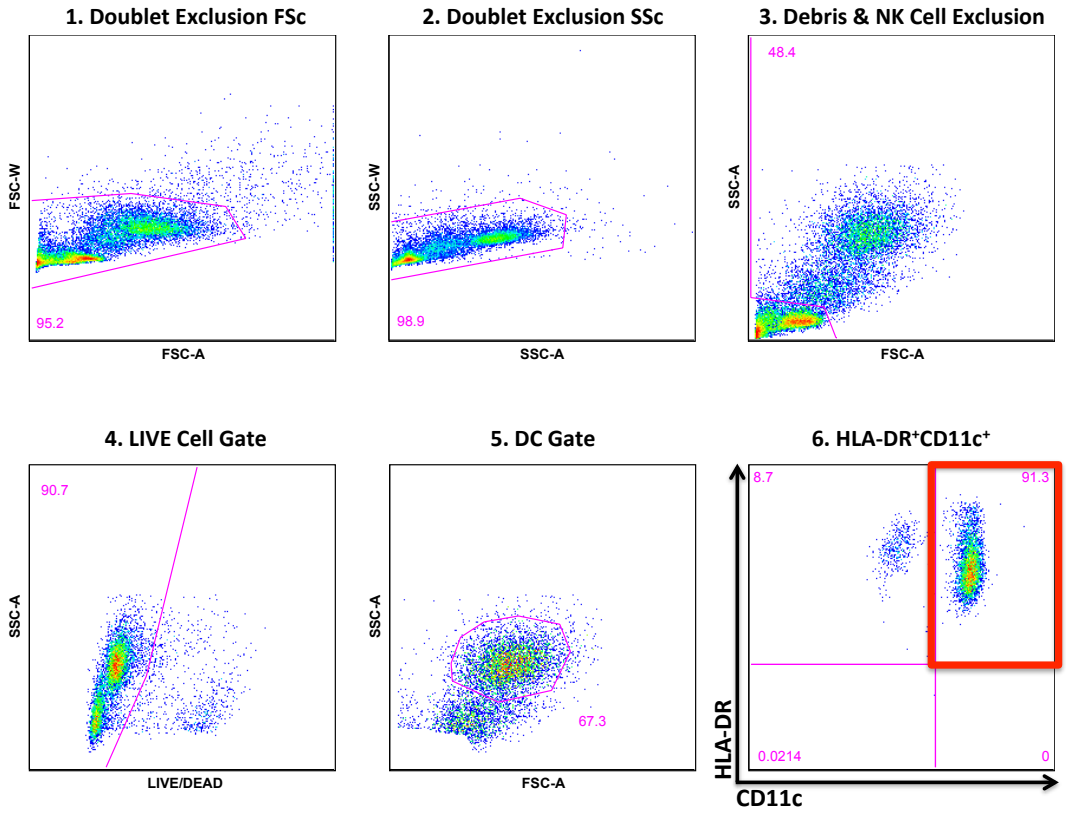

Figure 4.6. Strategy for DC gating within a mixed cell population
DC were identified within mixed cell populations according to the strategy illustrated above. Sequential gating achieved exclusion of doublets, debris, NK cells and dead cells. A gate encompassing the remaining cells that were of large size and positive for CD11c and HLA-DR constituted DC.

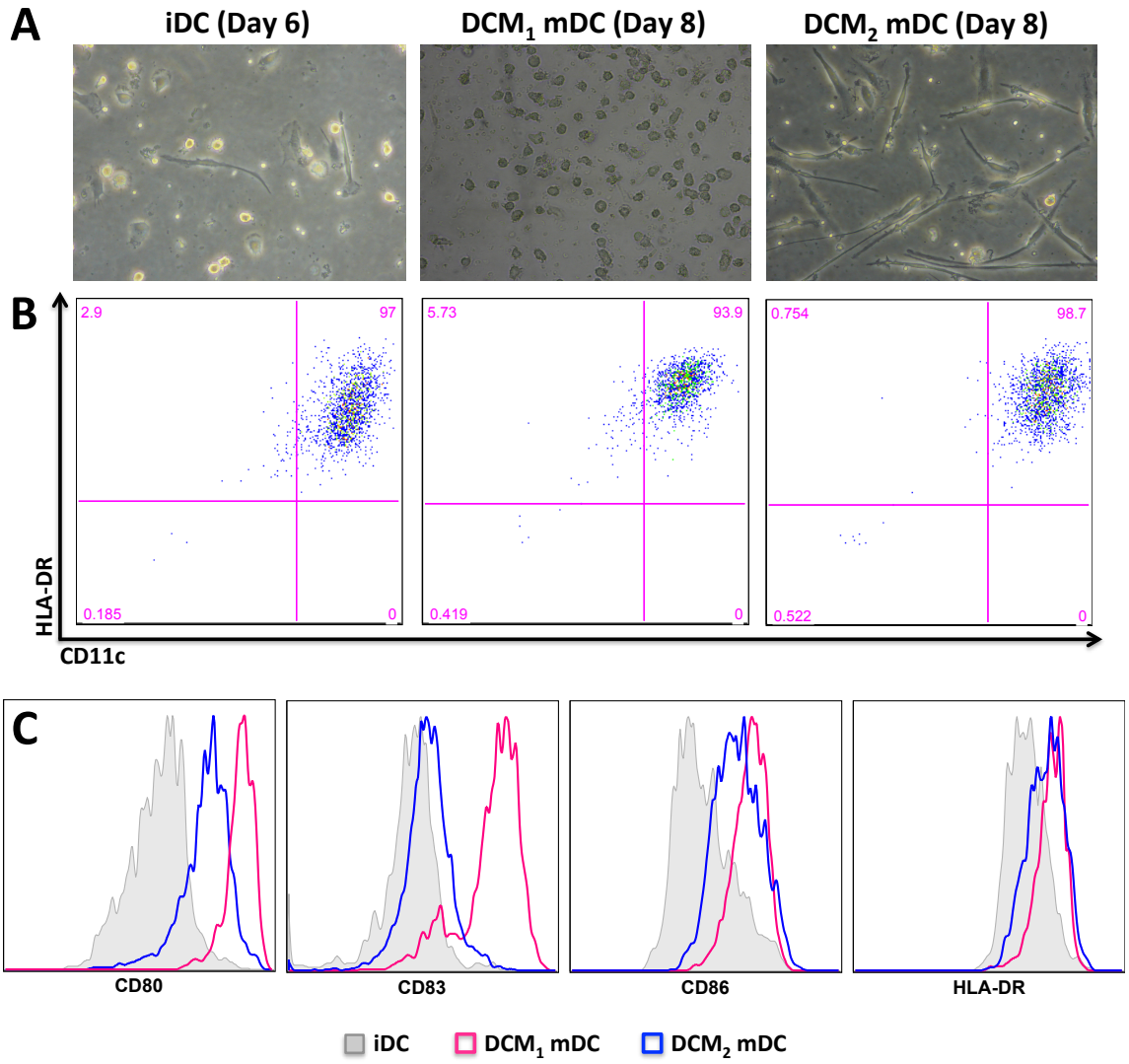

Figure 4.7. Morphology and CD11c+HLA-DR+ phenotype of monocyte derived iDC and mDC. Representative example of expression of DC maturation markers CD80, CD83, CD86 and HLA-DR by iDC and mDC

Panel A illustrates morphology of iDC, DCM_1 mDC and DCM_2 mDC with their corresponding CD11c+HLA-DR+ phenotype shown in Panel B. 10^5 DC were analysed and CD80, CD83, CD86 and HLA-DR expression profiles of iDC (grey) compared to DCM_1 mDC (pink) and DCM_2 mDC (blue).

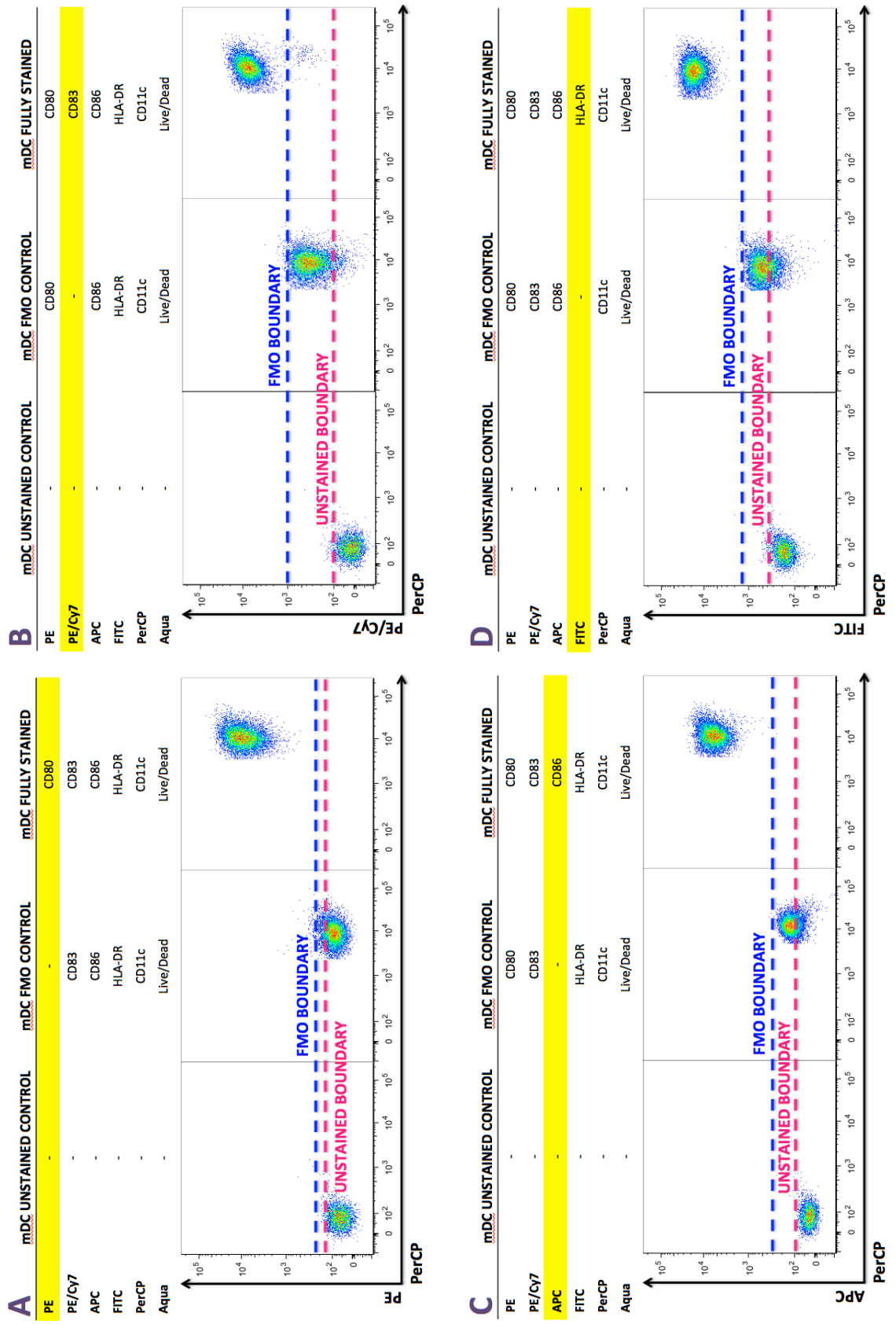

Figure 4.8. Illustration of the FMO control gating strategy used to assess expression of maturation markers by DC
FMO controls were used to identify and gate DC in the context of data spread due to the multiple fluorochromes. Compensation was correctly set using single stained controls and 10^5 mDC were stained as shown with all fluorochrome-conjugated antibodies except CD80-PE (panel A), CD83-PE/Cy7 (panel B), CD86-APC (panel C) or HLA-DR-FITC (panel D). Gating boundaries were determined for FMO stained DC (dotted blue line). Unstained DC boundaries are also shown (dotted pink line). Representative example of n=4 independent experiments.

4.5. *In vitro* assessment of DC maturation: preliminary co-cultures with anti-EGFR mAbs

To assess whether mAb-mediated activation of NK cells induced DC maturation, iDC were incubated with autologous NK cells and A431 tumour target cells at 1:1:1 ratio for 48 hours, with or without anti-EGFR mAbs. The cell ratio and assay duration used were those reported by the Ferris laboratory [97, 240]. Cell numbers and mAb concentrations were based on those used for *in vitro* studies of samples from patients recruited to the clinical trials discussed in section 1.12.4. The particulars of the preliminary co-cultures are summarised in Table 4.2. Notably, each of the cell types used in the co-culture had individual preparation requirements.

Table 4.2. DC maturation: conditions used for preliminary co-cultures with anti-EGFR mAb

Condition	Preparation Notes	Medium
Monocyte source	PBMC plastic adherence	RPMI
iDC	6-day monocyte differentiation (to synchronise with mDC)	DCD_1 (with 2% hAB) [a]
mDC	6-day monocyte differentiation +2-day maturation	DCD_1 (with 2% hAB) [a] DCM_1 (with 2% hAB) [a]
NK Cell	MACS negatively selected NK Cells (Straight *ex vivo* - NO recovery)	-
A431 Tumour	Seeded night before assay	DMEM (with 2% hAB) [a]
Assay Details	96-well flat bottom	RPMI (with 2% hAB) [a]
Assay Duration	48 hours [b]	
Cell ratio | Cell number	(1:1:1 ratio) [b] | 10^5 of each cell type [c]	
mAb concentration	10µg/ml [d]	

[a] 2%v/v hAB serum was used instead of 10% FBS, to minimise potential for xenoactivation of DC
[b] Assay duration and cell ratio from studies reported by the Ferris laboratory
[c] Cell number adapted from those used in previous clinical trials
[d] mAb concentration based on studies reported by the Ferris laboratory and previous clinical trials

4.5.1. Positive and negative controls for assessment of DC maturation

The positive control for maturation using cocktail DCM_1 is referred to in figures as [mDC POSITIVE CONTROL]. As a negative control, maturation marker expression on iDC immediately post-harvest was compared to iDC cultured alone for the duration of the assay, to assess any

spontaneous maturation in the absence of other cell types and in the absence of mAbs. These DC are referred to in figures as [iDC TIME ZERO] and [iDC NEGATIVE CONTROL] respectively. Apoptosis of JY cells in the absence of NK cells was induced by epitope ligation with GA101GE and was exploited to demonstrate that apoptotic tumour particulate was phagocytosed by iDC (Figure 4.4). Studies have demonstrated that DC phagocytosis of tumour particulate containing a high proportion of apoptotic material can induce DC maturation [324, 325]. Consequently, it was important to include a control to assess any maturation of DC in co-culture with tumour cells and mAb in the absence of NK cells. This presence and absence of NK cells in test conditions is referred to in figures as "+NK' and 'NO NK' respectively.

4.5.2. Preliminary results showed high levels of spontaneous DC maturation

DC maturation in the absence of stimulus has been observed for *in vitro* assays and attributed to changes in cytokine levels (personal communication with Dr Nathalie van Leeuwen and Dr Rebecca Prue - KCL). Preliminary results showed a substantial increase in expression of DC maturation markers in the iDC negative control (iDC cultured alone, without mAb) compared to iDC at time zero (immediately post-harvest), indicative of spontaneous maturation. This result is illustrated in Figure 4.9 using MFI peak overlays. CD86 showed the largest difference between iDC and mDC. Indeed, expression levels in the iDC negative control culture exceeded the positive control. CD80 and CD83 expression also appeared increased in the iDC negative control compared to iDC at time zero. When iDC, NK cells and A431 tumour cells were co-cultured in the presence of 10µg/ml imgatuzumab, the increase in expression of DC maturation markers did not surpass the high spontaneous maturation observed in the iDC negative control.

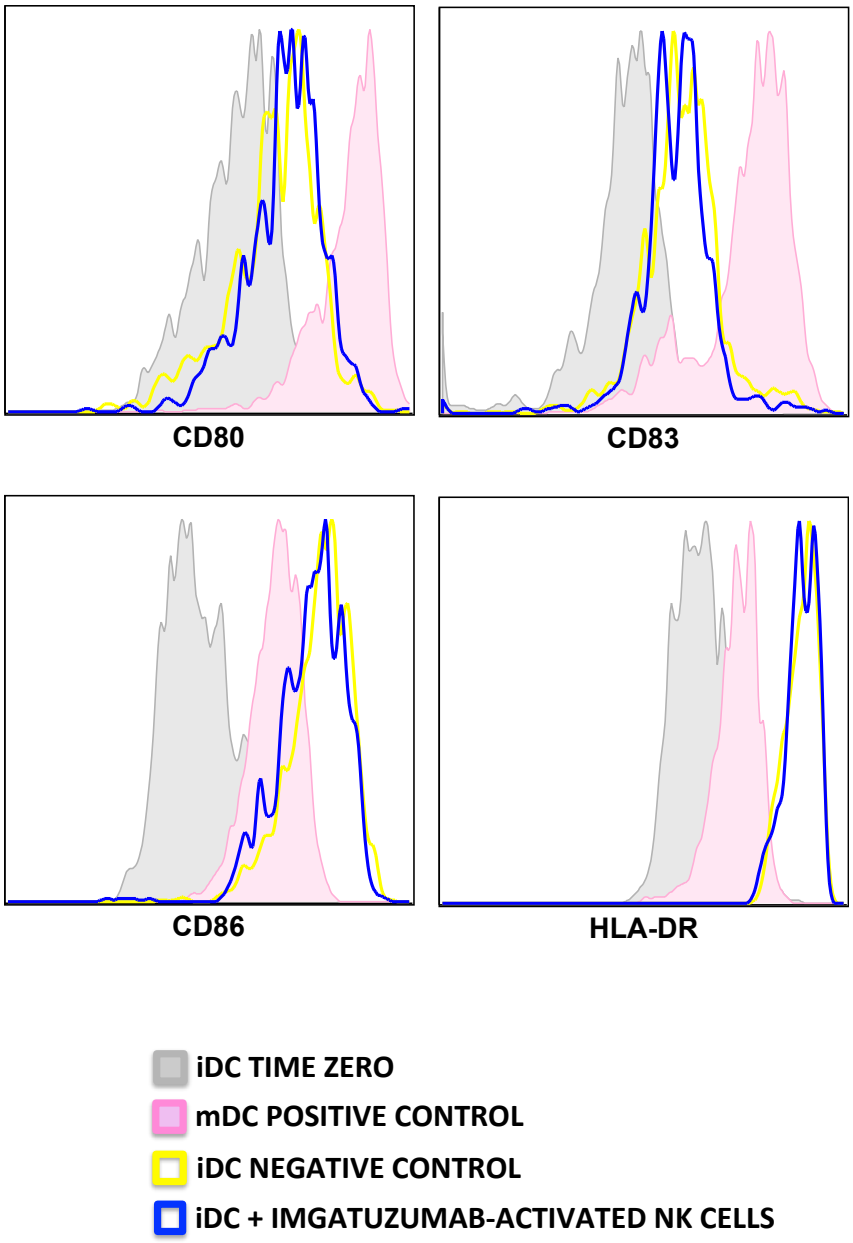

Figure 4.9. Preliminary results: high spontaneous maturation of iDC in negative control condition
10^5 DC post-harvest [iDC TIME ZERO] and cytokine matured mDC [mDC POSITIVE CONTROL] were screened for expression of maturation markers CD80, CD83, CD86 and HLA-DR and compared to iDC incubated for 48 hours either alone [iDC NEGATIVE CONTROL] or at 1:1:1 ratio with NK cells and A431 cells in the presence of imgatuzuamb (10µg/ml). Results are representative of two independent experiments.

4.6. *In vitro* assessment of DC maturation: optimisation of co-cultures with anti-EGFR mAbs reduced spontaneous DC maturation

A series of assay refinements were undertaken to reduce spontaneous maturation of iDC. Optimisation of the three-cell co-culture was undertaken in conjunction with the two-cell co-culture optimisation described in Chapter 3 (section 3.4) and details are as follows:

4.6.1. NK-cell recovery prior to co-culture

NK cells were recovered overnight in complete RPMI supplemented with low dose IL-2, prior to use in co-cultures rather than being used immediately after MACS isolation. The overnight recovery step minimised spontaneous NK-cell activation (Figure 3.7) and any potential for subsequent non-specific DC maturation.

4.6.2. Monocytes purified by magnetic cell separation as the source for moDC

The population of monocytes used to create moDC were originally obtained by plastic adherence of PBMC, but still contained small numbers of contaminating B, T and NK cells after washing. Therefore, monocytes isolated from PBMC by MACS rather than plastic adherence were used to create moDC for subsequent co-cultures. The MACS $CD14^+$ monocyte population obtained was of high purity (average 92.4% +/- 1.4% sd - 3 independent experiments). After differentiation, these purified monocytes yielded populations of $CD11c^+HLA\text{-}DR^+$ iDC with average purities of 96.5% (+/- 1.2% sd - 3 independent experiments) compared to an average purity of 78% (+/- 4.2% sd - 3 independent experiments) for pre-optimisation iDC, borne of plastic adhered monocytes.

4.6.3. Media standardisation and removal of human AB serum

Although 2% v/v hAB serum was the initially chosen to avoid xenoactivation of effector cells, reported protocols for DC maturation studies typically used 10% FBS [265, 266]. The media used in all cell preparations was standardised so that cells were not subjected to the shock and potential stimulatory effects of a media change when combined for co-culture and also to eliminate the detrimental affects of hAB on NK cells and A431 (detailed in section 3.4.2). The generation of iDC, *in vitro* maintenance of the A431 cell line and recovery of NK cells were all performed in complete RPMI, with relevant supplementation.

4.6.4. Reduction of co-culture duration and cell numbers

An assay duration of 18 hours was selected because there was less spontaneous NK-cell activation and NK-cell death (Figure 3.7) as well as less spontaneous DC maturation compared to the 48-hour assay duration (Figure 4.10).

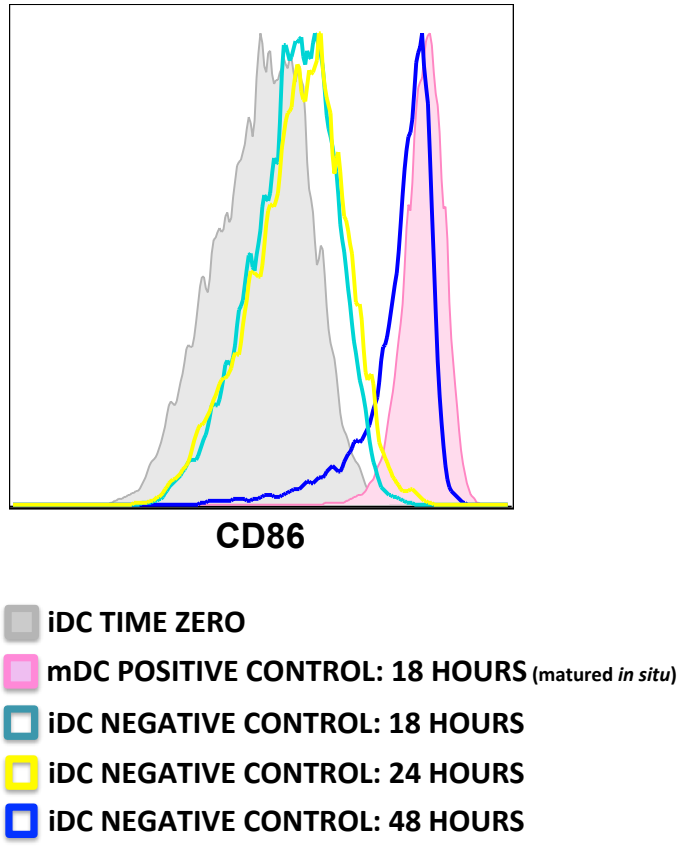

Figure 4.10. Optimisation of co-cultures with anti-EGFR mAbs: reduction of spontaneous DC maturation
$2.5x10^4$ iDC were incubated either alone or at 1:1:1 ratio with recovered NK cells and A431 tumour cells in the presence or absence of mAb at 10µg/ml. DC post-harvest [iDC TIME ZERO] were screened for expression of maturation markers and compared to [mDC POSITIVE CONTROL] and [iDC NEGATIVE CONTROL] at 18, 24 and 48 hours. Results are representative of two independent experiments.

As detailed in section 3.4.4 (Chapter 3), cell numbers were decreased from 10^5 of each type to $2.5x10^4$ of each type (while the co-culture volume, mAb concentration and 1:1:1 cell ratio were maintained) to allow for more economical use of limited donor material, without unduly compromising the flow cytometry results obtained (data from a minimum of 10,000 events was always collected).

4.6.5. Positive control: iDC matured *in situ*

Preliminary co-cultures used day 8 mDC as a positive control. For subsequent assays, cocktail DCM_1 was added to 6-day differentiated iDC directly in the co-culture to ensure that the iDC could mature during a shorter assay. Maturation *in situ* for 18 hours as opposed to 48 hours was still sufficient to promote increased expression of all maturation markers (illustrated in Figure 4.10) providing a distinct positive control population.

4.6.6. Imgatuzumab induces DC maturation

The cumulative effect of refinements detailed in sections 4.6.1 - 4.6.5 substantially reduced spontaneous DC maturation. Using the optimised assay conditions, the ability of imgatuzumab and cetuximab to induce DC maturation was assessed. Imgatuzuamb was found to promote expression of the DC maturation marker CD86 to the same extent as cetuximab at the mAb concentration of 10μg/ml (Figure 4.11).

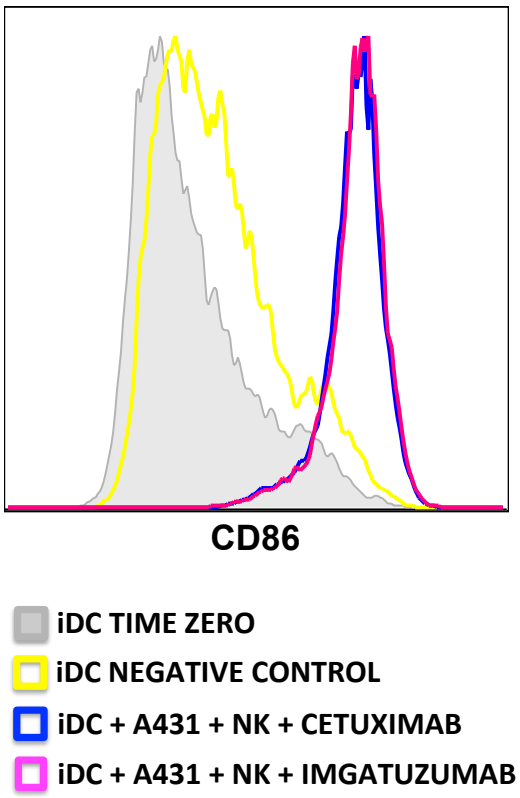

Figure 4.11. Imgatuzumab promotes increased expression of the DC maturation marker CD86
$2.5x10^4$ iDC were incubated either alone or at 1:1:1 ratio with recovered NK cells and A431 tumour cells in the presence or absence of mAb at 10µg/ml. DC post-harvest [iDC TIME ZERO] were screened for expression of maturation markers and compared to [iDC NEGATIVE CONTROL] and [iDC + mAb-ACTIVATED NK CELLS] co-culture conditions after 18 hours. Results are representative of two independent experiments.

Results presented in chapter 3 showed that, at low concentrations, imgatuzuamb promoted NK-cell activation and function to a significantly greater extent than cetuximab. A comparison of the ability of imgatuzumab and cetuximab to promote DC maturation at lower concentrations was therefore performed. The results are displayed in Figure 4.12 and show the increase in expression of the DC maturation marker CD86 induced with mAbs at concentrations between 10µg/ml and 1ng/ml relative to the iDC negative control. Imgatuzumab was found to promote DC maturation to a greater extent than cetuximab at the lower concentrations of 10ng/ml and 1ng/ml. These concentrations were used hereafter.

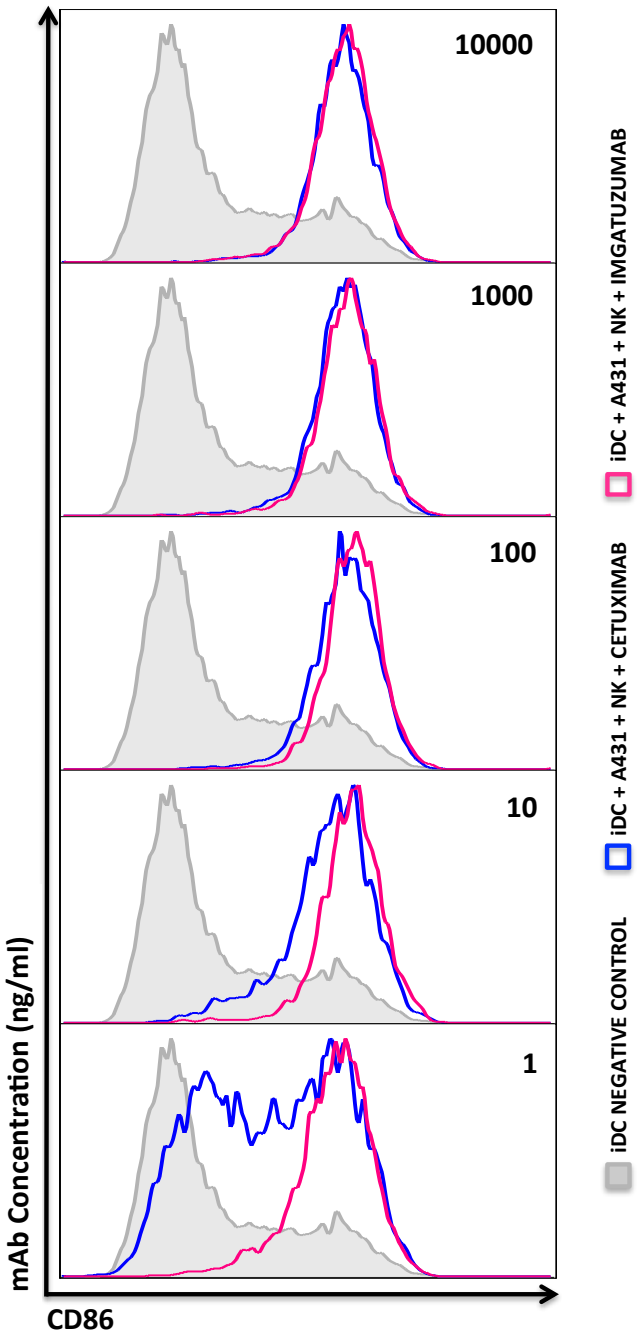

Figure 4.12. Imgatuzumab promotes increased expression of the DC maturation marker CD86 to a greater extent than cetuximab at the lower mAb concentrations

$2.5x10^4$ iDC were incubated either alone or at 1:1:1 ratio with recovered NK cells and A431 tumour cells in the presence or absence of mAbs at 10µg/ml, 1µg/ml, 100ng/ml, 10ng/ml and 1ng/ml. DC phenotyping was performed after 18 hours for the DC maturation marker CD86. Results are representative of two independent experiments.

4.6.7. Promotion of DC maturation by mAbs is NK-cell dependent

The mAb ligation of target antigen alone induced phagocytosis of apoptotic tumour particulate by DC (Figure 4.4). It was therefore important to assess whether the maturation of DC observed at low mAb concentrations was NK-cell dependent. Co-cultures were performed in the absence or presence of NK cells, with expression of DC maturation markers compared to the iDC negative control. Results presented in Figure 4.13 show that expression of CD80 was only detected when NK cells were present. Some upregulation for the maturation markers CD86 and HLA-DR was observed in the absence of NK cells (Figure 4.13 panel A), but was substantially higher when NK cells were present (Figure 4.13, panel B). Using CD86 as an example, in the presence of imgatuzumab the MFI was 191 arbitrary units (arbU) without NK cells and 913 arbU with NK cells; this 3.78-fold increase indicated that the DC maturation observed in these co-cultures was dependent on the presence of NK cells. The co-cultures without NK cells were included in all subsequent assays in order to assess the extent of NK-cell dependent DC maturation.

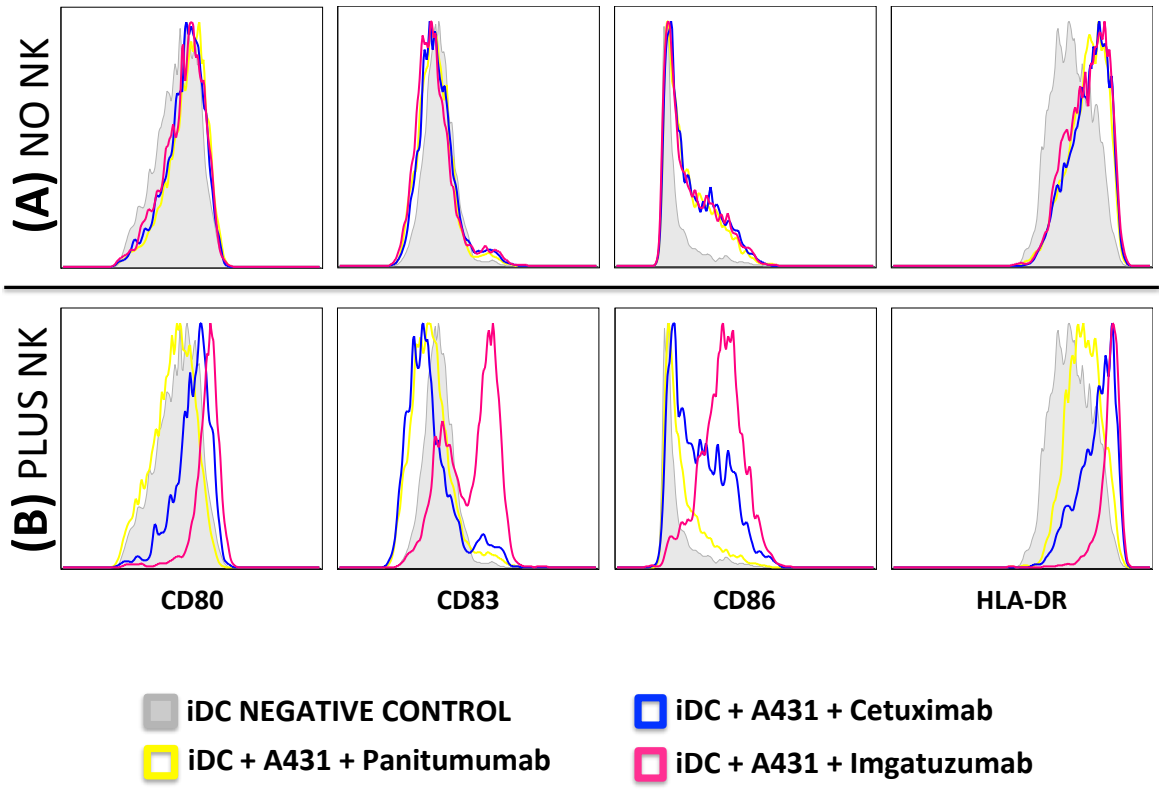

Figure 4.13. DC maturation is mediated by mAb-activated NK cells
$2.5x10^4$ iDC were incubated either alone or at 1:1 ratio with A431 tumour cells in the presence of panitumumab, cetuximab or imgatuzumab (1ng/ml). DC phenotyping was performed after 18 hours. Panel (A): co-cultures without NK cells, (B): Co-cultures with NK cells at 1:1:1 ratio. Representative example.

Table 4.3. Optimised conditions used for DC maturation in three-cell co-cultures

Condition	Preparation Notes	Medium [a]
Monocyte source	Negatively selected monocytes isolated by magnetic cell separation	-
iDC	6-day monocyte differentiation	DCD_1
mDC	6-day monocyte differentiation Matured during co-culture	DCD_1 DCM_1
NK Cell	Negatively selected NK cells isolated by magnetic cell separation and recovered for 16 hours	NKRM
A431 Tumour	Seeded 4 hours before assay	Complete RPMI
Assay Details	96-well v-bottom	Complete RPMI
Assay Duration	18 hours	
Cell ratio | Cell number	(1:1:1 ratio) | $2.5x10^4$ of each cell type	
mAb concentration	10ng/ml and 1ng/ml	

[a] All medium varieties comprised complete RPMI, with relevant supplementation

4.7. Comparison of DC maturation induced by the anti-EGFR mAbs imgatuzumab and cetuximab

4.7.1. Imgatuzumab-activated NK cells promote DC maturation to a greater extent than cetuximab at low mAb concentrations

Using the optimised three-cell co-culture conditions summarised in Table 4.3, cells isolated from 6 healthy donors were tested in the DC maturation assay. The effect of mAb-activated NK cells on DC are displayed in Figure 4.14 for the DC maturation markers CD80, CD83, CD86 and HLA-DR (rows) for all six donors (columns). The histogram overlays depict expression of the DC maturation markers for the DC alone negative control compared to DC maturation in the presence of mAb-activated NK cells (1ng/ml). For all donors, imgatuzumab consistently induced greater expression of DC maturation markers than cetuximab.

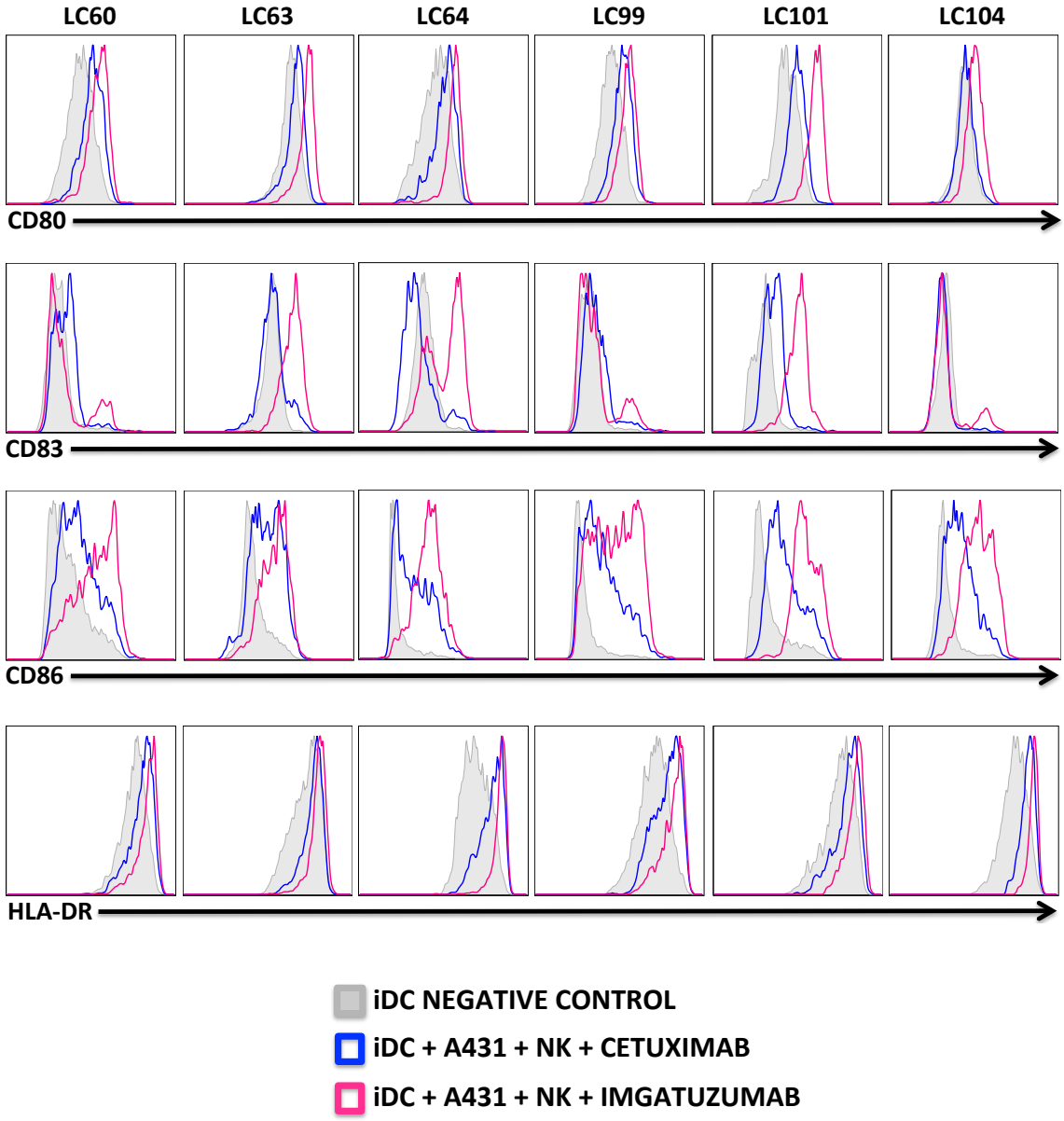

Figure 4.14. Imgatuzumab consistently promotes DC maturation to a greater extent than cetuximab using cells from six different donors
$2.5x10^4$ iDC were incubated either alone or at 1:1:1 ratio with recovered NK cells and A431 tumour cells in the presence of cetuximab or imgatuzumab (1ng/ml). DC phenotyping was performed after 18 hours. The rows represent the DC maturation markers CD80, CD83, CD86 and HLA-DR with a column for each of the six different donors (LC).

Analysis of two donors was repeated in duplicate to assess intra-donor variability. The expression of CD86 is displayed in Figure 4.15 and demonstrates reproducibility of results using a single donor in two independent experiments. These results were echoed with all other DC maturation markers and at both mAb concentrations. In light of this, the average of the replicates for LC60 and LC99 were used in subsequent statistical analyses.

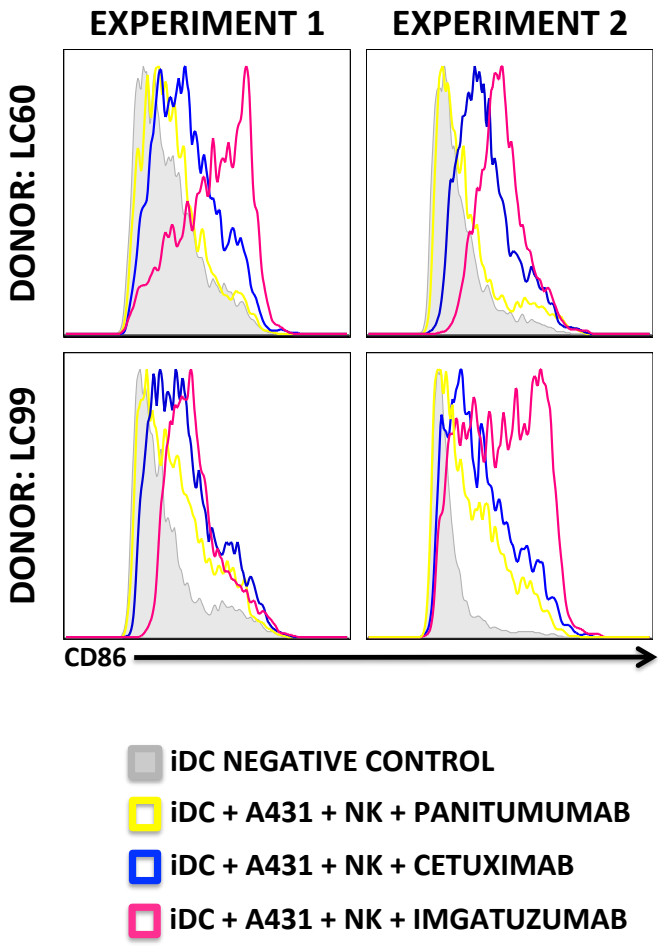

Figure 4.15. Replicate experiments illustrate that imgatuzumab induced DC maturation is reproducibly superior to non-GE mAbs

$2.5x10^4$ iDC were incubated either alone or at 1:1:1 ratio with recovered NK cells and A431 tumour cells in the presence of panitumumab, cetuximab or imgatuzumab (1ng/ml). DC phenotyping was performed after 18 hours. The rows represent each donor, with an independent replicate experiment in each column. Results are shown for the DC maturation marker CD86 only.

Statistical analyses were performed using fold change in DC maturation markers relative to the iDC negative control instead of absolute values because large variation in expression levels between different donor cell sources was observed (illustrated in Figure 4.14). Results for CD80, CD86 and HLA-DR are presented as fold change in MFI. Results for CD83 are presented as fold change in percentage positive due to a bi-modal expression profile (illustrated in Figure 4.14). The DC maturation results for six different donors tested with mAbs at 1ng/ml and 10ng/ml are presented in Figure 4.16.

At the low mAb concentration of 1ng/ml, NK cells activated by cetuximab did not promote expression of DC maturation markers above that seen with the non-IgG1 panitumumab control. In contrast, imgatuzumab-activated NK cells induced significantly greater fold increase in the expression of DC maturation markers CD80, CD83, CD86 and HLA-DR than cetuximab-activated NK cells ($p < 0.05$). When no NK cells were present, the same low level of DC maturation was observed with imgatuzumab, cetuximab and the panitumumab control. This showed that the DC maturation promoted by imgatuzumab was NK-cell mediated. Using CD86 as an example, imgatuzumab-activated NK cells induced a median 6-fold increase in MFI whereas median fold increase was 2.1 with cetuximab and 1.8 with panitumumab. At 10ng/ml, there was a trend to superior efficacy with imgatuzumab-activated NK cells compared to cetuximab, but differences were not statistically significant. Overall, there was less DC maturation at 10ng/ml than at 1ng/ml, but the reason for this remains unclear.

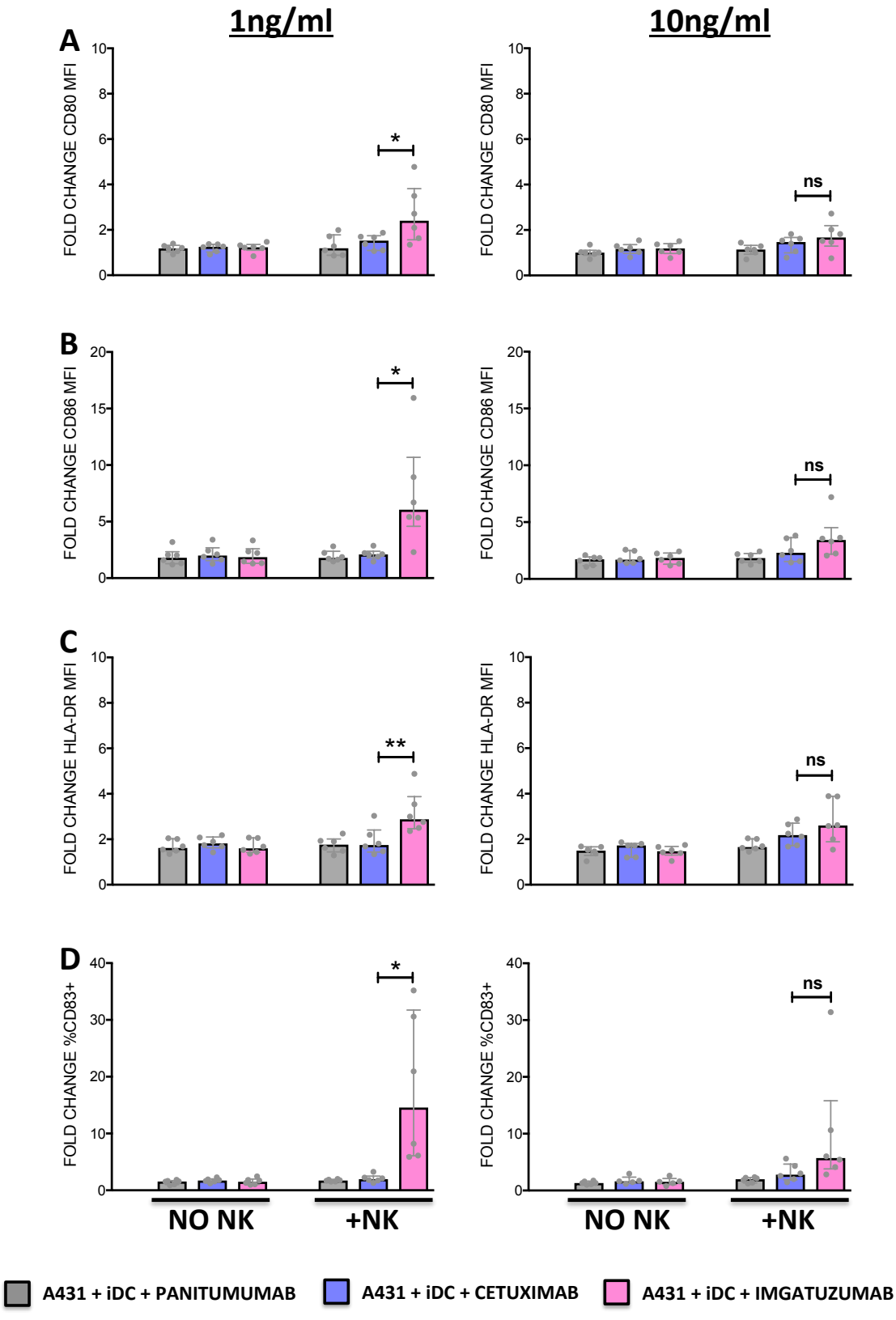

Figure 4.16. Imgatuzumab-activated NK cells promote expression of DC maturation markers to a significantly greater extent than cetuximab at 1ng/ml

$2.5x10^4$ iDC were incubated at 1:1 ratio with A431 tumour cells and panitumumab, cetuximab or imgatuzumab (1ng/ml and 10ng/ml) in the presence or absence of $2.5x10^4$ recovered NK cells. DC phenotyping was performed after 18 hours. Results shown are fold increase in (A) CD80, (B) CD86, (C) HLA-DR MFI and fold increase in $\%CD83^+$ (D) calculated compared to the iDC negative control condition. Plots display median and interquartile range for 6 independent experiments (n=6). *p<0.05 | **p<0.005 (Friedman's ANOVA, with Dunn's multiple comparison post hoc). No statistical differences were observed between the NO NK control samples

4.8. Comparison of NK-cell activation and function induced by the glyco-engineered anti-CD20 mAb GA101GE with the unmodified equivalent GA101WT

The ability of a GE-mAb to induce DC maturation was also assessed in the context of the anti-CD20 mAb model. In this setting, comparison of GA101GE with GA101WT that share the same epitope specificity enabled evaluation of the impact of the GE-modification *per se*. Rituximab, the widely used anti-CD20 therapeutic mAb, was also studied.

4.8.1. GA101GE-activated NK cells promote DC maturation to a greater extent than GA101WT at low mAb concentrations

Akin to the three-cell co-culture assays with anti-EGFR mAbs, cells isolated from 6 different healthy donors were studied using mAbs at concentrations of 1ng/ml and 10ng/ml. Experiments were performed in duplicate for one donor to confirm intra-donor replicability and the results were averaged. The fold changes in expression of the DC maturation markers are shown Figure 4.17.

At low mAb concentrations, neither GA101WT or rituximab promoted DC maturation above the background seen in control cultures without NK cells. In contrast, GA101GE induced significantly greater fold increases in expression of DC maturation markers at both 1ng/ml and 10 ng/ml compared to GA101WT. At 1ng/ml, CD80 and CD86 MFI, and %$CD83^+$ were significantly higher ($p < 0.05$) compared to the non-GE mAbs. Using %$CD83^+$ as an example, GA101GE--activated NK cells induced a median 6.3-fold enhancement in CD83 expression compared to 3.2-fold for GA101WT and 2.7 for rituximab. At 10ng/ml, CD86 and HLA-DR MFI, and %$CD83^+$ were significantly higher ($p < 0.05$) compared to the non-GE mAbs. Using CD86 MFI as an example, GA101GE--activated NK cells induced a median 5.2-fold enhancement in CD86 expression compared to 3.1-fold for GA101WT and 2.4 for rituximab. Of note, cells from donor LC64 were used in the anti-EGFR and anti-CD20 experiments, with superior DC maturation induced by GE-mAbs in both contexts. When no NK cells were present, the same low level of DC maturation was observed with GA101GE, GA101WT and rituximab. This showed that the DC maturation promoted by GA101GE was NK-cell mediated.

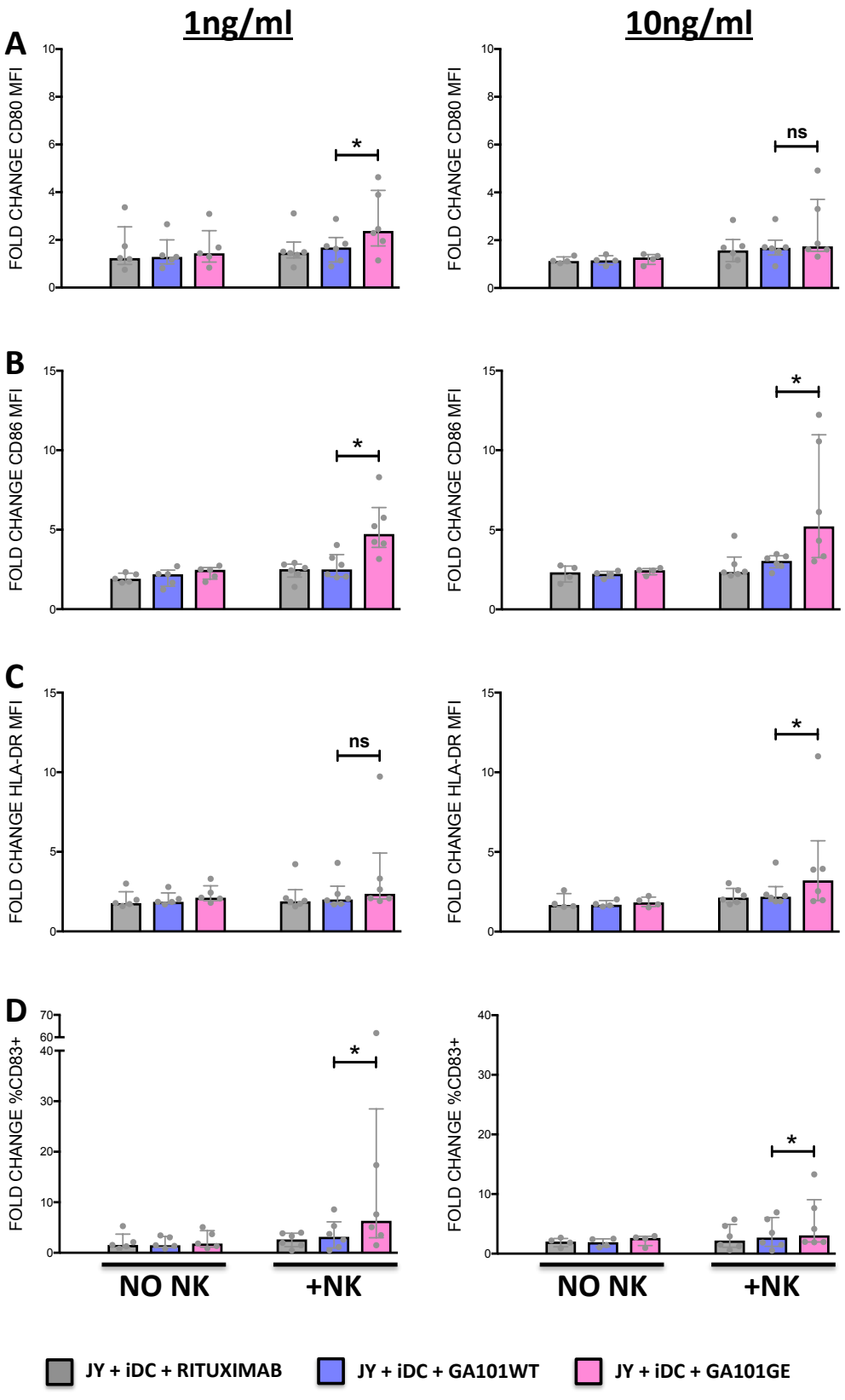

Figure 4.17. GA101GE-activated NK cells promote expression of DC maturation markers to a significantly greater extent than GA101WT at low mAb concentrations

$2.5x10^4$ iDC were incubated at 1:1 ratio with JY tumour cells and rituximab, GA101WT or GA101GE (1ng/ml and 10ng/ml) in the presence or absence of $2.5x10^4$ recovered NK cells. DC phenotyping was performed after 18 hours. Results shown are fold increase in (A) CD80, (B) CD86, (C) HLA-DR MFI and fold increase in $\%CD83^+$ (D) calculated compared to the iDC negative control condition. Plots display median and interquartile range for 6 independent experiments (n=6). *$p<0.05$ (Friedman's ANOVA, with Dunn's multiple comparison post hoc). No statistical differences were observed between the NO NK control samples

4.9. Discussion

The implications of NK:DC crosstalk and adaptive immune responses have been discussed for almost two decades, with activated NK cells regarded as pivotal to DC maturation, itself a precursor to antigen cross presentation [71, 85, 86, 96, 97, 263]. Despite this, it is only relatively recently that investigations of T-cell mediated cancer immunity have assessed the impact of mAb-activated NK cells on DC maturation and TA cross presentation [96, 97, 263], as earlier studies instead focussed on DC uptake of mAb-opsonised tumour cells in the absence of ADCC [239, 336].

The results presented in this chapter have demonstrated that GA101GE-coated tumour cells were ingested by DC. In addition, this is the first report to demonstrate that GE-mAb-activated NK cells can induce DC maturation, which is important for cross presentation.

4.9.1. GA101GE pre-treatment of tumour cells induces tumour phagocytosis

The 10μg/ml mAb pre-treatment of tumour cells before incubation with DC was intended to generate a high amount of apoptotic material. Under these conditions tumour particulate generated by GA101GE-mediated apoptosis was phagocytosed by DC to a significantly greater extent than untreated tumour cells. Importantly, this occurred without the need for any further manipulation of the tumour cells. Dhodapkar *et al* demonstrated that the coating of myeloma cells with the mAb anti-syndecan-I for 30 minutes at 4°C promoted cross presentation of TA to TA-specific T-cells by DC, in the absence of ADCC. They initially monitored DC uptake of mAb-coated myeloma cells via flow cytometry. Notably, phagocytosis of untreated or mAb-coated tumour cells was not observed. It was found that an additional 30 Gy γ-irradiation step was required to observe tumour^{+}DC and once irradiated, both untreated and mAb-coated tumour cells were ingested by DC to a similar extent. At a concentration of 1μg/ml, anti-syndecan-I mAb-binding alone did not induce sufficient tumour-cell apoptosis to elicit measurable phagocytosis [239]. Considering this point, it is perhaps surprising that untreated cells in this study were ingested by DC, albeit at low levels. This is perhaps due to the background level of apoptosis observed in JY cultures. Nevertheless, this was an indication that phagocytosis could occur in the co-culture model and was measurable, even with untreated tumour material harbouring a low percentage of apoptotic cells. Due to time constraints, a decision was taken not to include phagocytosis analysis that compared GA101GE and GA101WT mAbs in the presence of NK-cell mediated ADCC,

primarily because at the mAb concentrations required to generate large amounts of apoptotic material, it was assumed that there would be little measurable difference in apoptotic content of cell culture. However including all mAbs in this element of the study is a future consideration.

4.9.2. Imgatuzumab significantly enhances DC maturation compared to cetuximab

DC maturation was assessed via measurement of CD80, CD83 and CD86 expression. When compared to cetuximab, imgatuzumab-activated NK cells induced DC maturation marker upregulation to a significantly greater extent than cetuximab. Srivastava *et al* from the Ferris group demonstrated that cetuximab-activated NK cells induce DC maturation to a significantly greater extent than panitumumab-activated NK cells, by screening fold change of HLA-DR and CD80 expression [97]. This study used the same DC maturation markers, cell ratios, readout and therapeutic mAbs that were used by the Ferris group, but has extended their observations by novel exploration of imgatuzumab.

At 1ng/ml, only imgatuzumab-activated NK cells induced significant DC maturation and no differences were seen between panitumumab and cetuximab. While this trend of imgatuzumab-induced maturation was reproduced at 10ng/ml, results were not significantly different between the mAbs, suggesting that higher mAb concentrations, such as 10µg/ml used by the Ferris group, would have shown equivalent DC maturation.

Srivastava *et al* observed a mean 1.5-fold increase in DC CD80 expression and a mean 1.6-fold increase in DC HLA-DR expression induced by 10µg/ml panitumumab-activated NK-cells compared to control [97]. Interestingly, results in this current study also showed small fold increases in DC CD80 and HLA-DR expression induced by panitumumab-activated NK-cells compared to control. Although panitumumab lacks the ability to activate NK cells, it did appear to mediate downstream DC maturation, albeit low levels; which was also seen by Srivastava *et al*. Panitumumab has been shown to bind the EGFR with an 8-fold greater affinity than cetuximab [337]. It is possible that panitumumab induced a level of apoptosis in $EGFR^+$ tumour cells that subsequently induced a small amount of DC uptake and maturation.

By assessing DC maturation in the presence and absence of NK cells, this study was able to demonstrate that the significant level of GE-mAb-mediated DC maturation was NK-cell dependent. Srivastava *et al* did not include control conditions lacking NK cells, they did however

show that blocking of NKG2D abrogated IFNγ release and consequently DC maturation in transwell experiments. Transwell experiments are a possible future consideration for this study, since they indicate that maturation is also cytokine dependent and not just contact dependent. Another consideration for future experiments would be to assess DC functionality via measurement of IL-12 production. This could be achieved in the same way that NK cells were screened for intracellular cytokines in this study; and could potentially be correlated with DC ability to stimulate $CD8^+$ naïve T cells.

4.9.3. GA101GE significantly enhances DC maturation compared to GA101WT

Despite demonstrating that GE-mAb activity provided apoptotic tumour particulate for phagocytosis by DC, it is important to remember that efficient induction of TA-specific T-cells by DC may be hampered by peripheral tolerance if the TA is presented by DC that have not undergone maturation. In the absence of appropriate maturation stimuli, iDC present TA in the context of inhibitory signals [80], resulting in anergy of TA-specific $CD8^+$ T-cell clones and expansion of immunosuppressive T-regs [81, 82, 83]. In the context of CD20-mAb-activated NK-cells, results presented in Chapter 3 showed that GA101GE promoted significantly greater apoptosis of tumour cells and significantly greater activation of NK cells than GA101WT. It was therefore predicted that GA101GE-activated NK cells could promote maturation of DC and results presented in this chapter have indicated this. At 1ng/ml, only GA101GE-activated NK cells induced significant DC maturation and no differences were seen between GA101WT and rituximab. The trend of significant GA101GE-induced maturation was reproduced at 10ng/ml in all but one of the maturation markers.

These findings illustrate that the magnitude of NK-cell activation can directly affect the magnitude of DC maturation, and is important because maturation is a key stage of DC activity required for tumour-specific $CD8^+$ T-cell priming. When Dhodapkar *et al* demonstrated that the coating of myeloma cells with the mAb anti-syndecan-I promoted cross presentation of TA to TA-specific T-cells by DC, in the absence of ADCC it was of note that the coated myeloma cells induced only "partial" iDC maturation when compared to cytokine-matured iDC [239]. Results presented in this chapter show that at equivalent concentrations, GE-mAb activated NK cells elicit significantly more DC maturation than the unmodified mAbs. Therefore, it is reasonable to speculate that GE-

mAbs have better potential to present antigen in a context that will prime and activate TA-specific $CD8^+$ T cells than non-GE mAbs.

There are several concerns with the DC used in this study. The moDC may not be representative of all DC subtypes involved in antigen presentation. Although moDC are a gold standard and widely used in published literature because of their uniform phenotype and ease to obtain in sufficiently high numbers compared to DC directly isolated from peripheral blood [84], they may not provide the most appropriate setting for studying promotion of adaptive immunity. The majority of DC clinical trials to date have employed DC derived *in vitro* in the presence of IL4 and GM-CSF. In humans, most DC are derived from a common precursor; they do not arise from monocytes and are considered cDC. The moDC generated *in vitro* most closely resemble *in vivo* "inflammatory moDC", a recently identified subset which are not present in the steady state but differentiate from monocytes during infection/inflammation [338]. Despite their long history of use, there is a paucity of information on physiological mouse/human moDC equivalents and even less on the role of moDC in anti-cancer immune responses. A DC subtype resembling moDC in phenotype and morphology was recently found to be crucial for the induction of chemotherapy-induced anti-cancer immune responses within the tumour site in mice, providing the first evidence for a role for moDC in tumour immunity [339]. Conversely, an equivalent subset recently identified in the ascitic fluid from human breast and ovarian cancer patients was proposed to contribute to disease pathogenesis [338]. Consequently, generalization of observations made using *in vitro* generated moDC to activity of *in viv*o DC should be viewed with caution. In mice, moDC can be distinguished from cDC by their expression of dendritic cell-specific intercellular adhesion molecule-3-grabbing non-integrin (DC-SIGN) [340], therefore studies using mice lacking cDC may help address whether inflammatory moDC are able to promote adaptive immunity.

Another potential concern with studies involving moDC is the heterogeneity of the monocyte precursors used for *in vitro* generation of moDC. Passlick *et al* reported that human monocytes in the peripheral blood are heterogeneous. In addition to the classical $CD14^{++}$ monocytes, which comprise the major subset in the circulation, a subset of $CD14^+CD16^+$ monocytes is present, which make up 2.2% of total PBMC [341]. The $CD14^{++}CD16^-$ subtype represent 80% to 90% of blood monocytes. $CD16^+$ monocytes are usually divided into $CD14^{high}CD16^{low}$ ($CD14^{++}CD16^+$) and $CD14^{low}CD16^{high}$ ($CD14^+CD16^{++}$) subsets [92, 341]. Human $CD14^{++}$ $CD16^-$ monocytes express high levels of CCR2 and L-selectin (CD62L) but lower C-X_3-C chemokine receptor 1 (CX_3CR1) on

their surface. They have higher phagocytic activity and when stimulated with LPS, the cells produce higher levels of IL-10, but lower levels TNF-α and IL-1. In contrast, human $CD16^+$ monocytes express high levels of CX_3CR1 but lower CCR2, and are responsible for the production of TNF-α in response to LPS stimulation [342, 343]. Further studies have shown that $CD16^-$ and $CD16^+$ moDC behave differently. The latter express higher levels of CD86 and CD11c, and show lower expression of CD32 compared to $CD16^-$ moDC. LPS-stimulated $CD16^-$ moDC express lower levels of IL-12 mRNA and secrete lower amounts of IL-12 than $CD16^+$ moDC. Finally, $CD4^+$ T cells stimulated with $CD16^+$ moDC secrete increased amounts of IL-4 compared to those stimulated by $CD16^-$ moDC [343].

It is speculated that the moDC used in this study lacked CD16 expression, because the MACS monocyte isolation kit eluted $CD16^-$ monocytes (confirmed by personal communication with Miltenyi BioTech) and because CD16 has previously been described as absent on moDC [344].

The form in which tumour cells are ingested by DC influences the efficiency of TA presentation [326, 336]. DC express receptors that facilitate uptake of cells bearing specific moieties, such as the $\alpha_v\beta_3$ and CD36 receptors for apoptotic bodies; the lectin receptors (mannose receptors and DEC205) for heat shock proteins (associated with cellular stress) and the FcγR for IgG [345]. Despite variable expression, CD16-mediated internalisation very efficiently targets antigens to a unique DC specific antigen pathway that results in delivery to the cytosol [326, 336].

In retrospect, the use of $CD16^-$ moDC may have limited this study to a DC subtype more amenable to upregulation of maturation markers but with lower capacity for cross presentation via IL-12 stimulation of naïve T cells. The use of an alternative monocyte isolation kit that yields $CD16^+$ monocytes for differentiation to moDC could be a way of partially addressing this limitation.

Peripheral blood DC are known to express 2 other activating Fcγ receptors that can bind IgG - CD32a and CD64; however the expression of these receptors in *in vitro* generated moDC is highly selective (comprehensively reviewed by Guilliams *et al*, 2014 [346]). CD64 has been documented as absent or unstably expressed in moDC, attributed to the use of IL-4 during differentiation, which is known to downregulate CD64 expression. CD32a and the inhibitory receptor FCγRIIb (CD32b) are co-expressed on moDC and co-ligated by mAbs, where CD32a has been shown to limit CD32a-induced DC maturation [344]. In the co-culture model presented, DC maturation appeared to be NK-cell dependent. It was therefore speculated that the moDC used in

this study were limited in their capacity to be directly activated by the mAbs. It was felt that conducting these experiments in the presence and absence of NK cells adequately addressed the potential for direct mAb activation of DC and negated the need to screen extensively for activating receptors on DC.

Finally, by investigating only DC the critical events occurring in concert with other APC were indubitably missed. Although NK:DC crosstalk has been well studied, it has been shown for example that monocytes and macrophages also play a part in tumour-antigen presentation, via ADCP [233]. To enable a clearer picture of immune cell crosstalk, broader screening of a number of APC should be considered. For this to be adapted clinically however, more blood would be required and the impact of such sampling on cancer patients raises ethical concerns.

The interpretation of these findings is subject to the same limitations previously detailed in Chapter 3, viz: except in the case of GA101GE and GA101WT, the mAbs were not normalised to account for the differences in their binding sites or isotypes, restricting this study to comparison at equivalent concentration. Only one cell type was used to assess the process of DC maturation in both EGFR and CD20 contexts, making it hard to draw conclusions on wider applicability. Ideally future studies will incorporate multiple tumour cell types, including low passage primary tumour cells, with larger numbers of donors.

Despite these caveats, results obtained indicate that immunotherapeutic GE-mAbs specific for TA can induce efficient apoptosis of tumour cells and maturation of DC, so have the potential to elicit an adaptive response to TA. The results obtained herein support the findings of Srivastava *et al*, indicating that mAb-activated NK cells and dendritic cells collaborate to trigger TA-specific T-cell immunity [97]. In the same report, the authors demonstrated that EGFR-specific T-cell frequencies in cetuximab-treated patients were significantly higher than those of cetuximab-naïve patients; indicating that their *in vitro* findings were translated to their clinical setting.

Stimulation of an anti-TA reactive T-cell response remains challenging because most TA are self antigens to which the immune system is tolerant [347]. Exploration of the ability of GE-mAbs to promote DC cross presentation to TA-specific $CD8^+$ T cells is described in the following chapter.

Chapter 5. Results III: Evaluation of the ability of glyco-engineered monoclonal antibodies to promote tumour antigen cross presentation to $CD8^+$ T cells

5.1. Introduction

Results presented in the previous chapters have shown that GE-mAbs are able induce NK-cell mediated apoptosis of tumour cells, that tumour particulate generated by apoptosis is phagocytosed by DC and that GE-mAb activated NK cells induced DC maturation. These findings suggest that GE-mAbs have the potential to promote cross presentation of antigen by DC to TA-specific $CD8^+$ T cells.

Several studies have demonstrated cross presentation of TA to T cells by DC exposed to apoptotic tumour cells but, in most studies, the tumour particulate was generated in a non-physiological setting using UV- or γ-irradiation or heat shock [70, 106, 325, 348, 349]. Only the Ferris laboratory have previously described cross presentation of TA by DC in the setting where tumour particulate was generated by mAb-mediated ADCC [97]. Using *in vitro* co-cultures of the PCI-15B $EGFR^+$ cell line with NK cells, DC and EGFR-specific $CD8^+$ T-cells from HNSCC patients, they showed that cetuximab-activated NK cells induced DC maturation, antigen presentation and stimulation of IFNγ production by EGFR-specific $CD8^+$ T cells.

The final objective of the study reported here was to add TA-specific $CD8^+$ T cells to the *in vitro* co-culture model and assess whether GE-mAb-activated NK cells induce DC cross presentation of TA and stimulation of $CD8^+$ T-cell responses. The four-cell *in vitro* co-culture model depicted in Figure 5.1 exploits HLA-mismatched cell types to assess antigen cross presentation. The tumour cells are HLA-A*02 negative whereas the NK cells, DC and TA-specific T-cells are from an HLA-A*02 positive donor. In this setting, the T-cell is unable to recognise the tumour cell directly. The model is dependent upon ADCC-mediated lysis of HLA-$A*02^-$ tumour cells by NK cells, uptake of exogenous tumour particulate by DC, processing and binding of TA to HLA-A*02 and cross presentation by DC to HLA-A*02 restricted $CD8^+$ T cells. HLA-A*02 restricted TA-specific $CD8^+$ T cells for use in the model was a key requirement.

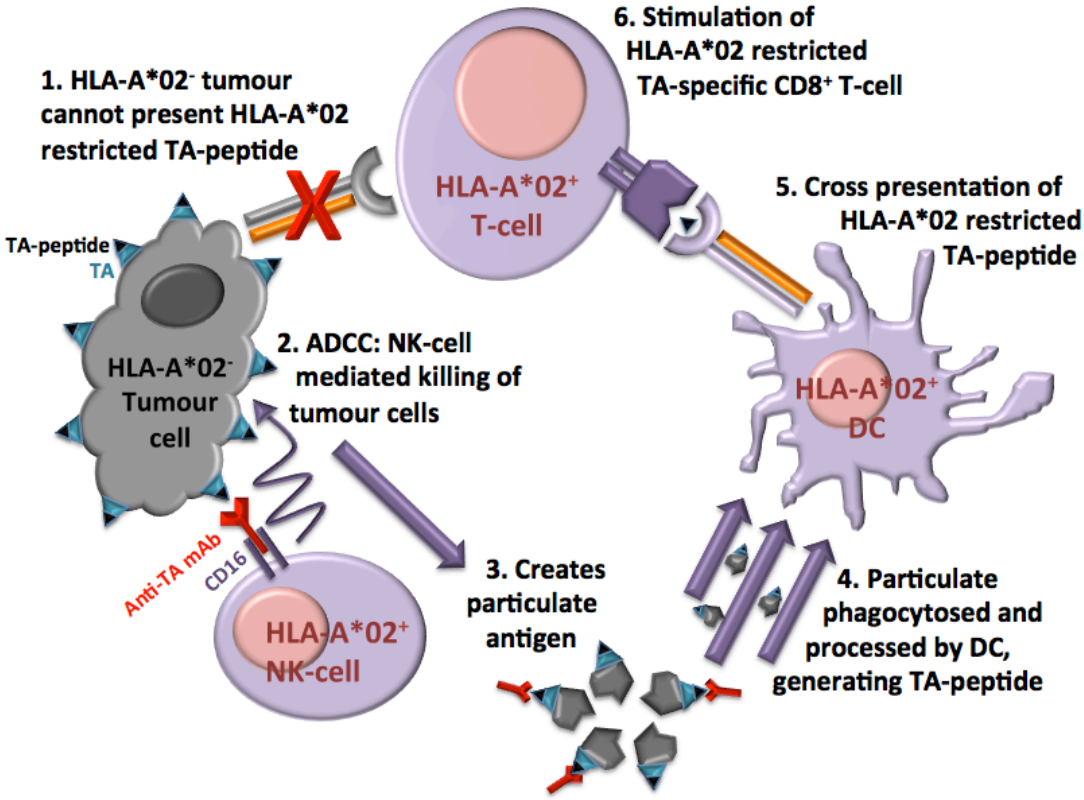

Figure 5.1. Schematic representation of a four-cell *in vitro* co-culture model using HLA-mismatched cells to assess TA cross presentation

5.2. Screening for HLA-A*02 restricted TA-specific CD8$^+$ T cells in cancer patients treated with anti-EGFR mAbs

A growing body of evidence from animal models [350] and in the clinical setting [351, 352, 353] indicates that TA-specific mAbs can elicit cellular immunity. Cancer patients treated with mAbs were therefore considered likely to have memory T cells specific for TA, and were investigated as a source of HLA-A*02 restricted TA-specific CD8$^+$ T cells for use in this study. Peripheral blood samples from CRC or HNSCC patients participating in a clinical trial to evaluate treatment with either cetuximab or imgatuzumab were screened for presence of EGFR-specific CD8$^+$ T cells.

Two previous reports have described identification of EGFR-specific CD8$^+$ T cells. Andrade Filho *et al* used *in silico* tools to predict the candidate HLA-A*02-binding peptide epitope $EGFR_{853}$ sequence ITDFGLAKL. After 10 days *in vitro* stimulation of peripheral blood from 5 HLA-A*02$^+$

healthy donors and 5 HLA-A*02^{+} HNSCC patients with the peptide, $EGFR_{853}$-specific CD8^{+} T cells were detected at mean frequencies of 0.4% and 0.6% respectively using MHC tetramers [282]. Schuler *et al* worked with two putative HLA-A*02-binding peptides, $EGFR_{479}$ sequence KLFGTSGQKT and $EGFR_{1138}$ sequence YLNTVQPTCV [240]. These peptides were previously reported to be recognised by antibodies present in pancreatic cancer patients [354]. Peripheral blood samples from 16 HLA-A*02^{+} HNSCC patients were stimulated *in vitro* with these peptides for four rounds and responses assessed by IFNγ enzyme linked immunospot (ELISPOT) assay. Mean T-cell frequencies of 0.28% specific for the $EGFR_{479}$ peptide and 0.56% for the $EGFR_{1138}$ peptide were detected [240].

In this study, peripheral blood samples from HLA-A*02+ CRC or HNSCC patients were stimulated *in vitro* with the previously reported HLA-A*02 restricted EGFR peptide epitopes and responses assessed after 10 days using MHC pentamers. Unfortunately, attempts to synthesise the HLA-A*02 pentamer for the $EGFR_{853}$ ITDFGLAKL peptide were not successful due to poor stability that was possibly the result of a low HLA-A*02 affinity score (ProImmune, personal communication). Therefore, only responses to $EGFR_{479}$ KLFGTSGQKT and $EGFR_{1138}$ YLNTVQPTCV were investigated. The work with patient samples was conducted in collaboration with Maeve McEnery (KCL - London, UK).

5.2.1. Patient samples

Samples available for study were unused frozen aliquots of PBMC remaining from other analytical studies after conclusion of three clinical trials involving imgatuzumb: BO21495 (ras mutant colorectal cancer), BP25438 (colorectal cancer) and BP22350 (HNSCC). PBMC numbers were low (1-2x10^{6} per aliquot) and frequently of poor quality (haemolysed with cell aggregates). Both the previously reported studies of EGFR-specific CD8^{+} T cells involved *in vitro* stimulation to promote proliferation and thereby increase numbers to a detectable range. Due to the low starting cell numbers available for this study, a protocol was devised that did not require purification of antigen-presenting cells or T cells and involved only minimal cell handling. The multiple rounds of *in vitro* stimulation conducted by Schuler *et al* [240] were not possible because all cells had to be committed to the initial stimulation. Thus, a protocol based on the study by Andrade Filho *et al* [282], using a single *in vitro* stimulation and assay with MHC-peptide multimers was employed. To assess whether anti-EGFR mAbs augment anti-tumour CD8^{+} T-cell immunity, PBMC samples

from each patient were tested at two time-points, one before and one during/after treatment with mAb infusions. Of 42 patients with appropriate paired samples, 18 were HLA-A*02^{+} and therefore suitable for study. These were 3 patients from trial BO21495, 3 from trial BP25438 and 12 from trial BP22350. All patients were treated with either cetuximAb or imgatuzumab.

The baseline samples for patients from trials BO21495 and BP22350 were thawed and a small aliquot of 10^5 PBMC used to screen for HLA-A*02 type with an anti-HLA-A*02 specific PE-labelled mAb and analysis by flow cytometry. For those samples found to be HLA-A*02^{+}, the PBMC paired sample during/after treatment was then immediately thawed and the antigen specific T-cell stimulation protocol performed simultaneously for the baseline and the during/after treatment samples. Patients from trial BP25438 had already previously been screened for HLA-A*02 type.

5.2.2. HLA-A*02 peptide-binding assay

The T2 assay was conducted to assess the HLA-A*02 binding ability of the EGFR-specific peptides relative to the highly immunogenic HLA-A*02 restricted peptide GILGFVFTL, derived from influenza A matrix protein-I (FLU.A-mp1$_{58}$). Stabilisation of the HLA-A*02 complex on the surface of TAP-deficient T2 cells correlates with the binding capacity of the specific peptide to HLA-A*02. In order to determine the binding capacity, the MFI of 'T2 cells + peptide' was divided by the MFI of 'T2 cells alone', resulting in a value between 1 and 2, in keeping with previous studies [240, 282]. The results displayed in Figure 5.2 show that binding of the EGFR$_{1138}$ YLNTVQPTCV peptide to HLA-A*02 was detected, but binding capacity was lower than for the FLU.A-mp1$_{58}$ positive control. The EGFR$_{479}$ KLFGTSGQKT peptide did not induce detectable stabilisation of HLA-A*02 expressed by T2 cells, indicating that it has much lower affinity for HLA-A*02 than the EGFR$_{1138}$ peptide.

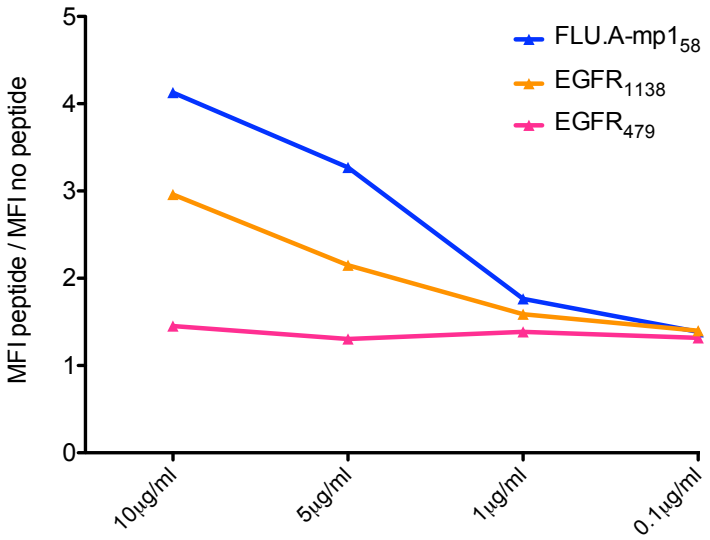

Figure 5.2. T2 stabilisation assay to assess relative HLA-A*02 binding affinities of EGFR peptides
$5x10^5$ T2 cells were cultured alone or in the presence of peptides at various concentrations. After 18 hours, T2 cells were screened for surface expression of HLA-A*02. The MFI was divided by the MFI of T2 alone to obtain a binding score.

5.2.3. Screening for HLA-A*02 restricted EGFR-specific CD8$^+$ T cells in cancer patient samples

There were insufficient patient PBMC to test the two HLA-A*02 restricted EGFR peptide epitopes individually, therefore, peptides were combined for *in vitro* stimulation. The EGFR$_{479}$ peptide was added at 10µg/ml as described by Schuler *et al* [240], and EGFR$_{1138}$ was added at the lower concentration of 5µg/ml in an attempt to limit dominance, as the results of the T2 peptide-binding assay indicated that EGFR$_{1138}$ had higher affinity for HLA-A*02. This decision was agreed with Roche Glycart. Patient PBMC were cultured with peptides in the presence of 5ng/ml IL-7. Every 3 days thereafter, IL-2 was added to a final concentration of 25U/ml. After 10 days, cultures were screened for the presence of EGFR-specific CD8$^+$ T cells (^{EGFR}T cells) using MHC class-I multimers (pentamers). PBMC from one healthy HLA-A*02$^+$ individual and patient PBMC were also screened for the HLA-A*02 restricted peptide NLVPMVATV derived from CMV pp65 protein (CMVpp65$_{495}$) as a positive control to validate the *in vitro* T-cell expansion protocol. Many individuals possess memory CMV-specific CD8$^+$ T cells (^{CMV}T cells) at frequencies detectable *ex vivo*, with a high probability of recall expansion [355].

MHC class-I multimer screening was performed according to the gating strategy illustrated in Figure 5.3. The antigen-specific T-cell phenotyping panel was designed to achieve clear segregation of Multimer^{+}CD8^{+} T cells within a mixed population. Because of the potential for CD8 downregulation after stimulation, CD4^{+}CD8^{-} cells were gated to determine fluorescence on multimer negative cells and this gate was then applied to CD8^{+} T cells as illustrated.

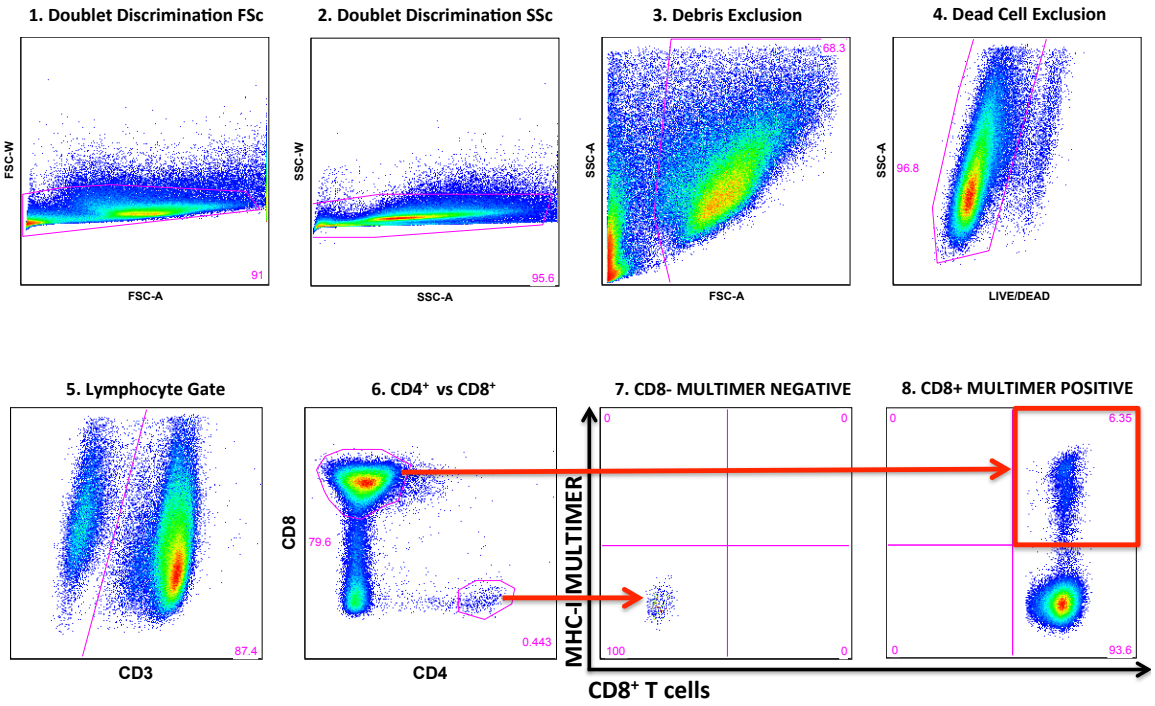

Figure 5.3. Gating strategy: identification of antigen specific CD8^{+} T cells using MHC class-I multimers
Antigen-specific CD8^{+} T cells within T-cell expansion cultures were identified according to the strategy illustrated. Sequential gating achieved exclusion of doublets, debris and dead cells, then CD3^{+} lymphocytes were separated into CD4^{+} and CD8^{+} subsets. CD4^{+}CD8^{-} cells were gated to determine fluorescence on MHC class-I multimer-negative cells and this gate was then applied to CD8^{+} T cells.

^{CMV}T cells were detected in the PBMC from one healthy individual *ex-vivo* (Day 0) and expanded robustly using the 10-day stimulation protocol. Results presented in Figure 5.4 A show expansion of ^{CMV}T cells from 0.776% at Day 0 to 30.5% of $CD8^+$ T cells after 10-day *in vitro* stimulation. Sufficient PBMC were available from six patients for *in vitro* stimulation with the $CMVpp65_{495}$ peptide. ^{CMV}T cells were detected in one culture established from BP22350 trial patient 1007. Ex-vivo analysis of PBMC from this patient showed expansion of ^{CMV}T cells from 2.81% at Day 0 to 21.7% of $CD8^+$ T cells after 10-days *in vitro* stimulation. This result demonstrated that the protocol could promote substantial *in vitro* expansion of antigen-specific memory $CD8^+$ T cells from patient PBMC. *In vitro* cultures were established from 18 HLA-A*02^+ patients using baseline and during/after treatment PBMC samples. Due to low cell numbers in many samples, priority was given to performing the EGFR peptide pool stimulation and then the $CMVpp65_{495}$ peptide culture if cell numbers were sufficient. Cultures performed are listed in Table 5.1.

Unfortunately, no ^{EGFR}T cells were detected in any cultures. A representative example of EGFR pentamer screening of cultures from baseline and progression samples is shown in Figure 5.4 B for patient 1007, from which expansion of ^{CMV}T cells was successfully achieved. The composition of all patient cultures after *in vitro* stimulation with EGFR peptides is shown in Table 5.2. Of the 36 cultures, 22 had a total cell viability below 50%, 27 had fewer than 100,000 viable T cells and 32 cultures contained less than 27% $CD8^+$ T-cells. Poor viability and limited cell numbers likely underlies the lack of detectable ^{EGFR}T cells in these patient samples. An alternative source of ^{EGFR}T cells was therefore sought.

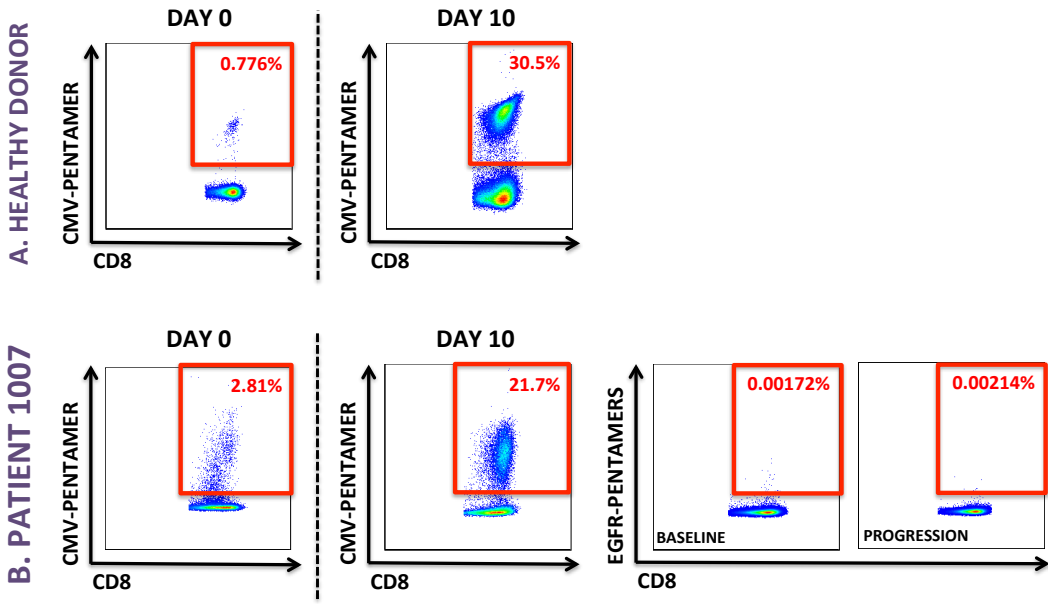

Figure 5.4. Representative example of pentamer screening of PBMC from a healthy individual and a patient before and after *in vitro* stimulation with peptides

$2x10^6$ PBMC were cultured in the presence of IL7 at a final concentration of 10ng/ml with peptides. IL-2 was added to a final concentration of 25U/ml every 3 days. After 10 days, cultures were harvested and screened for presence of peptide specific $CD8^+$ T cells using pentamers

Table 5.1. Details of patient sample allocation to T-cell expansion protocols

Samples from trial	HLA-A*02$^+$	EGFR	CMV
BP22350	12/32	12	6
BP25438	3	3	0
BO21495	3/11	3	0
Total	18	18	6

Table 5.2. Composition of T-cell expansion cultures after 10-day stimulation with EGFR peptides

Time point	Patient ID	% Live cells	% T cells	Number T cells	% $CD8^+$ T cells
BASELINE	1005	79	98	161000	13
	1007	97	98	1680000	23
	1037	35	94	45431	18
	1042	94	99	142000	18
	1051	3	92	245	87
	1057	27	96	522	1
	1065	32	99	24150	9
	1301	0	0	0	0
	1508	0	0	0	0
	2001	4	99	7507	21
	2037	14	0	0	0
	2039	7	93	1206	8
	2066	2	77	128	79
	3105	14	96	8042	7
	3304	98	99	104000	27
	3402	69	98	32166	10
	3502	0	0	0	0
	3503	0	0	0	0
PROGRESSION	1005	95	97	173000	10
	1007	95	98	1250000	23
	1037	36	99	2862	2
	1042	90	99	167000	23
	1051	7	91	1244	85
	1057	40	97	7951	12
	1065	90	98	133000	17
	1301	0	0	0	0
	1508	92	99	885000	27
	2001	9	99	1858	18
	2037	12	0	0	0
	2039	0	96	22	0
	2066	1	67	58	72
	3105	73	96	47159	14
	3304	96	99	32690	23
	3402	80	98	52101	14
	3502	5	75	58	0
	3503	91	72	2816	0

5.3. *In vitro* prime and expansion of HLA-A*02 restricted TA-specific CD8$^+$ T cells from the naïve repertoire of healthy donors

Because no HLA-A*02 restricted EGFR-specific T cells were detected in mAb-treated cancer patients, an *in vitro* prime of naïve T cells was attempted using PBMC from healthy donors. Many protocols have been described for *in vitro* expansion of antigen-specific T cells from the naïve repertoire, all involving the following steps:

1. APC selection
2. APC antigen loading
3. Responder T-cell selection
4. T-cell "prime" (initial combination of T cells and antigen loaded APCs)
5. T-cell "restimulation" (repeated exposure of T cells to antigen loaded APCs)
6. Screen for T-cell antigen specificity

The protocols vary greatly in terms of media, cytokines use, T-cell:APC ratios and duration of stimulation. Wolfl and Greenberg published a prescriptive protocol detailing the robust and reproducible expansion of CD8$^+$ antigen-specific T cells using IL-7, IL-15 and IL-21 to promote responder cells as opposed to the more widely used IL-2/IL-7 combination [264]. Their protocol exploited the properties of MelanA, an antigen that is overexpressed by melanoma cells and recognised by a large number of tumour infiltrating T cells in melanoma patients [356]. MelanA served as a model antigen because of the unusually high precursor frequencies of MelanA specific CD8$^+$ T cells (^{MelanA}T cells) found in HLA-A*02$^+$ healthy individuals [357, 358] and the identification of a heteroclytic peptide MelanA$_{26-35}$ ELAGIGILTV (A27L) that has enhanced HLA-A*02 binding which greatly improves ^{MelanA}T-cell expansion [281].

5.3.1. Naïve CD8$^+$ T-cell priming and expansion protocol

The MelanA antigen model was used to establish a modified version of the protocol described by Wolfl and Greenberg for use in this study. Purified naïve (CD45RO$^-$CD57$^-$CD62L$^+$) CD8$^+$ T cells were considered a more suitable responder population than more widely used total CD8 T-cell preparations because the fraction of naïve T cells varies considerably between donors. For 3 independent experiments, the average isolation purities after 2 stage selection were as follows:

$CD8^+$ fraction: 97.9% +/- 0.7% sd

$CD45RO^-$ fraction: 96.8% +/- 1.8% sd

$CD57^-$ fraction: 95.9% +/- 1.2% sd

$CD62L^+$ fraction: 68.9% +/- 2.9% sd

As APC, DC were matured in the presence of $MelanA_{26-35}$ peptide using an LPS/IFNγ cocktail as opposed to the more widely used TIP maturation cocktail to create ^{MelanA}DC. The PGE_2 component of TIP inhibits DC IL-12 production in a dose-dependent manner [359], as a consequence such DC are prone to exhaustion and show limited priming capacity [360]. In contrast, IFNγ primes the promoter region of IL-12 and LPS activates IL-12 production via TLR4 -triggering [360, 361]. A single stimulation of naïve $CD8^+$ T cells with ^{MelanA}DC was performed and MHC-dextramers used to identify ^{MelanA}T cells.

5.3.2. HLA-A*02$^+$ T cells

The frequency of HLA-A*02^+ individuals is approximately 46% within the Caucasian population; the highest allele frequency of any ethnicity [362]. 35 healthy donors were screened for HLA-A*02 status by flow cytometry, with 17 (48.6%) identified as HLA-A*02^+.

5.3.3. Successful *in vitro* priming and expansion of HLA-A*02 restricted MelanA-specific $CD8^+$ T cells

The modified T-cell stimulation protocol was used to assess expansion of MelanA-specific $CD8^+$ T cells from two donors in two independent experiments. Multiple cultures were set up for each donor and screened individually for expansion of ^{MelanA}T cells after 10 days using MelanA-dextramer. The results displayed in Table 5.3 and Figure 5.5 show reliable expansion of ^{MelanA}T cells. The ^{MelanA}T-cell frequency increased from 0.18% to a maximum 15.6% for LC66 and from 0.17% to a maximum 23% for LC97. The frequencies of ^{MelanA}T cells for LC66 and LC97 showed a median increase of 71- and 101-fold respectively; remarkable considering this was achieved without restimulation. There was variation in the frequencies of ^{MelanA}T cells attained in different cultures set up using cells from the same donor which indicated variation in the efficiency of *in vitro* T-cell priming and expansion.

Table 5.3. MelanA-specific CD8$^+$ T-cell frequencies achieved using the *in vitro* T-cell expansion protocol

DONOR	% MelanA-Specific T cells (D10)				
	TIME 0	CULTURE 1	CULTURE 2	CULTURE 3	CULTURE 4
LC66	0.177	9.24	12.7	15.6	-
LC97	0.169	12.3	15.9	18.4	23.1

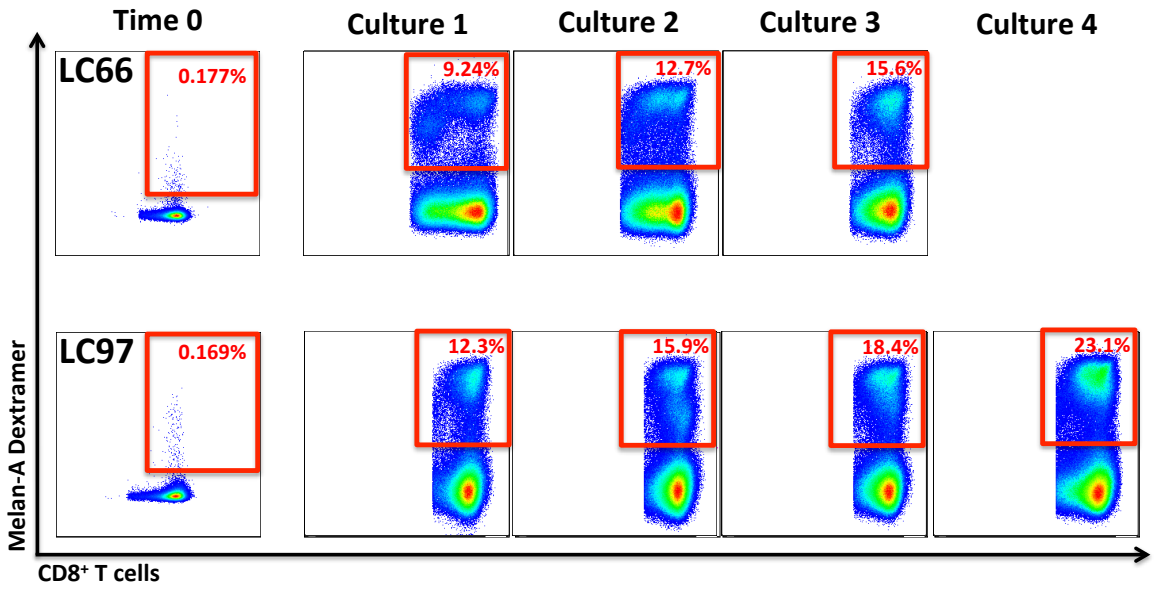

Figure 5.5. MelanA-specific T cells were robustly and reproducibly expanded *in vitro*
MelanA-specific T cells were expanded from naïve T cells and 10^5 cells were screened for specificity on day 10 of culture. Red boxes and text highlight the CD8$^+$ MelanA-dextramer$^+$ and frequency of ^{MelanA}T cells.

5.3.4. No *in vitro* expansion of HLA-A*02 restricted EGFR- or CD20-specific CD8$^+$ T cells

In light of the success expanding ^{MelanA}T cells, the modified protocol was used to attempt *in vitro* priming of EGFR- and CD20-specific CD8$^+$ T cells from healthy donors. MelanA stimulation was performed in parallel as a positive control. Duplicate cultures using cells from 3 healthy donors were screened on day 10 and the results for antigen-specific T-cell frequencies achieved are shown in Table 5.4 and displayed graphically in Figure 5.6. Although ^{MelanA}T cells were observed at high frequencies, neither CD20- nor EGFR-specific T cells were detected.

Table 5.4. TA-specific CD8$^+$ T-cell frequencies achieved using the *in vitro* T-cell expansion protocol

DONOR	% Antigen-Specific T cells after Expansion (Culture1 | Culture2)			
	$CD20_{188-196}$	$EGFR_{479-488}$	$EGFR_{1138-1147}$	$MelanA_{26-35}$
LC65	0.361 | 0.278	0.0254 | 0.0276	0.125 | 0.15	17.3 | 27.6
LC98	0.658 | 0.372	0.0142 | 0.0209	0.209 | 0.157	11.4 | 11.1
LC100	0.256 | 0.167	0.038 | 0.00841	0.382 | 0.358	5.72 | 2.32

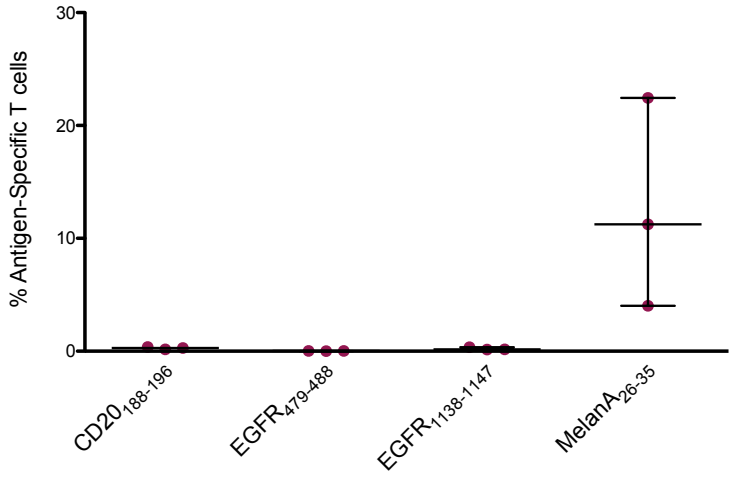

Figure 5.6. No expansion of CD20- or EGFR-specific CD8$^+$ T cells, despite robust expansion of ^{MelanA}T cells
Naïve T cells were stimulated with TA and 10^5 cells were screened for specificity after 10 days using MHC multimers. Graph depicts frequency of TA-specific T cells, with median and interquartile range for n=3 (duplicate average).

5.4. Modification of the four-cell *in vitro* co-culture model to assess cross presentation of MelanA

Because attempts to generate EGFR- or CD20-specific CD8$^+$ T cells were unsuccessful, the four-cell *in vitro* co-culture model was adapted to exploit the ^{MelanA}T cells that were successfully generated. Figure 5.7 depicts the modified cross presentation model in the context of anti-EGFR mAbs. A variant of the EGFR$^+$ tumour cell line A431 created to express MelanA protein was used so that NK-cell mediated lysis induced by an anti-EGFR mAb generates tumour particulate containing MelanA antigen for phagocytosis by DC and cross presentation to ^{MelanA}T cells.

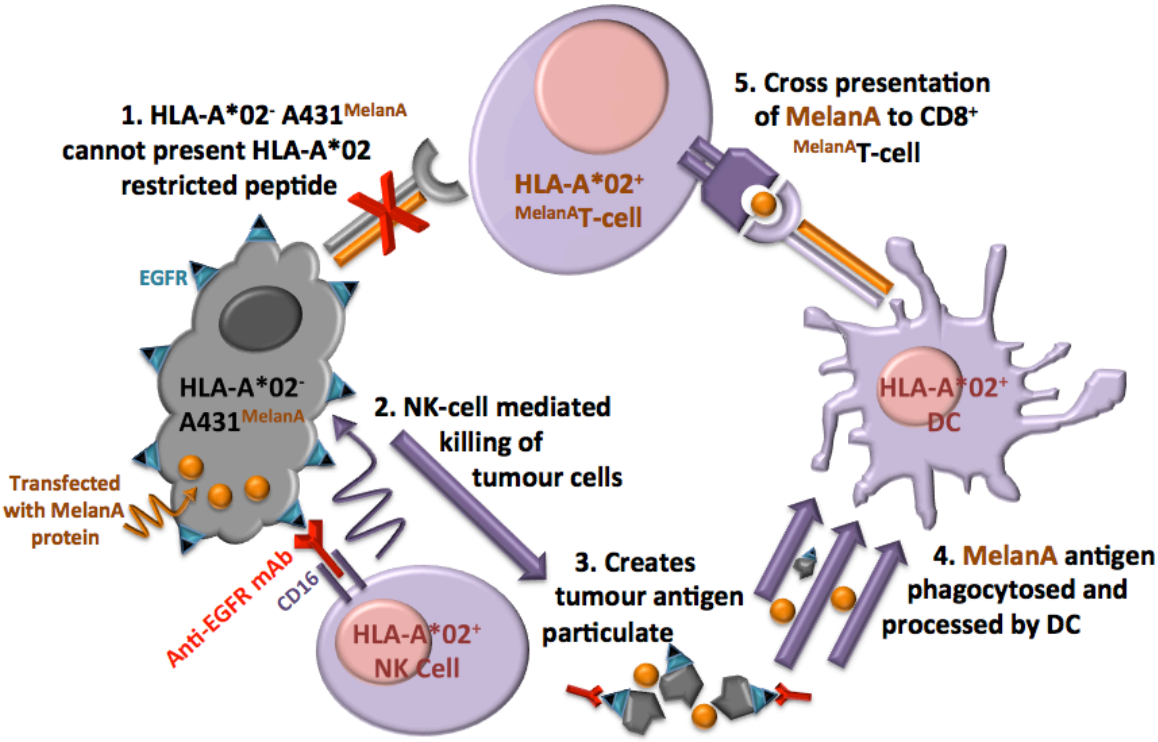

Figure 5.7. Schematic representation of the four-cell *in vitro* co-culture model, modified to assess cross presentation of MelanA antigen

5.4.1. Production of HLA*A-02^{-}EGFR^{+} A431 tumour cells that express MelanA protein

The EGFR^{+} cell lines A431 and H1299 were screened for expression of HLA-A*02 by flow cytometry and confirmed as HLA-A*02^{-} and HLA-A*02^{+} respectively (Figure 3.8). HLA-A*02^{+} H1299 cells and a MelanA^{+} transfected version of this cell line were needed as negative and positive controls respectively to stimulate HLA-A*02 restricted ^{MelanA}T cells. A431 and H1299 cells were transfected with the plasmid construct shown in Figure 2.1 to generate HLA-A*02^{-} EGFR^{+}MelanA^{+} tumour cells (A431^{MelanA}) and HLA-A*02^{+}EGFR^{+}MelanA^{+} tumour cells (H1299^{MelanA}). The DNA sequence for wild type MelanA was used because previous studies report that T cells generated using the heteroclytic peptide MelanA$_{26-35}$ ELAGIGILTV (A27L) effectively respond to wild type MelanA expressed by tumour cells [363] [364]. Fusion of the MelanA sequence to GFP enabled visualisation of transfected cells and incorporation of a puromycin resistance gene facilitated drug selection of transfected cells. A Control^{MA-} plasmid containing all elements except the MelanA sequence was transfected into A431 cells (A431^{CTRL}) and H1299^{CTRL} for use as negative controls in T-cell assays.

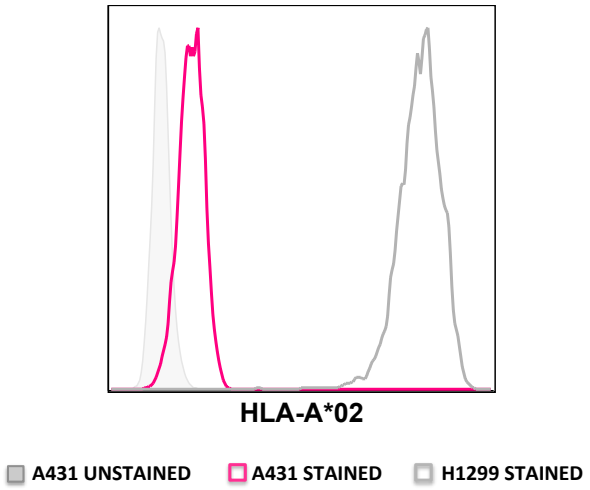

Figure 5.8. A431 and H1299 cell lines are HLA-A*02^{-} and HLA-A*02^{+} respectively
10^5 A431 and H1299 cells were stained with anti-HLA-A*02 PE-conjugated antibody

The model plasmid "p-Select", kindly provided by Dr Richard Beswick (KCL - London, UK) was used to optimise the transfection protocol. The p-select plasmid has previously been used to transfect a wide range of different cell types and produces high intensity expression of GFP 48 hours after transfection (Dr Beswick, personal communication). HLA-A*02^{-} A431 cells and HLA-A*02^{+} H1299 cells were transfected with either the Control^{MA-}, MelanA or p-Select plasmids in parallel.

Images presented in Figure 5.8 show successful transfection of adherent A431 and H1299 cells. Morphology of untransfected cells are displayed unfiltered in column 1 and compared to images taken 48 hours after transfection under either GFP daylight or GFP blackout filters. Transfection with the model p-Select plasmid elicited high intensity GFP^{+} cells that were visible in daylight (column 2-left) in both cell lines. GFP^{+} cells were present after transfection with Control^{MA-} or MelanA plasmids, but the signal was less intense requiring use of GFP blackout filters for visualisation. Transfection efficiency was lower for A431 cells (panel A) than H1299 cells (panel B). Mean transfection efficiency for the Control^{MA-} plasmid was 6.6% GFP^{+} (+/-2.9 sd) for A431 cells and 10.6% (+/-1.8 sd) for H1299 cells. Transfection efficiency was higher for the Control^{MA-} plasmid than the MelanA plasmid. Mean transfection efficiency of A431 cells was 6.6% GFP^{+} (+/-2.9 sd) with the Control^{MA-} plasmid and 3.6% (+/-0.6 sd) for the MelanA plasmid, with similar results observed for H1299 cells).

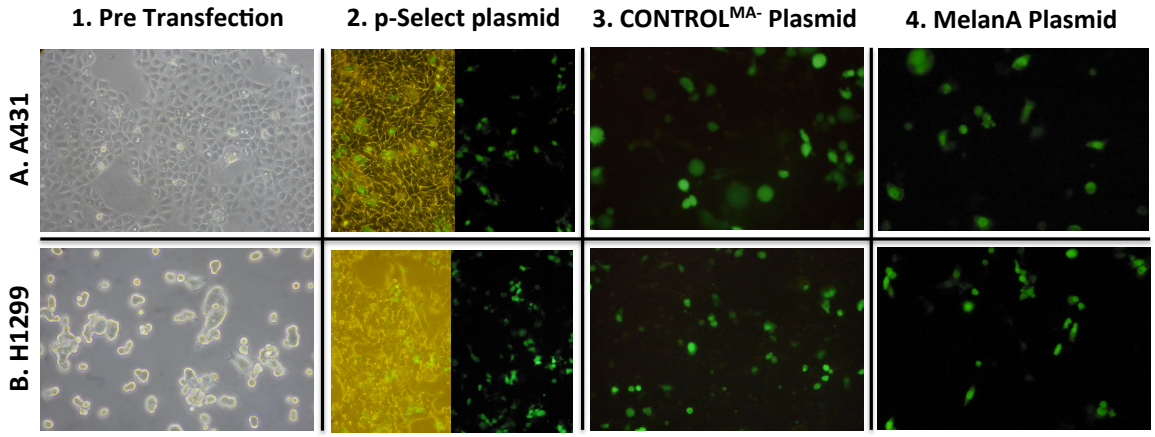

Figure 5.9. A431 and H1299 cells express GFP 48 hours after transfection
A431 (row A) and H1299 (rowB) cells were imaged pre-transfection (column 1) and post-transfection with the model plasmid p-Select (column 2) either in daylight (left) or darkness (right). Column 3: GFP^{+} variants of the A431 and H1299 cell lines were produced by transfection with the Control^{MA-} plasmid and imaged in darkness. Column 4: MelanA^{+}GFP^{+} variants of the A431 and H1299 cell lines were produced by transfection with the MelanA plasmid and imaged in darkness.

It was not possible to transfect suspension B-cell lines using calcium phosphate- or lipofectamine-based protocols, therefore cross presentation studies were limited to the EGFR setting. It was speculated that suspension cells were less permissive to transfection when using reagents optimised for use with adherent cell lines.

5.4.1.1. Selection of MelanA^{+}GFP^{+} cells after transfection

Cells were cultured in the presence of puromycin after transfection with the intention of selecting stably transfected cells that express the puromycin resistance gene. The puromycin concentration for selection was determined by dose titration of untransfected A431 and H1299 cells for 48 hours, and the lowest concentration that induced death of all cells was used. The minimum concentrations were 0.3µg/ml and 0.6µg/ml for A431 and H1299 respectively. Unfortunately, none of the cells survived puromycin selection after transfection. This was possibly due to the large size of the puromycin-resistance gene (600bp). Kim *et al* have reported that the translation efficiency of a gene placed downstream of an IRES can be low, particularly if larger than 80bp [285].

In the absence of puromycin selection pressure, the small percentage of transfected GFP^{+} cells disappeared after 6 days in culture (reduced to 2 days for frozen/thawed cells). Therefore, enrichment of GFP^{+} cells was attempted by FACS 48 hours post transfection, according to the gating strategy shown in Figure 5.9. The median post sort purity of GFP^{HIGH} cells was 91.9% (Figure 5.10). GFP^{HIGH} populations >90% pure were used in cross-presentation co-cultures immediately after sorting.

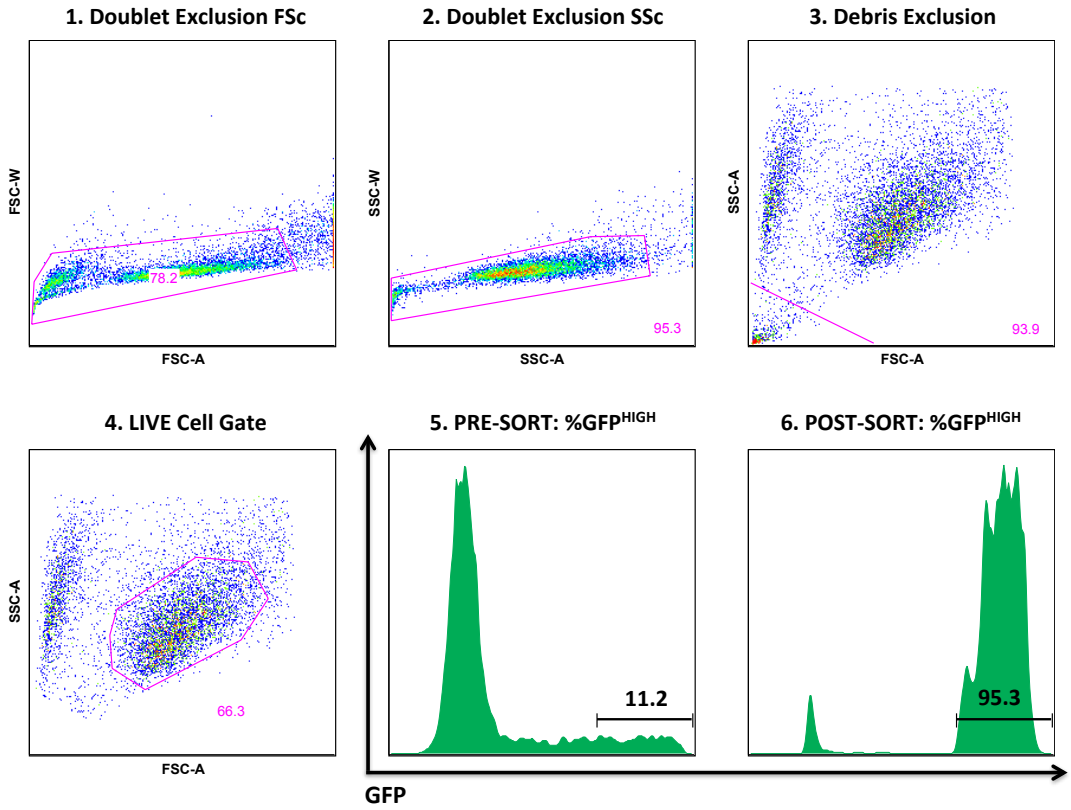

Figure 5.10. FACS gating for purification of GFP^{HIGH} cells
10^4 transfected cells were analysed. Sequential gating achieved exclusion of doublets, debris and dead cells. Pre-sort, transfected cells were gated based on GFP^{HIGH} expression (events > fourth log decade) and these events were collected into one sorting tube. The same GFP^{HIGH} gate was applied to a small aliquot of the post-sort sample, to assess purity of the sorted cells.

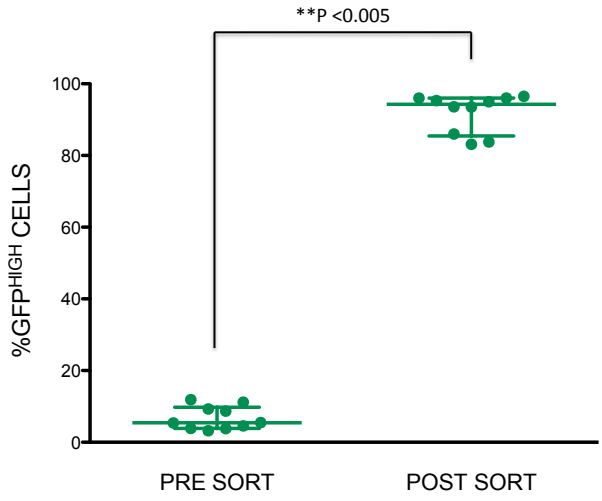

Figure 5.11. Populations of transfected cells expressing high levels of GFP obtained by FACS
10^4 transfected cells were screened for GFP expression. Graph depicts GFP^{HIGH} cell frequency before and after selection by FACS, with median and interquartile range for n=10 independent experiments **p <0.005 (Wilcoxon signed rank test).

5.4.1.2. Confirmation of intracellular MelanA expression

The presence of MelanA protein within GFP^+ sorted cells was confirmed by intracellular staining immediately after sorting. Untransfected cells were used as a negative control and the SKMEL30 cell line that endogenously expresses MelanA was used as a positive control. The majority of the transfected GFP^+ sorted cells expressed MelanA at levels equal to or above the levels in SKMEL30 cells. Representative examples of MelanA expression by transfected A431 and H1299 cells are shown in Figure 5.11.

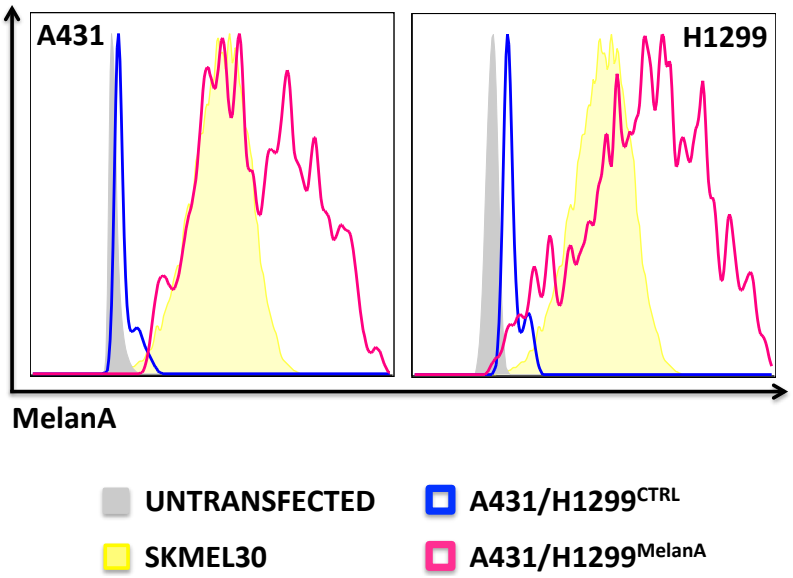

Figure 5.12. Transfected GFP^+ sorted tumour cells express intracellular MelanA
10^5 transfected cells were screened for intracellular expression of MelanA after sorting. $A431^{MelanA}$ and $H1299^{MelanA}$ were compared to either untransfected cells, negative control cells $A431^{CTRL}$ and $H1299^{CTRL}$, or positive control cells SKMEL30.

5.5. HLA-A*02 restricted $CD8^+$ ^{MelanA}T cells recognise $MelanA^+$HLA-$A*02^+$ cells

Recognition of antigen by the ^{MelanA}T cells generated by *in vitro* priming and expansion from the naïve T-cell repertoire of healthy donors (described in section 5.3) was assessed by stimulation with autologous DC loaded with MelanA peptide. Markers of T-cell activation shown in Table 5.5 were selected based on their use in studies previously published.

Table 5.5. T-cell marker modulation upon activation

T-cell Marker	Modulation Upon NK Activation	Reference
CD69	Upregulation	365, 366
CD71	Upregulation	366, 367
CD137	Upregulation	368, 369, 370
IFNγ	Upregulation	371

^{MelanA}T cells harvested after 10 days of *in vitro* expansion were restimulated with autologous DC pulsed with either MelanA peptide (^{MelanA}DC) or irrelevant $EGFR_{1138}$ peptide (^{EGFR}DC) in the presence of BFA. After 18 hours, IFNγ production by ^{MelanA}T cells was assessed. LAC was used as a positive control for T-cell activation and all results were compared to the negative control of unstimulated ^{MelanA}T cells. The results are displayed in Figure 5.13 and show that the majority of ^{MelanA}T cells expressed IFNγ after stimulation with ^{MelanA}DC (71.6%) and there was no response to DC pulsed with the irrelevant EGFR peptide. T cells that did not bind the MelanA dextramer did not produce IFNγ after stimulation.

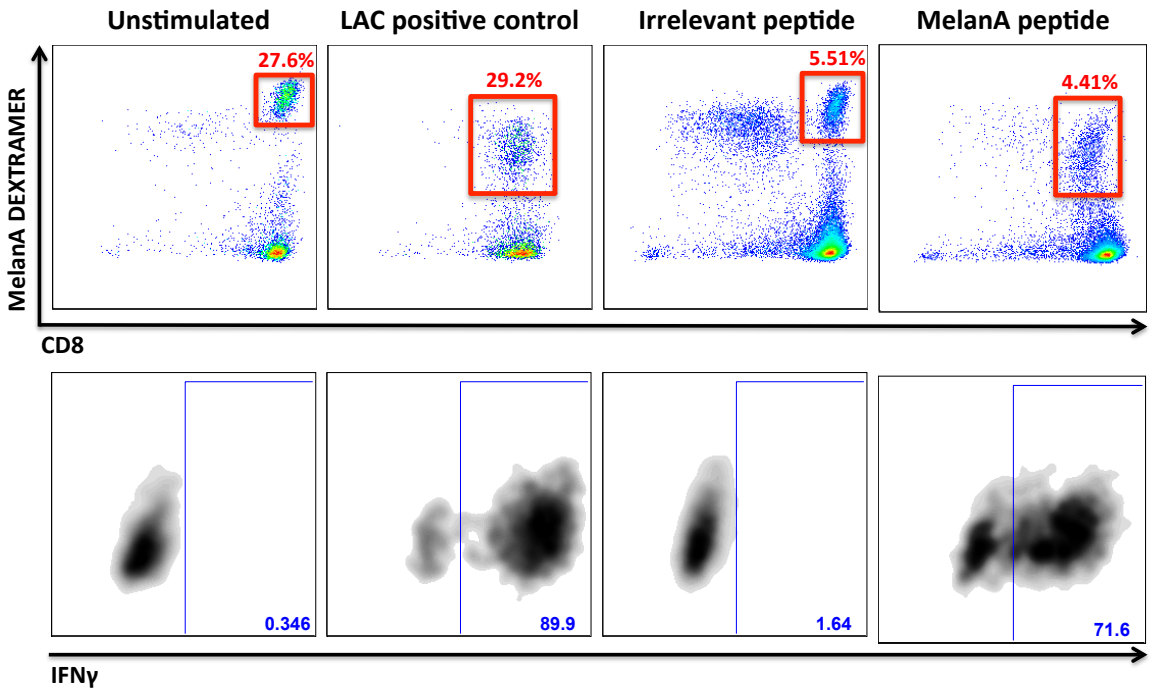

Figure 5.13. Freshly harvested ^{MelanA}T cells produce IFNγ when stimulated with MelanA peptide
^{MelanA}T cells were harvested on day 10 and stimulated using mDC pulsed with either $MelanA_{26-35}$ peptide (^{MelanA}DC) or irrelevant $EGFR_{1138-1147}$ peptide (^{EGFR}DC), at a T-cell:DC ratio of 4:1 in the presence of BFA. The positive control was T cells stimulated with LAC and the negative control was unstimulated ^{MelanA}T cells. After 18 hours, cells were stained for CD3, CD8, MelanA-dextramer and intracellular IFNγ. Red boxes and text highlight $CD8^+$ MelanA-dextramer$^+$ and the frequencies of ^{MelanA}T cells. Lower panel shows IFNγ production by ^{MelanA}T cells.

To avoid the logistical difficulties of co-ordinating ^{MelanA}T-cell harvests with A431^{MelanA} sorting, the feasibility of using frozen batches of ^{MelanA}T cells was evaluated. Previously frozen ^{MelanA}T cells were thawed and screened for antigen recognition and cross reactivity. Results displayed in Figure 5.13 confirmed that the previously frozen ^{MelanA}T cells expressed IFNγ specifically in response to ^{MelanA}DC in a similar vain to fresh ^{MelanA}T cells, but the number of T cells recovered was very low.

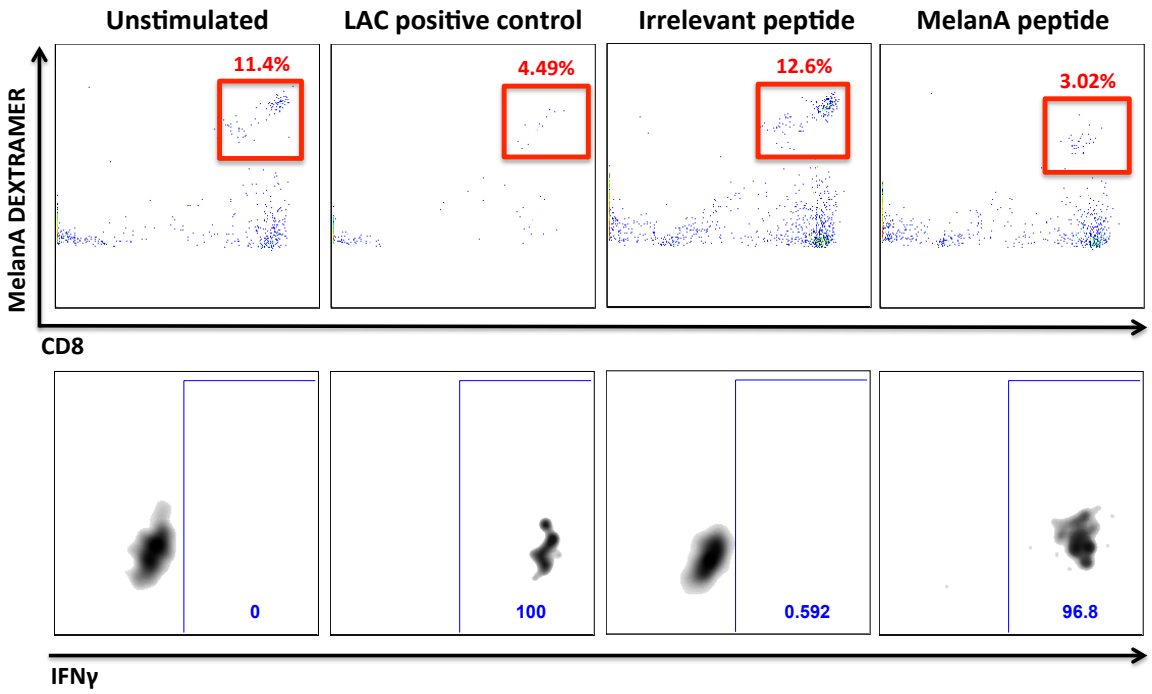

Figure 5.14. Previously frozen ^{MelanA}T cells produce IFNγ when stimulated with MelanA peptide
^{MelanA}T cells previously frozen were thawed and stimulated using mDC pulsed with either MelanA$_{26-35}$ peptide (^{MelanA}DC) or irrelevant EGFR$_{1138-1147}$ peptide (^{EGFR}DC), at a T-cell:DC ratio of 4:1 in the presence of BFA. The positive control was T cells stimulated with LAC and the negative control was unstimulated ^{MelanA}T cells. After 18 hours, cells were stained for CD3, CD8, MelanA-dextramer and intracellular IFNγ. Red boxes and text highlight CD8$^+$ MelanA-dextramer$^+$ and the frequencies of ^{MelanA}T cells. Lower panel shows IFNγ production by ^{MelanA}T cells.

To improve T-cell recovery, the response of thawed ^{MelanA}T cells was assessed based on increased expression of cell surface activation markers, thereby avoiding the fixation/permeabilization steps required for analysis of IFNγ that can cause cell loss. The results displayed in Figure 5.14 showed substantially better cell recovery and the ^{MelanA}T cells upregulated CD69, CD71 and CD137 specifically in response to MelanA antigen presented by HLA-A*02$^+$ DC exogenously loaded with peptide. T cells that did not bind the MelanA-dextramer did not upregulate expression of cell surface activation markers after stimulation.

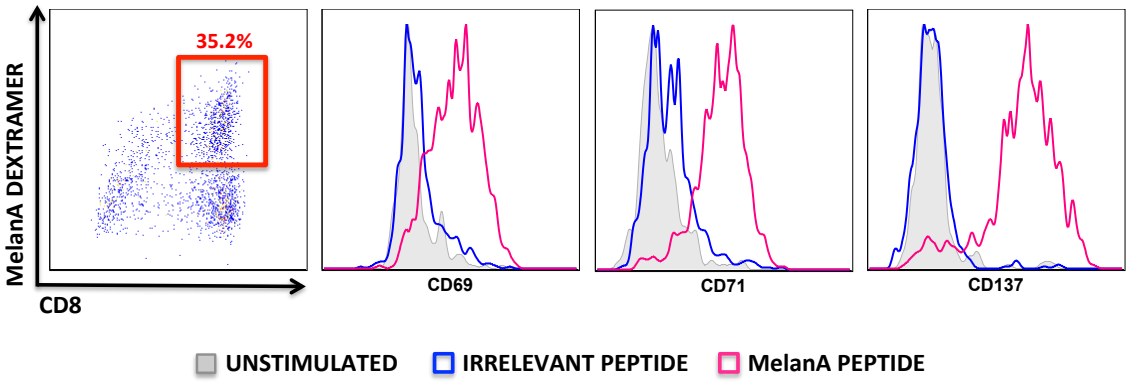

Figure 5.15. Previously frozen ^{MelanA}T cells upregulated surface activation markers when stimulated with MelanA peptide

^{MelanA}T cells previously frozen were thawed and stimulated using mDC pulsed with either MelanA$_{26-35}$ peptide (^{MelanA}DC) or irrelevant EGFR$_{1138-1147}$ peptide (^{EGFR}DC), at a T-cell:DC ratio of 4:1. The positive control was T cells stimulated with LAC and the negative control was unstimulated ^{MelanA}T cells. After 18 hours, cells were stained for CD3, CD8, MelanA-dextramer, CD69, CD71 and CD137. Red box and text highlight CD8$^+$ MelanA-dextramer$^+$ and frequency of ^{MelanA}T cells. Histograms show IFNγ production by ^{MelanA}T cells.

^{MelanA}T-cell recognition of endogenously processed MelanA presented by HLA-A*02$^+$ cells was assessed using the HLA-A*02$^+$ cell line SK-MEL-30 that naturally expresses MelanA and the HLA-A*02$^+$ H1299 cell line transfected to express MelanA (H1299^{MelanA}). A representative result from one of two donors tested is shown in Figure 5.16. Substantial increases in expression of CD69, CD71 and CD137 by ^{MelanA}T cells were observed after stimulation with MelanA$^+$ SK-MEL-30 cells and H1299^{MelanA} cells compared to unstimulated ^{MelanA}T cells or ^{MelanA}T cells stimulated with MelanA$^-$ HLA-A*02$^+$ H1299 cells. The response to SK-MEL-30 cells showed that ^{MelanA}T cells recognised natural endogenously processed MelanA antigen presented by HLA-A*02$^+$ tumour cells. The response of ^{MelanA}T cells to H1299^{MelanA} cells shows that the artificially created MelanA$^+$ EGFR$^+$ HLA-A*02$^+$ tumour cells generated by transfection with the MelanA plasmid also processed and presented MelanA antigen.

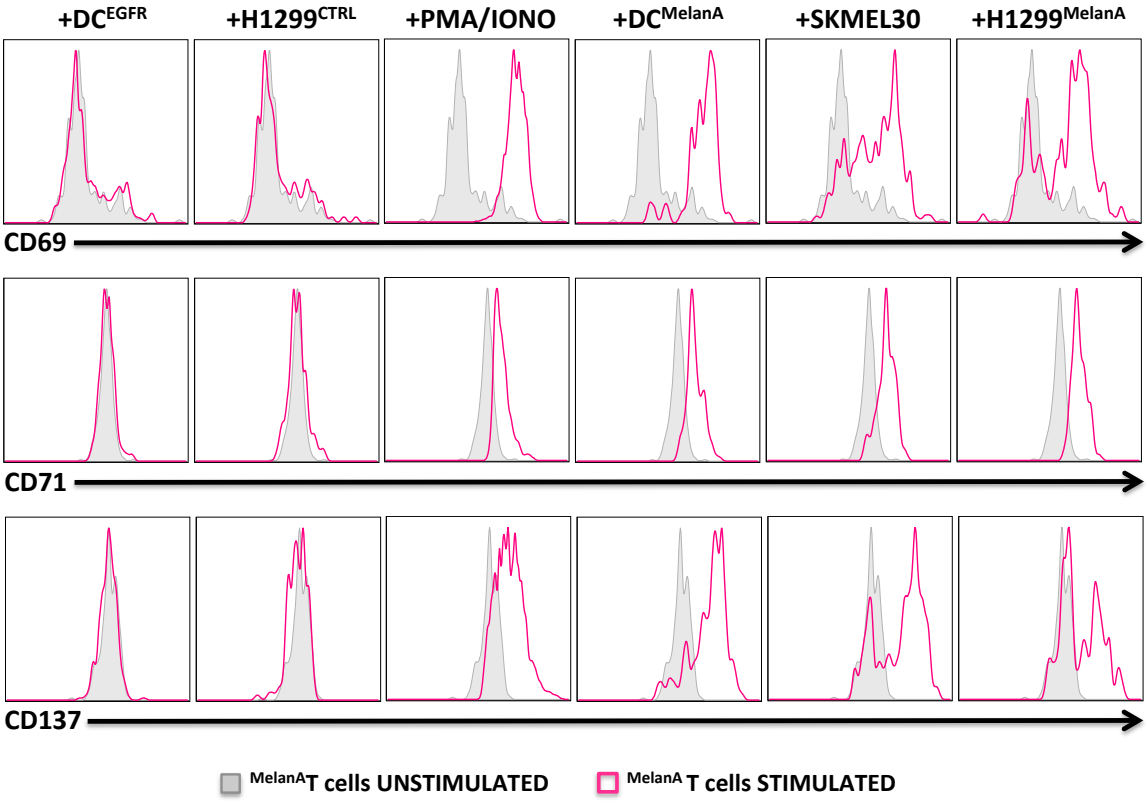

Figure 5.16. ^{MelanA}T cells recognise endogenously processed MelanA presented by HLA-A*02^{+} tumour cells
^{MelanA}T cells previously frozen were thawed and stimulated with HLA-A*02^{+} tumour cells at a 4:1 ratio. The negative controls were unstimulated ^{MelanA}T cells and culture with H1299^{CTRL} cells. After 18 hours, cells were stained for CD3, CD8, MelanA-dextramer, CD69, CD71 and CD137. Histograms show activation marker expression by ^{MelanA}T cells. Numbers in pink represent the frequency of activation marker expression by ^{MelanA}T cells and the grey shaded peak indicates marker expression on unstimulated ^{MelanA}T cells. Representative example of two independent experiments.

5.6. Assessment of MelanA cross presentation to HLA-A*02 restricted ^{MelanA}T cells

Having confirmed that ^{MelanA}T cells can recognise antigen processed and presented by HLA-A*02^{+} H1299^{MelanA} tumour cells, the modified four-cell *in vitro* co-culture model (Figure 5.7) was used with HLA-A*02^{-} A431^{MelanA} tumour cells to evaluate whether anti-EGFR mAb-activated NK cells could induce DC cross presentation of TA and stimulation of CD8^{+} T-cell responses. ^{MelanA}T cells from multiple donors detailed in Table 5.6 were batch frozen and used for the cross-presentation experiments.

Table 5.6. ^{MelanA}T-cell frequencies in frozen batches

DONOR	Total cells frozen	% ^{MelanA}T cells on Day 10
LC65	$2.1x10^6$	23.1
LC66	-	15.4
LC97	$2.6x10^6$	18.4
LC102	$1.4x10^6$	23.8
LC105	$1.5x10^6$	7.66
LC116	$1.5x10^6$	6.12
LC117	$1.6x10^6$	10.9
LC118	$1.2x10^6$	6.69
LC120	$0.8x10^6$	20.4
LC123	$5.4x10^6$	18.7

MelanA$^+$ EGFR$^+$ HLA-A*02$^-$ A431 (A431^{MelanA}) transfected tumour cells were incubated with NK cells, DC and ^{MelanA}T cells from the same HLA-A*02$^+$ donor, in the presence of cetuximab or imgatuzumab. After 18 hours, the ^{MelanA}T cells were assessed for upregulation of surface activation markers. Negative controls were co-cultures performed in the absence of mAbs and co-cultures conducted with A431^{CTRL}. The positive control was ^{MelanA}T cells stimulated with autologous MelanA peptide loaded DC. Upregulation of surface T-cell activation markers was compared to unstimulated ^{MelanA}T cells

5.6.1. MelanA can be cross presented to ^{MelanA}T cells in the absence of anti-EGFR mAb mediated tumour-cell lysis

The assessment of tumour cell death by annexin V staining described in section 3.6.4 showed that there was some spontaneous apoptotic tumour cell death in the absence of mAbs (Figure 3.21 C). Furthermore, in the analysis of phagocytosis by DC described in section 4.2.3, a low percentage of pHrodoRed$^+$ DC was observed after culture with untreated tumour cells (Figure 4.4) indicating that there was some uptake of tumour particulate in the absence of mAb-mediated lysis. Consequently, in the four-cell co-culture, there was potential for cross presentation of tumour antigen to ^{MelanA}T cells without mAbs present, and this needed to be evaluated. Results shown in Figure 5.17 depict CD69 expression on ^{MelanA}T cells after co-culture with NK cells, DC and A431^{CTRL} (5.17 A) or A431^{MelanA} (5.17 B) tumour cells, in the absence of anti-EGFR mAbs. The frequency of CD69$^+$ ^{MelanA}T cells was 3.2% without stimulation and 12.5% in the culture with

A431^{CTRL}, indicating some non-specific activation. The frequency of CD69^{+} ^{MelanA}T cells increased to 29.1% in the culture with A431^{MelanA}, with three possible explanations. Either some T-cell alloreactivity was observed upon incubation of HLA-A*02^{+} ^{MelanA}T cells and HLA-A*02^{-} A431^{MelanA}; or, some background cross presentation of MelanA antigen may have occurred without addition of anti-EGFR mAbs to promote tumour-cell lysis; or both of these scenarios occurred. The non-specific activation was however low enough to distinguish from the positive control.

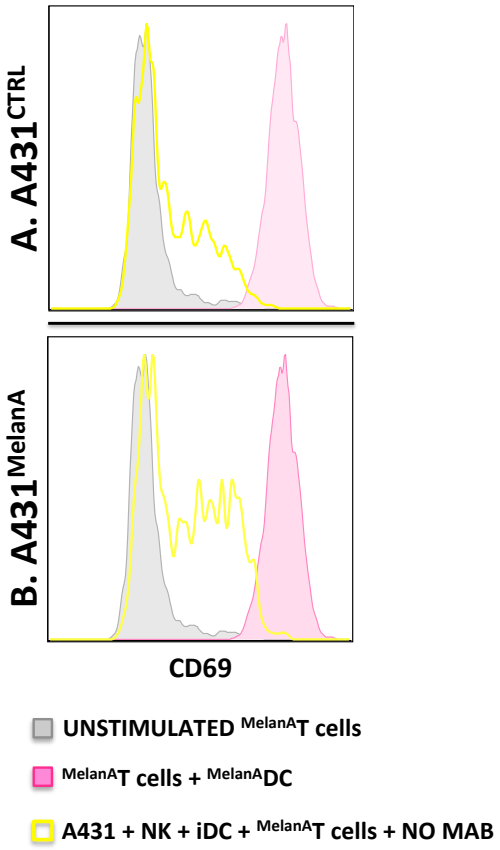

Figure 5.17. MelanA antigen can be cross presented to ^{MelanA}T cells in the absence of anti-EGFR mAb mediated tumour-cell lysis
2.5x10^{4} HLA-A*02^{-} A431^{CTRL} (A) or HLA-A*02^{-} A431^{MelanA} (B) were incubated with HLA-A*02^{+} NK cells, iDC and ^{MelanA}T cells at 1:1:1:4 ratio. After 18 hours, cells were stained for CD3, CD8, MelanA-dextramer and CD69. Histograms show CD69 expression by ^{MelanA}T cells. Representative example of two independent experiments with the same batch of ^{MelanA}T cells.

5.6.2. No detection of enhanced MelanA cross presentation to ^{MelanA}T cells in the presence of anti-EGFR mAb

The anti-EGFR mAbs imgatuzumab or cetuximab were added to the four-cell co-culture to induce mAb-mediated NK-cell lysis of tumour cells. A high concentration of 20µg/ml was used with the aim of maximising generation of tumour particulate. Results shown in Figure 5.18 depict

expression of the activation markers CD69, CD71 and CD137 on ^{MelanA}T cells after co-culture with NK cells, DC and A431^{CTRL} (5.18 A) or A431^{MelanA} (5.18 B) tumour cells in the presence of anti-EGFR mAbs. In the cultures with A431^{CTRL} that lack MelanA, CD69 was expressed by 39% of ^{MelanA}T cells in the presence of cetuximab and 40.9% in the presence of imgatuzumab, indicating very high non-specific activation. CD69 expression on ^{MelanA}T cells was only marginally higher in the cultures using A431^{MelanA}, rising to 47.3% with cetuximab and 48.8% with imgatuzumab. No upregulation was observed for the T-cell activation markers CD71 or CD137 in any of the test conditions.

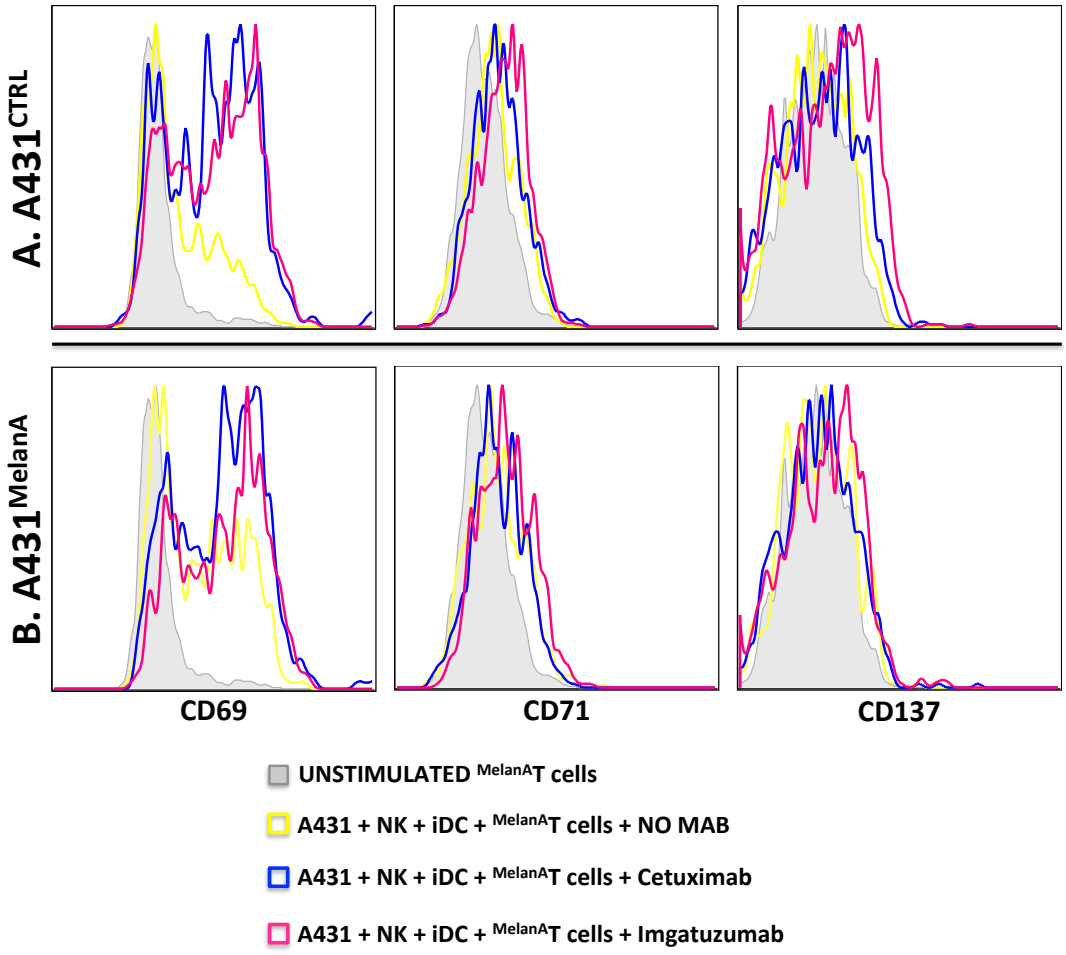

Figure 5.18. Presence of anti-EGFR mAb does not enhance MelanA cross presentation to ^{MelanA}T cells
$2.5x10^4$ HLA-A*02$^-$ A431^{CTRL} (A) or HLA-A*02$^-$A431^{MelanA} (B) were incubated with HLA-A*02$^+$ NK cells, iDC and ^{MelanA}T cells at 1:1:1:4 ratio in the presence of cetuximab or imgatuzumab (20µg/ml). After 18 hours, cells were stained for CD3, CD8, MelanA-dextramer, CD69, CD71 and CD137. Histograms show CD69, CD71 and CD137 expression by ^{MelanA}T cells. Representative example of two independent experiments with the same batch of ^{MelanA}T cells.

Similar results were obtained with ^{MelanA}T-cell batches from a further two donors, using only the A431^{MelanA} model (Figure 5.19).

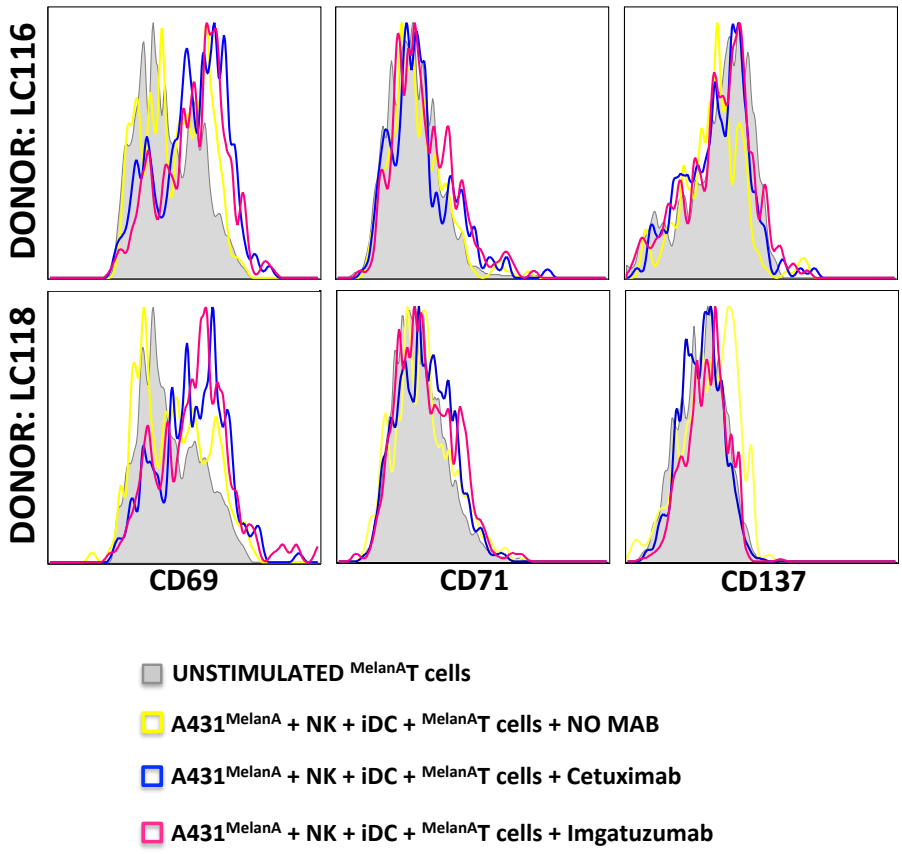

Figure 5.19. Anti-EGFR mAbs do not enhance MelanA cross presentation to ^{MelanA}T cells (donor replicates)
$2.5x10^4$ HLA-A*02$^-$A431^{MelanA} were incubated with HLA-A*02$^+$ NK cells, iDC and ^{MelanA}T cells at 1:1:1:4 ratio in the presence of cetuximab or imgatuzumab (20μg/ml). After 18 hours, cells were stained for CD3, CD8, MelanA-dextramer, CD69, CD71 and CD137. Histograms show CD69, CD71 and CD137 expression by ^{MelanA}T cells. Two independent experiments (n=2).

The following modifications to the four-cell co-culture model were investigated:

1. Reduction of co-culture duration from 18 hours to 6 hours
2. Titration of mAb concentrations from 20μg/ml to 1ng/ml
3. Alteration of T-cell:DC ratios (2:1, 4:1, 10:1)

Unfortunately, enhanced MelanA cross presentation to ^{MelanA}T cells in the presence of anti-EGFR mAbs was never detected.

5.7. Discussion

The role that anti-tumour mAb-therapy plays in initiating T-cell mediated cancer immune responses is still to be elucidated. The aim of the work presented in this chapter was to determine whether GE mAbs could induce cross presentation of TA to TA-specific T cells and the results and their limitations are discussed herein:

5.7.1. EGFR-specific T cells were not detected in patients

Attempts were made to generate EGFR-specific $CD8^+$ T cells (^{EGFR}T cells) for use in these studies. ^{EGFR}T cells were not detected in PBMC from any of the cancer patients after *in vitro* stimulation with peptides for 10 days. The T-cell expansion protocol and MHC-I multimer assay were successfully used to detect ^{CMV}T cells in healthy donor PBMC and also one of six patient samples. These results do not necessarily indicate that ^{EGFR}T cells were absent in these patients because the study had several limitations that may have prevented detection.

Foremost was the low number of viable PBMC available in the clinical trial samples. This necessitated a single *in vitro* stimulation without T-cell selection. After 10 days, the majority of cultures had fewer than 100,000 viable cells. Furthermore the low proportion of $CD8^+$ T cells meant the population screened for pentamer positivity was typically less than 25,000 cells. The only previous study describing detection of $CD8^+$ T cells specific for the $EGFR._{479}$ peptide KLFGTSGQKT and the $EGFR._{1138}$ peptide YLNTVQPTCV was conducted by Schuler *et al* (2011) and involved undertaking four rounds of *in vitro* stimulation over 28 days. Even then, low mean frequencies of 0.28% and 0.56% respectively were observed and only in patients with tumours expressing high levels of EGFR [240]. It seems likely that insufficient rounds of *in vitro* stimulation were performed in this study to increase the proportion of ^{EGFR}T cells to the range for detection using pentamers. It is also worth noting that samples in the Schuler *et al* study came from patients presenting with locoregionally advanced disease that was previously untreated. The samples available for this study came from patients who had failed 2nd line chemotherapy, the majority of whom presented with metastatic disease or disease progression. When compared, it was speculated that the cells of patients with more severe disease could be less viable, less amenable to long-term culture and less responsive.

This study was also hampered by the inability to obtain the $EGFR._{853}$ ITDFGLAKL pentamer used by Andrade Filho *et al* (2010) who reported detection of these EGFR-specific $CD8^+$ T cells after a

single 10-day *in vitro* stimulation [282]. The evaluation of enhancement of TA-specific $CD8^+$ T-cell responses in patients after GE-mAb therapy warrants further investigation, however larger numbers of PBMC ($\geq 5x10^7$) stored in multiple aliquots would be requisite to permit $CD8^+$ T-cell isolation and repeated rounds of *in vitro* stimulation where necessary.

5.7.2. EGFR-specific T cells were not detected in healthy donors

Attempts to generate ^{EGFR}T-cell lines by stimulation of naïve T cells from healthy individuals were not successful. The TA EGFR is a ubiquitous self-antigen for which the majority of potentially reactive T cells will have been deleted during development or maturation in the periphery. The frequency of circulating self-antigen-specific naïve T cells in healthy individuals is therefore expected to be extremely low, and the ability of these cells to bind MHC-I multimers to be weak [264]. As a notable exception to this observation, efforts were made to exploit the self-antigen MelanA, because HLA-A*02$^+$ healthy individuals possess unusually high precursor frequencies of ^{MelanA}T cells [358]. The success of ^{MelanA}T-cell expansion *in vitro* was in part due to use of the heteroclytic peptide [281]. If a heteroclytic peptide was available for EGFR or CD20 that showed similar success to MelanA, screening of patients for TA-specific T cells pre and post mAb-treatment could be viable.

5.7.3. MelanA-specific T cells recognise endogenous MelanA, but not processed MelanA

When expanded in this study, ^{MelanA}T cells recognised endogenously processed MelanA, but not MelanA cross-presented within the four-cell co-culture model. The cross presentation assessment was an ambitious undertaking and this part of the study also had several limitations, particularly with regards to incorporating MelanA into the experimental model. Stable transfection requires that the introduced DNA enters the nucleus and is integrated into the host genome, thereby sustaining transgene expression even after replication. With an efficient transfection it is expected that roughly 10% of events will be stably integrated and can then be selected in long-term culture [372]. The problems with puromycin selection and loss of GFP signal indicate that the MelanA expression in A431 was not stable. A stable transfection could have potentially allowed long-term culture of A431^{CTRL} and A431^{MelanA} tumour cells, rather than having to transfect and sort the tumour cells each time they were required for co-culture, eliminating a source of experimental variation. It is possible that the transiently transfected cell line exhibited potent DAMPs causing DC maturation. Linearizing the plasmid DNA prior to transfection and including nuclear

localisation sequences within the DNA are methods of enhancing insertion events [372] and could be incorporated into future experiments although it is not clear if this would be effective in suspension cells which are typically less permissive to transfection (personal communication Richard Beswick, KCL).

Another strategy to permanently modify a cell line is to use transduction. Transduction would have been applicable to both adherent and suspension cell types; allowing optimisation of this study in both EGFR and CD20 disease contexts. Ruben *et al* describe the use of MelanA transduced HL60 suspension cells in the study of induced T-cell immunity [106], monitoring IFNγ secretion by ^{MelanA}T cells after exposure to DC primed with MelanA^{+}HL60 cell lysates. However, even if stable MelanA^{+}A431 cells were achieved, detecting differences in the extent of cross presentation could still prove difficult because the ^{MelanA}T cells may have differentiated into an effector memory phenotype during expansion. Memory T cells have a lower threshold of activation and may have been triggered solely by the cytokines produced in the co-culture, an observation described by Geginat *et al* [373].

If all of these issues are addressed and spontaneous activation reduced to a minimum, in addition to upregulation of T-cell activation markers, T-cell proliferation measured by CFSE dilution could be an appropriate *in vitro* readout for cross presentation before proceeding to *in vivo* assessment.

5.7.4. Potential *in vivo* experiments to assess anti-tumour immunity

Gerdes *et al* demonstrated superior *in vivo* ADCC activity compared to cetuximab using a human tumour xeongraft model. Briefly, human FcγRIIIA transgenic SCID mice (which express human FcγRIIIA-positive transgenic murine NK cells as effectors) were injected with tumour cells exhibiting various levels of EGFR expression. Once tumours were established, animals received weekly doses of either cetuximab or imgatuzumab and OS was monitored. Median OS was significantly increased in animals receiving imgatuzumab compared with cetuximab, panitumumab or vehicle control for models of lung-, colorectal-, pancreatic- and breast-cancer [205].
At the time of writing, it was not possible to find a tumour xenograft mouse model assessing ADCC-induced anti-tumour immunity. It is instead proposed to adapt an established mouse model of ADCC in which both tumour cells and effector cells are adoptively transferred.

Chen *et al* (2016) observed tumourigenicity using LOVO CRC cells subcutaneously injected into BALB/c nude mice [374]. Mice receiving cetuximab plus NK cells showed the greatest tumour inhibition effect compared with NK cells or cetuximab alone. Although they did not see complete tumour clearance in any of their test conditions, this could possibly be achieved via careful optimisation of effector/target cell numbers and mAb concentration. Adapting this model for measurement of tumour immunity would involve infusing HLA-A*02^{-} tumour cells, followed by infusion of TA-specific mAb and adoptive transfer of NK cells, DC and a small percentage of TA-specific T cells from the same HLA-A*02^{+} donor. Like the *in vitro* model depicted in Figure 5.1, *in vivo* T-cells are unable to recognise tumour cells directly and T-cell stimulation is dependent upon ADCC-mediated lysis of HLA-A*02^{-} tumour cells, uptake of exogenous tumour particulate by DC and cross presentation by DC to HLA-A*02 restricted CD8^{+} T cells. Once the tumour is abolished, re-infusion of the same tumour could be a means of testing whether TA-specific T cells have expanded to a protective level, sufficient to prevent tumour recapitulation.

Chapter 6. Concluding remarks

6.1. Summary

The genetic alterations that accumulate in tumour cells endow them with the ability to resist cell death and evade growth suppression and destruction by immune cells [2]. An increased understanding of the tumour microenvironment and anti-tumour immunity has led to intense interest in manipulating the balance between the positive immune-stimulatory signals and negative regulatory signals involved in tumourigenesis [375]. Several immunotherapeutic strategies have been developed that aim to harness the power of the immune system to overcome immune tolerance to tumour cells. Therapeutic anti-TA mAbs such as cetuximab and rituximab are at the forefront of these strategies, with substantial pharmaceutical investment driven by relative ease of production and administration [142].

A major component of the therapeutic efficacy of these IgG_1 mAbs is their ability to recruit CD16-bearing NK cells to elicit ADCC. However, a common CD16 SNP (V158F) has been correlated with efficacy of clinical responses to these mAbs [210, 255]. Mechanistically, this polymorphism was found to modulate the affinity of CD16 for antibodies, in turn affecting the potency of ADCC [205, 209]. The observations connecting antibody/receptor affinity, ADCC efficiency and clinical outcomes were crucial, as they led to the prediction that enhancements of mAb affinity for CD16 would result in significant clinical benefits. GE mAbs show improved therapeutic potential because the glycosylation modification increases affinity for CD16 and leads to enhanced ADCC, irrespective of CD16 genotype [205, 232]. Therefore, GE-mAb mediated ADCC enhancement has the potential to benefit those patients in whom unmodified mAbs are either partially or totally ineffective, such as individuals with the low-affinity CD16 polymorphism [205, 232, 376] or KRAS gain-of-function mutations [377].

Studies have shown that the immune-cell interactions that follow ADCC of tumour cells can lead to the generation of T-cell mediated cancer immunity, via DC cross presentation of TA to $CD8^+$ T cells [97, 378]. The aim and novelty of the work described in this thesis was to build on and extend the evidence described for conventional therapeutic mAbs by investigating whether ADCC mediated by GE-mAbs could also lead to cross presentation of TA. This was examined by

assessing tumour cell apoptosis and NK-cell activation in the presence of GE-mAbs and the subsequent impact of ADCC-activated NK cells on DC maturation, because DC maturation is a prerequisite for efficient T-cell stimulation [87, 90]. The priming and establishment of TA-specific memory T cells is essential for long-term cancer immunosurveillance to prevent disease relapse [164].

The results detailed within this thesis have demonstrated that GE mAbs can induce the NK-cell activation, NK-cell function and DC maturation associated with adaptive cellular immune responses. Previous studies of GE-mAbs have been tumour-orientated and focused primarily on tumour:mAb interactions rather than the NK-cell activation and function associated with promoting adaptive cellular immunity. The work presented in this thesis has begun to elucidate the phenotype of primary NK cells activated by GE-mAb-mediated ADCC and their impact on DC maturation *in vitro*. Furthermore, the results presented have implied that, when compared at equivalent concentration, GE-mAbs promote NK-cell activity to a greater extent than unmodified mAbs. First, via enhanced NK-cell activation: the GE mAbs promoted expression of markers of NK-cell function and activation compared to unmodified mAbs, including significantly increased expression of CD107a, IFNγ, TNFα and CD69 and significant downregulation of CD16. Second, via enhanced provision of tumour particulate for DC: ADCC in the presence of GA101GE induced a significantly higher frequency of tumour-cell apoptosis compared to GA101WT. Importantly, it was also shown that GA101GE-treated tumour particulate was ingested by DC. Third, via enhanced DC maturation: GE-mAb activated NK cells induced DC maturation to a significantly greater extent than unmodified mAbs. These findings indicate that some of the essential pre-requisite criteria for DC cross presentation of TA, namely provision of tumour particulate, NK-cell activation and maturation of DC were induced by GE-mAbs and to a significantly greater extent at low concentrations compared with conventional therapeutic mAbs.

6.2. Limitations of the multi-cell *in vitro* co-culture model

The conclusions that can be drawn from the reported findings are limited by several caveats that have been acknowledged previously, including: lack of mAb normalisation, use of only a limited number of cell lines and relatively low sample numbers in experiments.

6.2.1. Limitations of established cell lines

Results chapters detailed some limitations of the effector cells used in this study however, it is also necessary to comment on the general use of established cancer cell lines as opposed to patient primary cancer cells as target populations. Although convenient, easy to handle and widely published, cell lines typically represent a single donor and are sometimes established from metastases raising debate about whether metastases will respond like their primary tumours. Serial passaging of cell lines over time can cause phenotypic and genotypic variation. Cells grown *in vitro* are subject to "selection pressure" where, for example, cells that gain mutations enabling faster growth will come to dominate a culture in time; or cultures grown at low density may select for cells capable of density independent growth. A widely cited bioinformatic analysis of proteomic phenotypes conducted by Pan *et al* revealed that the Hepa1–6 cell lines were deficient in mitochondria, reflecting rearrangement of metabolic pathways when compared to primary hepatocytes [379]. Researchers should therefore be careful about relying solely on data generated with cell lines. Primary cells are believed to be more biologically relevant and the current recommendation from the scientific community is to conduct key control experiments with primary cells of low passage to qualify and/or verify the findings seen in cell lines. With the emergence of newer technologies such as 3D culture, the use of primary cells is becoming increasingly prevalent and has further improved disease modelling and high-throughput therapeutic screening [380]. In future, using a variety of low passage patient primary cells from many different donors and cancer subtypes should be considered, to assess wider applicability of results and clinical relevance.

6.2.2. Limitations of the readout assay

The use of flow cytometry enabled multiparametric assessment of each individual cell type in the co-culture, but the technique has relatively low sensitivity. For example, a frequency of approximately 100 per 10^6 cells (0.01%) is necessary to obtain a positive measurement of IFNγ by ICS [381], however as low as 5 spot forming units/10^6 PBMC can be reliably detected in IFNγ enzyme-linked immune absorbent spot assays [382]. This increased sensitivity could be crucial in a setting where the population of interest is rare; such as the self-antigen specific T cells that proved difficult to obtain in this study. Another important consideration is that ICS measures the production and accumulation of a cytokine but not the release of it. Inhibition of protein transport is required for ICS analysis, but is non-physiological and can affect all cells. Notably, the protein

transport inhibitor BSA has been shown to prevent CD69 surface expression [288]; highlighting that study design and the choice of reagents plays an important role in study outcome.

An interesting advance in flow cytometric analysis is the development of Amnis® imaging flow cytometers (marketed by Merck Millipore). This technology combines surface and intracellular staining with the imaging of individual cells to enable assessment of internalisation, localisation and cell-to-cell interactions. Amnis® offers more economical use of study material as it removes the need for separate flow and microscopy staining; which could help to extend the results described herein as cell availability was a limitation. Future investigations should ideally include results reproduced using a variety of techniques that complement one-another.

6.3. Future directions

Although this study focused on mAbs used for malignancies expressing EGFR and CD20, in principle this glyco-engineering approach has wider applicability. Indeed, several other receptors are being targeted by anti-TA mAbs [141], notable examples of which include trastuzumab and daratumumab. Trastuzumab is currently approved for use in early stage and metastatic human epidermal growth factor receptor 2 positive ($HER2^{+}$) breast cancer, either alone or in combination with chemotherapy [383]. Trastuzumab is on the WHO list of essential medicines [384]. Daratumumab targets CD38 and is indicated for use in multiple myeloma and potential use in diffuse large B-cell lymphoma, follicular lymphoma, and mantle-cell lymphoma, all considered rare conditions. Daratumumab was given breakthrough therapy status in 2013 [385]. Endowing ligand-blocking mAbs with enhanced ADCC-triggering capabilities in such diseases may prove beneficial. However, as mAb manipulation becomes increasingly common, the work described in this thesis provides a cautionary note on the importance of selecting suitable target antigens. Results demonstrated that the enhanced efficacy seen with imgatuzumab over cetuximab was also observed when EGFR was expressed at lower levels. This has implications for normal cells that may express TA at low levels and suggests that GE-mAb effects may not spare healthy tissues.

Careful consideration must therefore be taken with antigen selection when using GE-mAbs. On this note, CD20 has proven to be an exemplary target because the expression of this glycoprotein is tightly restricted to B cells. In targeting CD20, GA101GE offers numerous advantages over rituximab. Cheadle and colleagues demonstrated that the induction of immunogenic cell death by

GA101GE had mechanistic differences compared with rituximab. After incubating $CD20^+$ Daudi cells with mAbs at 10µg/ml, they measured the release of DAMP molecules in the supernatant via western blot. DAMP molecules such as heat shock protein 90 (HSP90) and high mobility group box 1 protein (HMGB1) can prime DC maturation and subsequent T-cell activation. GA101GE induced significant release of HSP90 and HMGB1 compared to rituximab, and significantly enhanced DC maturation when these supernatants were incubated with iDC [332]. The comparison of GA101WT and GA101GE in this study has indicated that enhanced DC maturation is quite likely the result of glyco-engineering. When NK cells are present, these effects can be seen at lower mAb-concentrations than those used in the Cheadle study; concentrations that may more accurately represent the bioavailability of mAbs in tumour lesions [318, 319, 320].

Recent reviews on the use of mAbs for the treatment of B-cell malignancies predict that GA101GE will replace rituximab in most of the combined immunotherapy/chemotherapy regimens [297, 386]. Importantly, GA101GE may be combined with other immunotherapies to further enhance its therapeutic effect. Engagement of TLR expressed on DC can trigger a cascade of signalling pathways that lead to production of proinflammatory cytokines and polarization of T-cell responses. Synthetic agonists of TLR7/8 have been shown to activate pDC and myeloid DC, stimulating the production of type I interferons, strong T_H1 immunity and $CD8^+$ T-cell responses [387]. In early 2017, Cheadle and colleagues used a murine lymphoma model to demonstrate that the addition of the TLR agonist R848 (Resiquimod) enhanced the therapeutic efficacy of GA101GE in an NK-cell-dependent manner. This lead to long-term survival and anti-tumour immunity, providing proof of principle and rationale for translation to the clinic [388].

Other studies have shown promising results when combining rituximab with tyrosine kinase inhibitors (TKI). The Bruton TKI ibrutinib inhibits the migration and adhesion of CLL cells into the protective microenvironment, thereby leading to a redistribution and mobilization of these cells from the lymphoid tissue to the peripheral blood, which can be seen in the peripheral blood as transient lymphocytosis. Because lymphocytosis remains largely asymptomatic and can persist for long periods (up to 124 weeks), the combination of ibrutinib with other agents that clear the peripheral blood of CLL cells is a reasonable therapeutic approach [389]. A recent phase II trial evaluated rituximab plus ibrutinib in 40 patients with high-risk CLL/small lymphocytic lymphoma. An ORR of 95% was achieved, with 3 complete remissions and 1 minimal residual disease

(MRD)–negative case [390]. However, Cramer *et al* considered the combination of ibrutinib and GA101GE a more attractive option. They speculated that as ibrutinib redistributes the CLL cells from their homing organs to the peripheral blood, GA101GE would eliminate the leukaemic cells with greater efficiency than rituximab. Furthermore, they suggested that adding the Bcl-2 antagonist venetoclax could further intensify this treatment in CLL patients with a specific chromosomal abnormality known as 17p deletion (del(17p)/TP53) and that this combination, in the absence of chemotherapy, may hold the potential to achieve a deep remission with an eradication of residual CLL cells, thus leading to long-term remissions of CLL [391].

Cramer and colleagues recently reported the results of a sequential combination therapy comprising bendamustine debulking followed by ibrutinib and GA101GE (BIG regimen) in a heterogeneous group of 61 CLL patients [392]. The BIG regimen appeared to improve the efficacy of CLL therapy in both a frontline and relapsed/refractory setting. An ORR of 100% and a MRD negativity rate of 47.5% compared favourably with ibrutinib monotherapy response rates of 86% in CLL: first-line treatment [393], and 71% in CLL: relapsed/refractory [394]. A similar ORR of 95% was reached in a combination study using rituximab and ibrutinib in a high-risk CLL population, but only 1 out of 40 patients was MRD negative [395].

Another promising direction in cancer therapeutics is the advent of 'universal' antibody-mediated cell therapy (uACT). The uACT comprises T cells engineered for use irrespective of HLA barriers and incorporating a signalling chimeric FcγRIIIa receptor (cFcR) for use in combination with existing therapeutic mAbs [396]. Etuk *et al* recently generated a uACT by transduction of healthy donor cells with a self-inactivating lentiviral 'terminal' vector. This platform coupled cFcR expression with CRISPR/Cas9-mediated scission via precise incorporation of a single guide RNA element into the ΔU3 3' lentiviral long terminal repeat. Delivery of Cas9 mRNA by electroporation resulted in highly efficient modification of the T-cell receptor (TCR) α-chain locus and automated magnetic bead-mediated depletion enabled enrichment of highly homogenous (>90%) $FcγRIIIa^{+}$ (>99%) TCR^{-} populations. *In vitro* cytotoxicity studies confirmed that uACTs specifically killed Daudi lymphoma cells in combination with rituximab or SKBR3 breast cancer cells in combination with trastuzumab. In contrast, uACTs alone or antibody alone produced no effect [396]. Preliminary *in vivo* experiments investigated anti-leukaemic efficacy using serial bioluminescence in a humanised immunodeficient murine tumour model. Complete tumour clearance was observed in 100% of mice (n=5) infused with uACT effectors in combination with rituximab when compared to

uACT alone, untransduced or vehicle control groups and sustained for 25 days post tumour challenge. Bone marrow harvests further corroborated these findings with an indication to extend experimental duration to assess whether rituximab per se can also sustain tumour clearance. The uACT production processes were scalable and adaptable to GMP compliant manufacturing [396], providing a route to clinical phase evaluation in an allogeneic setting, potentially in combination with GE-mAbs.

A major challenge in cancer therapy is tumour escape, often characterised by treatment related loss or downregulation of TA [317]. This may be overcome by simultaneously targeting receptors that are co-expressed on tumour cells. Antibodies harbouring dual specificities were briefly discussed in section 1.10.1.3, however these were standard, unmodified antibodies, which recruited T cells for ADCC via CD3 ligation [152, 153]. Recently, Schanzer and colleagues from Roche-Glycart described the design and *in vitro*/*in vivo* characterisation of XGFR*, a novel GE-bispecific antibody targeting both EGFR and the insulin-like growth factor-1 receptor (IGF-1R) [397]. Mechanistically this antibody combines potent signalling and tumour growth inhibition with enhanced ADCC induction, mediated by an afucosylated Fc portion. XGFR* potently inhibited EGFR- and IGF-1R-dependent receptor phosphorylation, reduced tumour cell proliferation in cells with heterogeneous levels of EGFR and IGF-1R expression and induced strong ADCC *in vitro*. Pancreatic cancers frequently show a high degree of EGFR/IGF-1R co-expression, thus the authors employed the murine orthotopic MiaPaCa-2 pancreatic xenograft model to explore XGFR* *in vivo* efficacy. Administration of XGFR* resulted in nearly complete tumour growth inhibition, with a significant number of tumour remissions compared to control. Interestingly, several human colorectal carcinoma models showed minimal or no sensitivity to XGFR*, highlighting the importance of appropriate disease indications in addition to appropriate antigen selection [397].

While *in vitro* and pre-clinical *in vivo* mouse studies are the first test of feasibility and a foundation from which to build upon, the ultimate test of any new agent is its clinical performance. Although novel anti-CD20 agents such as GA101GE are claimed to have high potency, it is a concern that much higher doses than those used in a standard rituximab regimen were chosen to show superior efficacy [398]. Indeed a more recent clinical study comparing imgatuzumab and cetuximab has also perpetuated this dosing inequality [399]. Chang *et al* highlight these points and emphasise

that clinical comparisons require parallel cohorts in which novel candidate mAbs are administered in similar or even lower doses and schedules to prove superiority [400].

Studies of clinical effectiveness of novel immunotherapeutic strategies require accompanying research to obtain knowledge of the underlying immune-cell crosstalk mechanisms. The work presented in this thesis indicates that GE-mAbs may be able to promote $CD8^+$ T-cell mediated immunity and supports their use and further development as immunotherapeutic agents.

Chapter 7. Appendix

Details of the DNA sequences of the plasmid expression vectors, custom made by Oxford Genetics, are provided. The data were arranged using SnapGeneViewer Software, version 2.82 (GSL Biotech LLC | Chicago, USA - 2016) and are displayed in the GenBank flat file format described by the National Center for Biotechnology Information (NCBI) [401].

7.1. Control Plasmid “CMV-P2A.eGFP-IRES-Puro”

```
LOCUS       pSF_CMV_P2A_eGFP_IRES_Puro   6164bp   DNA circular   16-MAR-2015
DEFINITION
ACCESSION
VERSION
SOURCE
ORGANISM
COMMENT     Oxford Genetics GenBank Format File

FEATURES             Location/Qualifiers
     source          1..6164
                     /organism="E.coli"
                     /strain="XL1 Blue"
                     /mol_type="plasmid DNA"

     misc_feature    18..89
                     /note="BetaGlobin Insulator"

     promoter        238..810
                     /note="CMV"

     RBS             893..906
                     /note="KOZAK_ShineDalgarno"

     CDS             907..1692
                     /note="P2A_eGFP"

     misc_feature    910..972
                     /note="P2A Tag"

     misc_feature    1717..1727
                     /note="Stop codons x 3"

     misc_feature    1768..2318
                     /note="EMCV IRES"

     CDS             2321..2920
                     /note="Puromycin Resistance"

     misc_feature    2928..2938
                     /note="Stop codons x 3"

     polyA_site      2961..3152
                     /note="SV40 PolyA"

     terminator      3206..3253
                     /note="T7"

     terminator      3283..3419
                     /note="RrnG"

     misc_feature    3463..3534
```

```
                     /note="BetaGlobin Insulator"

     rep_origin      3700..4584
                     /note="pUC Origin"

     promoter        5009..5037
                     /note="Selection Gene"

     CDS             5094..5888
                     /note="Kanamycin Resistance"

     terminator      5902..6038
                     /note="RrnG"

ORIGIN
        1 GCGATCGCGG CTCCCGACAT CTTGGACCAT TAGCTCCACA GGTATCTTCT TCCCTCTAGT
       61 GGTCATAACA GCAGCTTCAG CTACCTCTCA ATTCAAAAAA CCCCTCAAGA CCCGTTTAGA
      121 GGCCCCAAGG GGTTATGCTA TCAATCGTTG CGTTACACAC ACAAAAAACC AACACACATC
      181 CATCTTCGAT GGATAGCGAT TTTATTATCT AACTGCTGAT CGAGTGTAGC CAGATCTAGT
      241 AATCAATTAC GGGGTCATTA GTTCATAGCC CATATATGGA GTTCCGCGTT ACATAACTTA
      301 CGGTAAATGG CCCGCCTGGC TGACCGCCCA ACGACCCCCG CCCATTGACG TCAATAATGA
      361 CGTATGTTCC CATAGTAACG CCAATAGGGA CTTTCCATTG ACGTCAATGG GTGGAGTATT
      421 TACGGTAAAC TGCCCACTTG GCAGTACATC AAGTGTATCA TATGCCAAGT ACGCCCCCTA
      481 TTGACGTCAA TGACGGTAAA TGGCCCGCCT GGCATTATGC CCAGTACATG ACCTTATGGG
      541 ACTTTCCTAC TTGGCAGTAC ATCTACGTAT TAGTCATCGC TATTACCATG CTGATGCGGT
      601 TTTGGCAGTA CATCAATGGG CGTGGATAGC GGTTTGACTC ACGGGGATTT CCAAGTCTCC
      661 ACCCCATTGA CGTCAATGGG AGTTTGTTTT GGCACCAAAA TCAACGGGAC TTTCCAAAAT
      721 GTCGTAACAA CTCCGCCCCA TTGACGCAAA TGGGCGGTAG GCGTGTACGG TGGGAGGTCT
      781 ATATAAGCAG AGCTGGTTTA GTGAACCGTC AGATCAGATC TTTGTCGATC CTACCATCCA
      841 CTCGACACAC CCGCCAGCGG CCGCTGCCAA GCTTCCGAGC TCTCGAATTC AAAGGAGGTA
      901 CCCACCATGG GAAGCGGAGA GGGCAGAGGA AGTCTGCTAA CATGCGGTGA CGTCGAGGAG
      961 AATCCTGGAC CTATGGTGTC CAAGGGAGAA GAGCTGTTCA CGGGAGTTGT TCCAATTCTT
     1021 GTTGAGCTGG ATGGGGATGT TAACGGCCAT AAATTCTCCG TAAGCGGGGA GGGCGAGGGA
     1081 GACGCCACTT ACGGGAAGCT TACCTTGAAA TTTATTTGCA CTACAGGAAA GCTGCCAGTG
     1141 CCCTGGCCTA CGCTGGTCAC TACCTTGACC TACGGGGTTC AGTGCTTCTC CAGGTATCCG
     1201 GATCATATGA AACAGCATGA TTTCTTTAAA AGCGCCATGC CAGAGGGTTA TGTACAGGAA
     1261 CGAACGATCT TCTTTAAGGA TGACGGGAAC TACAAGACCC GCGCAGAGGT GAAATTTGAA
     1321 GGAGATACGC TGGTGAACAG AATAGAGCTG AAGGGGATCG ACTTCAAAGA AGATGGCAAC
     1381 ATCCTGGGCC ACAAGCTTGA ATATAACTAC AACAGCCATA ACGTATATAT CATGGCTGAC
     1441 AAGCAGCGAA ATGGAATTAA GGCCAACTTC AAGATTCGGC ACAACATCGA AGACGGGAGC
     1501 GTGCAGCTGG CCGACCATTA CCAGCAGAAC ACCCCTATCG GGGATGGCCC AGTGCTGCTG
     1561 CCTGATAATC ATTATCTCAG CACGCAGTCT GCCCTGTCTA AAGACCCCAA CGAGAAAAGG
     1621 GACCATATGG TCCTGCTGGA ATTTGTGACA GCAGCTGGCA TCACCCTGGG AATGGATGAA
     1681 CTCTACAAGT AGTCTAGAAG TTGTCTCCTC CTGCACTGAC TGACTGATAC AATCGATATG
     1741 CCAAAAGCAA AGCGCTATCG CGCCTTACGT TACTGGCCGA AGCCGCTTGG AATAAGGCCG
     1801 GTGTGCGTTT GTCTATATGT TATTTTCCAC CATATTGCCG TCTTTTGGCA ATGTGAGGGC
     1861 CCGGAAACCT GGCCCTGTCT TCTTGACGAG CATTCCTAGG GGTCTTTCCC CTCTCGCCAA
     1921 AGGAATGCAA GGTCTGTTGA ATGTCGTGAA GGAAGCAGTT CCTCTGGAAG CTTCTTGAAG
     1981 ACAAACAACG TCTGTAGCGA CCCTTTGCAG GCAGCGGAAC CCCCCACCTG GCGACAGGTG
     2041 CCTCTGCGGC CAAAAGCCAC GTGTATAAGA TACACCTGCA AAGGCGGCAC AACCCCAGTG
     2101 CCACGTTGTG AGTTGGATAG TTGTGGAAAG AGTCAAATGG CTCCCCTCAA GCGTATTCAA
     2161 CAAGGGGCTG AAGGATGCCC AGAAGGTACC CCATTGTATG GGATCTGATC TGGGGCCTCG
     2221 GTGCACATGC TTTTCATGTG TTTAGTCGAG GTTAAAAAAC GTCTAGGCCC CCCGAACCAC
     2281 GGGGACGTGG TTTTCCTTTG AAAAACACGA TGATAATAAC ATGACCGAGT ACAAGCCCAC
     2341 GGTGCGCCTC GCCACCCGCG ACGACGTCCC CAGGGCCGTA CGCACCCTCG CCGCCGCGTT
     2401 CGCCGACTAC CCCGCCACGC GCCACACCGT CGATCCGGAC CGCCACATCG AGCGGGTCAC
     2461 CGAGCTGCAA GAACTCTTCC TCACGCGCGT CGGGCTCGAC ATCGGCAAGG TGTGGGTCGC
     2521 GGACGACGGC GCCGCGGTGG CGGTCTGGAC CACGCCGGAG AGCGTCGAAG CGGGGGCGGT
     2581 GTTCGCCGAG ATCGGCCCGC GCATGGCCGA GTTGAGCGGT TCCCGGCTGG CCGCGCAGCA
     2641 ACAGATGGAG GGCCTCCTGG CGCCGCACCG GCCCAAGGAG CCCGCGTGGT TCCTGGCCAC
     2701 CGTCGGCGTC TCGCCCGACC ACCAGGGCAA GGGTCTGGGC AGCGCCGTCG TGCTCCCCGG
     2761 AGTGGAGGCC GCCGAGCGCG CCGGGGTGCC CGCCTTCCTG GAGACCTCCG CGCCCCGCAA
     2821 CCTCCCCTTC TACGAGCGGC TCGGCTTCAC CGTCACCGCC GACGTCGAGG TGCCCGAAGG
     2881 ACCGCGCACC TGGTGCATGA CCCGCAAGCC CGGTGCCTAG GCTAGCTTGA CTGACTGAGA
     2941 TACAGCGTAC CTTCAGCTCA CAGACATGAT AAGATACATT GATGAGTTTG GACAAACCAC
     3001 AACTAGAATG CAGTGAAAAA AATGCTTTAT TTGTGAAATT TGTGATGCTA TTGCTTTATT
     3061 TGTAACCATT ATAAGCTGCA ATAAACAAGT TAACAACAAC AATTGCATTC ATTTTATGTT
     3121 TCAGGTTCAG GGGGAGGTGT GGGAGGTTTT TTAAAGCAAG TAAAACCTCT ACAAATGTGG
     3181 TATTGGCCCA TCTCTATCGG TATCGTAGCA TAACCCCTTG GGGCCTCTAA ACGGGTCTTG
     3241 AGGGGTTTTT TGTGCCCCTC GGGCCGGATT GCTATCTACC GGCATTGGCG CAGAAAAAAA
     3301 TGCCTGATGC GACGCTGCGC GTCTTATACT CCCACATATG CCAGATTCAG CAACGGATAC
     3361 GGCTTCCCCA ACTTGCCCAC TTCCATACGT GTCCTCCTTA CCAGAAATTT ATCCTTAAGG
     3421 TCGTCAGCTA TCCTGCAGGC GATCTCTCGA TTTCGATCAA GACATTCCTT TAATGGTCTT
```

```
3481 TTCTGGACAC CACTAGGGGT CAGAAGTAGT TCATCAAACT TTCTTCCCTC CCTAATCTCA
3541 TTGGTTACCT TGGGCTATCG AAACTTAATT AACCAGTCAA GTCAGCTACT TGGCGAGATC
3601 GACTTGTCTG GGTTTCGACT ACGCTCAGAA TTGCGTCAGT CAAGTTCGAT CTGGTCCTTG
3661 CTATTGCACC CGTTCTCCGA TTACGAGTTT CATTTAAATC ATGTGAGCAA AAGGCCAGCA
3721 AAAGGCCAGG AACCGTAAAA AGGCCGCGTT GCTGGCGTTT TTCCATAGGC TCCGCCCCCC
3781 TGACGAGCAT CACAAAAATC GACGCTCAAG TCAGAGGTGG CGAAACCCGA CAGGACTATA
3841 AAGATACCAG GCGTTTCCCC CTGGAAGCTC CCTCGTGCGC TCTCCTGTTC CGACCCTGCC
3901 GCTTACCGGA TACCTGTCCG CCTTTCTCCC TTCGGGAAGC GTGGCGCTTT CTCATAGCTC
3961 ACGCTGTAGG TATCTCAGTT CGGTGTAGGT CGTTCGCTCC AAGCTGGGCT GTGTGCACGA
4021 ACCCCCCGTT CAGCCCGACC GCTGCGCCTT ATCCGGTAAC TATCGTCTTG AGTCCAACCC
4081 GGTAAGACAC GACTTATCGC CACTGGCAGC AGCCACTGGT AACAGGATTA GCAGAGCGAG
4141 GTATGTAGGC GGTGCTACAG AGTTCTTGAA GTGGTGGCCT AACTACGGCT ACACTAGAAG
4201 AACAGTATTT GGTATCTGCG CTCTGCTGAA GCCAGTTACC TTCGGAAAAA GAGTTGGTAG
4261 CTCTTGATCC GGCAAACAAA CCACCGCTGG TAGCGGTGGT TTTTTTGTTT GCAAGCAGCA
4321 GATTACGCGC AGAAAAAAAG GATCTCAAGA AGATCCTTTG ATCTTTTCTA CGGGGTCTGA
4381 CGCTCAGTGG AACGAAAACT CACGTTAAGG GATTTTGGTC ATGAGATTAT CAAAAAGGAT
4441 CTTCACCTAG ATCCTTTTAA ATTAAAAATG AAGTTTTAAA TCAATCTAAA GTATATATGA
4501 GTAAACTTGG TCTGACAGTT ACCAATGCTT AATCAGTGAG GCACCTATCT CAGCGATCTG
4561 TCTATTTCGT TCATCCATAG TTGCATTTAA ATTTCCGAAC TCTCCAAGGC CCTCGTCGGA
4621 AAATCTTCAA ACCTTTCGTC CGATCCATCT TGCAGGCTAC CTCTCGAACG AACTATCGCA
4681 AGTCTCTTGG CCGGCCTTGC GCCTTGGCTA TTGCTTGGCA GCGCCTATCG CCAGGTATTA
4741 CTCCAATCCC GAATATCCGA GATCGGGATC ACCCGAGAGA AGTTCAACCT ACATCCTCAA
4801 TCCCGATCTA TCCGAGATCC GAGGAATATC GAAATCGGGG CGCGCCTGGT GTACCGAGAA
4861 CGATCCTCTC AGTGCGAGTC TCGACGATCC ATATCGTTGC TTGGCAGTCA GCCAGTCGGA
4921 ATCCAGCTTG GGACCCAGGA AGTCCAATCG TCAGATATTG TACTCAAGCC TGGTCACGGC
4981 AGCGTACCGA TCTGTTTAAA CCTAGATATT GATAGTCTGA TCGGTCAACG TATAATCGAG
5041 TCCTAGCTTT TGCAAACATC TATCAAGAGA CAGGATCAGC AGGAGGCTTT CGCATGATTG
5101 AACAAGATGG ATTGCACGCA GGTTCTCCGG CGGCTTGGGT GGAGAGGCTA TTCGGCTATG
5161 ACTGGGCACA ACAGACAATC GGCTGCTCTG ATGCCGCCGT GTTCCGGCTG TCAGCGCAGG
5221 GGCGTCCGGT TCTTTTTGTC AAGACCGACC TGTCCGGTGC CCTGAATGAA CTGCAAGACG
5281 AGGCAGCGCG GCTATCGTGG CTGGCGACGA CGGGCGTTCC TTGCGCGGCT GTGCTCGACG
5341 TTGTCACTGA AGCGGGAAGG GACTGGCTGC TATTGGGCGA AGTGCCGGGG CAGGATCTCC
5401 TGTCATCTCA CCTTGCTCCT GCCGAGAAAG TATCCATCAT GGCTGATGCA ATGCGGCGGC
5461 TGCATACGCT TGATCCGGCT ACCTGCCCAT TCGACCACCA AGCGAAACAT CGCATCGAGC
5521 GAGCACGTAC TCGGATGGAA GCCGGTCTTG TCGATCAGGA TGATCTGGAC GAAGAGCATC
5581 AGGGGCTCGC GCCAGCCGAA CTGTTCGCCA GGCTCAAGGC GTCTATGCCC GACGGCGAGG
5641 ATCTCGTCGT GACCCACGGC GATGCCTGCT TGCCGAATAT CATGGTGGAA AATGGCCGCT
5701 TTTCTGGATT CATCGACTGT GGCCGTCTGG GTGTGGCGGA CCGCTATCAG GACATAGCGT
5761 TGGCTACCCG TGATATTGCT GAAGAGCTTG GCGGCGAATG GGCTGACCGC TTCCTTGTGC
5821 TTTACGGTAT CGCCGCGCCC GATTCGCAGC GCATCGCCTT CTATCGCCTT CTTGACGAGT
5881 TCTTCTGACC GATTCTAGGT GCATTGGCGC AGAAAAAAAT GCCTGATGCG ACGCTGCGCG
5941 TCTTATACTC CCACATATGC CAGATTCAGC AACGGATACG GCTTCCCCAA CTTGCCCACT
6001 TCCATACGTG TCCTCCTTAC CAGAAATTTA TCCTTAAGGT CGTTTAAACT CGACTCTGGC
6061 TCTATCGAAT CTCCGTCGTT TCGAGCTTAC GCGAACAGCC GTGGCGCTCA TTTGCTCGTC
6121 GGGCATCGAA TCTCGTCAGC TATCGTCAGC TTACCTTTTT GGCA
//
```

7.2. MelanA Plasmid “CMV-MelanA.P2A.eGFP-IRES-Puro”

```
LOCUS       pSF_CMV_MelanA_P2A_eGFP_IRES_Puro  6515bp  DNA circular  17-MAR-2015
DEFINITION
ACCESSION
VERSION
SOURCE
ORGANISM
COMMENT     Oxford Genetics GenBank Format File

FEATURES             Location/Qualifiers
     source          1..6515
                     /organism="E.coli"
                     /strain="XL1 Blue"
                     /mol_type="plasmid DNA"

     misc_feature    18..89
                     /note="BetaGlobin Insulator"

     promoter        238..810
                     /note="CMV"

     RBS             893..906
                     /note="KOZAK_ShineDalgarno"

     CDS             907..2043
                     /note="MelanA_P2A_eGFP"

     misc_feature    1261..1323
                     /note="P2A Tag"

     misc_feature    2068..2078
                     /note="Stop codons x 3"

     misc_feature    2119..2669
                     /note="EMCV IRES"

     CDS             2672..3271
                     /note="Puromycin Resistance"

     misc_feature    3279..3289
                     /note="Stop codons x 3"

     polyA_site      3312..3503
                     /note="SV40 PolyA"

     terminator      3557..3604
                     /note="T7"

     terminator      3634..3770
                     /note="RrnG"

     misc_feature    3814..3885
                     /note="BetaGlobin Insulator"

     rep_origin      4051..4935
                     /note="pUC Origin"

     promoter        5360..5388
                     /note="Selection Gene"

     CDS             5445..6239
                     /note="Kanamycin Resistance"

     terminator      6253..6389
                     /note="RrnG"
```

ORIGIN

```
        1 GCGATCGCGG CTCCCGACAT CTTGGACCAT TAGCTCCACA GGTATCTTCT TCCCTCTAGT
       61 GGTCATAACA GCAGCTTCAG CTACCTCTCA ATTCAAAAAA CCCCTCAAGA CCCGTTTAGA
      121 GGCCCCAAGG GGTTATGCTA TCAATCGTTG CGTTACACAC ACAAAAAACC AACACACATC
      181 CATCTTCGAT GGATAGCGAT TTTATTATCT AACTGCTGAT CGAGTGTAGC CAGATCTAGT
      241 AATCAATTAC GGGGTCATTA GTTCATAGCC CATATATGGA GTTCCGCGTT ACATAACTTA
      301 CGGTAAATGG CCCGCCTGGC TGACCGCCCA ACGACCCCCG CCCATTGACG TCAATAATGA
      361 CGTATGTTCC CATAGTAACG CCAATAGGGA CTTTCCATTG ACGTCAATGG GTGGAGTATT
      421 TACGGTAAAC TGCCCACTTG GCAGTACATC AAGTGTATCA TATGCCAAGT ACGCCCCCTA
      481 TTGACGTCAA TGACGGTAAA TGGCCCGCCT GGCATTATGC CCAGTACATG ACCTTATGGG
      541 ACTTTCCTAC TTGGCAGTAC ATCTACGTAT TAGTCATCGC TATTACCATG CTGATGCGGT
      601 TTTGGCAGTA CATCAATGGG CGTGGATAGC GGTTTGACTC ACGGGGATTT CCAAGTCTCC
      661 ACCCCATTGA CGTCAATGGG AGTTTGTTTT GGCACCAAAA TCAACGGGAC TTTCCAAAAT
      721 GTCGTAACAA CTCCGCCCCA TTGACGCAAA TGGGCGGTAG GCGTGTACGG TGGGAGGTCT
      781 ATATAAGCAG AGCTGGTTTA GTGAACCGTC AGATCAGATC TTTGTCGATC CTACCATCCA
      841 CTCGACACAC CCGCCAGCGG CCGCTGCCAA GCTTCCGAGC TCTCGAATTC AAAGGAGGTA
      901 CCCACCATGC CAAGAGAAGA TGCTCACTTC ATCTATGGTT ACCCCAAGAA GGGGCACGGC
      961 CACTCTTACA CCACGGCTGA AGAGGCCGCT GGGATCGGCA TCCTGACAGT GATCCTGGGA
     1021 GTCTTACTGC TCATCGGCTG TTGGTATTGT AGAAGACGAA ATGGATACAG AGCCTTGATG
     1081 GATAAAAGTC TTCATGTTGG CACTCAATGT GCCTTAACAA GAAGATGCCC ACAAGAAGGG
     1141 TTTGATCATC GGGACAGCAA AGTGTCTCTT CAAGAGAAAA ACTGTGAACC TGTGGTTCCC
     1201 AATGCTCCAC CTGCTTATGA GAAACTCTCT GCAGAACAGT CACCACCACC TTATTCACCT
     1261 GGAAGCGGAG AGGGCAGAGG AAGTCTGCTA ACATGCGGTG ACGTCGAGGA GAATCCTGGA
     1321 CCTATGGTGT CCAAGGGAGA AGAGCTGTTC ACGGGAGTTG TTCCAATTCT TGTTGAGCTG
     1381 GATGGGGATG TTAACGGCCA TAAATTCTCC GTAAGCGGGG AGGGCGAGGG AGACGCCACT
     1441 TACGGGAAGC TTACCTTGAA ATTTATTTGC ACTACAGGAA AGCTGCCAGT GCCCTGGCCT
     1501 ACGCTGGTCA CTACCTTGAC CTACGGGGTT CAGTGCTTCT CCAGGTATCC GGATCATATG
     1561 AAACAGCATG ATTTCTTTAA AAGCGCCATG CCAGAGGGTT ATGTACAGGA ACGAACGATC
     1621 TTCTTTAAGG ATGACGGGAA CTACAAGACC CGCGCAGAGG TGAAATTTGA AGGAGATACG
     1681 CTGGTGAACA GAATAGAGCT GAAGGGGATC GACTTCAAAG AAGATGGCAA CATCCTGGGC
     1741 CACAAGCTTG AATATAACTA CAACAGCCAT AACGTATATA TCATGGCTGA CAAGCAGCGA
     1801 AATGGAATTA AGGCCAACTT CAAGATTCGG CACAACATCG AAGACGGGAG CGTGCAGCTG
     1861 GCCGACCATT ACCAGCAGAA CACCCCTATC GGGGATGGCC CAGTGCTGCT GCCTGATAAT
     1921 CATTATCTCA GCACGCAGTC TGCCCTGTCT AAAGACCCCA ACGAGAAAAG GGACCATATG
     1981 GTCCTGCTGG AATTTGTGAC AGCAGCTGGC ATCACCCTGG GAATGGATGA ACTCTACAAG
     2041 TAGTCTAGAA GTTGTCTCCT CCTGCACTGA CTGACTGATA CAATCGATAT GCCAAAAGCA
     2101 AAGCGCTATC GCGCCTTACG TTACTGGCCG AAGCCGCTTG GAATAAGGCC GGTGTGCGTT
     2161 TGTCTATATG TTATTTTCCA CCATATTGCC GTCTTTTGGC AATGTGAGGG CCCGGAAACC
     2221 TGGCCCTGTC TTCTTGACGA GCATTCCTAG GGGTCTTTCC CCTCTCGCCA AAGGAATGCA
     2281 AGGTCTGTTG AATGTCGTGA AGGAAGCAGT TCCTCTGGAA GCTTCTTGAA GACAAACAAC
     2341 GTCTGTAGCG ACCCTTTGCA GGCAGCGGAA CCCCCCACCT GGCGACAGGT GCCTCTGCGG
     2401 CCAAAAGCCA CGTGTATAAG ATACACCTGC AAAGGCGGCA CAACCCCAGT GCCACGTTGT
     2461 GAGTTGGATA GTTGTGGAAA GAGTCAAATG GCTCCCCTCA AGCGTATTCA ACAAGGGGCT
     2521 GAAGGATGCC CAGAAGGTAC CCCATTGTAT GGGATCTGAT CTGGGGCCTC GGTGCACATG
     2581 CTTTTCATGT GTTTAGTCGA GGTTAAAAAA CGTCTAGGCC CCCCGAACCA CGGGGACGTG
     2641 GTTTTCCTTT GAAAAACACG ATGATAATAA CATGACCGAG TACAAGCCCA CGGTGCGCCT
     2701 CGCCACCCGC GACGACGTCC CCAGGGCCGT ACGCACCCTC GCCGCCGCGT TCGCCGACTA
     2761 CCCCGCCACG CGCCACACCG TCGATCCGGA CCGCCACATC GAGCGGGTCA CCGAGCTGCA
     2821 AGAACTCTTC CTCACGCGCG TCGGGCTCGA CATCGGCAAG GTGTGGGTCG CGGACGACGG
     2881 CGCCGCGGTG GCGGTCTGGA CCACGCCGGA GAGCGTCGAA GCGGGGGCGG TGTTCGCCGA
     2941 GATCGGCCCG CGCATGGCCG AGTTGAGCGG TTCCCGGCTG GCCGCGCAGC AACAGATGGA
     3001 GGGCCTCCTG GCGCCGCACC GGCCCAAGGA GCCCGCGTGG TTCCTGGCCA CCGTCGGCGT
     3061 CTCGCCCGAC CACCAGGGCA AGGGTCTGGG CAGCGCCGTC GTGCTCCCCG GAGTGGAGGC
     3121 CGCCGAGCGC GCCGGGGTGC CCGCCTTCCT GGAGACCTCC GCGCCCCGCA ACCTCCCCTT
     3181 CTACGAGCGG CTCGGCTTCA CCGTCACCGC CGACGTCGAG GTGCCCGAAG GACCGCGCAC
     3241 CTGGTGCATG ACCCGCAAGC CCGGTGCCTA GGCTAGCTTG ACTGACTGAG ATACAGCGTA
     3301 CCTTCAGCTC ACAGACATGA TAAGATACAT TGATGAGTTT GGACAAACCA CAACTAGAAT
     3361 GCAGTGAAAA AAATGCTTTA TTTGTGAAAT TTGTGATGCT ATTGCTTTAT TTGTAACCAT
     3421 TATAAGCTGC AATAAACAAG TTAACAACAA CAATTGCATT CATTTTATGT TTCAGGTTCA
     3481 GGGGGAGGTG TGGGAGGTTT TTTAAAGCAA GTAAAACCTC TACAAATGTG GTATTGGCCC
     3541 ATCTCTATCG GTATCGTAGC ATAACCCCTT GGGGCCTCTA AACGGGTCTT GAGGGGTTTT
     3601 TTGTGCCCCT CGGGCCGGAT TGCTATCTAC CGGCATTGGC GCAGAAAAAA ATGCCTGATG
     3661 CGACGCTGCG CGTCTTATAC TCCCACATAT GCCAGATTCA GCAACGGATA CGGCTTCCCC
     3721 AACTTGCCCA CTTCCATACG TGTCCTCCTT ACCAGAAATT TATCCTTAAG GTCGTCAGCT
     3781 ATCCTGCAGG CGATCTCTCG ATTTCGATCA AGACATTCCT TTAATGGTCT TTTCTGGACA
     3841 CCACTAGGGG TCAGAAGTAG TTCATCAAAC TTTCTTCCCT CCCTAATCTC ATTGGTTACC
     3901 TTGGGCTATC GAAACTTAAT TAACCAGTCA AGTCAGCTAC TTGGCGAGAT CGACTTGTCT
     3961 GGGTTTCGAC TACGCTCAGA ATTGCGTCAG TCAAGTTCGA TCTGGTCCTT GCTATTGCAC
     4021 CCGTTCTCCG ATTACGAGTT TCATTTAAAT CATGTGAGCA AAAGGCCAGC AAAAGGCCAG
     4081 GAACCGTAAA AAGGCCGCGT TGCTGGCGTT TTTCCATAGG CTCCGCCCCC CTGACGAGCA
     4141 TCACAAAAAT CGACGCTCAA GTCAGAGGTG GCGAAACCCG ACAGGACTAT AAAGATACCA
     4201 GGCGTTTCCC CCTGGAAGCT CCCTCGTGCG CTCTCCTGTT CCGACCCTGC CGCTTACCGG
     4261 ATACCTGTCC GCCTTTCTCC CTTCGGGAAG CGTGGCGCTT TCTCATAGCT CACGCTGTAG
```

```
4321 GTATCTCAGT TCGGTGTAGG TCGTTCGCTC CAAGCTGGGC TGTGTGCACG AACCCCCCGT
4381 TCAGCCCGAC CGCTGCGCCT TATCCGGTAA CTATCGTCTT GAGTCCAACC CGGTAAGACA
4441 CGACTTATCG CCACTGGCAG CAGCCACTGG TAACAGGATT AGCAGAGCGA GGTATGTAGG
4501 CGGTGCTACA GAGTTCTTGA AGTGGTGGCC TAACTACGGC TACACTAGAA GAACAGTATT
4561 TGGTATCTGC GCTCTGCTGA AGCCAGTTAC CTTCGGAAAA AGAGTTGGTA GCTCTTGATC
4621 CGGCAAACAA ACCACCGCTG GTAGCGGTGG TTTTTTTGTT TGCAAGCAGC AGATTACGCG
4681 CAGAAAAAAA GGATCTCAAG AAGATCCTTT GATCTTTTCT ACGGGGTCTG ACGCTCAGTG
4741 GAACGAAAAC TCACGTTAAG GGATTTTGGT CATGAGATTA TCAAAAAGGA TCTTCACCTA
4801 GATCCTTTTA AATTAAAAAT GAAGTTTTAA ATCAATCTAA AGTATATATG AGTAAACTTG
4861 GTCTGACAGT TACCAATGCT TAATCAGTGA GGCACCTATC TCAGCGATCT GTCTATTTCG
4921 TTCATCCATA GTTGCATTTA AATTTCCGAA CTCTCCAAGG CCCTCGTCGG AAAATCTTCA
4981 AACCTTTCGT CCGATCCATC TTGCAGGCTA CCTCTCGAAC GAACTATCGC AAGTCTCTTG
5041 GCCGGCCTTG CGCCTTGGCT ATTGCTTGGC AGCGCCTATC GCCAGGTATT ACTCCAATCC
5101 CGAATATCCG AGATCGGGAT CACCCGAGAG AAGTTCAACC TACATCCTCA ATCCCGATCT
5161 ATCCGAGATC CGAGGAATAT CGAAATCGGG GCGCGCCTGG TGTACCGAGA ACGATCCTCT
5221 CAGTGCGAGT CTCGACGATC CATATCGTTG CTTGGCAGTC AGCCAGTCGG AATCCAGCTT
5281 GGGACCCAGG AAGTCCAATC GTCAGATATT GTACTCAAGC CTGGTCACGG CAGCGTACCG
5341 ATCTGTTTAA ACCTAGATAT TGATAGTCTG ATCGGTCAAC GTATAATCGA GTCCTAGCTT
5401 TTGCAAACAT CTATCAAGAG ACAGGATCAG CAGGAGGCTT TCGCATGATT GAACAAGATG
5461 GATTGCACGC AGGTTCTCCG GCGGCTTGGG TGGAGAGGCT ATTCGGCTAT GACTGGGCAC
5521 AACAGACAAT CGGCTGCTCT GATGCCGCCG TGTTCCGGCT GTCAGCGCAG GGGCGTCCGG
5581 TTCTTTTTGT CAAGACCGAC CTGTCCGGTG CCCTGAATGA ACTGCAAGAC GAGGCAGCGC
5641 GGCTATCGTG GCTGGCGACG ACGGGCGTTC CTTGCGCGGC TGTGCTCGAC GTTGTCACTG
5701 AAGCGGGAAG GGACTGGCTG CTATTGGGCG AAGTGCCGGG GCAGGATCTC CTGTCATCTC
5761 ACCTTGCTCC TGCCGAGAAA GTATCCATCA TGGCTGATGC AATGCGGCGG CTGCATACGC
5821 TTGATCCGGC TACCTGCCCA TTCGACCACC AAGCGAAACA TCGCATCGAG CGAGCACGTA
5881 CTCGGATGGA AGCCGGTCTT GTCGATCAGG ATGATCTGGA CGAAGAGCAT CAGGGGCTCG
5941 CGCCAGCCGA ACTGTTCGCC AGGCTCAAGG CGTCTATGCC CGACGGCGAG GATCTCGTCG
6001 TGACCCACGG CGATGCCTGC TTGCCGAATA TCATGGTGGA AAATGGCCGC TTTTCTGGAT
6061 TCATCGACTG TGGCCGTCTG GGTGTGGCGG ACCGCTATCA GGACATAGCG TTGGCTACCC
6121 GTGATATTGC TGAAGAGCTT GGCGGCGAAT GGGCTGACCG CTTCCTTGTG CTTTACGGTA
6181 TCGCCGCGCC CGATTCGCAG CGCATCGCCT TCTATCGCCT TCTTGACGAG TTCTTCTGAC
6241 CGATTCTAGG TGCATTGGCG CAGAAAAAAA TGCCTGATGC GACGCTGCGC GTCTTATACT
6301 CCCACATATG CCAGATTCAG CAACGGATAC GGCTTCCCCA ACTTGCCCAC TTCCATACGT
6361 GTCCTCCTTA CCAGAAATTT ATCCTTAAGG TCGTTTAAAC TCGACTCTGG CTCTATCGAA
6421 TCTCCGTCGT TTCGAGCTTA CGCGAACAGC CGTGGCGCTC ATTTGCTCGT CGGGCATCGA
6481 ATCTCGTCAG CTATCGTCAG CTTACCTTTT TGGCA
```
//

References

1. Vogelstein, B. *et al.* Cancer Genome Landscapes. *Science* **339**, 1546-1558 (2013).

2. Hanahan, D. & Weinberg, Robert A. Hallmarks of Cancer: The Next Generation. *Cell* **144**, 646-674 (2011).

3. Hogquist, K.A., Baldwin, T.A. & Jameson, S.C. Central tolerance: learning self-control in the thymus. *Nature reviews. Immunology* **5**, 772-782 (2005).

4. Arnold, B., Schonrich, G. & Hammerling, G.J. Multiple levels of peripheral tolerance. *Immunol. Today* **14**, 12-14 (1993).

5. Erlich, P. Über den jetzigen Stand der Karzinomforschung. *Ned. Tijdschr. Geneeskd.* **5**, 273-290 (1909).

6. Burnet, M. Cancer—A Biological Approach: I. The Processes Of Control. II. The Significance of Somatic Mutation. *Br. Med. J.* **1**, 779-786 (1957).

7. Thomas, L. Cellular and humoral aspects of the hypersensitive states. *Acta Med. Scand.* **170**, 128-128 (1961).

8. Burnet, F.M. Immunological surveillance in neoplasia. *Transplant. Rev.* **7**, 3-25 (1971).

9. Thomas, L. On immunosurveillance in human cancer. *Yale J. Biol. Med.* **55**, 329-333 (1982).

10. Old, L.J. & Boyse, E.A. Immunology of experimental tumors. *Annu. Rev. Med.* **15**, 167-186 (1964).

11. Stutman, O. Tumor development after 3-methylcholanthrene in immunologically deficient athymic-nude mice. *Science* **183**, 534-536 (1974).

12. Stutman, O. Chemical carcinogenesis in nude mice: comparison between nude mice from homozygous matings and heterozygous matings and effect of age and carcinogen dose. *J. Natl. Cancer Inst.* **62**, 353-358 (1979).

13. Stutman, O. in Proceedings of the International Workshop on Nude Mice (eds. Rygaard, J. & Povlsen, C.). **1**, 257-264 (1973).

14. Outzen, H.C., Custer, R.P., Eaton, G.J. & Prehn, R.T. Spontaneous and induced tumor incidence in germfree "nude" mice. *J. Reticuloendothel. Soc.* **17**, 1-9 (1975).

15. Stutman, O. in The Nude Mouse in Experimental and Clinical Research (eds. Fogh, J. & Giovanella, B. C.). *Academic, New York*, 411-435 (1978).

16. Rygaard, J. & Povlsen, C.O. The mouse mutant nude does not develop spontaneous tumours. An argument against immunological surveillance. *Acta Pathol Microbiol Scand B Microbiol Immunol* **82**, 99-106 (1974).

17. Heidelberger, C. Chemical carcinogenesis. *Annu. Rev. Biochem.* **44**, 79-121 (1975).

18. Dunn, G.P., Bruce, A.T., Ikeda, H., Old, L.J. & Schreiber, R.D. Cancer immunoediting: from immunosurveillance to tumor escape. *Nat Immunol* **3**, 991-998 (2002).

19. Ikehara, S., Pahwa, R.N., Fernandes, G., Hansen, C.T. & Good, R.A. Functional T cells in athymic nude mice. *Proc. Natl. Acad. Sci. U. S. A.* **81**, 886-888 (1984).

20. Maleckar, J.R. & Sherman, L.A. The composition of the T cell receptor repertoire in nude mice. *J. Immunol.* **138**, 3873-3876 (1987).

21. Yeadon, J. Immunodeficient mice for cancer studies: which host strain should I use? *The Jackson Laboratory: JAX Notes* (2017).

22. Dighe, A.S., Richards, E., Old, L.J. & Schreiber, R.D. Enhanced in vivo growth and resistance to rejection of tumor cells expressing dominant negative IFN gamma receptors. *Immunity* **1**, 447-456 (1994).

23. van den Broek, M.E. *et al.* Decreased tumor surveillance in perforin-deficient mice. *J. Exp. Med.* **184**, 1781-1790 (1996).

24. Jenkins, M.R. *et al.* Failed CTL/NK cell killing and cytokine hypersecretion are directly linked through prolonged synapse time. *J. Exp. Med.* **212**, 307-317 (2015).

25. Clementi, R. *et al.* A proportion of patients with lymphoma may harbor mutations of the perforin gene. *Blood* **105**, 4424-4428 (2005).

26. Gatti, R.A. & Good, R.A. Occurrence of malignancy in immunodeficiency diseases. A literature review. *Cancer* **28**, 89-98 (1971).

27. Penn, I. Posttransplant malignancies. *Transplant. Proc.* **31**, 1260-1262 (1999).

28. Sheil, A.G. Cancer after transplantation. *World J. Surg.* **10**, 389-396 (1986).

29. Pham, S.M. *et al.* Solid tumors after heart transplantation: lethality of lung cancer. *Ann. Thorac. Surg.* **60**, 1623-1626 (1995).

30. Birkeland, S.A. *et al.* Cancer risk after renal transplantation in the Nordic countries, 1964-1986. *Int. J. Cancer* **60**, 183-189 (1995).

31. Penn, I. Tumors of the immunocompromised patient. *Annu. Rev. Med.* **39**, 63-73 (1988).

32. McFarlane, G.A. & Munro, A. Helicobacter pylori and gastric cancer. *Br. J. Surg.* **84**, 1190-1199 (1997).

33. Silva, J., Cerqueira, F. & Medeiros, R. Chlamydia trachomatis infection: implications for HPV status and cervical cancer. *Arch. Gynecol. Obstet.* **289**, 715-723 (2014).

34. de Martel, C. & Franceschi, S. Infections and cancer: Established associations and new hypotheses. *Crit. Rev. Oncol./Hematol.* **70**, 183-194 (2009).

35. Gallimore, A.M. & Simon, A.K. Positive and negative influences of regulatory T cells on tumour immunity. *Oncogene* **27**:45, 5886-5893 (2008).

36. Gleave, M.E. *et al.* Interferon gamma-1b compared with placebo in metastatic renal-cell carcinoma. Canadian Urologic Oncology Group. *N. Engl. J. Med.* **338**, 1265-1271 (1998).

37. Jett, J.R. *et al.* Phase III trial of recombinant interferon gamma in complete responders with small-cell lung cancer. *J. Clin. Oncol.* **12**, 2321-2326 (1994).

38. Wiesenfeld, M. *et al.* Controlled clinical trial of interferon-gamma as postoperative surgical adjuvant therapy for colon cancer. *J. Clin. Oncol.* **13**, 2324-2329 (1995).

39. Vesely, M.D. & Schreiber, R.D. Cancer Immunoediting: antigens, mechanisms and implications to cancer immunotherapy. *Ann. N. Y. Acad. Sci.* **1284**, 1-5 (2013).

40. Mendes, F. *et al.* The role of immune system exhaustion on cancer cell escape and anti-tumor immune induction after irradiation. *Biochim. Biophys. Acta* **1865**, 168-175 (2016).

41. Raval, R.R., Sharabi, A.B., Walker, A.J., Drake, C.G. & Sharma, P. Tumor immunology and cancer immunotherapy: summary of the 2013 SITC primer. *Journal for immunotherapy of cancer* **2**, 14 (2014).

42. Dunn, G.P., Old, L.J. & Schreiber, R.D. The Immunobiology of Cancer Immunosurveillance and Immunoediting. *Immunity* **21**, 137-148 (2004).

43. Medeiros, L.R., Rosa, D.D., da Rosa, M.I., Bozzetti, M.C. & Zanini, R.R. Efficacy of human papillomavirus vaccines: a systematic quantitative review. *International journal of gynecological cancer : official journal of the International Gynecological Cancer Society* **19**, 1166-1176 (2009).

44. Rampias, T., Sasaki, C., Weinberger, P. & Psyrri, A. E6 and e7 gene silencing and transformed phenotype of human papillomavirus 16-positive oropharyngeal cancer cells. *J. Natl. Cancer Inst.* **101**, 412-423 (2009).

45. van der Bruggen, P. *et al.* A gene encoding an antigen recognized by cytolytic T lymphocytes on a human melanoma. *Science* **254**, 1643-1647 (1991).

46. Kwak, L.W. *et al.* Induction of immune responses in patients with B-cell lymphoma against the surface-immunoglobulin idiotype expressed by their tumors. *N. Engl. J. Med.* **327**, 1209-1215 (1992).

47. Vigneron, N., Stroobant, V., Van den Eynde, B.J. & van der Bruggen, P. Database of T cell-defined human tumor antigens: the 2013 update. *Cancer immunity* **13**, 15 [6 pages] (2013).

48. Sang, M., Lian, Y., Zhou, X. & Shan, B. MAGE-A family: attractive targets for cancer immunotherapy. *Vaccine* **29**, 8496-8500 (2011).

49. Grunert, F., Luckenbach, G.A., Haderlie, B., Schwarz, K. & von Kleist, S. Comparison of colon-, lung-, and breast-derived carcinoembryonic antigen and cross-reacting antigens by monoclonal antibodies and fingerprint analysis. *Ann. N. Y. Acad. Sci.* **417**, 75-85 (1983).

50. Turriziani, M. *et al.* Carcinoembryonic antigen (CEA)-based cancer vaccines: recent patents and antitumor effects from experimental models to clinical trials. *Recent patents on anti-cancer drug discovery* **7**, 265-296 (2012).

51. Beatson, R.E., Taylor-Papadimitriou, J. & Burchell, J.M. MUC1 immunotherapy. *Immunotherapy* **2**, 305-327 (2010).

52. Vermeij, R. *et al.* Immunological and clinical effects of vaccines targeting p53-overexpressing malignancies. *J Biomed Biotechnol* **2011**, Article ID: 702146 (2011).

53. Bocchia, M. *et al.* Specific human cellular immunity to bcr-abl oncogene-derived peptides. *Blood* **87**, 3587-3592 (1996).

54. Bocchia, M. *et al.* Specific binding of leukemia oncogene fusion protein peptides to HLA class I molecules. *Blood* **85**, 2680-2684 (1995).

55. Taylor, T.E., Furnari, F.B. & Cavenee, W.K. Targeting EGFR for treatment of glioblastoma: molecular basis to overcome resistance. *Curr Cancer Drug Targets* **12**, 197-209 (2012).

56. Copier, J. & Dalgleish, A. Tumour Immunology. *eLS*. John Wiley & Sons, Ltd, 2013.

57. Murphy, K. *Janeway's Immunobiology*, 8th edn. Garland Science, Taylor & Francis Group LLC: USA, 2012.

58. Vivier, E., Ugolini, S., Blaise, D., Chabannon, C. & Brossay, L. Targeting natural killer cells and natural killer T cells in cancer. *Nature reviews. Immunology* **12**, 239-252 (2012).

59. Riganti, C., Massaia, M., Davey, M.S. & Eberl, M. Human gammadelta T-cell responses in infection and immunotherapy: common mechanisms, common mediators? *Eur. J. Immunol.* **42**, 1668-1676 (2012).

60. Giannattasio, A. *et al.* Cytotoxicity and infiltration of human NK cells in in vivo-like tumor spheroids. *BMC Cancer* **15**, 351 (2015).

61. Mani, N.L. *et al.* Quantitative assessment of the spatial heterogeneity of tumor-infiltrating lymphocytes in breast cancer. *Breast cancer research : BCR* **18**, 78 (2016).

62. Peng, L.S. *et al.* Altered phenotypic and functional characteristics of CD3+CD56+ NKT-like cells in human gastric cancer. *Oncotarget* **7**:34, 55222-55230 (2016).

63. Rong, L. *et al.* Analysis of tumor-infiltrating gamma delta T cells in rectal cancer. *World journal of gastroenterology : WJG* **22**, 3573-3580 (2016).

64. Linnebacher, M. & Maletzki, C. Tumor-infiltrating B cells: The ignored players in tumor immunology. *Oncoimmunology* **1**, 1186-1188 (2012).

65. Tran Janco, J.M., Lamichhane, P., Karyampudi, L. & Knutson, K.L. Tumor-infiltrating dendritic cells in cancer pathogenesis. *J. Immunol.* **194**, 2985-2991 (2015).

66. Herberman, R.B., Nunn, M.E., Holden, H.T. & Lavrin, D.H. Natural cytotoxic reactivity of mouse lymphoid cells against syngeneic and allogeneic tumors. II. Characterization of effector cells. *Int. J. Cancer* **16**, 230-239 (1975).

67. Herberman, R.B., Nunn, M.E. & Lavrin, D.H. Natural cytotoxic reactivity of mouse lymphoid cells against syngeneic acid allogeneic tumors. I. Distribution of reactivity and specificity. *Int. J. Cancer* **16**, 216-229 (1975).

68. Cooper, M.A., Fehniger, T.A. & Caligiuri, M.A. The biology of human natural killer-cell subsets. *Trends Immunol* **22**, 633-640 (2001).

69. Biassoni, R. Human natural killer receptors, co-receptors, and their ligands. *Current protocols in immunology / edited by John E. Coligan ... [et al.]* **Chapter 14**, Unit 14.10 (2009).

70. Ruben, J.M. *et al.* Apoptotic blebs from leukemic cells as a preferred source of tumor-associated antigen for dendritic cell-based vaccines. *Cancer Immunol. Immunother.* **63**, 335-345 (2014).

71. Agaugue, S., Marcenaro, E., Ferranti, B., Moretta, L. & Moretta, A. Human natural killer cells exposed to IL-2, IL-12, IL-18, or IL-4 differently modulate priming of naive T cells by monocyte-derived dendritic cells. *Blood* **112**, 1776-1783 (2008).

72. Ferlazzo, G. *et al.* Human dendritic cells activate resting natural killer (NK) cells and are recognized via the NKp30 receptor by activated NK cells. *J. Exp. Med.* **195**, 343-351 (2002).

73. Gerosa, F. *et al.* Reciprocal activating interaction between natural killer cells and dendritic cells. *J. Exp. Med.* **195**, 327-333 (2002).

74. Vitale, M. *et al.* NK-dependent DC maturation is mediated by TNFalpha and IFNgamma released upon engagement of the NKp30 triggering receptor. *Blood* **106**, 566-571 (2005).

75. Choi, P.J. & Mitchison, T.J. Imaging burst kinetics and spatial coordination during serial killing by single natural killer cells. *Proc. Natl. Acad. Sci. U. S. A.* **110**, 6488-6493 (2013).

76. Wu, J. *et al.* A novel polymorphism of FcgammaRIIIa (CD16) alters receptor function and predisposes to autoimmune disease. *J. Clin. Invest.* **100**, 1059-1070 (1997).

77. Steinman RM, C.Z. Identification of a novel cell type in peripheral lymphoid organs of mice. I. Morphology, quantitation, tissue distribution. . *J. Exp. Med.* **137**, 1142-1162 (1973).

78. Vacchelli, E. *et al.* Trial watch: Dendritic cell-based interventions for cancer therapy. *Oncoimmunology* **2** (2013).

79. Steinman, R.M. Decisions about dendritic cells: past, present, and future. *Annu. Rev. Immunol.* **30**, 1-22 (2012).

80. Steinman, R.M. & Nussenzweig, M.C. Avoiding horror autotoxicus: the importance of dendritic cells in peripheral T cell tolerance. *Proc. Natl. Acad. Sci. U. S. A.* **99**, 351-358 (2002).

81. Steinman, R.M. & Banchereau, J. Taking dendritic cells into medicine. *Nature* **449**, 419-426 (2007).

82. Yamazaki, S., Inaba, K., Tarbell, K.V. & Steinman, R.M. Dendritic cells expand antigen-specific Foxp3+ CD25+ CD4+ regulatory T cells including suppressors of alloreactivity. *Immunol. Rev.* **212**, 314-329 (2006).

83. Steinman, R.M., Hawiger, D. & Nussenzweig, M.C. Tolerogenic dendritic cells. *Annu. Rev. Immunol.* **21**, 685-711 (2003).

84. Castiello, L. *et al.* Monocyte-derived DC maturation strategies and related pathways: a transcriptional view. *Cancer Immunol. Immunother.* **60**, 457-466 (2011).

85. Walzer, T., Dalod, M., Robbins, S.H., Zitvogel, L. & Vivier, E. Natural-killer cells and dendritic cells: "l'union fait la force". *Blood* **106**, 2252-2258 (2005).

86. Walzer, T., Dalod, M., Vivier, E. & Zitvogel, L. Natural killer cell-dendritic cell crosstalk in the initiation of immune responses. *Expert opinion on biological therapy* **5 Suppl 1**, S49-59 (2005).

87. Steinman, R.M. Dendritic cells: understanding immunogenicity. *Eur. J. Immunol.* **37 Suppl 1**, S53-60 (2007).

88. Curtsinger, J.M. *et al.* Inflammatory cytokines provide a third signal for activation of naive CD4+ and CD8+ T cells. *J. Immunol.* **162**, 3256-3262 (1999).

89. Gill, R.G., Coulombe, M. & Lafferty, K.J. Pancreatic islet allograft immunity and tolerance: the two-signal hypothesis revisited. *Immunol. Rev.* **149**, 75-96 (1996).

90. Valenzuela, J., Schmidt, C. & Mescher, M. The roles of IL-12 in providing a third signal for clonal expansion of naive CD8 T cells. *J. Immunol.* **169**, 6842-6849 (2002).

91. Curtsinger, J.M. & Mescher, M.F. Inflammatory cytokines as a third signal for T cell activation. *Curr. Opin. Immunol.* **22**, 333-340 (2010).

92. Ziegler-Heitbrock, L. *et al.* Nomenclature of monocytes and dendritic cells in blood. *Blood* **116**, e74-80 (2010).

93. MacDonald, K.P. *et al.* Characterization of human blood dendritic cell subsets. *Blood* **100**, 4512-4520 (2002).

94. Ueno, H., Palucka, A.K. & Banchereau, J. The expanding family of dendritic cell subsets. *Nat. Biotechnol.* **28**, 813-815 (2010).

95. Belz, G.T. & Nutt, S.L. Transcriptional programming of the dendritic cell network. *Nature reviews. Immunology* **12**, 101-113 (2012).

96. Lee, S.C., Srivastava, R.M., Lopez-Albaitero, A., Ferrone, S. & Ferris, R.L. Natural killer (NK): dendritic cell (DC) cross talk induced by therapeutic monoclonal antibody triggers tumor antigen-specific T cell immunity. *Immunol. Res.* **50**, 248-254 (2011).

97. Srivastava, R.M. *et al.* Cetuximab-activated natural killer and dendritic cells collaborate to trigger tumor antigen-specific T-cell immunity in head and neck cancer patients. *Clin. Cancer Res.* **19**, 1858-1872 (2013).

98. Piccioli, D., Sbrana, S., Melandri, E. & Valiante, N.M. Contact-dependent stimulation and inhibition of dendritic cells by natural killer cells. *J. Exp. Med.* **195**, 335-341 (2002).

99. Seth, S. *et al.* Heterogeneous expression of the adhesion receptor CD226 on murine NK and T cells and its function in NK-mediated killing of immature dendritic cells. *J. Leukoc. Biol.* **86**, 91-101 (2009).

100. Fernandez, N.C. *et al.* Dendritic cells directly trigger NK cell functions: cross-talk relevant in innate anti-tumor immune responses in vivo. *Nat. Med.* **5**, 405-411 (1999).

101. Germain, R.N. T-cell development and the CD4-CD8 lineage decision. *Nature reviews. Immunology* **2**, 309-322 (2002).

102. Aspinall, R. T cell development, ageing and Interleukin-7. *Mech. Ageing Dev.* **127**, 572-578 (2006).

103. Flannagan, R.S., Jaumouille, V. & Grinstein, S. The cell biology of phagocytosis. *Annual review of pathology* **7**, 61-98 (2012).

104. Alfaro, C. *et al.* Dendritic cells take up and present antigens from viable and apoptotic polymorphonuclear leukocytes. *PloS one* **6**, e29300 (2011).

105. Bracher, M., Gould, H.J., Sutton, B.J., Dombrowicz, D. & Karagiannis, S.N. Three-colour flow cytometric method to measure antibody-dependent tumour cell killing by cytotoxicity and phagocytosis. *J. Immunol. Methods* **323**, 160-171 (2007).

106. Ruben, J.M. *et al.* loading of skin dendritic cells with apoptotic bleb-derived antigens for the induction of tumor-directed immunity. *Oncoimmunology* **3**, e946360 (2014).

107. Mantegazza, A.R., Magalhaes, J.G., Amigorena, S. & Marks, M.S. Presentation of phagocytosed antigens by MHC class I and II. *Traffic (Copenhagen, Denmark)* **14**, 135-152 (2013).

108. Rangarajan, S. & Mariuzza, R.A. T cell receptor bias for MHC: co-evolution or co-receptors? *Cell. Mol. Life Sci.* **71**, 3059-3068 (2014).

109. Cresswell, P. Invariant chain structure and MHC class II function. *Cell* **84**, 505-507 (1996).

110. Peaper, D.R. & Cresswell, P. Regulation of MHC class I assembly and peptide binding. *Annu. Rev. Cell Dev. Biol.* **24**, 343-368 (2008).

111. Butler, M.O. & Hirano, N. Human cell-based artificial antigen-presenting cells for cancer immunotherapy. *Immunol. Rev.* **257**, 191-209 (2014).

112. Hirano, N. *et al.* Expression of costimulatory molecules in human leukemias. *Leukemia* **10**, 1168-1176 (1996).

113. Pogge von Strandmann, E., Shatnyeva, O. & Hansen, H.P. NKp30 and its ligands: emerging players in tumor immune evasion from natural killer cells. *Annals of translational medicine* **3**:20, 314-317 (2015).

114. Rudd, C.E., Taylor, A. & Schneider, H. CD28 and CTLA-4 coreceptor expression and signal transduction. *Immunol. Rev.* **229**, 12-26 (2009).

115. LeBien, T.W. & Tedder, T.F. B lymphocytes: how they develop and function. *Blood* **112**, 1570-1580 (2008).

116. Corfe, S.A. & Paige, C.J. The many roles of IL-7 in B cell development; Mediator of survival, proliferation and differentiation. *Semin. Immunol.* **24**, 198-208 (2012).

117. Rickert, R.C. New insights into pre-BCR and BCR signalling with relevance to B cell malignancies. *Nature reviews. Immunology* **13**, 578-591 (2013).

118. Schroeder, H.W., Radbruch, A. & Berek, C. 7 - B-Cell Development and Differentiation. In: Rich, R.R. *et al.* (eds). *Clinical Immunology (Fifth Edition)*. London, 107-118 [e101] (2019)

119. Suryani, S. *et al.* Differential expression of CD21 identifies developmentally and functionally distinct subsets of human transitional B cells. *Blood* **115**:3, 519-529 (2010).

120. Pillai, S. & Cariappa, A. The follicular versus marginal zone B lymphocyte cell fate decision. *Nature reviews. Immunology* **9**, 767-777 (2009).

121. Desiderio, S.V. B-cell activation. *Curr. Opin. Immunol.* **4**, 252-256 (1992).

122. Waldmann, H. & Munro, A. B cell activation. *Immunol. Rev.* **23**, 213-222 (1975).

123. Cambier, J.C., Gauld, S.B., Merrell, K.T. & Vilen, B.J. B-cell anergy: from transgenic models to naturally occurring anergic B cells? *Nature reviews. Immunology* **7**, 633-643 (2007).

124. Vidarsson, G., Dekkers, G. & Rispens, T. IgG subclasses and allotypes: from structure to effector functions. *Frontiers in Immunology* **5**, 520 [17 pages] (2014).

125. Schneider-Merck, T. *et al.* Human IgG2 antibodies against epidermal growth factor receptor effectively trigger antibody-dependent cellular cytotoxicity but, in contrast to IgG1, only by cells of myeloid lineage. *J. Immunol.* **184**, 512-520 (2010).

126. Schwartz-Albiez, R., Laban, S., Eichmuller, S. & Kirschfink, M. Cytotoxic natural antibodies against human tumours: an option for anti-cancer immunotherapy? *Autoimmun Rev* **7**, 491-495 (2008).

127. Pal, S., Chatterjee, M., Bhattacharya, D.K., Bandhyopadhyay, S. & Mandal, C. Identification and purification of cytolytic antibodies directed against O-acetylated sialic acid in childhood acute lymphoblastic leukemia. *Glycobiology* **10**, 539-549 (2000).

128. Schwartz-Albiez, R., Monteiro, R.C., Rodriguez, M., Binder, C.J. & Shoenfeld, Y. Natural antibodies, intravenous immunoglobulin and their role in autoimmunity, cancer and inflammation. *Clin. Exp. Immunol.* **158**, 43-50 (2009).

129. Weiner, L.M., Surana, R. & Wang, S. Antibodies and cancer therapy: versatile platforms for cancer immunotherapy. *Nature reviews. Immunology* **10**, 317-327 (2010).

130. Shiraishi, K. *et al.* Inhibition of MMP activity can restore NKG2D ligand expression in gastric cancer, leading to improved NK cell susceptibility. *J. Gastroenterol.* (2016).

131. O'Connell, J., O'Sullivan, G.C., Collins, J.K. & Shanahan, F. The Fas counterattack: Fas-mediated T cell killing by colon cancer cells expressing Fas ligand. *J. Exp. Med.* **184**, 1075-1082 (1996).

132. Dong, H. *et al.* Tumor-associated B7-H1 promotes T-cell apoptosis: a potential mechanism of immune evasion. *Nat. Med.* **8**, 793-800 (2002).

133. van der Pol, E., Boing, A.N., Harrison, P., Sturk, A. & Nieuwland, R. Classification, functions, and clinical relevance of extracellular vesicles. *Pharmacol. Rev.* **64**, 676-705 (2012).

134. Clayton A, M.J., Court J, Linnane S, Mason MD, Tabi Z. Human tumor-derived exosomes down-modulate NKG2D expression. *J. Immunol.* **11**, 7249-7258 (2008).

135. Kloss, S. *et al.* Increased sMICA and TGFbeta1 levels in HNSCC patients impair NKG2D-dependent functionality of activated NK cells. *Oncoimmunology* **4**, e1055993 (2015).

136. Massimo Ghio, P.C., Simone Negrini, Silvia Boero, Alessandra Musso and Alessandro Poggi. Soluble HLA-I-mediated secretion of TGF-b1 by human NK cells and consequent down-regulation of anti-tumor cytolytic activity. *Eur. J. Immunol.* **39**, 3459-3468 (2009).

137. Buggins, A.G. *et al.* Microenvironment produced by acute myeloid leukemia cells prevents T cell activation and proliferation by inhibition of NF-kappaB, c-Myc, and pRb pathways. *J. Immunol.* **167**, 6021-6030 (2001).

138. Garrido, F., Cabrera, T. & Aptsiauri, N. "Hard" and "soft" lesions underlying the HLA class I alterations in cancer cells: implications for immunotherapy. *Int. J. Cancer* **127**, 249-256 (2010).

139. Pedrinaci, S. *et al.* Selective upregulation of MHC class I expression in metastatic colonies derived from tumor clones of a murine fibrosarcoma. *Int. J. Clin. Lab. Res.* **29**, 166-173 (1999).

140. Kohler, G. & Milstein, C. Continuous cultures of fused cells secreting antibody of predefined specificity. *Nature* **256**, 495-497 (1975).

141. Liu, L. Antibody glycosylation and its impact on the pharmacokinetics and pharmacodynamics of monoclonal antibodies and Fc-fusion proteins. *J. Pharm. Sci.* **104**, 1866-1884 (2015).

142. Gaughan, C.L. The present state of the art in expression, production and characterization of monoclonal antibodies. *Mol. Divers.* **20**, 255-270 (2016).

143. Ventola, C.L. Biosimilars: part 1: proposed regulatory criteria for FDA approval. *P & T : a peer-reviewed journal for formulary management* **38**, 270-287 (2013).

144. Kaplon, H. & Reichert, J.M. Antibodies to watch in 2018. *MAbs* **10**, 183-203 (2018).

145. Imai, K. & Takaoka, A. Comparing antibody and small-molecule therapies for cancer. *Nature reviews. Cancer* **6**, 714-727 (2006).

146. Laffleur, B., Pascal, V., Sirac, C. & Cogne, M. Production of human or humanized antibodies in mice. *Methods Mol. Biol.* **901**, 149-159 (2012).

147. Norderhaug, L., Olafsen, T., Michaelsen, T.E. & Sandlie, I. Versatile vectors for transient and stable expression of recombinant antibody molecules in mammalian cells. *J. Immunol. Methods* **204**, 77-87 (1997).

148. Leach, D.R., Krummel, M.F. & Allison, J.P. Enhancement of antitumor immunity by CTLA-4 blockade. *Science* **271**, 1734-1736 (1996).

149. Pegram, M.D. *et al.* Phase I dose escalation pharmacokinetic assessment of intravenous humanized anti-MUC1 antibody AS1402 in patients with advanced breast cancer. *Breast Cancer Research* **11**:5, R73 [8 pages] (2009).

150. Seiwert TY, H.R., Gupta S, et al. Antitumor activity and safety of pembrolizumab in patients (pts) with advanced squamous cell carcinoma of the head and neck (SCCHN): Preliminary results from KEYNOTE-012 expansion cohort (supplement; abstract LBA6008). *J. Clin. Oncol.* **33** (2015).

151. Seiwert TY, B.B.B., Weiss J, et al. A phase Ib study of MK-3475 in patients with human papillomavirus (HPV)-associated and non-HPV–associated head and neck (H/N) cancer (supplement; abstract 6011). *J. Clin. Oncol.* **32** (2014).

152. Bargou, R. *et al.* Tumor regression in cancer patients by very low doses of a T cell-engaging antibody. *Science* **321**, 974-977 (2008).

153. Aigner, M. *et al.* T lymphocytes can be effectively recruited for ex vivo and in vivo lysis of AML blasts by a novel CD33/CD3-bispecific BiTE antibody construct. *Leukemia* **27**, 1107-1115 (2013).

154. Lutterbuese, R. *et al.* T cell-engaging BiTE antibodies specific for EGFR potently eliminate KRAS- and BRAF-mutated colorectal cancer cells. *Proc. Natl. Acad. Sci. U. S. A.* **107**, 12605-12610 (2010).

155. Flygare, J.A., Pillow, T.H. & Aristoff, P. Antibody-Drug Conjugates for the Treatment of Cancer. *Chemical Biology & Drug Design* **81**, 113-121 (2013).

156. Kantarjian, H. *et al.* Inotuzumab ozogamicin, an anti-CD22-calecheamicin conjugate, for refractory and relapsed acute lymphocytic leukaemia: a phase 2 study. *The Lancet. Oncology* **13**, 403-411 (2012).

157. (INO), C.g. Search Term: Inotuzumab Ozogamicin. 2018.

158. Rosenberg, S.A. *et al.* Use of tumor-infiltrating lymphocytes and interleukin-2 in the immunotherapy of patients with metastatic melanoma. A preliminary report. *N. Engl. J. Med.* **319**, 1676-1680 (1988).

159. Chia, W.K. *et al.* Adoptive T-cell transfer and chemotherapy in the first-line treatment of metastatic and/or locally recurrent nasopharyngeal carcinoma. *Molecular therapy : the journal of the American Society of Gene Therapy* **22**, 132-139 (2014).

160. Galluzzi, L. *et al.* Trial watch: Dendritic cell-based interventions for cancer therapy. *Oncoimmunology* **1**, 1111-1134 (2012).

161. Bonifaz, L.C. *et al.* In vivo targeting of antigens to maturing dendritic cells via the DEC-205 receptor improves T cell vaccination. *J. Exp. Med.* **199**, 815-824 (2004).

162. Munich, S., Sobo-Vujanovic, A., Buchser, W.J., Beer-Stolz, D. & Vujanovic, N.L. Dendritic cell exosomes directly kill tumor cells and activate natural killer cells via TNF superfamily ligands. *Oncoimmunology* **1**, 1074-1083 (2012).

163. Pan, W.Y. *et al.* Cancer immunotherapy using a membrane-bound interleukin-12 with B7-1 transmembrane and cytoplasmic domains. *Molecular therapy : the journal of the American Society of Gene Therapy* **20**, 927-937 (2012).

164. Chen, Z. *et al.* Efficient antitumor immunity derived from maturation of dendritic cells that had phagocytosed apoptotic/necrotic tumor cells. *Int. J. Cancer* **93**, 539-548 (2001).

165. Kandalaft, L.E. *et al.* Autologous lysate-pulsed dendritic cell vaccination followed by adoptive transfer of vaccine-primed ex vivo co-stimulated T cells in recurrent ovarian cancer. *Oncoimmunology* **2**, e22664 (2013).

166. Mayordomo, J.I. *et al.* Bone marrow-derived dendritic cells pulsed with synthetic tumour peptides elicit protective and therapeutic antitumour immunity. *Nat. Med.* **1**, 1297-1302 (1995).

167. Boczkowski, D., Nair, S.K., Nam, J.H., Lyerly, H.K. & Gilboa, E. Induction of tumor immunity and cytotoxic T lymphocyte responses using dendritic cells transfected with messenger RNA amplified from tumor cells. *Cancer Res.* **60**, 1028-1034 (2000).

168. Song, W. *et al.* Dendritic cells genetically modified with an adenovirus vector encoding the cDNA for a model antigen induce protective and therapeutic antitumor immunity. *J. Exp. Med.* **186**, 1247-1256 (1997).

169. Wang, J., Saffold, S., Cao, X., Krauss, J. & Chen, W. Eliciting T cell immunity against poorly immunogenic tumors by immunization with dendritic cell-tumor fusion vaccines. *J. Immunol.* **161**, 5516-5524 (1998).

170. Plosker, G.L. Sipuleucel-T: in metastatic castration-resistant prostate cancer. *Drugs* **71**, 101-108 (2011).

171. Costello, R.T. *et al.* Defective expression and function of natural killer cell-triggering receptors in patients with acute myeloid leukemia. *Blood* **99**, 3661-3667 (2002).

172. Ingram, W. *et al.* Human CD80/IL2 lentivirus-transduced acute myeloid leukaemia (AML) cells promote natural killer (NK) cell activation and cytolytic activity: implications for a phase I clinical study. *Br. J. Haematol.* **145**, 749-760 (2009).

173. Ingram, W. *et al.* Human CD80/IL2 lentivirus transduced acute myeloid leukaemia cells enhance cytolytic activity in vitro in spite of an increase in regulatory CD4+ T cells in a subset of cultures. *Cancer Immunol. Immunother.* **58**, 1679-1690 (2009).

174. Smits, E.L. *et al.* The Toll-like receptor 7/8 agonist resiquimod greatly increases the immunostimulatory capacity of human acute myeloid leukemia cells. *Cancer Immunol. Immunother.* **59**, 35-46 (2010).

175. Wang, L.X. *et al.* Low dose decitabine treatment induces CD80 expression in cancer cells and stimulates tumor specific cytotoxic T lymphocyte responses. *PloS one* **8**, e62924 (2013).

176. Davila, M.L. & Sadelain, M. Biology and clinical application of CAR T cells for B cell malignancies. *Int. J. Hematol.* **104**, 6-17 (2016).

177. Biglari, A., Southgate, T.D., Fairbairn, L.J. & Gilham, D.E. Human monocytes expressing a CEA-specific chimeric CD64 receptor specifically target CEA-expressing tumour cells in vitro and in vivo. *Gene Ther.* **13**, 602-610 (2006).

178. Rischer, M. *et al.* Human gammadelta T cells as mediators of chimaeric-receptor redirected anti-tumour immunity. *Br. J. Haematol.* **126**, 583-592 (2004).

179. Imai, C., Iwamoto, S. & Campana, D. Genetic modification of primary natural killer cells overcomes inhibitory signals and induces specific killing of leukemic cells. *Blood* **106**, 376-383 (2005).

180. Zah, E., Lin, M.Y., Silva-Benedict, A., Jensen, M.C. & Chen, Y.Y. T Cells Expressing CD19/CD20 Bispecific Chimeric Antigen Receptors Prevent Antigen Escape by Malignant B Cells. *Cancer immunology research* **4**, 498-508 (2016).

181. Qasim, W. *et al.* First Clinical Application of Talen Engineered Universal CAR19 T Cells in B-ALL. *Blood* **126**:23, 2046 (2015).

182. Qasim, W. *et al.* Molecular remission of infant B-ALL after infusion of universal TALEN gene-edited CAR T cells. *Science Translational Medicine* **9**:374 [8 pages] (2017).

183. Khalil, D.N., Smith, E.L., Brentjens, R.J. & Wolchok, J.D. The future of cancer treatment: immunomodulation, CARs and combination immunotherapy. *Nature reviews. Clinical oncology* **13**, 273-290 (2016).

184. Citri A, Y.Y. EGF-ERBB signalling: towards the systems level. *Nat Rev Mol Cell Biol* **7**, 505-516 (2006).

185. Lampri, E.S. *et al.* Biomarkers of head and neck cancer, tools or a gordian knot? *International journal of clinical and experimental medicine* **8**, 10340-10357 (2015).

186. Ling, Y. *et al.* Overexpression of mutant EGFR protein indicates a better survival benefit from EGFR-TKI therapy in non-small cell lung cancer. *Oncotarget* **7**:33, 52862-52869 (2016).

187. Markman, B., Javier Ramos, F., Capdevila, J. & Tabernero, J. EGFR and KRAS in colorectal cancer. *Adv. Clin. Chem.* **51**, 71-119 (2010).

188. de Gramont, A. *et al.* Leucovorin and fluorouracil with or without oxaliplatin as first-line treatment in advanced colorectal cancer. *Journal of clinical oncology : official journal of the American Society of Clinical Oncology* **18**, 2938-2947 (2000).

189. Douillard, J.Y. Irinotecan and high-dose fluorouracil/leucovorin for metastatic colorectal cancer. *Oncology* **14**, 51-55 (2000).

190. Giacchetti, S. *et al.* Long-term survival of patients with unresectable colorectal cancer liver metastases following infusional chemotherapy with 5-fluorouracil, leucovorin, oxaliplatin and surgery. *Annals of oncology : official journal of the European Society for Medical Oncology / ESMO* **10**, 663-669 (1999).

191. Goldberg, R.M. *et al.* A randomized controlled trial of fluorouracil plus leucovorin, irinotecan, and oxaliplatin combinations in patients with previously untreated metastatic colorectal cancer. *Journal of clinical oncology : official journal of the American Society of Clinical Oncology* **22**, 23-30 (2004).

192. Grothey, A. & Goetz, M.P. Oxaliplatin plus oral fluoropyrimidines in colorectal cancer. *Clin Colorectal Cancer* **4**:Suppl 1, S37-42 (2004).

193. Kohne, C.H. *et al.* Phase III study of weekly high-dose infusional fluorouracil plus folinic acid with or without irinotecan in patients with metastatic colorectal cancer: European Organisation for Research and Treatment of Cancer Gastrointestinal Group Study 40986. *Journal of clinical oncology : official journal of the American Society of Clinical Oncology* **23**, 4856-4865 (2005).

194. Laurent-Puig, P., Lievre, A. & Blons, H. Mutations and response to epidermal growth factor receptor inhibitors. *Clinical cancer research : an official journal of the American Association for Cancer Research* **15**, 1133-1139 (2009).

195. Maughan, T.S. *et al.* Addition of cetuximab to oxaliplatin-based first-line combination chemotherapy for treatment of advanced colorectal cancer: results of the randomised phase 3 MRC COIN trial. *Lancet* **377**, 2103-2114 (2011).

196. Saltz, L. Irinotecan-based combinations for the adjuvant treatment of stage III colon cancer. *Oncology* **14**, 47-50 (2000).

197. Tournigand, C. *et al.* FOLFIRI followed by FOLFOX6 or the reverse sequence in advanced colorectal cancer: a randomized GERCOR study. *Journal of clinical oncology : official journal of the American Society of Clinical Oncology* **22**, 229-237 (2004).

198. Bianco, R., Gelardi, T., Damiano, V., Ciardiello, F. & Tortora, G. Rational bases for the development of EGFR inhibitors for cancer treatment. *Int. J. Biochem. Cell Biol.* **39**, 1416-1431 (2007).

199. Specenier, P., and Vermorken Jan, B. . Cetuximab: its unique place in head and neck cancer treatment. *Biologics* **7**, 77-90 (2013).

200. Amado, R.G. *et al.* Wild-type KRAS is required for panitumumab efficacy in patients with metastatic colorectal cancer. *Journal of clinical oncology : official journal of the American Society of Clinical Oncology* **26**, 1626-1634 (2008).

201. Karapetis, C.S. *et al.* K-ras mutations and benefit from cetuximab in advanced colorectal cancer. *The New England journal of medicine* **359**, 1757-1765 (2008).

202. Bokemeyer, C. *et al.* Fluorouracil, leucovorin, and oxaliplatin with and without cetuximab in the first-line treatment of metastatic colorectal cancer. *Journal of clinical oncology : official journal of the American Society of Clinical Oncology* **27**, 663-671 (2009).

203. Van Cutsem, E. *et al.* Cetuximab and chemotherapy as initial treatment for metastatic colorectal cancer. *The New England journal of medicine* **360**, 1408-1417 (2009).

204. Ciardiello, F. & Tortora, G. EGFR antagonists in cancer treatment. *N Engl J Med* **358**, 1160-1174 (2008).

205. Gerdes, C.A. *et al.* GA201 (RG7160): A Novel, Humanized, Glycoengineered Anti-EGFR Antibody with Enhanced ADCC and Superior In Vivo Efficacy Compared with Cetuximab. *Clinical cancer research : an official journal of the American Association for Cancer Research* **19**, 1126-1138 (2013).

206. Pessino, A. *et al.* First-line single-agent cetuximab in patients with advanced colorectal cancer. *Ann. Oncol.* **19**, 711-716 (2008).

207. Baselga, J. *et al.* Phase I studies of anti-epidermal growth factor receptor chimeric antibody C225 alone and in combination with cisplatin. *J. Clin. Oncol.* **18**, 904-914 (2000).

208. Thomson, D. National Cancer Drugs Fund List Ver5.1. NHS England; 2015. p. 11.

209. Taylor, R.J. *et al.* FcgammaRIIIa polymorphisms and cetuximab induced cytotoxicity in squamous cell carcinoma of the head and neck. *Cancer immunology, immunotherapy : CII* **58**, 997-1006 (2009).

210. Zhang, W. *et al.* FCGR2A and FCGR3A polymorphisms associated with clinical outcome of epidermal growth factor receptor expressing metastatic colorectal cancer patients treated with single-agent cetuximab. *Journal of clinical oncology : official journal of the American Society of Clinical Oncology* **25**, 3712-3718 (2007).

211. Umana, P., Jean-Mairet, J., Moudry, R., Amstutz, H. & Bailey, J.E. Engineered glycoforms of an antineuroblastoma IgG1 with optimized antibody-dependent cellular cytotoxic activity. *Nat. Biotechnol.* **17**, 176-180 (1999).

212. Ferrara, C., Stuart, F., Sondermann, P., Brunker, P. & Umana, P. The carbohydrate at FcgammaRIIIa Asn-162. An element required for high affinity binding to non-fucosylated IgG glycoforms. *The Journal of biological chemistry* **281**, 5032-5036 (2006).

213. Ferrara, C. *et al.* Unique carbohydrate-carbohydrate interactions are required for high affinity binding between FcgammaRIII and antibodies lacking core fucose. *Proc. Natl. Acad. Sci. U. S. A.* **108**, 12669-12674 (2011).

214. Wormald, M.R. *et al.* Conformational studies of oligosaccharides and glycopeptides: complementarity of NMR, X-ray crystallography, and molecular modelling. *Chem. Rev.* **102**, 371-386 (2002).

215. Beck-Sickinger, A.G. & Mörl, K. Posttranslational Modification of Proteins. Expanding Nature's Inventory. By Christopher T. Walsh. *Angewandte Chemie International Edition* **45**, 1020-1020 (2006).

216. Becker, D.J. & Lowe, J.B. Fucose: biosynthesis and biological function in mammals. *Glycobiology* **13**, 41r-53r (2003).

217. Burda, P. & Aebi, M. The dolichol pathway of N-linked glycosylation. *Biochim. Biophys. Acta* **1426**, 239-257 (1999).

218. Dean, N. Asparagine-linked glycosylation in the yeast Golgi. *Biochim. Biophys. Acta* **1426**, 309-322 (1999).

219. Frenkel, Z., Gregory, W., Kornfeld, S. & Lederkremer, G.Z. Endoplasmic reticulum-associated degradation of mammalian glycoproteins involves sugar chain trimming to Man6-5GlcNAc2. *J. Biol. Chem.* **278**, 34119-34124 (2003).

220. Shields, R.L. *et al.* Lack of fucose on human IgG1 N-linked oligosaccharide improves binding to human Fcgamma RIII and antibody-dependent cellular toxicity. *J. Biol. Chem.* **277**, 26733-26740 (2002).

221. Umana, P., Jean-Mairet, J., Moudry, R., Amstutz, H. & Bailey, J.E. Engineered glycoforms of an antineuroblastoma IgG1 with optimized antibody-dependent cellular cytotoxic activity. *Nat. Biotechnol.* **17**, 176-180 (1999).

222. Dicker, M. & Strasser, R. Using glyco-engineering to produce therapeutic proteins. *Expert opinion on biological therapy* **15**, 1501-1516 (2015).

223. Ferrara, C. *et al.* Modulation of therapeutic antibody effector functions by glycosylation engineering: influence of Golgi enzyme localization domain and co-expression of heterologous beta1, 4-N-acetylglucosaminyltransferase III and Golgi alpha-mannosidase II. *Biotechnol. Bioeng.* **93**, 851-861 (2006).

224. Kanda, Y. *et al.* Comparison of cell lines for stable production of fucose-negative antibodies with enhanced ADCC. *Biotechnol. Bioeng.* **94**, 680-688 (2006).

225. Yamane-Ohnuki, N. *et al.* Establishment of FUT8 knockout Chinese hamster ovary cells: an ideal host cell line for producing completely defucosylated antibodies with enhanced antibody-dependent cellular cytotoxicity. *Biotechnol. Bioeng.* **87**, 614-622 (2004).

226. Malphettes, L. *et al.* Highly efficient deletion of FUT8 in CHO cell lines using zinc-finger nucleases yields cells that produce completely nonfucosylated antibodies. *Biotechnol. Bioeng.* **106**, 774-783 (2010).

227. Mori, K. *et al.* Engineering Chinese hamster ovary cells to maximize effector function of produced antibodies using FUT8 siRNA. *Biotechnol. Bioeng.* **88**, 901-908 (2004).

228. Mizuochi, T., Taniguchi, T., Shimizu, A. & Kobata, A. Structural and numerical variations of the carbohydrate moiety of immunoglobulin G. *J. Immunol.* **129**, 2016-2020 (1982).

229. Daeron, M. Fc receptor biology. *Annu. Rev. Immunol.* **15**, 203-234 (1997).

230. Nimmerjahn, F. & Ravetch, J.V. Fcgamma receptors as regulators of immune responses. *Nature reviews. Immunology* **8**, 34-47 (2008).

231. Thomann, M. *et al.* In vitro glycoengineering of IgG1 and its effect on Fc receptor binding and ADCC activity. *PloS one* **10**, e0134949 (2015).

232. Mossner, E. *et al.* Increasing the efficacy of CD20 antibody therapy through the engineering of a new type II anti-CD20 antibody with enhanced direct and immune effector cell-mediated B-cell cytotoxicity. *Blood* **115**, 4393-4402 (2010).

233. Herter, S. *et al.* Glycoengineering of therapeutic antibodies enhances monocyte/macrophage-mediated phagocytosis and cytotoxicity. *J. Immunol.* **192**, 2252-2260 (2014).

234. Paz-Ares, L.G. *et al.* Phase I pharmacokinetic and pharmacodynamic dose-escalation study of RG7160 (GA201), the first glycoengineered monoclonal antibody against the epidermal growth factor receptor, in patients with advanced solid tumors. *J. Clin. Oncol.* **29**, 3783-3790 (2011).

235. Alter, G., Malenfant, J.M. & Altfeld, M. CD107a as a functional marker for the identification of natural killer cell activity. *J. Immunol. Methods* **294**, 15-22 (2004).

236. Giard, D.J. *et al.* In vitro cultivation of human tumors: establishment of cell lines derived from a series of solid tumors. *J. Natl. Cancer Inst.* **51**, 1417-1423 (1973).

237. Lozzio, C.B. & Lozzio, B.B. Human chronic myelogenous leukemia cell-line with positive Philadelphia chromosome. *Blood* **45**, 321-334 (1975).

238. Oppenheim, D.E. *et al.* Glyco-engineered anti-EGFR mAb elicits ADCC by NK cells from colorectal cancer patients irrespective of chemotherapy. *Br. J. Cancer* **110**, 1221-1227 (2014).

239. Dhodapkar, K.M., Krasovsky, J., Williamson, B. & Dhodapkar, M.V. Antitumor monoclonal antibodies enhance cross-presentation ofcCellular antigens and the generation of myeloma-specific killer T cells by dendritic cells. *J. Exp. Med.* **195**, 125-133 (2002).

240. Schuler, P.J. *et al.* EGFR-specific T cell frequencies correlate with EGFR expression in head and neck squamous cell carcinoma. *Journal of Translational Medicine* **9**, 168 [8 pages] (2011).

241. Lehmann, P.V., Forsthuber, T., Miller, A. & Sercarz, E.E. Spreading of T-cell autoimmunity to cryptic determinants of an autoantigen. *Nature* **358**, 155-157 (1992).

242. Lehmann, P.V., Sercarz, E.E., Forsthuber, T., Dayan, C.M. & Gammon, G. Determinant spreading and the dynamics of the autoimmune T-cell repertoire. *Immunol. Today* **14**, 203-208 (1993).

243. Butterfield, L.H. *et al.* Determinant spreading associated with clinical response in dendritic cell-based immunotherapy for malignant melanoma. *Clin. Cancer Res.* **9**, 998-1008 (2003).

244. Vanderlugt, C.L. & Miller, S.D. Epitope spreading in immune-mediated diseases: implications for immunotherapy. *Nature reviews. Immunology* **2**, 85-95 (2002).

245. Yang, X.D., Jia, X.C., Corvalan, J.R., Wang, P. & Davis, C.G. Development of ABX-EGF, a fully human anti-EGF receptor monoclonal antibody, for cancer therapy. *Crit. Rev. Oncol. Hematol.* **38**, 17-23 (2001).

246. Masui, H. *et al.* Growth inhibition of human tumor cells in athymic mice by anti-epidermal growth factor receptor monoclonal antibodies. *Cancer Res.* **44**, 1002-1007 (1984).

247. Goldstein, N.I., Prewett, M., Zuklys, K., Rockwell, P. & Mendelsohn, J. Biological efficacy of a chimeric antibody to the epidermal growth factor receptor in a human tumor xenograft model. *Clin. Cancer. Res.* **1**:11, 1311-1318 (1995).

248. Modjtahedi, H., Styles, J.M. & Dean, C.J. The human EGF receptor as a target for cancer therapy: six new rat mAbs against the receptor on the breast carcinoma MDA-MB 468. *Br. J. Cancer* **67**, 247-253 (1993).

249. Queen, C. *et al.* A humanized antibody that binds to the interleukin 2 receptor. *Proc. Natl. Acad. Sci. U. S. A.* **86**, 10029-10033 (1989).

250. Tedder, T.F. & Engel, P. CD20: a regulator of cell-cycle progression of B lymphocytes. *Immunol. Today* **15**, 450-454 (1994).

251. Lam, K.P., Kuhn, R. & Rajewsky, K. In vivo ablation of surface immunoglobulin on mature B cells by inducible gene targeting results in rapid cell death. *Cell* **90**, 1073-1083 (1997).

252. Duhren-von Minden, M. *et al.* Chronic lymphocytic leukaemia is driven by antigen-independent cell-autonomous signalling. *Nature* **489**, 309-312 (2012).

253. Rafiq, S. *et al.* Comparative assessment of clinically utilized CD20-directed antibodies in chronic lymphocytic leukemia cells reveals divergent NK cell, monocyte, and macrophage properties. *J. Immunol.* **190**, 2702-2711 (2013).

254. Jaglowski, S.M., Alinari, L., Lapalombella, R., Muthusamy, N. & Byrd, J.C. The clinical application of monoclonal antibodies in chronic lymphocytic leukemia. *Blood* **116**, 3705-3714 (2010).

255. Cartron, G. *et al.* Therapeutic activity of humanized anti-CD20 monoclonal antibody and polymorphism in IgG Fc receptor FcgammaRIIIa gene. *Blood* **99**, 754-758 (2002).

256. Goede, V. *et al.* Obinutuzumab plus chlorambucil in patients with CLL and coexisting conditions. *N. Engl. J. Med.* **370**, 1101-1110 (2014).

257. Morschhauser, F.A. *et al.* Obinutuzumab (GA101) Monotherapy in Relapsed/Refractory Diffuse Large B-Cell Lymphoma or Mantle-Cell Lymphoma: Results From the Phase II GAUGUIN Study. *J. Clin. Oncol.* **31**, 2912-2919 (2013).

258. Vitolo, U. *et al.* Obinutuzumab or Rituximab Plus CHOP in Patients with Previously Untreated Diffuse Large B-Cell Lymphoma: Final Results from an Open-Label, Randomized Phase 3 Study (GOYA). *Blood* **128**:22, 470 (2016).

259. (NCT01287741), C.g. A Study of Obinutuzumab in Combination With CHOP Chemotherapy Versus Rituximab With CHOP in Participants With CD20-Positive Diffuse Large B-Cell Lymphoma (GOYA). (2018).

260. Adams, R.A., Flowers, A. & Davis, B.J. Direct implantation and serial transplantation of human acute lymphoblastic leukemia in hamsters, SB-2. *Cancer Res.* **28**, 1121-1125 (1968).

261. Reff, M.E. *et al.* Depletion of B cells in vivo by a chimeric mouse human monoclonal antibody to CD20. *Blood* **83**:2, 435 (1994).

262. Poppema, S.a.V., L. Preparation and application of monoclonal antibodies: B cell panel and parafin tissue reactive panel. *Biotest Bulletin* **3**, 131-139 (1987).

263. Trivedi, S. *et al.* Anti-EGFR Targeted Monoclonal Antibody Isotype Influences Antitumor Cellular Immunity in Head and Neck Cancer Patients. *Clin. Cancer. Res.* **22**, 5229-5237 (2016).

264. Wolfl, M. & Greenberg, P.D. Antigen-specific activation and cytokine-facilitated expansion of naive, human CD8+ T cells. *Nature protocols* **9**, 950-966 (2014).

265. Dauer, M. *et al.* Mature dendritic cells derived from human monocytes within 48 hours: a novel strategy for dendritic cell differentiation from blood precursors. *J. Immunol.* **170**, 4069-4076 (2003).

266. Lopez-Albaitero, A. *et al.* Maturation pathways of dendritic cells determine TAP1 and TAP2 levels and cross-presenting function. *J. Immunother.* **32**, 465-473 (2009).

267. Inc, T.S. Extinction Coefficients: A guide to understanding extinction coefficients, with emphasis on spectrophotometric determination of protein concentration. (2013).

268. Pace, C.N., Vajdos, F., Fee, L., Grimsley, G. & Gray, T. How to measure and predict the molar absorption coefficient of a protein. *Protein Sci.* **4**, 2411-2423 (1995).

269. Carney, D.N. *et al.* Establishment and identification of small cell lung cancer cell lines having classic and variant features. *Cancer Res.* **45**, 2913-2923 (1985).

270. Terhorst, C., Parham, P., Mann, D.L. & Strominger, J.L. Structure of HLA antigens: amino-acid and carbohydrate compositions and NH2-terminal sequences of four antigen preparations. *Proc. Natl. Acad. Sci. U. S. A.* **73**, 910-914 (1976).

271. Lozzio, B.B. & Lozzio, C.B. Properties and usefulness of the original K-562 human myelogenous leukemia cell line. *Leuk. Res.* **3**, 363-370 (1979).

272. Atlas, T.H.P. MLANA. 2015 [cited 2015 28/07/15] Available from: http://www.proteinatlas.org/ENSG00000120215-MLANA/cell/HPA048662

273. Letsch, A. *et al.* High frequencies of circulating melanoma-reactive CD8+ T cells in patients with advanced melanoma. *Int. J. Cancer* **87**, 659-664 (2000).

274. DeMars, R., Chang, C.C., Shaw, S., Reitnauer, P.J. & Sondel, P.M. Homozygous deletions that simultaneously eliminate expressions of class I and class II antigens of EBV-transformed B-lymphoblastoid cells. I. Reduced proliferative responses of autologous and allogeneic T cells to mutant cells that have decreased expression of class II antigens. *Hum. Immunol.* **11**, 77-97 (1984).

275. Salter, R.D. & Cresswell, P. Impaired assembly and transport of HLA-A and -B antigens in a mutant TxB cell hybrid. *EMBO J.* **5**, 943-949 (1986).

276. van Kuppeveld, F.J. *et al.* Genus- and species-specific identification of mycoplasmas by 16S rRNA amplification. *Appl. Environ. Microbiol.* **58**, 2606-2615 (1992).

277. Uphoff, C.C., Denkmann, S.A. & Drexler, H.G. Treatment of mycoplasma contamination in cell cultures with Plasmocin. *J Biomed Biotechnol* **2012**, Article ID: 267678 [8 pages] (2012).

278. Dietz, A.B. *et al.* A novel source of viable peripheral blood mononuclear cells from leukoreduction system chambers. *Transfusion* **46**, 2083-2089 (2006).

279. Neron, S. *et al.* Characterization of mononuclear cells remaining in the leukoreduction system chambers of apheresis instruments after routine platelet collection: a new source of viable human blood cells. *Transfusion* **47**, 1042-1049 (2007).

280. Keogh, E. *et al.* Identification of new epitopes from four different tumor-associated antigens: recognition of naturally processed epitopes correlates with HLA-A*0201-binding affinity. *J. Immunol.* **167**, 787-796 (2001).

281. Romero, P. *et al.* Antigenicity and immunogenicity of Melan-A/MART-1 derived peptides as targets for tumor reactive CTL in human melanoma. *Immunol. Rev.* **188**, 81-96 (2002).

282. Andrade Filho, P.A., Lopez-Albaitero, A., Gooding, W. & Ferris, R.L. Novel immunogenic HLA-A*0201-restricted epidermal growth factor receptor-specific T-cell epitope in head and neck cancer patients. *J. Immunother.* **33**, 83-91 (2010).

283. Vandeventer, P.E. *et al.* Multiphasic DNA adsorption to silica surfaces under varying buffer, pH, and ionic strength conditions. *The journal of physical chemistry. B* **116**, 5661-5670 (2012).

284. McGuigan, F.E. & Ralston, S.H. Single nucleotide polymorphism detection: allelic discrimination using TaqMan. *Psychiatr. Genet.* **12**, 133-136 (2002).

285. Kim, J.H. *et al.* High cleavage efficiency of a 2A peptide derived from porcine teschovirus-1 in human cell lines, zebrafish and mice. *PloS one* **6**, e18556 (2011).

286. Biolabs, N.E. NEB® 5-alpha Competent E. coli (Subcloning Efficiency). (2016) [cited 2016 25/04/16] Available from: https://www.neb.com/products/c2988-neb-5-alpha-competent-e-coli-subcloning-efficiency - tabselect0

287. GmbH, B.L. Transfection. (2016) [cited 2015 23/01/15] Available from: http://www.biontex.com/con_4_6_4/cms/front_content.php?idcat=52

288. Nylander S., K.I. Brefeldin A, but not monensin, completely blocks CD69 expression on mouse lymphocytes: efficacy of inhibitors of protein secretion in protocols for intracellular cytokine staining by flow cytometry. *J. Immunol. Methods* **224**, 69-76 (1999).

289. Miksa, M., Komura, H., Wu, R., Shah, K.G. & Wang, P. A novel method to determine the engulfment of apoptotic cells by macrophages using pHrodo succinimidyl ester. *J. Immunol. Methods* **342**, 71-77 (2009).

290. Coulter, B. CytoFuge II. 2016.

291. Kelley, T.F., Petithory, H.A. & Soares, T.W. Cytology centrifuge apparatus. Google Patents; 1997.

292. Mahnke, Y.D. & Roederer, M. Optimizing a multicolor immunophenotyping assay. *Clin. Lab. Med.* **27**, 469-485, v (2007).

293. Maecker, H.T. & Trotter, J. Flow cytometry controls, instrument setup, and the determination of positivity. *Cytometry. Part A : the journal of the International Society for Analytical Cytology* **69**, 1037-1042 (2006).

294. McLaughlin, B.E. *et al.* Nine-color flow cytometry for accurate measurement of T cell subsets and cytokine responses. Part II: Panel performance across different instrument platforms. *Cytometry. Part A : the journal of the International Society for Analytical Cytology* **73**, 411-420 (2008).

295. GraphPad Software, I. GraphPad Statistics Guide. (2015) [cited 24/06/16] Available from: http://www.graphpad.com/guides/prism/6/statistics/

296. Habibzadeh, F. Common statistical mistakes in manuscripts submitted to biomedical journals. *European Science Editing* **39**, 92-94 (2013).

297. Awasthi, A. *et al.* Obinutuzumab (GA101) compared to rituximab significantly enhances cell death and antibody-dependent cytotoxicity and improves overall survival against CD20(+) rituximab-sensitive/-resistant Burkitt lymphoma (BL) and precursor B-acute lymphoblastic leukaemia (pre-B-ALL): potential targeted therapy in patients with poor risk CD20(+) BL and pre-B-ALL. *Br. J. Haematol.* **171**, 763-775 (2015).

298. Peruzzi, G. *et al.* Membrane-type 6 matrix metalloproteinase regulates the activation-induced downmodulation of CD16 in human primary NK cells. *J. Immunol.* **191**, 1883-1894 (2013).

299. North, J. *et al.* Tumor-primed human natural killer cells lyse NK-resistant tumor targets: evidence of a two-stage process in resting NK cell activation. *J. Immunol.* **178**, 85-94 (2007).

300. Fogel, L.A., Sun, M.M., Geurs, T.L., Carayannopoulos, L.N. & French, A.R. Markers of Nonselective and Specific NK Cell Activation. *J. Immunol.* **190**:12,6269-6276 (2013).

301. Chen, X., Trivedi, P.P., Ge, B., Krzewski, K. & Strominger, J.L. Many NK cell receptors activate ERK2 and JNK1 to trigger microtubule organizing center and granule polarization and cytotoxicity. *Proc. Natl. Acad. Sci. U. S. A.* **104**, 6329-6334 (2007).

302. Bryceson, Y.T., March, M.E., Ljunggren, H.G. & Long, E.O. Synergy among receptors on resting NK cells for the activation of natural cytotoxicity and cytokine secretion. *Blood* **107**, 159-166 (2006).

303. Muller, P.Y., Milton, M., Lloyd, P., Sims, J. & Brennan, F.R. The minimum anticipated biological effect level (MABEL) for selection of first human dose in clinical trials with monoclonal antibodies. *Curr. Opin. Biotechnol.* **20**, 722-729 (2009).

304. Suh, H.Y., Peck, C.C., Yu, K.S. & Lee, H. Determination of the starting dose in the first-in-human clinical trials with monoclonal antibodies: a systematic review of papers published between 1990 and 2013. *Drug design, development and therapy* **10**, 4005-4016 (2016).

305. Khoo, B.L. *et al.* Single-cell profiling approaches to probing tumor heterogeneity. *Int. J. Cancer* **139**, 243-255 (2016).

306. Derer, S. *et al.* Impact of epidermal growth factor receptor (EGFR) cell surface expression levels on effector mechanisms of EGFR antibodies. *J. Immunol.* **189**, 5230-5239 (2012).

307. Franz, S. *et al.* After shrinkage apoptotic cells expose internal membrane-derived epitopes on their plasma membranes. *Cell Death Differ.* **14**, 733-742 (2007).

308. Vermes, I., Haanen, C., Steffens-Nakken, H. & Reutelingsperger, C. A novel assay for apoptosis. Flow cytometric detection of phosphatidylserine expression on early apoptotic cells using fluorescein labelled Annexin V. *J. Immunol. Methods* **184**, 39-51 (1995).

309. Biosciences, B. FITC Annexin V Apoptosis Detection Kit I. 2016 [cited 27.11.15] Available from: http://www.bdbiosciences.com/eu/applications/research/apoptosis/apoptosis-kits-sets/fitc-annexin-v-apoptosis-detection-kit-i/p/556547

310. Koopman, G. *et al.* Annexin V for flow cytometric detection of phosphatidylserine expression on B cells undergoing apoptosis. *Blood* **84**, 1415-1420 (1994).

311. Cardarelli, P.M. *et al.* Binding to CD20 by anti-B1 antibody or F(ab')(2) is sufficient for induction of apoptosis in B-cell lines. *Cancer Immunol. Immunother.* **51**, 15-24 (2002).

312. Shan, D., Ledbetter, J.A. & Press, O.W. Apoptosis of malignant human B cells by ligation of CD20 with monoclonal antibodies. *Blood* **91**, 1644-1652 (1998).

313. Deans, J.P., Li, H. & Polyak, M.J. CD20-mediated apoptosis: signalling through lipid rafts. *Immunology* **107**, 176-182 (2002).

314. Testi, R., D'Ambrosio, D., De Maria, R. & Santoni, A. The CD69 receptor: a multipurpose cell-surface trigger for hematopoietic cells. *Immunol. Today* **15**, 479-483 (1994).

315. Haining, W.N. Travels in time: assessing the functional complexity of T cells. *Proc. Natl. Acad. Sci. U. S. A.* **109**, 1359-1360 (2012).

316. Han, Q. *et al.* Polyfunctional responses by human T cells result from sequential release of cytokines. *Proc. Natl. Acad. Sci. U. S. A.* **109**, 1607-1612 (2012).

317. Small, G.W., McLeod, H.L. & Richards, K.L. Analysis of innate and acquired resistance to anti-CD20 antibodies in malignant and nonmalignant B cells. *PeerJ* **1**, e31 (2013).

318. Lammerts van Bueren, J.J. *et al.* Effect of target dynamics on pharmacokinetics of a novel therapeutic antibody against the epidermal growth factor receptor: implications for the mechanisms of action. *Cancer Res.* **66**, 7630-7638 (2006).

319. Thurber, G.M., Schmidt, M.M. & Wittrup, K.D. Antibody tumor penetration: Transport opposed by systemic and antigen-mediated clearance. *Adv. Drug Del. Rev.* **60**:12, 1421-1434 (2008).

320. Weinstein, J.N. *et al.* The pharmacology of monoclonal antibodies. *Ann. N. Y. Acad. Sci.* **507**, 199-210 (1987).

321. Tan, A.R. *et al.* Pharmacokinetics of cetuximab after administration of escalating single dosing and weekly fixed dosing in patients with solid tumors. *Clin. Cancer Res.* **12**, 6517-6522 (2006).

322. Yi, C.H. *et al.* Function characterization of a glyco-engineered anti-EGFR monoclonal antibody cetuximab in vitro. *Acta pharmacologica Sinica* **35**, 1439-1446 (2014).

323. Kanda, Y. *et al.* Comparison of biological activity among nonfucosylated therapeutic IgG1 antibodies with three different N-linked Fc oligosaccharides: the high-mannose, hybrid, and complex types. *Glycobiology* **17**, 104-118 (2007).

324. Parameswaran, S., Khalil, M., Ahmed, K.A., Sharma, R.K. & Xiang, J. Enhanced protective immunity derived from dendritic cells with phagocytosis of CD40 ligand transgene-engineered apoptotic tumor cells via increased dendritic cell maturation. *Tumori* **101**:6, 637-643 (2015).

325. von Euw, E.M. *et al.* Monocyte-derived dendritic cells loaded with a mixture of apoptotic/necrotic melanoma cells efficiently cross-present gp100 and MART-1 antigens to specific CD8(+) T lymphocytes. *Journal of translational medicine* **5**, 19 [13 pages] (2007).

326. Moeller, I., Spagnoli, G.C., Finke, J., Veelken, H. & Houet, L. Uptake routes of tumor-antigen MAGE-A3 by dendritic cells determine priming of naive T-cell subtypes. *Cancer Immunol. Immunother.* **61**, 2079-2090 (2012).

327. Orange, J.S. Formation and function of the lytic NK-cell immunological synapse. *Nature reviews. Immunology* **8**, 713-725 (2008).

328. Hampton, M.B., Vissers, M.C. & Winterbourn, C.C. A single assay for measuring the rates of phagocytosis and bacterial killing by neutrophils. *J. Leukoc. Biol.* **55**, 147-152 (1994).

329. Lin, Z. *et al.* Detection of murine leukemia virus in the Epstein-Barr virus-positive human B-cell line JY, using a computational RNA-Seq-based exogenous agent detection pipeline, PARSES. *J. Virol.* **86**, 2970-2977 (2012).

330. Olejniczak, S.H., Stewart, C.C., Donohue, K. & Czuczman, M.S. A quantitative exploration of surface antigen expression in common B-cell malignancies using flow cytometry. *Immunol. Invest.* **35** 93-114 (2006).

331. Oestergaard, M.Z. *et al.* Superiority of Obinutuzumab over Rituximab in a New Molecular Follicular Lymphoma-like Subgroup of DLBCL: Results from an Exploratory Analysis of the Phase 3 GOYA Trial. *Blood* **130:**Suppl 1, 1543 (2017).

332. Cheadle, E.J. *et al.* The induction of immunogenic cell death by type II anti-CD20 monoclonal antibodies has mechanistic differences compared with type I rituximab. *Br. J. Haematol.* **162**, 842-845 (2013).

333. Golay, J. *et al.* Glycoengineered CD20 antibody obinutuzumab activates neutrophils and mediates phagocytosis through CD16B more efficiently than rituximab. *Blood* **122**, 3482-3491 (2013).

334. Haller Hasskamp, J., Zapas, J.L. & Elias, E.G. Dendritic cell counts in the peripheral blood of healthy adults. *Am. J. Hematol.* **78**, 314-315 (2005).

335. Shannon, J.G., Cockrell, D.C., Takahashi, K., Stahl, G.L. & Heinzen, R.A. Antibody-mediated immunity to the obligate intracellular bacterial pathogen Coxiella burnetii is Fc receptor- and complement-independent. *BMC Immunol* **10**, 26 [8 pages] (2009).

336. Signorino, E. *et al.* Contribution of dendritic cells' FcgammaRI and FcgammaRIII to cross-presentation of tumor cells opsonized with the anti-MHC class I monoclonal antibodies. *Cancer biology & therapy* **6**, 1932-1937 (2007).

337. Kim, G.P. & Grothey, A. Targeting colorectal cancer with human anti-EGFR monoclonocal antibodies: focus on panitumumab. *Biologics : Targets & Therapy* **2**, 223-228 (2008).

338. Segura, E. *et al.* Human inflammatory dendritic cells induce Th17 cell differentiation. *Immunity* **38**, 336-348 (2013).

339. Ma, Y. *et al.* Anticancer chemotherapy-induced intratumoral recruitment and differentiation of antigen-presenting cells. *Immunity* **38**, 729-741 (2013).

340. Cheong, C. *et al.* Microbial stimulation fully differentiates monocytes to DC-SIGN/CD209(+) dendritic cells for immune T cell areas. *Cell* **143**, 416-429 (2010).

341. Passlick, B., Flieger, D. & Ziegler-Heitbrock, H.W. Identification and characterization of a novel monocyte subpopulation in human peripheral blood. *Blood* **74**, 2527-2534 (1989).

342. Randolph, G.J., Sanchez-Schmitz, G., Liebman, R.M. & Schakel, K. The CD16(+) (FcgammaRIII(+)) subset of human monocytes preferentially becomes migratory dendritic cells in a model tissue setting. *J. Exp. Med.* **196**, 517-527 (2002).

343. Sanchez-Torres, C., Garcia-Romo, G.S., Cornejo-Cortes, M.A., Rivas-Carvalho, A. & Sanchez-Schmitz, G. CD16+ and CD16- human blood monocyte subsets differentiate in vitro to dendritic cells with different abilities to stimulate CD4+ T cells. *Int. Immunol.* **13**, 1571-1581 (2001).

344. Boruchov, A.M. *et al.* Activating and inhibitory IgG Fc receptors on human DCs mediate opposing functions. *J. Clin. Invest.* **115**, 2914-2923 (2005).

345. Nouri-Shirazi, M. *et al.* Dendritic Cells Capture Killed Tumor Cells and Present Their Antigens to Elicit Tumor-Specific Immune Responses. *The Journal of Immunology* **165**:7, 3797-3803 (2000).

346. Guilliams, M., Bruhns, P., Saeys, Y., Hammad, H. & Lambrecht, B.N. The function of Fcgamma receptors in dendritic cells and macrophages. *Nature reviews. Immunology* **14**, 94-108 (2014).

347. Chaux, P., Vantomme, V., Coulie, P., Boon, T. & van der Bruggen, P. Estimation of the frequencies of anti-MAGE-3 cytolytic T-lymphocyte precursors in blood from individuals without cancer. *Int. J. Cancer* **77**, 538-542 (1998).

348. Barrio, M.M. *et al.* Human macrophages and dendritic cells can equally present MART-1 antigen to CD8(+) T cells after phagocytosis of gamma-irradiated melanoma cells. *PloS one* **7**, e40311 (2012).

349. Chiang, C.L. *et al.* Day-4 myeloid dendritic cells pulsed with whole tumor lysate are highly immunogenic and elicit potent anti-tumor responses. *PloS one* **6**, e28732 (2011).

350. Kim, P.S. *et al.* Antibody association with HER-2/neu-targeted vaccine enhances CD8 T cell responses in mice through Fc-mediated activation of DCs. *J. Clin. Invest.* **118**, 1700-1711 (2008).

351. Disis, M.L. *et al.* Concurrent trastuzumab and HER2/neu-specific vaccination in patients with metastatic breast cancer. *J. Clin. Oncol.* **27**, 4685-4692 (2009).

352. Tomita, Y. *et al.* Identification of immunogenic LY6K long peptide encompassing both CD4+ and CD8+ T-cell epitopes and eliciting CD4+ T-cell immunity in patients with malignant disease. *Oncoimmunology* **3**, e28100 (2014).

353. Yoshitake, Y., Nishimura, Y., Nakamura, Y. & Shinohara, M. A clinical trial of multiple peptides vaccination for advanced head and neck cancer patients induced immune responses and prolonged OS. *Oncoimmunology* **4**, e1022307 (2015).

354. Tanaka, M. *et al.* Development of a new diagnostic tool for pancreatic cancer: simultaneous measurement of antibodies against peptides recognized by cytotoxic T lymphocytes. *Kurume Med. J.* **53**, 63-70 (2006).

355. Kleihauer, A. *et al.* Ex vivo generation of human cytomegalovirus-specific cytotoxic T cells by peptide-pulsed dendritic cells. *Br. J. Haematol.* **113**, 231-239 (2001).

356. Coulie, P.G. *et al.* A new gene coding for a differentiation antigen recognized by autologous cytolytic T lymphocytes on HLA-A2 melanomas. *J. Exp. Med.* **180**, 35-42 (1994).

357. Alanio, C., Lemaitre, F., Law, H.K., Hasan, M. & Albert, M.L. Enumeration of human antigen-specific naive CD8+ T cells reveals conserved precursor frequencies. *Blood* **115**, 3718-3725 (2010).

358. Pittet, M.J. *et al.* High frequencies of naive Melan-A/MART-1-specific CD8(+) T cells in a large proportion of human histocompatibility leukocyte antigen (HLA)-A2 individuals. *J. Exp. Med.* **190**, 705-715 (1999).

359. Kalinski, P., Vieira, P.L., Schuitemaker, J.H., de Jong, E.C. & Kapsenberg, M.L. Prostaglandin E(2) is a selective inducer of interleukin-12 p40 (IL-12p40) production and an inhibitor of bioactive IL-12p70 heterodimer. *Blood* **97**, 3466-3469 (2001).

360. Langenkamp, A., Messi, M., Lanzavecchia, A. & Sallusto, F. Kinetics of dendritic cell activation: impact on priming of TH1, TH2 and nonpolarized T cells. *Nat Immunol* **1**, 311-316 (2000).

361. Ma, X. *et al.* The interleukin 12 p40 gene promoter is primed by interferon gamma in monocytic cells. *J. Exp. Med.* **183**, 147-157 (1996).

362. HLA-Matchmaker. HLAMatchmaker: % chance of HLA allele expressed in an individual 2014 [Online] Cited 26.02.14. Available from: http://www.hlamatchmaker.net. (2014).

363. Valmori, D. *et al.* Enhanced generation of specific tumor-reactive CTL in vitro by selected Melan-A/MART-1 immunodominant peptide analogues. *J. Immunol.* **160**, 1750-1758 (1998).

364. Ayyoub, M. *et al.* Activation of human melanoma reactive CD8+ T cells by vaccination with an immunogenic peptide analog derived from Melan-A/melanoma antigen recognized by T cells-1. *Clin. Cancer Res.* **9**, 669-677 (2003).

365. Li, J. *et al.* Human T cells upregulate CD69 after coculture with xenogeneic genetically-modified pig mesenchymal stromal cells. *Cell. Immunol.* **285**, 23-30 (2013).

366. Lio, D. *et al.* In vitro T cell activation in elderly individuals: failure in CD69 and CD71 expression. *Mech. Ageing Dev.* **89**, 51-58 (1996).

367. Fadel, F.I. *et al.* Lymphocyte Activation Markers in Pediatric Kidney Transplant Recipients. *International journal of biomedical science : IJBS* **11**, 121-130 (2015).

368. Gros, A. *et al.* PD-1 identifies the patient-specific CD8(+) tumor-reactive repertoire infiltrating human tumors. *J. Clin. Invest.* **124**, 2246-2259 (2014).

369. Wolfl, M., Kuball, J., Eyrich, M., Schlegel, P.G. & Greenberg, P.D. Use of CD137 to study the full repertoire of CD8+ T cells without the need to know epitope specificities. *Cytometry. Part A : the journal of the International Society for Analytical Cytology* **73**, 1043-1049 (2008).

370. Wolfl, M. *et al.* Activation-induced expression of CD137 permits detection, isolation, and expansion of the full repertoire of CD8+ T cells responding to antigen without requiring knowledge of epitope specificities. *Blood* **110**, 201-210 (2007).

371. Sattler, A., Wagner, U., Rossol, M., Sieper, J., Wu, P., Krause, A., Schmidt, W.A., Radmer, S., Kohler, S., Romagnani, C. and Thiel, A. . Effector memory T helper cells secrete IFN-γ upon stimulation with cytokines: a role in chronic inflammation. *MACS&more* **13**:1, 17-23 (2011).

372. Kim, T.K. & Eberwine, J.H. Mammalian cell transfection: the present and the future. *Anal. Bioanal. Chem.* **397**, 3173-3178 (2010).

373. Geginat, J., Sallusto, F. & Lanzavecchia, A. Cytokine-driven proliferation and differentiation of human naive, central memory and effector memory CD4+ T cells. *Pathol. Biol. (Paris).* **51**, 64-66 (2003).

374. Chen, S., Li, X., Chen, R., Yin, M. & Zheng, Q. Cetuximab intensifies the ADCC activity of adoptive NK cells in a nude mouse colorectal cancer xenograft model. *Oncology Letters* **12**, 1868-1876 (2016).

375. Honeychurch, J., Cheadle, E.J., Dovedi, S.J. & Illidge, T.M. Immuno-regulatory antibodies for the treatment of cancer. *Expert opinion on biological therapy* **15**, 787-801 (2015).

376. Wu, J. *et al.* A novel polymorphism of FcgammaRIIIa (CD16) alters receptor function and predisposes to autoimmune disease. *The Journal of clinical investigation* **100**, 1059-1070 (1997).

377. Lievre, A. *et al.* KRAS mutation status is predictive of response to cetuximab therapy in colorectal cancer. *Cancer Res.* **66**, 3992-3995 (2006).

378. Trivedi, S. *et al.* Anti-EGFR targeted monoclonal antibody isotype influences anti-tumor cellular immunity in head and neck cancer patients. *Clin. Cancer Res.* **22**:21, 5229-5237 (2016).

379. Pan, C., Kumar, C., Bohl, S., Klingmueller, U. & Mann, M. Comparative proteomic phenotyping of cell lines and primary cells to assess preservation of cell type-specific functions. *Molecular & cellular proteomics : MCP* **8**, 443-450 (2009).

380. Short, S.P., Costacurta, P.W. & Williams, C.S. Using 3D Organoid Cultures to Model Intestinal Physiology and Colorectal Cancer. *Current colorectal cancer reports* **13**, 183-191 (2017).

381. Roederer, M. How many events is enough? Are you positive? *Cytometry. Part A : the journal of the International Society for Analytical Cytology* **73**, 384-385 (2008).

382. Moodie, Z. *et al.* Response definition criteria for ELISPOT assays revisited. *Cancer Immunol. Immunother.* **59**, 1489-1501 (2010).

383. Nahta, R. & Esteva, F.J. HER-2-targeted therapy: lessons learned and future directions. *Clin. Cancer Res.* **9**, 5078-5084 (2003).

384. WHO. WHO Model List of Essential Medicines. 2015.

385. GenmAb. Daratumumab Receives Breakthrough Therapy Designation from US Food and Drug Administration. 2013 [cited 13.11.16] Available from: http://ir.genmab.com/releasedetail.cfm?releaseid=760960

386. Bagacean, C., Zdrenghea, M., Tempescul, A., Cristea, V. & Renaudineau, Y. Anti-CD20 monoclonal antibodies in chronic lymphocytic leukemia: from uncertainties to promises. *Immunotherapy* **8**, 569-581 (2016).

387. Kobold, S., Wiedemann, G., Rothenfusser, S. & Endres, S. Modes of action of TLR7 agonists in cancer therapy. *Immunotherapy* **6**, 1085-1095 (2014).

388. Cheadle, E.J. *et al.* A TLR7 agonist enhances the antitumor efficacy of obinutuzumab in murine lymphoma models via NK cells and CD4 T cells. *Leukemia* (2017).

389. Byrd, J.C. *et al.* Three-year follow-up of treatment-naive and previously treated patients with CLL and SLL receiving single-agent ibrutinib. *Blood* **125**, 2497-2506 (2015).

390. Burger, J.A. *et al.* Safety and activity of ibrutinib plus rituximab for patients with high-risk chronic lymphocytic leukaemia: a single-arm, phase 2 study. *The Lancet. Oncology* **15**, 1090-1099 (2014).

391. Cramer, P., Langerbeins, P. & Hallek, M. Combination of Targeted Drugs to Control Chronic Lymphocytic Leukemia: Harnessing the Power of New Monoclonal Antibodies in Combination With Ibrutinib. *Cancer journal (Sudbury, Mass.)* **22**, 62-66 (2016).

392. von Tresckow, J. *et al.* CLL2-BIG: sequential treatment with bendamustine, ibrutinib and obinutuzumab (GA101) in chronic lymphocytic leukemia. *Leukemia* [12 pages] e-published ahead of print (2018).

393. Burger, J.A. *et al.* Ibrutinib as Initial Therapy for Patients with Chronic Lymphocytic Leukemia. *New Engl. J. Med.* **373**, 2425-2437 (2015).

394. Byrd, J.C. *et al.* Targeting BTK with Ibrutinib in Relapsed Chronic Lymphocytic Leukemia. *New Engl. J. Med.* **369**, 32-42 (2013).

395. Burger, J.A. *et al.* Safety and activity of ibrutinib plus rituximab for patients with high-risk chronic lymphocytic leukaemia: a single-arm, phase 2 study. *The Lancet Oncology* **15**, 1090-1099 (2014).

396. Etuk A., G.C., Preece R. and Qasim W. Abstract: Universal Antibody-Mediated Cell Therapy (uACT). *BSGCT Autumn Conference - London, UK* (2018).

397. Schanzer, J.M. *et al.* XGFR*, a novel affinity-matured bispecific antibody targeting IGF-1R and EGFR with combined signaling inhibition and enhanced immune activation for the treatment of pancreatic cancer. *mAbs* **8**, 811-827 (2016).

398. Salles, G. *et al.* Phase 1 study results of the type II glycoengineered humanized anti-CD20 monoclonal antibody obinutuzumab (GA101) in B-cell lymphoma patients. *Blood* **119**, 5126-5132 (2012).

399. Temam, S. *et al.* An exploratory, open-label, randomized, multicenter study to investigate the pharmacodynamics of a glycoengineered antibody (imgatuzumab) and cetuximab in patients with operable head and neck squamous cell carcinoma. *Annals of oncology : official journal of the European Society for Medical Oncology* **28**, 2827-2835 (2017).

400. Chang, C.-H., Rossi, E.A. & Goldenberg, D.M. Monoclonal antibodies targeting CD20. *mAbs* **5**, 335-336 (2013).

401. NCBI. NCBI Sample GenBank Record: GenBank Flat File Format. 2006 23/10/06 [cited 01/05/16] Available from: http://www.ncbi.nlm.nih.gov/Sitemap/samplerecord.html

“Men have forgotten this truth,” said the fox. “But you must not forget it. You become responsible, forever, for what you have tamed.”

The Little Prince - Antoine de Saint-Exupéry